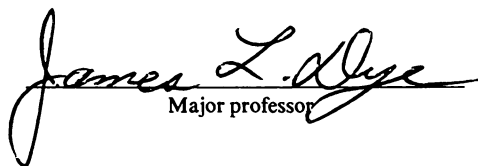This is to certify that the

dissertation entitled

Solid State Alkali Metal NMR
Spectra and Magnetic Susceptibilities
of Alkalides, Electrides and Their
Related Compounds

presented by

Jineun Kim

has been accepted towards fulfillment
of the requirements for

___Ph.D.___ degree in __Chemistry__

James L. Dye
Major professor

Date_ 6 / 28 / 89 _

DATE DUE	DATE DUE	DATE DUE

SOLID STATE ALKALI METAL NMR SPECTRA AND

MAGNETIC SUSCEPTIBILITIES OF ALKALIDES, ELECTRIDES AND

THEIR RELATED COMPOUNDS

By

Jineun Kim

A DISSERTATION

Submitted to
Michigan State University
in partial fulfillment of the requirements
for the degree of

DOCTOR OF PHILOSOPHY

Department of Chemistry

1989

ABSTRACT

SOLID STATE ALKALI METAL NMR SPECTRA AND MAGNETIC SUSCEPTIBILITIES OF ALKALIDES, ELECTRIDES AND THEIR RELATED COMPOUNDS

By

Jineun Kim

The position of NMR lines in single crystals as a function of orientation was described as a function of the chemical shift parameters (δ_{XX}, δ_{YY}, δ_{ZZ}), a quadrupolar coupling constant (χ), an asymmetry parameter (η^Q) for quadrupolar interactions, and Eulerian angles (α, β, γ). Solid state NMR powder patterns were explained by the superposition of single crystal NMR lines at different orientations of the crystal with respect to the external field, taking into account the probabilities of various orientations.

A nuclear quadrupolar coupling constant of 0.1763 MHz ($\eta^Q = 0$) for Na^- in $Na^+C222 \cdot Na^-$ was obtained by a single crystal NMR method, in addition to a quadrupolar coupling constant of 1.268 MHz ($\eta^Q = 0$) for Na^+. A quadrupolar coupling constant of 0.605 MHz ($\eta^Q = 0$) for Na^+ in $Na^+C222 \cdot Br^-$ was determined by a single crystal NMR study.

Nonaxially symmetric quadrupolar coupling and chemical shift tensors (χ = 0.5810 MHz, η^Q = 0.4755, δ_{XX} = 62.0 ppm, δ_{YY} = 46.1 ppm, and δ_{ZZ} = -28.4 ppm) for Cs^+ in tetragonal $Cs^+(15C5)_2 \cdot I^-$ were obtained by a single crystal NMR study. Simulations of the powder patterns of numerous Na^+ and Cs^+ salts by the program VMASS yielded quadrupolar coupling constants, asymmetry parameters, and chemical shift parameters. The powder patterns are inhomogeneously broadened in spite of the presence of strong proton-proton and proton-alkali cation interactions.

Alkali metal NMR spectra of $M^+BH_4^-$ (M = Li, Na, K, Rb, Cs) and M^+TPB^- ($TPB^- = B(C_6H_5)_4^-$) were investigated. The most diamagnetically shifted alkali metal cations ever found were present in the M^+TPB^- salts.

A spin echo technique with phase cycling allowed the observation of K^+ and Rb^+ in crystalline alkalides, electrides and their related compounds.

The magnetic behaviors of three electrides, $Cs^+(18C6)_2 \cdot e^-$, $Cs^+(15C5)_2 \cdot e^-$, and $K^+C222 \cdot e^-$ were discussed in relation to their structures. The magnetic susceptibility data of $Li^+C211 \cdot e^-$ fit a modified Oguchi theory of magnetism, yielding a coupling constant, J/k = -13.9 K, a Weiss temperature, -20.6 K, and a Néel temperature, T_N = 17.0 K.
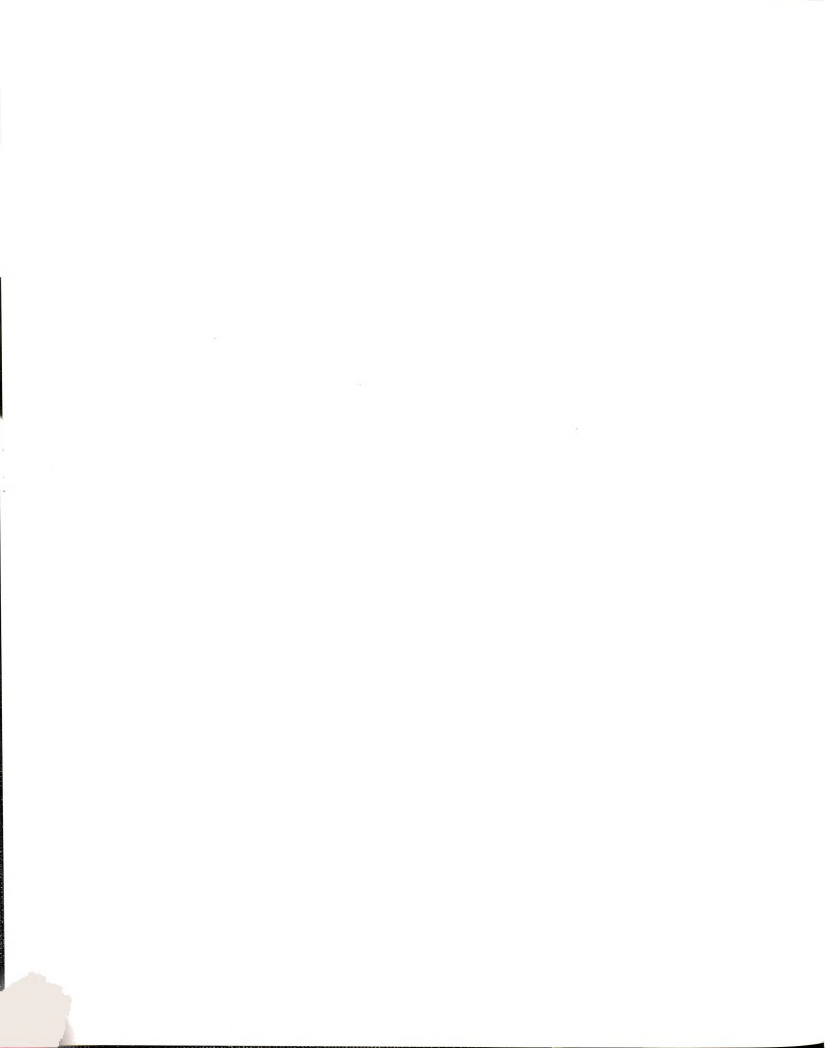
To my wife,

BoYoung

ACKNOWLEDGEMENTS

TABLE OF CONTENTS

CH

AP

LI

LIST OF TABLES

LIST OF FIGURES

Page

Figure

Figure

Figure

Figure

Figure

Figure

Figure

Figure

Figure

Figure

Figure

Figure 39

Figure 40

Figure 41

Figure 42

Figure 43

Figure 44

Figure 45

Figure 46

Figure 47

Figure 48

Figure 49

Figure 50

Figure 51

Figure 52

Figure 53

Figure 54

Figure 55

Figure 56

Figure 57

Figure

Figure

So

molecul

proper

bondin

covale

number

electr

these

comple

methyl

alkali

electr

F

Na^+C22

$Cs^+(18$

been i

and ch

includ

magnet

photol

CHAPTER I

INTRODUCTION

Solids are composed of basic units such as atoms, molecules, and ions held together by chemical bonds. The properties of solids are very much dependent on the type of bonding. There are five main types of bonding: ionic, covalent, Van der Waals, hydrogen, and metallic. Recently a number of new ionic crystals known as alkalides and electrides have been synthesized and characterized [1,2]. In these solids the cations (M^+L_n) are alkali metal cations complexed by macrocyclic or macrobicyclic polyethers or fully methylated aza-crown ethers [Figure 1] and the anions are alkali metal anions (N^-) in alkalides or solvent free trapped electrons in electrides.

Following the synthesis of the first alkalide $Na^+C222 \cdot Na^-$ [3] and the first crystalline electride $Cs^+(18C6)_2 \cdot e^-$ [4], about 30 alkalides and 7 electrides have been isolated. Much work has been focussed on the synthesis and characterization of new compounds by numerous techniques including optical spectroscopy, chemical analysis, NMR, EPR, magnetic susceptibility, and conductivity. Recently photoluminescence [5], photoelectron emission and thermionic

1
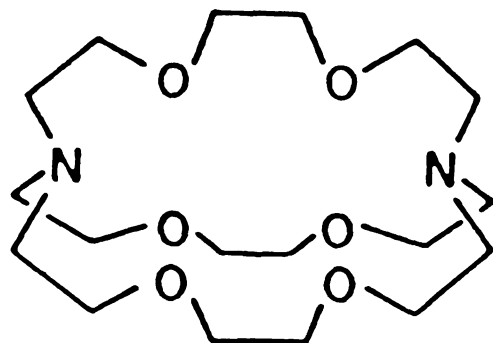
a) Cryptand 222 (C222)
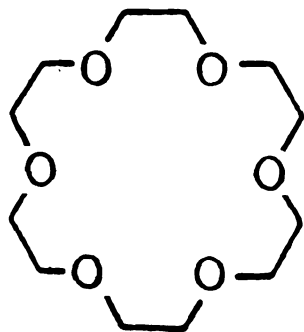
b) 18-Crown-6 (18C6)
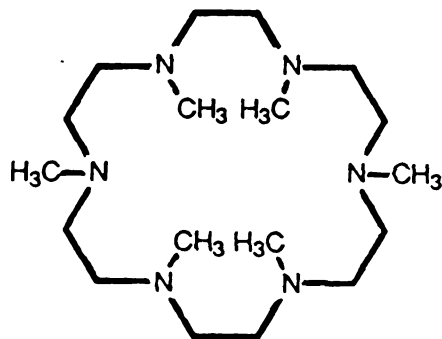
c) Hexamethyl hexacyclen (HMHCY)

Figure 1 Representative complexants.

emissic

structu

compour

contair

been o

ether,

success

single

and th

have p

electr

fully

stable

T

[11] e

study

spinni

and Cs

were c

not pe

extens

The n

they

spher

quest

by

ident

emission [6] have been investigated to study the band structures of these materials. However, the study of these compounds has been hindered by decomposition of the solution containing M^+L_n, N^-, and solvated electrons. This problem has been overcome by using aprotic solvents such as dimethyl ether, trimethyl amine, and diethyl ether [7]. Since the successful development of methods to grow and handle good single crystals [8,9], the crystal structures of 15 alkalides and three electrides have been determined. The structures have provided a better understanding of the nature of trapped electrons and alkali metal anions in these materials. With fully methylated aza-crown ethers, relatively thermally stable compounds have been synthesized [10].

The first identification of alkali metal anions by NMR [11] established this technique as an excellent tool for the study of alkalides and electrides. Magic angle sample spinning (MAS) NMR was used to identify Li^+, Na^+, Na^-, Cs^+, and Cs^- in these materials [12-14]. The species K^- and Rb^- were observed in potassides and rubidides [15,16], but it was not possible to study complexes of these cations because of extensive quadrupolar line broadening and low sensitivity. The narrow NMR lines of alkali metal anions indicate that they are almost unperturbed ions with two electrons in a spherically symmetric ns orbital. However there remains a question whether these relatively narrow lines are broadened by quadrupolar interactions. In addition to the identification of species, NMR has been used to study some

phys

quad

obta

The

know

low

the

cati

inte

stat

1, 2

tha

amo

alk

oth

com

phe

tem

K^+C

bel

[22

cla

[25

ant

exp

str

physical properties of these compounds. For example, a quadrupolar coupling constant of 1.2 ± 0.1 MHz for Na^+ was obtained by simulating the MAS spectrum of $Na^+C222 \cdot Na^-$ [17]. The temperature dependence of the ^{133}Cs Knight shifts and the known magnetic susceptibility of $Cs^+(18C6)_2 \cdot e^-$ yielded a very low fraction of cesium s-orbital character, 3.3×10^{-4}, for the trapped electron [14]. This indicates that the cesium cations are well screened from the unpaired electrons by interaction with the crown ethers. Summaries of the solid state NMR results from previous studies are listed in Tables 1, 2, 3, and 4.

The ns^2 electronic configuration of alkalides predicts that they are diamagnetic. Although the presence of small amounts of trapped electrons gives EPR signals [18,21], alkalides are indeed diamagnetic [22]. Electrides, on the other hand, show a wide range of magnetic properties. The compounds $Li^+C211 \cdot e^-$ and $K^+C222 \cdot e^-$ exhibit spin pairing phenomena below their transition temperatures. The transition temperature (temperature of maximum susceptibility) of $K^+C222 \cdot e^-$ has not been observed since the compound decomposes below its critical temperature. $Cs^+(18C6)_2 \cdot e^-$ is paramagnetic [22], while $Cs^+(15C5)_2 \cdot e^-$ [8] and $Li^+PMPCY \cdot e^-$ [23] behave as classical antiferromagnetics. $Li^+C211 \cdot e^-$ [24] and $K^+C222 \cdot e^-$ [25] might be classified as limiting cases of antiferromagnetics since the magnetic behavior may be explained by invoking only small interactions between more strongly coupled electron pairs. These versatile magnetic

l nemdence of the chemical shift

Table 1 Proton decoupled and frequency dependence of the chemical shift and linewidth of ^{23}Na NMR [18]

| Compound | ^{1}H decoupled 52.94 MHz | | ^{1}H coupled | | | | | |
| | | | 52.94 MHz | | 95.29 MHz | | 132.35 MHz | |
	δ,ppm	$\Delta\nu_{1/2}$,Hz	δ,ppm	$\Delta\nu_{1/2}$,Hz	δ,ppm	$\Delta\nu_{1/2}$,Hz	δ,ppm	$\Delta\nu_{1/2}$,Hz
Na^{+}18C6·SCN^{-}	-22	610	-22	700	---	----	-13	310
Na^{+}C222·I^{-}	-20	680	-21	1300	---	----	-10	514
N<u>a</u>$^{+}$C222·Na^{-}	-20	860	-24	1200	-11	720	-9	610
Na^{+}C222·N<u>a</u>$^{-}$	-61	30	-61	290	-61	190	-61	250
K^{+}C222·Na^{-}	-62	30	-61	170	-61	210	-61	84
Rb^{+}C222·Na^{-}	-63	60	-63	225	-57	270	---	---
K^{+}18C6·Na^{-}	-58	78	-56	120	-60	185	-57	223
Rb^{+}18C6·Na^{-}	-60	40	-60	90	-60	50	-61	109
Cs^{+}(18C6)$_{2}$·Na^{-}	-63	70	-63	75	-62	75	---	---
K^{+}(15C5)$_{2}$·Na^{-}	-61	45	-61	90	-61	64	---	---
K^{+}(12C4)$_{2}$·Na^{-}	-61	33	-61	51	-61	48	-61	85

Table

Compou
K^+(15C
Rb^+(15
Cs^+(15
KRb18C
Cs^+(18
K^+C222

[a] Chemi
dilut:
[b] Prob

Table

Compo
KRb(1
Rb^+(1
Cs^+(1
Cs^+(1
KRb18

[a] Chem
dilut:

Table 2 ^{39}K MAS NMR results [19]

Compound	δ, ppm[a]	$\Delta\nu_{1/2}$, Hz
$K^+(15C5)_2 \cdot K^-$	-105(1)	70
$Rb^+(15C5)_2 \cdot K^{-}$[b]	-105(2)	120
$Cs^+(15C5)_2 \cdot K^-$	-105(5)	220
KRb18C6[b]	no signal	
$Cs^+(18C6)_2 \cdot K^-$	-115(10)	150
$K^+C222 \cdot Rb^-$	no signal	

[a]Chemical shifts are referenced to K^+(aq) at infinite dilution. Uncertainty of the last digit given in parentheses.
[b]Probably contain K^- and Rb^- as indicated by rubidium XANES.

Table 3 ^{87}Rb MAS NMR results [19]

Compound	δ, ppm[a]	$\Delta\nu_{1/2}$, Hz
$KRb(15C5)_2$	-191(1)	370(30)
$Rb^+(15C5)_2 \cdot Rb^-$	-191(1)	460(30)
$Cs^+(15C5)_2 \cdot Rb^-$	-189(2)	490(30)
$Cs^+(18C6)_2 \cdot Rb^-$	-194(1)	650(30)
KRb18C6	no signal	

[a]Chemical shifts are referenced to Rb^+(aq) at infinite dilution. Uncertainty of the last digit given in parentheses.

Table 4 ^{133}Cs MAS NMR results [18]

	42.24 MHz		65.61 MHz	
	δ^a, ppm	$\Delta\nu_{1/2}$, Hz	δ^a, ppm	$\Delta\nu_{1/2}$, Hz
0.7 M CsI(aq)	-23	30	-23	90
CsSCN	+190	190	---	---
CsCl	+232	125	---	---
CsBr	+264	---	---	---
CsI	+284	420	---	---
Cs^+TPB^-	---	---	---	---
$Cs^+18C6 \cdot SCN^-$	+73	100	---	---
$Cs^+18C6 \cdot I^-$ [b]	+171	280	179	700
$Cs^+(18C6)_2 \cdot SCN^-$	-59	70	---	---
$Cs^+(18C6)_2 \cdot I^-$	-59	47	-59	80
$Cs^+(18C6)_2 \cdot TPB^-$	-43	80	-47	200
$Cs^+C222 \cdot SCN^-$ [c]	+50, +275	210, 420	---	---
$Cs^+C222 \cdot SCN^-$ [d]	+238	140	238	133

Table 4 continues.

Table 4 continued.

	42.24 MHz		65.61 MHz	
	δ^a, ppm	$\Delta\nu_{1/2}$, Hz	δ^a, ppm	$\Delta\nu_{1/2}$, Hz
$Cs^+C222 \cdot Cl^{-d}$	+167	860	--	--
$Cs^+C222 \cdot I^{-d}$	+232, +254	63, 135	--	--
$Cs^+(18C6)_2 \cdot e^-$	+81	135	+89	235
$Cs^+(18C6)_2 \cdot Na^-$	-61	40	-62	160
$Cs^+(18C6)_2 \cdot K^-$	-58	85	-58	188
$Cs^+(18C6)_2 \cdot Rb^-$	-57	115	-57	65
$\underline{Cs}^+(18C6)_2 \cdot Cs^-$	-61	175	-49, -40	168, 300
$Cs^+(18C6)_2 \cdot \underline{Cs}^-$	-228	350	-230	435
$Cs^+C222 \cdot e^-$	+138, +238	320, 140	+134, +240	500, 350

[a] Referenced to infinitely diluted Cs^+(aq).
[b] Triplet peak.
[c] Sample prepared according to the directions of Weiss et al. [20]
[d] Sample prepared by solvent evaporation from a methanol solution.

prop

elec

inte

elec

trap

resu

rela

envi

the

pat

NMR

lin

met

and

the

Ohy

bee

Li^+

operties depend on the communication between the trapped
ectrons. At this time it is not clear whether these
teractions depend primarily on the distance between the
ectrons or on the presence of channels that interconnect
apped electron sites in the structure.

In this thesis research, the theory and experimental
sults of single crystal NMR will be described to obtain
latively accurate parameters associated with the local
vironment of the nuclei of interest. With the background of
e position of NMR lines in single crystals, the powder
tterns of static and variable angle sample spinning (VAS)
2 will be described. In order to understand the NMR
eshapes of alkalides and electrides, complexed alkali
al salts have been used as models to investigate static
magic angle sample spinning (MAS) NMR techniques. Also,
modification of the Oguchi theory of magnetism by
a-Nishiguchi (based on the Heisenberg Hamiltonian) has
applied to explain the magnetic susceptibility of
211·e$^-$.

gen

wid

by

int

che

ani

to

how

a

obt

sta

suc

2-c

anc

ter

nuc

in

to

CHAPTER II

THEORY OF SOLID STATE NMR

It is well known that the NMR spectrum of a liquid
nerally consists of numerous sharp lines, typically with
dths of less than a few Hz. These lines are characterized
the isotropic chemical shifts and scalar spin-spin
teractions. All possible anisotropic interactions, namely,
emical shift anisotropy, dipole-dipole interactions, and
isotropic quadrupolar interactions are averaged to zero due
the rapid isotropic molecular motion. In the solid state,
ever, all these anisotropic interactions are retained and
more or less bell shaped, structureless line may be
ained. In this sense, the goal of high resolution solid
te NMR can be described as utilizing or designing methods,
as decoupling, magic angle sample spinning, and
mensional NMR, to observe the interactions to be studied
to suppress or separate unwanted interactions.

The nuclear spin Hamiltonian consists of a number of
that describe physically different interactions of the
ar spins. Some of these terms are related to the
action of the nuclear spin with the apparatus, and some
e physical properties of the sample. These terms

desc

ther

inte

high

II.

whe

$\mathcal{H}_{in}$

Zee

mag

ext

pro

$B_1($

can

nuc

sun

$\mathcal{H} =$

wh

$\mathcal{H}_{\bullet,}$

$\mathcal{H}_{i}$

scribe the shifts and broadening of the NMR lines. It is
erefore necessary to understand basic nuclear spin
teractions in solids to design experiments that achieve
gh resolution solid state NMR.

. A. Nuclear Spin Interactions in Solids

In this work most experiments have been done in a regime
ere the magnitude of $\mathcal{H}_0$ and $\mathcal{H}_1$ is much larger than that of
$_t$ (not always $\mathcal{H}_1 > \mathcal{H}_Q$). The terms $\mathcal{H}_0$ and $\mathcal{H}_1$ represent the
eman interactions with the external static and dynamic
gnetic fields, $\mathbf{B}_0$ and $\mathbf{B}_1(t)$, respectively. The resulting
ternal Hamiltonian, $\mathcal{H}_{ext}$, depends, apart from nuclear
operties, only on external parameters (external fields $\mathbf{B}_0$,
(t)), which are under the control of the experimenter. One
use this control to distinguish interactions between
lear spins and external fields and internal fields. In
mary then:

$$\mathcal{H}_{int} + \mathcal{H}_{ext} \tag{2.1}$$

e

$$= \mathcal{H}_0 + \mathcal{H}_1.$$

The nuclear spin Hamiltonian $\mathcal{H}_{int}$ may be written as:

$$\mathcal{H}_{II} + \mathcal{H}_{SS} + \mathcal{H}_{IS} + \mathcal{H}_Q + \mathcal{H}_{SH} + \mathcal{H}_{SR} + \mathcal{H}_L \tag{2.2}$$

wher

indi

spi

bot

cas

and

(ch

is

all

all

fre

int

ter

vec

χ :

ma

χ_0

χ_1

wh

ere $\mathscr{H}_{II}$, $\mathscr{H}_{SS}$, and $\mathscr{H}_{IS}$ represent the direct as well as

direct interactions among I spins, S spins and between I

ins and S spins, respectively. Note that one can consider

th the homonuclear case ($\omega_I = \omega_S$) and the heteronuclear

se ($\omega_I \neq \omega_S$). $\mathscr{H}_Q$ is the quadrupolar Hamiltonian of the I

d S spins, while $\mathscr{H}_{SH}$ includes all shift interactions

nemical shift and Knight shift) of the I and S spins, $\mathscr{H}_{SR}$

the spin rotation interaction Hamiltonian and $\mathscr{H}_L$ contains

l spin lattice interactions. It is convenient to express

l Hamiltonians in tensorial form and to use angular

equency units throughout. One can assume that all spin

eractions can be expressed by second rank Cartesian

sors. For example, if one lets **I** and **S** represent general

tors and A a general Cartesian tensor, one has

$$\mathbf{I} \cdot \mathbf{A} \cdot \mathbf{S} = (I_x, \ I_y, \ I_z) \begin{bmatrix} A_{xx} & A_{xy} & A_{xz} \\ A_{yx} & A_{yy} & A_{yz} \\ A_{zx} & A_{zy} & A_{zz} \end{bmatrix} \begin{bmatrix} S_x \\ S_y \\ S_z \end{bmatrix} \qquad (2.3)$$

The Zeeman interaction of spin I with the external field

also be written in this form as:

$$= \mathbf{I} \cdot \mathbf{Z} \cdot \mathbf{B}_0 \qquad (2.4)$$

$$= \mathbf{I} \cdot \mathbf{Z} \cdot \mathbf{B}_1(t) \qquad (2.5)$$

re

B$_0$

and

1 =

The

pre

tra

rad

ru.

li

su

χ_1

Th

(d

ir

th

tr

a

D

$_0 = (B_x, B_y, B_z)$, $\mathbf{B}_1(t) = 2(B_{1x}(t), B_{1y}(t), B_{1z}(t)) \cos\omega t$

d $Z = -\gamma_I 1$ with the unit matrix

$$= \begin{bmatrix} 1 & 0 & 0 \\ 0 & 1 & 0 \\ 0 & 0 & 1 \end{bmatrix}.$$

e $2I + 1$ Zeeman energy levels are separated by ω_L in the resence of the external magnetic field $\mathbf{B}_0$. Magnetic dipole ansitions between these levels can be induced by a dio-frequency field $\mathbf{B}_1$ transverse to $\mathbf{B}_0$. The selection les are $\Delta m = \pm 1$; hence there is a single magnetic resonance ne at the Larmor frequency, ω_L, comprised of $2I$ perimposed components.

One can express the coupling between I and S spins as

$$_S = \mathbf{I} \cdot \mathbf{D}_{IS} \cdot \mathbf{S} \tag{2.6}$$

e tensor $\mathbf{D}_{IS}$ covers both direct spin-spin interactions ipolar interaction) as well as indirect spin-spin teractions (scalar coupling). Although not generally so, in e case of the dipolar interaction, D is symmetric and aceless. In this case $D_{\alpha\beta}$ (α, β = x, y, z) may be written

$$= \frac{\gamma_I \gamma_S}{R^3} \left(\delta_{\alpha\beta} - 3 \frac{\hat{e}_\alpha \cdot \hat{e}_\beta}{R^2} \right) \tag{2.7}$$

re R is the distance between the spins and $\delta_{\alpha\beta}$ is the

Kron

dege

$\ell_{Q} =$

wher

in

elec

sec

the

Sin

the

gra

ten

and

not

fro

per

des

nuc

sit

int

dis

sat

int

co

ecker delta.

The quadrupolar Hamiltonian $\mathcal{H}_Q$ can be considered as a

nerate case of $\mathcal{H}_{IS}$ with

$$\mathbf{I} \cdot \mathbf{Q} \cdot \mathbf{I} \qquad\qquad (2.8)$$

e $Q = [eQ/2I(2I-1)\hbar] \cdot V$ with $V = \{V_{\alpha\beta}\}$ (α, β = x, y, z)

hich Q is the nuclear quadrupole moment and V is the

tric field gradient tensor. One may interpret V as the

nd derivative of the potential due to charges external to

nucleus, i.e. $\nabla^2 V = 0$. Hence, the trace of V vanishes.

e the quadrupolar interaction is the interaction between

nuclear electric quadrupole moment and electric field

ient around the nucleus. The electric field gradient

r V is very sensitive to the electronic configuration

oordination of the surrounding atoms. It is important to

that the quadrupolar interaction vanishes if V arises

a spherically symmetric charge distribution or if it has

ct cubic symmetry. When imperfections or impurities

oy the local symmetry at the site of each resonant

us, electric field gradients which vary from site to

arise. The NMR line is then broadened by quadrupolar

actions, the line shape being determined by the

ibution of the electric field gradient. Only the

lites are broadened in first order by quadrupolar

actions. If the second order broadening of the central

nent is large, indicating a large distribution of field

gra

cou

the

ℓ_s

The

is

be

S :

wh

ar

pr

el

nc

th

th

if

re

c

p

e

dients, the satellites may be too broad to be observed.

The shift Hamiltonian of spin I can be given as the pling of the spin I with the static magnetic field $\mathbf{B}_0$ via shift tensor S: '

$$\mathbf{I} \cdot \mathbf{S} \cdot \mathbf{B}_0 . \tag{2.9}$$

tensor is no longer the unit matrix, since the coupling established via the electronic surroundings rather than g direct. In the case of the chemical shift,

$$\gamma_I \begin{pmatrix} \delta_{xx} & \delta_{xy} & \delta_{xz} \\ \delta_{yx} & \delta_{yy} & \delta_{yz} \\ \delta_{zx} & \delta_{zy} & \delta_{zz} \end{pmatrix} \tag{2.10}$$

e S is the chemical shift tensor and $\delta_{\alpha\beta}(\alpha, \beta = x, y, z)$ the elements of the chemical shift tensor. The dot uct $\mathbf{S} \cdot \mathbf{B}_0$ is the magnetic field induced by the surrounding trons at the site of the spin I. In general S has a anishing trace and is not necessarily symmetric. However antisymmetric components of the tensor S contribute to chemical shift only in second order and can usually be red. Like the quadrupolar effect, this interaction ects the electronic environment around the nuclei.

The spin rotation interaction $\mathcal{H}_{SR}$, which represents the ling of the nuclear spin I with the magnetic moment uced by the angular momentum $\mathbf{J}$ of the molecule, can be essed as

$\mathcal{H}_{SR}$

The

com

wit

int

sol

lat

of

in

ter

be

ro

II

ex

pr

to

is

Eu

X_{t}

ma

$$= \mathbf{I} \cdot \mathbf{C} \cdot \mathbf{J} . \qquad (2.11)$$

spin rotation interaction tensor C has some features in
mon with the shift tensor S, since both are associated
th the motion of the electrons, whether by $\mathbf{B}_0$ or by $\mathbf{J}$. This
eraction, however, is weak and may often be neglected in
id state NMR. It plays a somewhat important role in spin
tice relaxation of liquid samples.

The spin lattice interaction $\mathscr{H}_L$ involves the scattering
a phonon by the spin in solids.

These internal spin interactions can be expressed either
terms of Cartesian tensors as done above or by spherical
sors. The advantage of the spherical tensor notation will
fully exploited in following sections, when unitary
ation transformations have to be performed.

B. Transformation Properties of Spin Interactions in Real
   Space and a Single Crystal NMR Line

In the previous section, the spin interactions have been
ressed by second rank tensors. The transformation
perties of those tensors will be discussed here in order
xpress the interactions in different reference frames. It
necessary to define these reference frames and the
rian angles. The Zeeman axis system will be expressed by
Y_H, and Z_H. Of course, Z_H is parallel to the static
etic field direction and Y_H is in the plane of Z_H and the

gon

is

coi

cry

of

ax:

the

Z_g

de

re

sy

la

an

Eu

(

to

ca

t]

x

t

t

s

r

e

t

e

oniometer Z_g axis (or spinning axis). The goniometer X_g axis

s in the plane of Z_H and Z_g. Hence, X_H and Y_g are

oincident. These axis systems are shown in Figure 2. The

rystal axis system is expressed by x, y and z, at least one

f which is customarily coincident with a crystallographic

xis. At the beginning of an experiment one can often set

ese axes x, y, and z to be coincident with the X_g, Y_g, and

, respectively. The principal axes, X, Y, and Z, will be

fined later. One set of Eulerian angles, α, β, and γ,

lates the principal axis system to the goniometer axis

stem. Transformation from the goniometer frame to the

boratory frame can be described by another set of Eulerian

gles, ϕ, θ, and ψ. Here the sign conventions and the

lerian angle definition of Rose [26] are adopted.

A right-handed frame of axes is chosen and a positive

r counterclockwise when viewed down the positive axis

ward the origin) rotation is defined as one which would

rry a right-handed screw in the positive direction along

at axis. Thus a rotation about the z-axis which carries the

axis into the original position of the y-axis is considered

be positive. Suppose one wishes to make a rotational

ansformation from the axis system x, y, z to a new axis

stem x''', y''', z'''. The axes x', y', z' (after the first

ation) are produced by rotation about the z-axis through

angle α (or ϕ) counterclockwise relative to x, y, z. Note

at z' and z are coincident. Then the next rotation is made

out the y'-axis counterclockwise through an angle β (or θ).
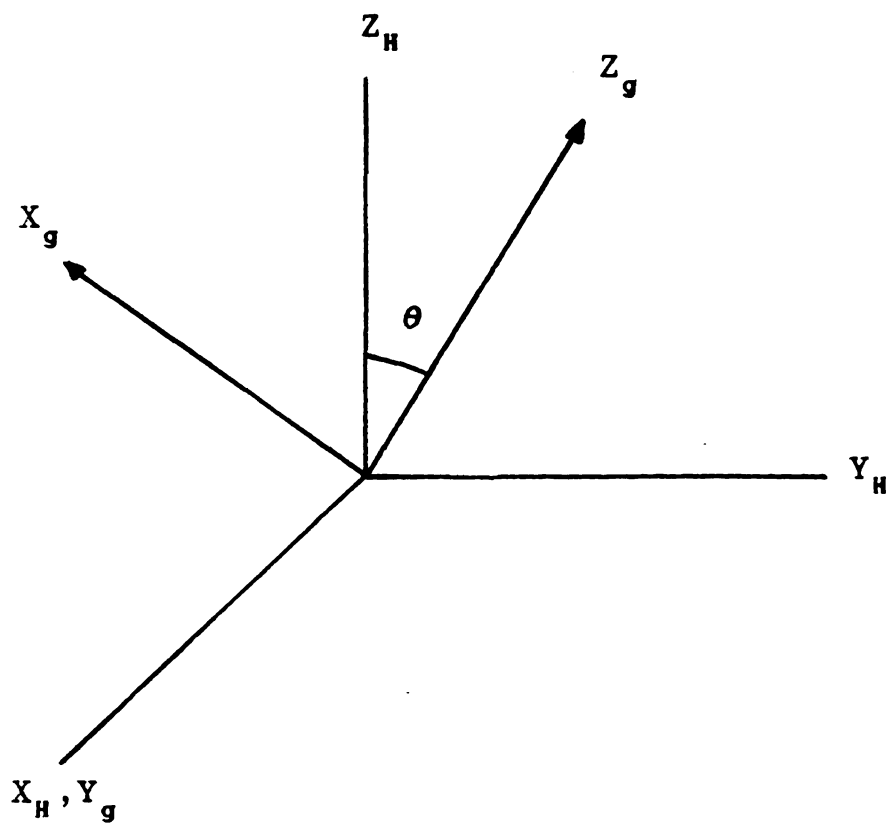
Figu

re 2 Relation between the goniometer axes, X_g, Y_g, Z_g and the laboratory axes, X_H, Y_H, Z_H.

The

is

yie

the

wel

bet

sec

A'

sys

to

a

R'

No

R(

A'

wh

A'

a

new axes become x'', y'', z''. The third and final rotation
through an angle γ (or ψ) counterclockwise about z'',
lding the new x''', y''', z'''-axis system. In Figure 3,
se transformations are shown.

Suppose a single crystal is mounted on a goniometer in a
l defined fashion with Eulerian angles, α, β, and γ
ween X, Y, Z and X_g, Y_g, Z_g as noted above. Let A be a
ond rank tensor expressed in the principal axis system and
be the same tensor expressed in the goniometer axis
tem. Any vector $\mathbb{R}'$ in the X_g, Y_g, Z_g axis system is related
the corresponding vector $\mathbb{R}$ in the principal axis system by
itary rotation $R(\alpha,\beta,\gamma)$ i.e.

$$= R(\alpha,\beta,\gamma)\mathbb{R} \tag{2.12}$$

A$'$ and A are related by the unitary transformation matrix
$\beta,\gamma)$ through:

$$R(\alpha,\beta,\gamma) \ A \ R^{-1}(\alpha,\beta,\gamma), \tag{2.13}$$

e

$$\begin{bmatrix} A_{xx} & A_{xy} & A_{xz} \\ A_{xy} & A_{yy} & A_{yz} \\ A_{zx} & A_{zy} & A_{zz} \end{bmatrix}, \quad A = \begin{bmatrix} A_{XX} & 0 & 0 \\ 0 & A_{YY} & 0 \\ 0 & 0 & A_{ZZ} \end{bmatrix},$$
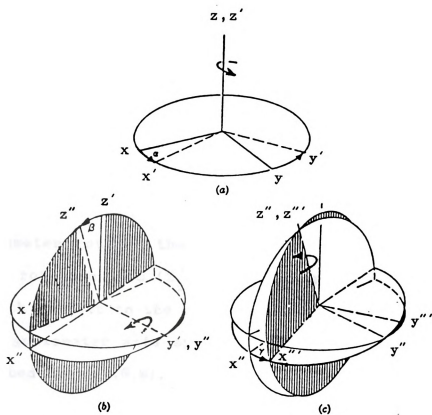
Figure 3 Rotational transformations from the axis system, x, y, z to a new axis system, x′′′, y′′′, z′′′ through Eulerian angles, α, β, γ.

$R(\alpha,\beta,$

$$= \begin{pmatrix} c \\ -c \\ c \end{pmatrix}$$

Then

matrix

$A'_{ij} =$

The g

about

$= \pi/2$

from

be de

$R'(\phi,$

The

inter

$A'' =$

or

$A''_{mn} =$

$,\beta,\gamma) = \{r_{ij}\}$

$$\begin{bmatrix} \cos\alpha\cos\beta\cos\gamma-\sin\alpha\sin\gamma & \sin\alpha\cos\beta\cos\gamma+\cos\alpha\sin\gamma & -\sin\beta\cos\gamma \\ -\cos\alpha\cos\beta\sin\gamma-\sin\alpha\cos\gamma & -\sin\alpha\cos\beta\sin\gamma+\cos\alpha\cos\gamma & \sin\beta\sin\gamma \\ \cos\alpha\sin\beta & \sin\alpha\sin\beta & \cos\beta \end{bmatrix}$$

n the Cartesian tensor A′ can be easily expressed by

rix multiplication as

$$_{j} = \sum_{kl} A_{kl}\ r_{ik}\ r_{jl}.\tag{2.14}$$

goniometer rotates the crystal clockwise by an angle ϕ

ut its rotation axis (Z_g), which has an angle θ (usually θ

/2) with respect to the magnetic field. The transformation

n the goniometer axis system to the laboratory frame may

lescribed by R′(ϕ,θ,ψ):

$$,\theta,\psi) = R'_{g\hat{z}}(\psi)\ R'_{g\hat{y}}(\theta)\ R'_{g\hat{z}}(\phi).\tag{2.15}$$

second rank Cartesian tensor representing the spin

:ractions can then be expressed by

$$R'A'R'^{-1}\tag{2.16}$$

$$= \sum_{kl} A'_{kl}\ r'_{mk}\ r'_{nl}\ =\ \sum_{ijkl} A_{ij}\ r'_{mk}\ r'_{nl}\ r_{mi}\ r_{1j}$$

wher

and

of t

firs

inte

A''_{zz}

whe

C_0

C_1

S_1

C_2

S_2

In

go

te

de

is

π

A'

r'_{mk}, r'_{n1}, r'_{mi}, and r_{1j} are the matrix elements of R'

respectively. In most cases only the Z-component (A''_{zz})

e tensor A'' is measured in an experiment, leading to the

order expression for chemical shift and quadrupolar

actions [27]:

$$C_0 + C_1\cos\phi + S_1\sin\phi + C_2\cos2\phi + S_2\sin2\phi \qquad (2.17)$$

$1/2\ (A'_{xx} + A'_{yy})(r'^2_{zx} + r'^2_{zy}) + A'_{zz}r'^2_{zz}$

$(A'_{xz} + A'_{zx})r'_{zx}r'_{zz} + (A'_{yz} + A'_{zy})r'_{zy}r'_{zz}$

$(A'_{yz} + A'_{zy})r'_{zx}r'_{zz} - (A'_{xz} + A'_{zx})r'_{zy}r'_{zz}$

$(A'_{xy} + A'_{yx})r'_{zx}r'_{zy} + 1/2\ (A'_{xx} - A'_{yy})(r'^2_{zx} - r'^2_{zy})$

$1/2\ (A'_{xy} + A'_{yx})(r'^2_{zx} - r'^2_{zy}) + (A'_{yy} - A'_{xx})r'_{zx}r'_{zy}.$

neral A''_{zz} is not invariant under a π rotation. If the

meter axis does not concide with a principal axis of the

r, five of six possible tensor elements can be

mined from one orientation plot. If the goniometer axis

thogonal to the magnetic field, A''_{zz} has a periodicity of

C_1 and S_1 vanish, which results in [27,28]

$$C_0 + C_2\cos2\phi + S_2\sin2\phi \qquad (2.18)$$

$= 1/2$ (

Si

quadrup

$$\omega_{\blacksquare}^{Q(2)} =$$

$4(c_2(\blacksquare)$

$(c_y^2 - c_z^2$

$+ [(c_2($

$\times \sin 4$

where

$a_x = 1/$

$b_x = 1/$

$c_x = 1/$

$c_y = 1,$

$c_z = 1,$

$c_1(\blacksquare)$

$c_2(\blacksquare)$

$2 (A'_{xx} + A'_{yy}) + 1/2 (A'_{xx} - A'_{yy})\cos2\phi + 1/2 (A'_{xy} + A'_{yx})\sin2\phi.$

Similarly one can obtain the second order terms for the rupolar Hamiltonian [28]:

$) = -(\omega_Q^2/144\omega_L)\Big[[18c_2(m)a_x^2 + (c_2(m) - 4c_1(m))(b_x^2 + c_x^2) +$

$(m) - c_1(m))(c_y^2 + c_z^2) + [-12c_2(m)a_xb_x + 4(c_2(m) + c_1(m)) \times$

$c_z^2)]\cos2\phi + [-12c_2(m)a_xc_x + 8(c_2(m) + c_1(m))c_yc_z]\sin2\phi$

$c_2(m) + 4c_1(m))(b_x^2 - c_x^2)]\cos4\phi + 2(c_2(m) + 4c_1(m))b_xc_x$

$n4\phi\Big]$

$$(2.19)$$

e

$1/2 (A'_{xx} + A'_{yy})$

$1/2 (A'_{xx} - A'_{yy})$

$1/2 (A'_{yz} + A'_{zy})$

$1/2 (A'_{zx} + A'_{xz})$

$1/2 (A'_{xy} + A'_{yx})$

$) = 24m(m-1) - 4I(I + 1) + 9$

$) = 6m(m-1) - 2I(I + 1) + 3$

$\omega_Q = \overline{2}$

if Z_g

freque

$\omega_\blacksquare = \omega$

where

an ori

of si

matrix

can th

In add

diagor

unders

irredu

descr

orien

geome

compo

secon

const

$A = A$

A^0 is

$$_q = \frac{3e^2qQ}{2I(2I - 1)\hbar} = \frac{3\pi\chi}{I(2I - 1)} \quad , \quad (\chi = \frac{e^2qQ}{h})$$

f Z_g is perpendicular to the field direction. Then, the requency of the NMR line of a single crystal is given by

$$_n = \omega_L(1 + A''^{CSA}_{zz}) - (m - \frac{1}{2})\omega_Q A''^{Q}_{zz} + \omega^{Q(2)}_m \qquad (2.20)$$

here m indicates a transition between m and m − 1. Fitting n orientation plot with these equations gives at least three f six tensor elements. Therefore one can obtain all six atrix elements from two or more rotation plots. The matrix an then be diagonalized to yield three principal components. n addition, three Eulerian angles can be calculated from the iagonalization matrix by comparison with $R(\alpha, \beta, \gamma)$.

Although Cartesian tensors lead to a direct physical nderstanding in terms of direction cosines, the use of the rreducible tensor operator is a very powerful way to escribe the rotation transformation since the change in the rientation of the crystal is the simple rotation of a eometrical factor without changing its magnitude. The nine omponents A_{ij} (i, j = x, y, z) of a Cartesian tensor of econd rank can be decomposed into their irreducible onstituents with respect to the full 3d rotation group, O_3^+:

$$= A^0 + A^1 + A^2. \qquad (2.21)$$

is the isotropic constituent

$A^0 = 1/$

R is a

tracele

$A^1_{ij} =$

with tl

(2.21)

A^2_{ij}

with

delta.

transf

zero,

W

$\dot{e}_{10} =$

the c

terms

$A_{1q} =$

or

$A_{10} =$

$$= 1/3 \ Tr\{ \ R \ \}\cdot 1 = R\cdot 1. \tag{2.22}$$

is a scalar and 1 is the unit dyadic. The term A^1 is a
aceless antisymmetric tensor of first rank:

$$= 1/2 \ (A_{ij} - A_{ji}) \tag{2.23}$$

th three independent components. The third term in Equation
21) is the traceless symmetric second rank tensor A^2:

$$= 1/2 \ (A_{ij} + A_{ji}) - R\delta_{ij} \tag{2.24}$$

h five independent components, where δ_{ij} is Kronecker
ta. The components of the three quantities A^0, A^1, and A^2
nsform in the same way as the spherical harmonics of order
o, one, and two, respectively.

With the spherical unit vectors

$$= \hat{e}_z \ ; \ \hat{e}_{1\pm1} = \mp 1/\sqrt{2}(\hat{e}_x \pm i\hat{e}_y) \tag{2.25}$$

components of a first rank irreducible tensor A_{1q} in
ns of the Cartesian components (A_x, A_y, A_z) are given by

$$= \hat{e}_{1q}\cdot A = \hat{e}_{1q}\cdot(A_x\hat{e}_x + A_y\hat{e}_y + A_z\hat{e}_z) \tag{2.26}$$

$$= A_z \ ; \ A_{1\pm1} = -1/\sqrt{2}(A_x - iA_y).$$

To def

Cartes.

obtaine

rule f

[29]:

$$\dot{e}_{kq} = [$$

$$= (2k$$

where $\left[\right.$

The ir

Cartes

two ir

$$A_{kq} = \dot{e}$$

$$= (2k+$$

where

$$A = \sum_{ij}$$

as

define the irreducible tensor components in terms of the

rtesian components, first the appropriate unit vectors are

tained. The spherical unit vectors are constructed from the

le for the product of two irreducible tensor operators

9]:

$$= [e^1 \times e^1]_{kq}$$

$$(2k + 1)^{1/2} \sum_{q_1 q_2} (-1)^{-q} \begin{bmatrix} 1 & 1 & k \\ q_1 & q_2 & -q \end{bmatrix} \hat{e}_{1q_1} \cdot \hat{e}_{1q_2} \qquad (k = 0, 1, 2),$$

$$(2.27)$$

re $\begin{bmatrix} 1 & 1 & k \\ q_1 & -q_2 & q \end{bmatrix}$ is the Wigner 3-j symbol [26].

e irreducible spherical tensor components in terms of the

rtesian tensor components are obtained as the product of

irreducible tensor operators:

$$= \hat{e}_{kq} \cdot A$$

$$2k+1)^{1/2} \sum_{q_1 q_2} (-1)^q \begin{bmatrix} 1 & 1 & k \\ q_1 & q_2 & -q \end{bmatrix} A_{1q_1} A_{1q_2},$$

$$(2.28)$$

re

$$\sum_{ij} \hat{e}_i \cdot \hat{e}_j A_{ij} \qquad (i, j = x, y, z)$$

$A_{00} = -$

$A_{10} = -$

$A_{1\pm1} =$

$A_{20} = 1$

$A_{2\pm1} =$

$A_{2\pm2} =$

In exp

-, an

additi

T

produc

the c

Hamilt

$\ell = \sum_{k=1}^{}$

Here

inter

invol

compo

param

types

$$_0 = -1/\sqrt{3} \ (A_{xx} + A_{yy} + A_{zz})$$

$$_0 = -i/\sqrt{2} \ (A_{xy} - A_{yx})$$

$$_{\pm 1} = -1/2 \ [A_{zx} - A_{xz} \pm i(A_{zy} - A_{yz})]$$

$$_{} = 1/\sqrt{6} \ [3A_{zz} - (A_{xx} + A_{yy} + A_{zz})]$$

$$_{\pm 1} = \mp 1/2 \ [A_{xz} + A_{zx} \pm i(A_{yz} + A_{zy})]$$

$$_{\pm 2} = 1/2 \ [A_{xx} - A_{yy} \pm i(A_{xy} + A_{yx})].$$

expressing the components of a tensor, the subscripts, +,

and ± belong to the second subscript and do not mean

ition or subtraction.

The Hamiltonians are usually expressed as scalar

ducts of corresponding irreducible tensors A^k and T^k with

components A_{kq} and T_{kq}, respectively, leading to a

iltonian of the form

$$\sum_{=-q}^{+q} (-1)^q A_{kq}(t) T_{k-q}(t') . \tag{2.29}$$

A_{kq} contains physical constants appropriate to the

eractions including the magnetogyric ratios of the species

olved. A_{kq} and T_{k-q} are irreducible spherical tensor

ponents of the tensor of rank k, which express the lattice

ameters and spin variables respectively. Two different

es of time dependences are involved in Equation (2.29).

The or

static

$A_{kq}(t)$

what

domina

rotat:

time

indepe

$$\chi = \sum_{k=}$$

Table

in te

omit

rank,

0, 1

inter

k =

tensc

antis

contr

whicl

elem

prin

is c

axis

The one imposed on $T_{k-q}(t')$ stems from spin precession in the static magnetic field $\mathbf{B}_0$, whereas the time dependence of $A_{kq}(t)$ results from the sample spinning. In nearly all of what follows the Zeeman interaction will be overwhelmingly dominant. Tensor T can be transformed to a coordinate system rotating (in spin space) at a Larmor frequency ω_L to remove time dependences in T_{k-q}. For static NMR A_{kq} is time independent; the Hamiltonian can then be rewritten as

$$\mathcal{H} = \sum_{k=-q}^{+q} (-1)^q A_{kq} T_{k-q}. \qquad (2.30)$$

Tables 5 and 6 enable us to express all internal Hamiltonians in terms of irreducible tensor operators (A_{kq}, T_{k-q}). One may omit interactions requiring tensors of higher than second rank, e.g. magnetic octapole, electric hexadecapole, so k = 0, 1, 2 only. In the case of dipolar and quadrupolar interactions A_{00} and A_{1q} vanish, and only the five terms with = 2 will be nonzero. Chemical shift and Knight shift tensors, however, do have non-zero traces and, of course, antisymmetric parts in general, i.e. A_{00} and A_{1q} do contribute.

The principal axis system (X, Y, Z) is the frame in which the symmetric part (A_{2q}) is diagonal. The diagonal elements in the principal axis system (PAS) are called principal components, A_{XX}, A_{YY}, A_{ZZ}. The following convention is chosen to label the principal axes of one of the principal axis systems:

Table 5 C
       t

Interact

Chemical

Dipole-d

J coupli

Spin rot

Quadrupo

le 5 Connection between Cartesian tensors and spherical
tensors for spin interactions [27]

	Cartesian	Spherical tensor
eraction	$A_{\alpha\beta}(\alpha,\beta=x,y,z)$	A_{kq}
mical shift	$\gamma\delta_{\alpha\beta}$	$A_{00} = -1/\sqrt{3}\ (A_{xx}+A_{yy}+A_{zz})$
ole-dipole	$D_{\alpha\beta}$	$A_{10} = -i/\sqrt{2}\ (A_{xy}-A_{yx})$
oupling	$J_{\alpha\beta}$	$A_{1\pm1} = -1/2\ [A_{zx}-A_{xz}\pm i(A_{zy}-A_{yz})]$
n rotation	$C_{\alpha\beta}$	$A_{20} = 1/\sqrt{6}\ [3A_{zz}-(A_{xx}+A_{yy}+A_{zz})]$
drupole	$\dfrac{eQ}{2I(2I-1)\hbar}V_{\alpha\beta}$	$A_{2\pm1} = \mp1/2\ [A_{xx}-A_{yy}\pm i(A_{xy}+A_{yx})]$

Table 6 Spherical tensor representation of spin operators [27]

	Chemical shift	Dipole-dipole	J coupling	Spin rotation	Quadrupole
T_{00}	$-\dfrac{1}{\sqrt{3}}I_z B_0$	0	$-\dfrac{1}{\sqrt{3}}\mathbf{I}\cdot\mathbf{S}$	$-\dfrac{1}{\sqrt{3}}\mathbf{I}\cdot\mathbf{J}$	0
T_{10}	0	0	$\dfrac{-1}{2\sqrt{2}}(I^+S^- - I^-S^+)$	$\dfrac{-1}{2\sqrt{2}}(I^+S^- - I^-S^+)$	0
$T_{1\pm1}$	$-\dfrac{1}{2}I^\pm B_0$	0	$\dfrac{1}{2\sqrt{2}}(I_z S^\pm - I^\pm S_z)$	$\dfrac{1}{2\sqrt{2}}(I_z J^\pm - I^\pm J_z)$	0
T_{20}	$\sqrt{\dfrac{2}{3}}I_z B_0$	$\dfrac{1}{\sqrt{6}}(3I_z S_z - \mathbf{I}\cdot\mathbf{S})$	$\dfrac{1}{\sqrt{6}}(3I_z S_z - \mathbf{I}\cdot\mathbf{S})$	$\dfrac{1}{\sqrt{6}}(3I_z S_z - \mathbf{I}\cdot\mathbf{J})$	$\dfrac{1}{\sqrt{6}}(3I_z^2 - I(I+1))$
$T_{2\pm1}$	$\mp\dfrac{1}{2}I^\pm B_0$	$\mp\dfrac{1}{2}(I_z S^\pm + I^\pm S_z)$	$\mp\dfrac{1}{2}(I_z S^\pm + I^\pm S_z)$	$\mp\dfrac{1}{2}(I_z J^\pm + I^\pm J_z)$	$\mp\dfrac{1}{2}(I_z I^\pm + I^\pm I_z)$
$T_{2\pm2}$	0	$\dfrac{1}{2}I^\pm S^\pm$	$\dfrac{1}{2}I^\pm S^\pm$	$\dfrac{1}{2}I^\pm J^\pm$	$\dfrac{1}{2}I^\pm I^\pm$

$|A_{zz} -$

where

$A_{iso} =$

If the
angles

I
princi
$A_{iso},$

$\delta = A_z$

$\eta = (A$

Then
axis

$A_{00} =$

$A_{10} =$

$A_{1\pm1} =$

$A_{20} =$

$A_{2\pm1} =$

$$_{ZZ} - A_{iso}| \geq |A_{XX} - A_{iso}| \geq |A_{YY} - A_{iso}| \qquad (2.31)$$

ere

$$_{o} = 1/3 \ tr\{ \ A \ \} = 1/3 \ (A_{XX} + A_{YY} + A_{ZZ}).$$

the principal axis systems are noncoincident, Eulerian
les between one axis system and another must be defined.

It is often convenient to introduce instead of the three
ncipal components three new parameters, one of which is
$_{o}$, and the other two, δ, and η, are defined by

$$A_{ZZ} - A_{iso}, \qquad (2.32)$$

$$(A_{YY} - A_{XX})/(A_{ZZ} - A_{iso}) = (A_{YY} - A_{XX})/\delta. \qquad (2.33)$$

n the spherical tensor A can be expressed in the principal
s system as

$$= -\sqrt{3} \ A_{iso}$$

$$= 0$$

$$_{1} = 0$$

$$= \sqrt{3/2} \ \delta$$

$$_{1} = 0$$

$A_{2\pm2} = -$

Th

followi

$\omega_m = \omega_L$

$6/\omega_L$ ([

$\times [A_{2\pm2}^{\prime Q}$

where

A_{kq}^{CSA})

respec

in ter

conven

spheri

of ran

the ir

$A_{kq}^{\prime\prime} = R$

$A_{kp}^{\prime} =$

where

$D_{m'm}^{k}(0$

and

$$A_{2\pm2} = -1/2 \ \eta\delta. \tag{2.34}$$

The observed spectral frequency is determined by the following equation:

$$\omega_m = \omega_L (1 \ -1/\sqrt{3} \ A_{00}^{CSA} + \sqrt{2/3} \ A_{20}''^{CSA}) - (m - 1/2)\sqrt{6} \ A_{20}''^Q +$$

$$1/\omega_L \ ([24m(m - 1) - 4a + 9][A_{2\pm1}''^Q]^2 - [6m(m - 1) -4a + 3]$$

$$[A_{2\pm2}''^Q]^2) \tag{2.35}$$

here the quadrupolar and chemical shift terms ($A_{kq}''^Q$ and $A_{kq}''^{CSA}$) are correct through second order and first order, respectively. In order to express A_{kq}'' in the laboratory frame in terms of principal tensor components A_{kq} via A_{kq}', it is convenient to use a spherical representation. In this spherical representation the irreducible spherical tensor A^k of rank k with 2k + 1 components A_{kq} transforms according to the irreducible representation D^k of the rotation group

$$A_{kq}' = R(\phi,\theta,\psi)A_{kq}'R^{-1}(\phi,\theta,\psi) = \sum_{k=-k}^{+k} A_{kp}' D_{pq}^k(\phi,\theta,\psi) \tag{2.36}$$

$$A_{1p} = \sum A_{k1} D_{1p}^k(\alpha,\beta,\gamma), \tag{2.37}$$

here

$$D_{m'm}^k(\alpha,\beta,\gamma) = e^{-im'\alpha} \ d_{m'm}^k(\beta) \ e^{-im\gamma} \tag{2.38}$$

nd

$$d^k_{\blacksquare,\blacksquare}(\beta) = \sum_{\blacksquare}$$

$$\times \ ($$

The

obtained

Equation

$$A'_{20} = 1/2$$

$$A'_{2\pm1} = \pm \sqrt{}$$

$i\sin\beta\sin2$

$$A'_{2\pm2} = 1/2$$

$i2\cos\beta\sin$

and

$$A''_{20} = 1/2$$

$c\sin(\gamma +$

$$A''_{2\pm1} = \pm\sqrt{3}$$

$c\sin(\gamma +$

$i(-\cos\theta[b$

$e\cos2(\gamma$

$$,'_{\blacksquare}(\beta) = \sum_n (-1)^n \frac{[(k+m)!(k-m)!(k+m')!(k-m')]^{1/2}}{(k-m'-n)!(k+m-n)!(n+m'-m)!n!}$$

$$\times (\cos \frac{\beta}{2})^{2k+m-m'-2n} (-\sin \frac{\beta}{2})^{m'-m+2n} .$$

The geometrical parts A'_{kp} and A''_{kq} of the operator are
tained by inserting Equation (2.40) into Equation (2.36)and
uation (2.37):

$$_0 = 1/2 \sqrt{3/2} \, \delta \, (3\cos^2\beta - 1 - \eta\sin^2\beta\cos 2\alpha)$$

$$_{\pm 1} = \pm \sqrt{3/2} \, \delta \, (\sqrt{3/2}\sin\beta\cos\beta + \eta/\sqrt{6} \, [\sin\beta\cos\beta\cos 2\alpha \pm$$

$$in\beta\sin 2\alpha])e^{\mp\gamma i}$$

$$_{\pm 2} = 1/2 \sqrt{3/2} \, \delta \, (\sqrt{3/2}\sin^2\beta - \eta/\sqrt{6} \, [(1 + \cos^2\beta)\cos 2\alpha \mp$$

$$\cos\beta\sin 2\alpha])e^{\mp 2\gamma i} \qquad\qquad (2.39)$$

$$= 1/2 \sqrt{3/2} \, \delta \, (\, a(3\cos^2\theta - 1) - \sqrt{6}\sin\theta\cos\theta[b\cos(\gamma + \phi) +$$

$$in(\gamma + \phi)] + \sqrt{3/2}\sin^2\theta[d\cos 2(\gamma + \phi) + e\sin 2(\gamma + \phi)])$$

$$_{\pm 1} = \pm\sqrt{3/2} \, \delta \, \left[1/2 \sqrt{3/2}a\sin\theta\cos\theta - (2\sin^2\theta - 1)[b\cos(\gamma + \phi) +\right.$$

$$n(\gamma + \phi)] - \sin\theta\cos\theta[d\cos 2(\gamma + \phi) - e\sin 2(\gamma + \phi)] \mp$$

$$\cos\theta[b\sin(\gamma + \phi) - c\cos(\gamma + \phi)] + \sin\theta[d\sin 2(\gamma + \phi) +$$

$$\left. s2(\gamma + \phi)])\right]e^{\mp\psi i}$$

$A''_{z\pm 2} = \sqrt{}$

$c\sin(\gamma$

$\zeta(\sin\theta[$

$e\cos2(\gamma$

and

$a = 1/2$

$b = \sqrt{3}/$

$c = -\eta/$

$d = 1/$

$e = -\eta/$

The fi

produc

orient

of th

chemic

the ex

around

contra

intera

~ 1) a

spaced

$$_{\pm 2} = \sqrt{3/2}\ \delta\ \left[\sqrt{3/8}\ a\sin^2\theta + \sin\theta\cos\theta[b\cos(\gamma+\phi) + \right.$$

$$\sin(\gamma+\phi)] + 1/2\ (1+\cos^2\theta)[d\cos2(\gamma+\phi) - e\sin2(\gamma+\phi)] \pm$$

$$\sin\theta[b\sin(\gamma+\phi) - c\cos(\gamma+\phi)] + \cos\theta[d\sin2(\gamma+\phi) +$$

$$\left.\cos2(\gamma+\phi)]) \right]e^{\mp2\psi i} \tag{2.40}$$

d

$$= 1/2\ (3\cos^2\beta - 1 - \eta\sin^2\beta\cos2\alpha)$$

$$= \sqrt{3/2}\sin\beta\cos\beta + \eta/\sqrt{6}\ \sin\beta\cos\beta\cos2\alpha$$

$$= -\eta/\sqrt{6}\ \sin\beta\sin2\alpha$$

$$= 1/2\ [\sqrt{3/2}\sin^2\beta - \eta/\sqrt{6}\ (1+\cos^2\beta)\cos2\alpha]$$

$$= -\eta/\sqrt{6}\ \cos\beta\sin2\alpha.$$

e first order terms of the chemical shift interaction
oduce the same shift for all transitions at a certain
ientation of the crystal, while small second order effects
the chemical shift interaction can be ignored. The
emical shift in frequency units is directly proportional to
external magnetic field since the induced magnetic field
ound a nuclear spin depends on the applied field. In
trast the two resonance lines due to quadrupolar
eractions (transitions between m and m - 1 and between -(m
) and -m), which are called satellites, lie almost equally
ced on opposite sides of the center of gravity of each

pair. Th

II comp

between

1), and

units).

constant

the qu

satellit

first

multipli

remains

since tl

In seco

satelli

proport

satelli

quadrup

anisotr

fundame

program

researc

crystal

Th

informa

depende

second

powder

pair. The magnetic resonance line is therefore split into its 2I components. The relative intensity of the transition between m and m - 1 is very nearly equal to $I(I + 1) - m(m - 1)$, and the positions are field independent (in frequency units). The quadrupolar frequency ω_Q or quadrupolar coupling constant (QCC), χ, is a convenient measure of the strength of the quadrupolar interaction. The distance between two satellites has exactly the same orientation dependence as the first order chemical shift interaction except for the multiplicative constants. For half-integral spins there remains a central component that is unshifted in first order since the first order term contains the multiplier $(m - 1/2)$. In second order, however, the central component and all satellites are shifted and these shifts are inversely proportional to the field. It is important to note that the satellite center of gravity is unshifted by the first order quadrupolar interaction and is only shifted by chemical shift anisotropy and higher order quadrupolar interactions. These fundamental relationships are illustrated in Figure 4. The program XTAL (Appendix A), written as part of this thesis research, can calculate the resonance positions for a single crystal. The program is based on Equations (2.35) and (2.40).

The NMR spectrum of a powdered sample provides some information about anisotropic interactions since the angular dependences of the chemical shift, and the first order and second order quadrupolar interactions are different. The powder pattern results from the sum of all individual single

a)

b)

Figure 4

a)

$m = -3/2$

$-1/2$

$1/2$

$3/2$

$B_0 = 0$ $B_0 \neq 0$ $B_0 \neq 0$ $B_0 \neq 0$

$\chi = 0$ $\chi \neq 0$ $\chi \neq 0$

E_Z $E_Q^{(1)}$ $E_Q^{(2)}$

10

Zeeman transition

3   4   3

First Order Splitting

b)

3   4   3

Second Order Shift

ν_L
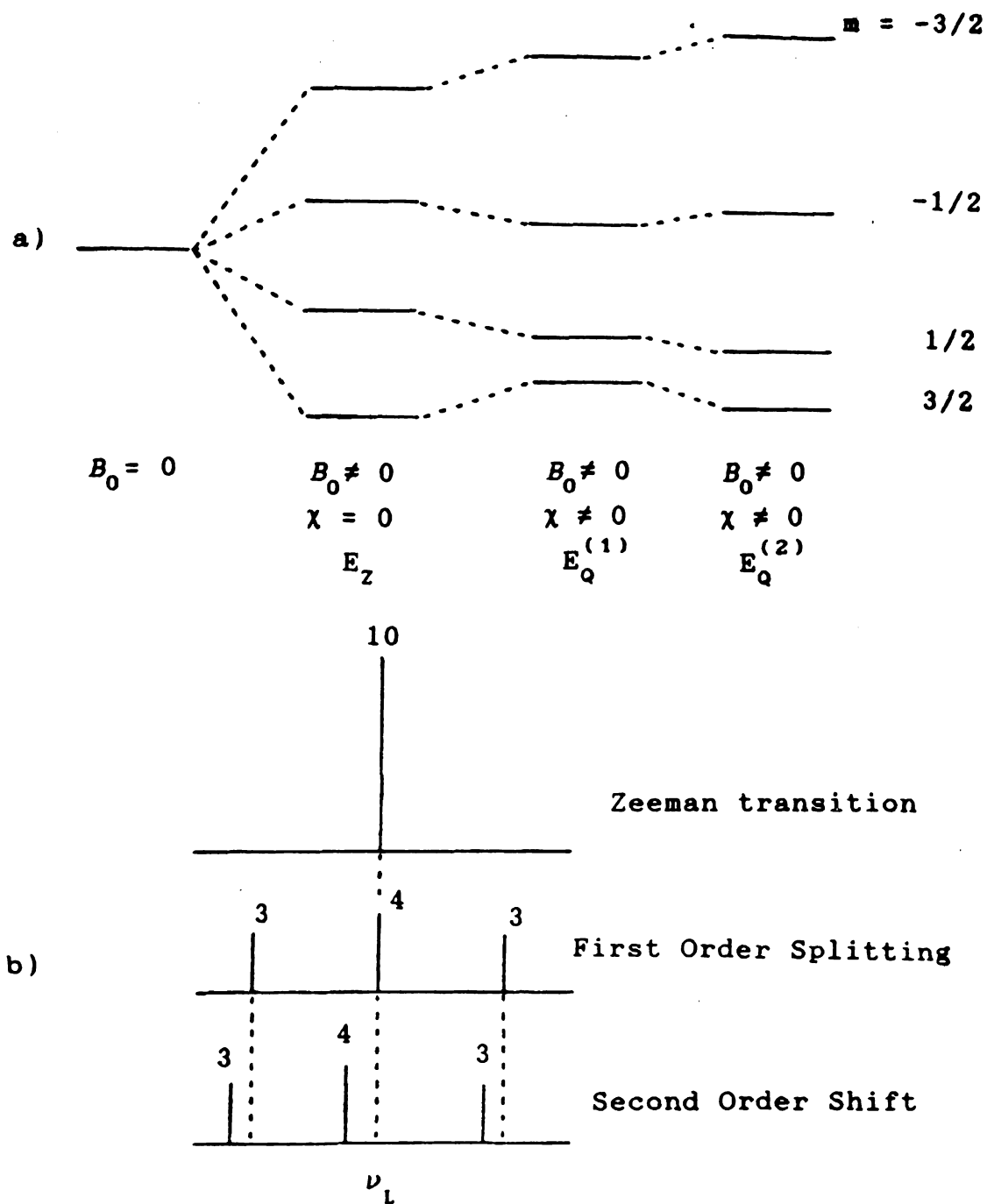
Figure 4 Quadrupolar splitting of the magnetic resonance of
spin 3/2 in a single crystal at an arbitrary
orientation.
a) Energy level diagrams;
b) Theoretical NMR spectra without linebroadening.
The numerals indicate relative intensities.

crystal lir

fields prov

quadrupolar

technique (

used to stu

II. C. Powd

The

polycrystal

continuous

the powder

all the nuc

line is ter

II. C. 1. S

In a

written as

between th

invariant

Thus the M

angle γ.

coordinate

system ar

respective

rystal lines. In addition the NMR spectra at different

ields provide more information about both chemical shift and

uadrupolar interactions. The variable angle sample spinning

echnique (including magic angle sample spinning) can also be

sed to study anisotropic interactions in solids.

I. C. Powder Patterns

The random distribution of orientations in a

olycrystalline or powdered specimen gives rise to a

ontinuous distribution of frequencies. The NMR spectrum of

he powder sample is a superposition of the NMR lines from

ll the nuclei of all the grains of the sample. The resulting

ine is termed a powder pattern.

. C. 1. Static Powder Patterns

In a single crystal, the resonance position can be

ritten as a function of a set of Eulerian angles (α, β, γ)

tween the field and the principal axis systems and is

variant under the sample rotation around the field axis.

us the NMR line position does not depend on the Eulerian

gle γ. In addition, it should be noted that the polar

ordinates ϕ and θ of Z_H with respect to the principal axis

stem are identical with the Eulerian angles α, and β,

spectively.

$\omega = \omega(\alpha, \beta)$

or

$\omega = \omega(\alpha, \mu)$,

The normal
number of
+ dω.

$P(\omega) = (4\pi$

where dΩ
resonance
Equation
principle,
condition
be readily
on both β
possible,
computer
transitio
Equation

$\omega_n = \omega_L \left(1 \right.$

$- (n - 1/$

$$\omega = \omega(\alpha,\beta) = \omega(\phi,\theta),$$

or

$$\omega = \omega(\alpha,\mu), \quad \mu = \cos\beta. \tag{2.41}$$

The normalized lineshape function $P(\omega)$ is proportional to the number of nuclei whose NMR lines fall into the interval $\omega \sim \omega + d\omega$.

$$P(\omega) = (4\pi)^{-1}d\omega^{-1}\int_{\omega}^{\omega+d\omega}d\Omega \tag{2.42}$$

where $d\Omega$ is an element of solid angle ($d\Omega = -d\mu d\alpha$). The resonance condition (Equation (2.35)) is inserted into Equation (2.42) and the powder pattern $P(\omega)$ can, at least in principle, be calculated. It turns out that if the resonance condition is only a function of μ and not of α, then $P(\omega)$ can be readily calculated in closed form. However, when ω depends on both μ and α, a closed form for $P(\omega)$ is not generally possible, and one must calculate the powder pattern with a computer [30]. The resonance peak position ω_m for a transition from level m to m $-$ 1 can be obtained from Equation (2.35):

$$\omega_m = \omega_L\left[1 + \delta_{iso}^{CSA} + \delta^{CSA}(3\cos^2\beta - 1 - \eta^{CSA}\sin^2\beta\cos2\alpha)\right]$$

$$- (m - 1/2)\omega_Q(3\cos^2\beta - 1 - \eta^Q\sin^2\beta\cos2\alpha) + (\omega_Q^2/12\omega_L)$$

$\times \left[[24m(m - 1 \right.$

$+ \eta^Q \cos 2\alpha + \frac{\eta}{3}$

$- [6m(m - 1)$

$|- \frac{3}{4} + \frac{\eta^{Q2}}{6} -$

where $a = I($
the principa
value of $\cos$
$\mu-\alpha$ space wi
powder patte
$+ d\omega$; every
correspondin
space.

Up to
interactions
considered.
theoretical
absorption F

$I(\omega) = \int_{-\infty}^{\infty} P(\omega'$

where $F(\omega$ -
due to di

$$\times \left[[24m(m-1) - 4a + 9][\frac{\eta^{Q2}}{6}(1 - \cos^2 2\alpha) + \cos^2\beta(\frac{3}{2} - \frac{\eta^{Q2}}{6} \right.$$

$$+ \eta^Q\cos2\alpha + \frac{\eta^{Q2}}{3}\cos^2 2\alpha) + \cos^4\beta(-\frac{3}{2} - \eta^Q\cos2\alpha - \frac{\eta^{Q2}}{6}\cos^2 2\alpha)]$$

$$- [6m(m-1) - 2a + 3][\frac{3}{8} - \frac{\eta^Q}{4}\cos2\alpha + \frac{\eta^{Q2}}{24}\cos^2 2\alpha + \cos^2\beta \times$$

$$\left. (-\frac{3}{4} + \frac{\eta^{Q2}}{6} - \frac{\eta^{Q2}}{12}\cos^2 2\alpha) + \cos^4\beta(\frac{3}{8} + \frac{\eta^Q}{4}\cos2\alpha + \frac{\eta^{Q2}}{24}\cos^2 2\alpha)] \right]$$

$$(2.43)$$

where $a = I(I + 1)$. In a powder sample, all orientations of the principal axis system are equally probable, i.e. the value of $\cos\beta$ and α in Equation (2.43) are distributed in the μ-α space with equal probability. Thus one can obtain the powder pattern by counting $P(\omega)$ for ω_m lying between ω and ω + dω; every combination of values of μ and α should be chosen corresponding to the lattice points of an equally divided μ-α space.

Up to this point the effects of dipole-dipole interactions and the spin-spin relaxation have not been considered. These effects will broaden and smooth out the theoretical powder pattern. Mathematically, the true absorption pattern $I(\omega)$ will be given by

$$I(\omega) = \int_{-\infty}^{\infty} p(\omega')F(\omega - \omega')d\omega', \qquad (2.44)$$

where $F(\omega - \omega')$ is a function that describes the broadening due to dipole-dipole interaction or/and the spin-spin

relaxation.

multispin sys

as Gaussian

sufficiently

assumption t

[31],

F(ω - ω′) = [

The peak-to-

equal to 2σ

width". Figu

which are ca

This program

part of thi

Gaussian cor

static and m

program ass

quadrupolar

all transit

(Equation (

axes and th

with respec

may have t

from six po

the two te

pattern.

relaxation. This process is known as convolution. In a multispin system, the distribution of spins may be considered as Gaussian. In most cases considered in this work, sufficiently accurate results are obtained with the assumption that $F(\omega - \omega')$ is a normalized Gaussian function [31],

$$F(\omega - \omega') = [1/(2\ \sigma^2 \pi^{1/2})]\exp[-(\omega - \omega')^2/(2\sigma^2)]. \qquad (2.45)$$

The peak-to-peak width of the derivative of $F(\omega - \omega')$ is equal to 2σ, which shall be referred to as the "dipolar width". Figures 5 and 6 show some computer simulated spectra which are calculated by using the program VMASS (Appendix B). This program has been modified from the program POWPAT as part of this thesis research to permit simulation of the Gaussian convoluted lineshape of all transitions obtained by static and magic angle or variable angle sample spinning. The program assumes coincidence of the chemical shift and quadrupolar principal axis systems and the same linewidth for all transitions. In this case one may choose the convention (Equation (2.31)) to determine three quadrupolar principal axes and then three elements of a CSA tensor will be fixed with respect to the quadrupolar coupling tensor. However one may have to calculate six powder patterns with parameters from six possible combinations between the six elements of the two tensors in order to simulate an observed powder pattern.

100

Figure

δ_{XX} δ_{YY} δ_{ZZ}(ppm)

25.0   25.0   -50.0

37.5   12.5   -50.0

-50.0   0.0   50.0

-37.5   -12.5   50.0

-25.0   -25.0   50.0

100   0   -100

ppm
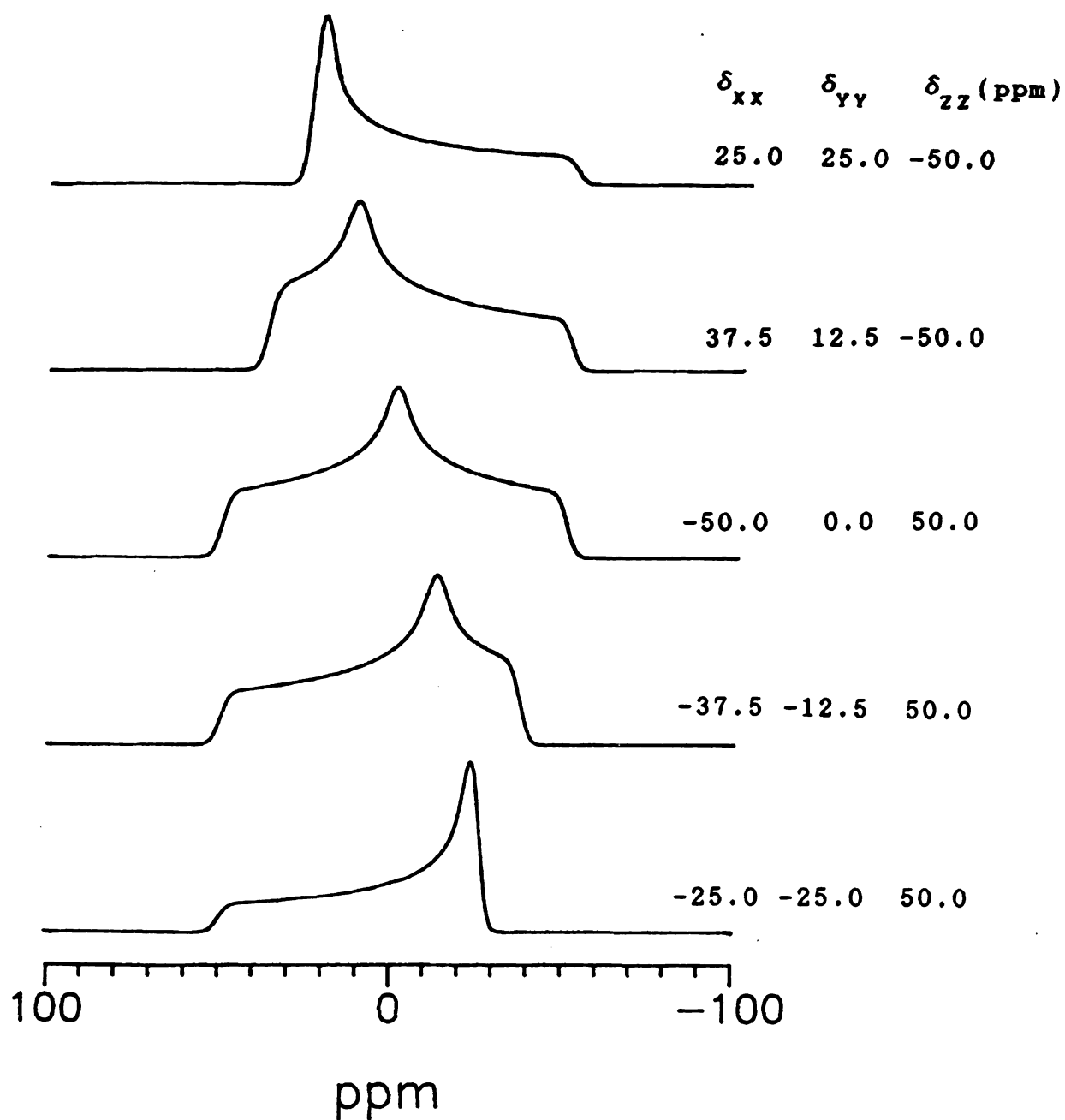
Figure 5 Computer simulated static CSA lineshapes for a
transition (1/2,-1/2).

4
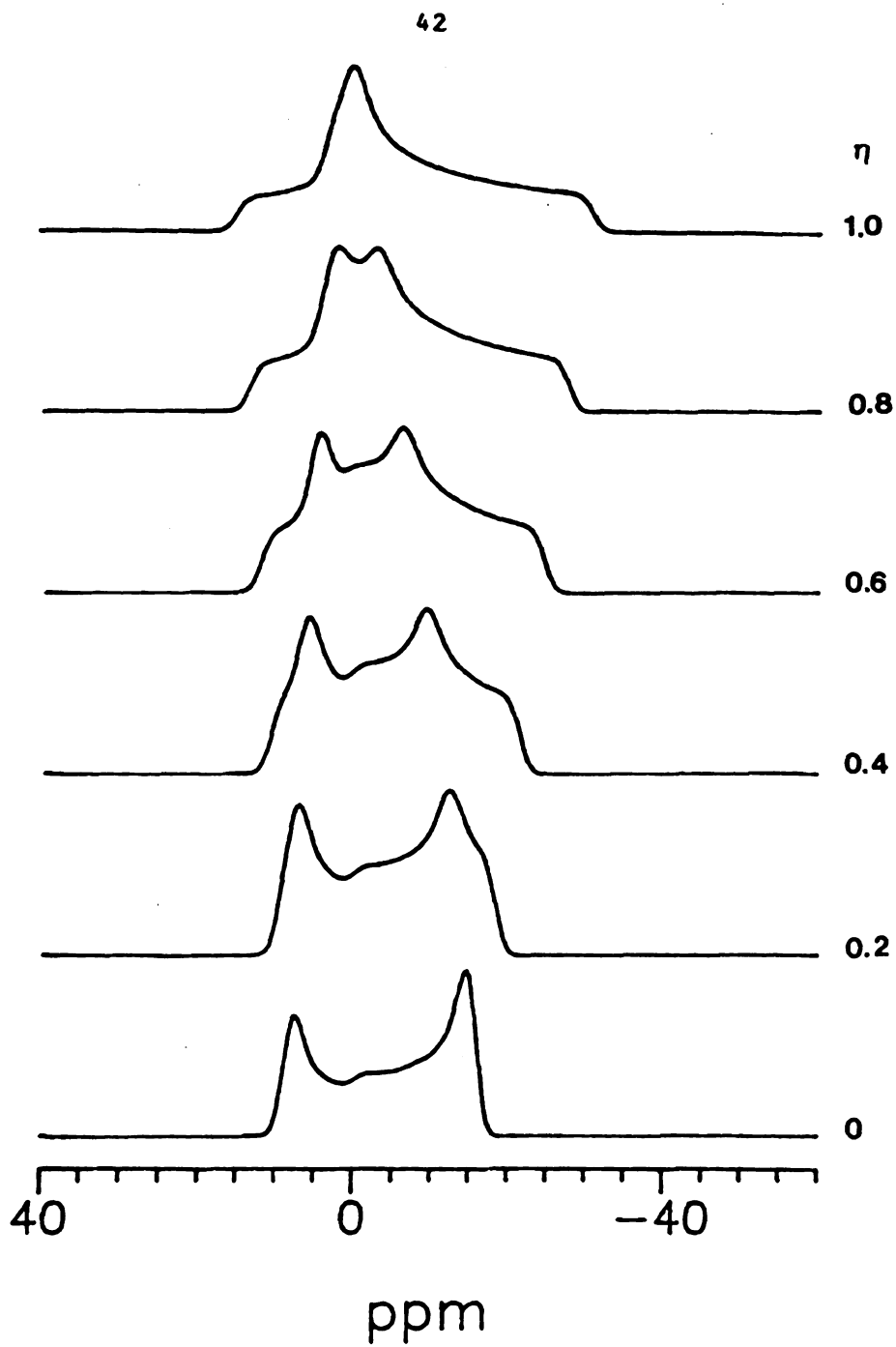
Figure 6 C
1
9

Figure 6 Computer simulated static second order quadrupolar
lineshapes for the central transition of a
quadrupolar nucleus.

When a

to the ext

dependent.

size of the

anisotropic

single line

observed at

However, s

dependence

a single ax

Substantial

can be ach

Variable an

promising n

in solids.

interaction

line-broade

static spec

anisotropic

For a

time-depend

respect to

$_r$. The ex

static sing

spinning si

II. C. 2. Variable Angle Sample Spinning

When a sample is spun at the "magic angle" with respect to the external field all spin interactions become time dependent. If the spinning rate ω_r is much larger than the size of the anisotropic spin interaction, small first order anisotropic interactions are averaged to zero and a narrow single line with negligible spinning side bands will be observed at the isotropic value of the chemical shift. However, second order terms have a different angular dependence and cannot be averaged to zero by spinning about a single axis, thus producing a second order powder pattern. Substantial line narrowing of the second order powder pattern can be achieved at angles other than the magic angle. Variable angle (including magic angle) sample spinning is a promising new approach for obtaining high-resolution spectra in solids. In the slow spinning regime the anisotropic interactions are only partially averaged for inhomogeneous line-broadening, and the spinning side bands map out the static spectrum of the sample. This permits one to study the anisotropic interactions in yet another way.

For a polycrystalline sample, the Hamiltonian becomes time-dependent when the sample is spun at an angle θ with respect to the magnetic field $\mathbf{B}_0$ and with an angular velocity ω_r. The expression for the frequency of an NMR line of a static single crystal can be used in variable angle sample spinning simply by replacing the Eulerian angle ϕ by $\phi_0 + \omega_r t$

and setting

variable ang

through one

quadrupolar

compared wi

the expressi

single crys

(2.40) as:

$$\omega_{_{R}} = \omega_{_{L}}\left[1 + \right.$$

$$\left. \sin^2\beta\cos2\alpha\right)$$

$$\cos2\alpha) + \frac{\omega_{_{Q}}^{^{2}}}{12\alpha}$$

$$6\cos^2\theta + \cos$$

$$\cos^2 2\alpha + \cos$$

$$\frac{\eta^{Q2}}{24}\cos^2 2\alpha))$$

$$- \frac{1}{2}(1 - \cos$$

$$+ \cos^2\beta(\frac{3}{2})$$

$$\eta^{Q}\cos2\alpha - \frac{\eta^{Q}}{6}$$

and setting the two Eulerian angles ψ and θ to 0 and the variable angle θ. For rapid sample spinning, one can average through one cycle of spinning if the magnitudes of the quadrupolar and chemical shift interactions are small compared with the spinning frequency ω_r [32,33]. Therefore the expression for the frequency of an NMR line of a rotating single crystal can be derived from Equations (2.35) and (2.40) as:

$$\omega_m = \omega_L \left[1 + \delta_{iso}^{CSA} + \frac{1}{4} \delta^{CSA} (3\cos^2\theta - 1)(3\cos^2\beta - 1 - \eta^{CSA} \times \right.$$

$$\left. \sin^2\beta\cos2\alpha) \right] - \frac{1}{4}(m - \frac{1}{2})\omega_Q (3\cos^2\theta - 1)(3\cos^2\beta - 1 - \eta^Q\sin^2\beta \times$$

$$\cos2\alpha) + \frac{\omega_Q^2}{12\omega_L} \left[(\frac{1}{2}(1 - \cos^4\theta)[24m(m - 1) - 4a + 9] - \frac{1}{8}(1 + \right.$$

$$6\cos^2\theta + \cos^4\theta)[6m(m - 1) - 2a + 3])(\frac{3}{8} - \frac{\eta^Q}{4}\cos2\alpha + \frac{\eta^{Q2}}{24} \times$$

$$\cos^2 2\alpha + \cos^2\beta (-\frac{3}{4} + \frac{\eta^{Q2}}{6} - \frac{\eta^{Q2}}{12}\cos^2 2\alpha) + \cos^4\beta(\frac{3}{8} + \frac{\eta^Q}{4}\cos2\alpha +$$

$$\frac{\eta^{Q2}}{24}\cos^2 2\alpha)) + (\frac{1}{2}(1 - 3\cos^2\theta + 4\cos^4\theta)[24m(m - 1) - 4a + 9]$$

$$- \frac{1}{2}(1 - \cos^4\theta)[6m(m - 1) - 2a + 3])(\frac{\eta^{Q2}}{6} - \frac{\eta^{Q2}}{6}\cos^2 2\alpha$$

$$\cos^2\beta(\frac{3}{2} - \frac{\eta^{Q2}}{6} + \eta^Q\cos2\alpha + \frac{\eta^{Q2}}{3}\cos^2 2\alpha) + \cos^4\beta (-\frac{3}{2} -$$

$$\eta^Q\cos2\alpha - \frac{\eta^{Q2}}{6}\cos^2 2\alpha)) + (\frac{3}{2}(\cos^2\theta - \cos^4\theta) - \frac{3}{8}(1 - 2\cos^2\theta$$

$+ \cos^4\theta))(\frac{1}{4}$

$- \frac{\eta^{Q2}}{2} \cos^2 2\alpha)$

If the spec

angle) with

order chemic

zero. When

expression

Some simula

illustrated

When t

anisotropic

spinning si

anisotropic

decay (FID

Equation (

spinning-in

into two pa

moderate va

spin echoes

after Four

information

The envelo

magic angle

the isotro

discussed

$$+ \cos^4\theta)) (\frac{1}{4} + \frac{\eta^Q}{2} \cos2\alpha + \frac{\eta^{Q2}}{4} \cos^2 2\alpha + \cos^2\beta(- \frac{3}{2} - 2\eta^Q\cos2\alpha$$

$$- \frac{\eta^{Q2}}{2} \cos^2 2\alpha) + \cos^4\beta(\frac{9}{4} + \frac{3}{2} \eta^Q\cos2\alpha + \frac{\eta^{Q2}}{4} \cos^2 2\alpha)) \Big] \qquad (2.46)$$

If the specimen is rotated at an angle of $54.7356°$ (magic angle) with respect to the applied magnetic field, the first order chemical shift and quadrupolar terms can be averaged to zero. When the variable angle is equal to zero, this expression reduces to Equation (2.43) for a static sample. Some simulated variable angle sample spinning spectra are illustrated in Figures 7 and 8.

When the spinning speed is small (not enough to average anisotropic interactions), a peak at the isotropic value with spinning side bands will result due to partial averaging of anisotropic interactions. Calculation of the free induction decay (FID) requires integration of Equation (2.35) with Equation (2.40) and $\phi = \phi_0 + \omega_r t$ which brings out the spinning-induced periodicities. This can often be separated into two parts, one of which is simple. One may find that for moderate values of ω_r, the FID assumes the form of rotational spin echoes, which correspond to sets of distinct sidebands after Fourier transformation. The shape of echoes carry information about δ^{CSA}, η^{CSA}, δ^Q and η^Q of Equation (2.40). The envelope of the echoes is governed by δ_{iso} under the magic angle spinning condition, and therefore is related to the isotropic spectrum of a liquid sample. This problem is discussed in detail by others [34,35].

δ_{xx} δ
-37.5 -1

Figur

δ_{XX} δ_{YY} δ_{ZZ} (ppm)
-37.5 -12.5 50.0

Variable Angle ( )

90

80

70

54.74

40

30

20

10

75   0   −75

ppm
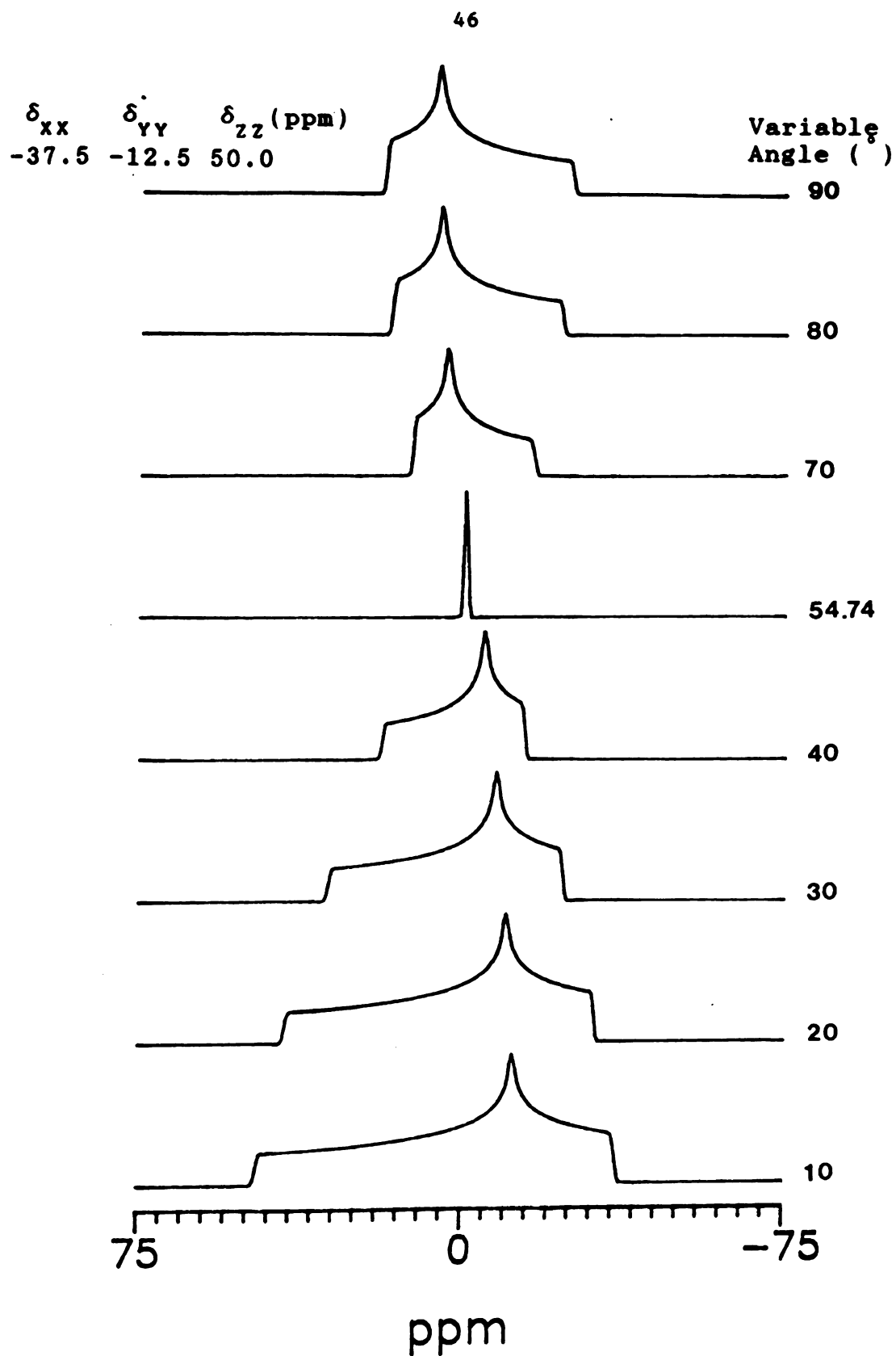
Figure 7 Computer simulated VAS CSA lineshapes for a transition (1/2,-1/2).

20   0   -
ppm

η = 0
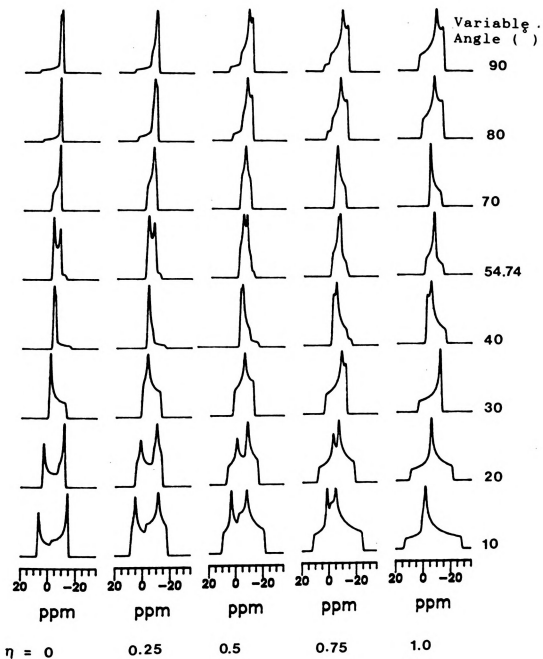
Figure 8

Figure 8 Computer simulated VAS second order quadrupolar
lineshapes for the central transition of a
quadrupolar nucleus.

A numbe

width of a

of the appli

can be redu

magnetic di

broadening

broaden the

second orde

lattice rel

population

the lifetim

resonance l

Uncertainty

In thi

dipole coup

the Zeeman

will be ign

small magne

nuclei. Th

magnetic mo

$$E = \frac{\hat{\mu}_1 \cdot \hat{\mu}_2}{R_{12}^3}$$

where R_{12}

II. D. Magnetic Dipolar Broadening

A number of physical phenomena may contribute to the width of a resonance line. One of them is the inhomogeneity of the applied field. This is not a serious problem since it can be reduced to a few milligauss out of 10^4 Gauss. The magnetic dipolar interaction is the dominant source of broadening in solids. Also the quadrupolar interaction can broaden the observed line due to first order splittings or second order shift as already discussed. The fact that spin lattice relaxation (T_1) processes produce an equilibrium population by balancing rates of transitions puts a limit on the lifetime of Zeeman states, which effectively broadens the resonance lines by an energy of the order of $\hbar/T_1$ due to the Uncertainty Principle.

In this section, however, the contribution of magnetic dipole coupling between the various nuclei to the width of the Zeeman transition will be considered, and other effects will be ignored. Magnetically active nuclei ($I \neq 0$) behave as small magnets and create magnetic fields at the surrounding nuclei. The classical interaction energy E between two magnetic moments $\hat{\mu}_1$ and $\hat{\mu}_2$ is

$$E = \frac{\hat{\mu}_1 \cdot \hat{\mu}_2}{R_{12}^3} - \frac{3(\hat{\mu}_1 \cdot \mathbb{R}_{12})(\hat{\mu}_2 \cdot \mathbb{R}_{12})}{R_{12}^5} \qquad (2.47)$$

where $\mathbb{R}_{12}$ is the radius vector from $\hat{\mu}_1$ to $\hat{\mu}_2$ and R_{12} is the

magnitude c

Hamiltonian

usual:

$$\hat{\mu}_1 = \gamma_I \hbar \mathbf{I}$$

$$\hat{\mu}_2 = \gamma_S \hbar \mathbf{S}.$$

The dipolar

$$\mathcal{H} = \gamma_I \gamma_S R_{IS}^{-3} \hbar$$

Also the

"dipolar al

$$\mathcal{H}_{IS} = \frac{\gamma_I \gamma_S \hbar}{R_{IS}^3}$$

where

$$A = (1 - 3$$

$$B = -1/4 \ ($$

$$= 1/2 \ (1$$

$$C = -3/2 \ s$$

$$D = C^* = $$

magnitude of the vector $\mathbf{R}_{12}$. For a quantum mechanical Hamiltonian one simply substitutes operators for $\hat{\mu}_1$ and $\hat{\mu}_2$ as usual:

$$\hat{\mu}_1 = \gamma_I \hbar \mathbf{I}$$

$$\hat{\mu}_2 = \gamma_S \hbar \mathbf{S}. \tag{2.48}$$

The dipolar Hamiltonian then becomes

$$\mathcal{H} = \gamma_I \gamma_S R_{IS}^{-3} \hbar \left[\mathbf{I} \cdot \mathbf{S} - \frac{3(\mathbf{I} \cdot \mathbf{R}_{IS})(\mathbf{S} \cdot \mathbf{R}_{IS})}{R_{IS}^2} \right]. \tag{2.49}$$

Also the dipolar Hamiltonian can be expanded into the "dipolar alphabet" [36]

$$\mathcal{H}_{IS} = \frac{\gamma_I \gamma_S \hbar}{R_{IS}^3} [A + B + C + D + E + F] \tag{2.50}$$

where

$$A = (1 - 3\cos^2\theta) I_z S_z$$

$$B = -1/4 \, (1 - 3\cos^2\theta)(I^+ S^- - I^- S^+)$$

$$= 1/2 \, (1 - 3\cos^2\theta)(I_z S_z - \mathbf{I} \cdot \mathbf{S})$$

$$C = -3/2 \, \sin\theta\cos\theta(I_z S^+ + I^+ S_z) e^{-i\phi}$$

$$D = C^* = -3/2 \, \sin\theta\cos\theta(I_z S^- + I^- S_z) e^{i\phi}$$

$E = -3/4 \sin$

$F = E^* = -3/$

Wavefunctior

numbers m_I

term A, whi

diagonal an

On the oth

connects or

usually sai

the other u

representat

states, wh

degenerate.

determined

Terms C an

both spins

are off-di

zero-order

admixture

methods. /

transition

extra peal

disregarde

terms C,

to drop C

truncated

$$E = -3/4 \sin^2\theta \; I^+ S^+ e^{-2i\phi}$$

$$F = E^* = -3/4 \sin^2\theta \; I^- S^- e^{2i\phi}$$

Wavefunctions can be given in terms of the individual quantum numbers m_I and m_S, which are eigenvalues of I_z and S_z. The term A, which is proportional to $I_z S_z$, is clearly completely diagonal and it connects the state $|m_I m_S\rangle$ with state $\langle m_I m_S|$. On the other hand, B is proportional to $I^+ S^- + I^- S^+$, and connects only $|m_I m_S\rangle$ to $\langle m_{I+1} m_{S-1}|$ or to $\langle m_{I-1} m_{S+1}|$. It is usually said that B simultaneously flips one spin down and the other up. B has no diagonal matrix elements for the $m_I m_S$ representation, but it has off-diagonal elements between two states, which become important when the states are nearly degenerate. When the proper zero-order functions are determined, B turns out to have diagonal matrix elements. Terms C and D each flip one spin only. Finally E and F flip both spins up or both spins down. The terms C, D, E, and F are off-diagonal. The effect of these four terms is to admix zero-order states into the exact states. The amount of the admixture can be computed by second-order perturbation methods. A consequence of the admixture of states is that transitions at $\omega = 2\omega_0$ and near $\omega = 0$ can be induced. The extra peaks at 0 and $2\omega_0$ are very weak and may usually be disregarded. Since they are the principal effects of the terms C, D, E, and F, it will be an excellent approximation to drop C, D, E, and F from the Hamiltonian. Therefore the truncated dipolar Hamiltonian becomes

$$\mathcal{H}_{IS} = -1/4 \ \gamma$$

For   va

becomes simi

one can eas

zero by spi

chemical sh

interaction

this term t

spins can s

time averag

the sample

magnetic f

important

interaction

In or

samples, o

Hamiltonian

since $I_{jz}S$

each other

Vleck [37]

compute th

eigenstate

is defined

$$\mathcal{H}_{IS} = -1/4 \; \gamma_I \gamma_S \hbar \sum \frac{(3\cos^2\theta_{jk} - 1)}{R_{jk}^3} \; (3I_{jz}S_{kz} - \mathbf{I}_j \cdot \mathbf{S}_k) \qquad (2.51)$$

For variable angle sample spinning this expression becomes similar to the first order equation of CSA. Of course one can easily see that this interaction will be averaged to zero by spinning the sample at the magic angle just as with chemical shift anisotropy and the first order quadrupolar interaction. It is clear that one can theoretically average this term to zero if $3\cos^2\theta_{jk} - 1 = 0$. Although only a few spins can satisfy this condition under static conditions, the time averaged $\cos^2\theta_{jk}$ can be made to equal $1/3$ by spinning the sample at the magic angle with respect to the applied magnetic field $\mathbb{B}_0$. The dipolar Hamiltonian $\mathcal{H}_{IS}$ is very important in considering homogeneous and inhomogeneous interactions in solids.

In order to estimate the dipolar broadening of static samples, one has to obtain the eigenvalues of the total Hamiltonian and it is a formidable task to solve this problem since $I_{jz}S_{kz}$ and $\mathbf{I}_j \cdot \mathbf{S}_k$ operators do not commute with each other. In fact, there is a clever technique by Van Vleck [37], called moment analysis, which enables one to compute the dipolar width without solving explicitly for the eigenstates and eigenvalues of energy. The nth moment of $f(\omega)$ is defined by the equations

$$\langle \omega^n \rangle = \frac{\int_0^\infty \omega^n}{\int_0^\infty}$$

and

$$\langle \Delta \omega^n \rangle = \frac{\int_0^\infty}{}$$

Equation (2

expressions

single crys

$$\langle \Delta \omega_I^2 \rangle_{II} = \frac{3}{4}$$

for intera

$$\langle \Delta \omega_I^2 \rangle_{IS} = \frac{1}{}$$

for intera

R_{jk} is th

angle betw

The subsc

respective

replaced b

    For

$$\langle \Delta \omega^2 \rangle = 0.$$

$$\langle\omega^n\rangle = \frac{\int_0^\infty \omega^n f(\omega)d\omega}{\int_0^\infty f(\omega)d\omega} \tag{2.52}$$

and

$$\langle\Delta\omega^n\rangle = \frac{\int_0^\infty (\omega - \langle\omega\rangle)^n f(\omega)d\omega}{\int_0^\infty f(\omega)d\omega} \tag{2.53}$$

Equation (2.53) for n = 2 is called the "second moment". The expressions for the second moment of nuclei of type I in a single crystal are

$$\langle\Delta\omega_I^2\rangle_{II} = \frac{3}{4} \gamma_I^4 \hbar^2 I(I+1) \sum_k \frac{(1 - 3\cos^2\theta_{jk})^2}{R_{jk}^6} \tag{2.54}$$

for interactions between like spins and

$$\langle\Delta\omega_I^2\rangle_{IS} = \frac{1}{3} \gamma_I^2 \gamma_S^2 \hbar^2 S(S+1) \sum_k \frac{(1 - 3\cos^2\theta_{jk})^2}{R_{jk}^6} \tag{2.55}$$

for interactions between unlike spins. In these expressions R_{jk} is the distance between nuclei j and k and θ_{jk} is the angle between the $\mathbf{R}_{jk}$ vector and the external field direction. The subscripts II and IS indicate like and unlike spins, respectively. For a powder pattern $\sum_k (1 - 3\cos^2\theta_{jk})^2$ can be replaced by its average value 4/5.

For a Gaussian line shape, the second moment is given by

$$\langle\Delta\omega^2\rangle = 0.721(\frac{1}{2}\Delta\omega_{1/2})^2 \text{ or } \Delta\nu_{1/2} = 2.355\sqrt{\langle\Delta\nu^2\rangle}, \tag{2.56}$$

where $\Delta\omega_{1/2}$

The a

calculations

and Ollom [

nuclei. Thre

spins in id

inequivalent

modification

involves si

(2.54) by ar

$$F_a = \frac{4}{3} I(I +$$

$$F_b = \frac{4}{3} I(I$$

In case (c)

the same a

unsplit lin

II. E. Homo

Inte

As mer

shifted by

shapes, ho

result for

A hom

where $\Delta\omega_{1/2}$ is full width at half-height.

The appropriate modifications of Van Vleck's calculations have been carried out in first order by Kambe and Ollom [38] for the central component of quadrupolar nuclei. Three cases are considered: (a) broadening by like spins in identical sites, (b) broadening by like nuclei in inequivalent sites, (c) broadening by unlike nuclei. The modification for dipolar broadening in cases (a) and (b) involves simply the replacement of $3I(I + 1)$ in Equation (2.54) by an appropriate factor F_x (x = a, b).

$$F_a = \frac{4}{3} I(I + 1) + [\ 2I^2(I + 1)^2 + 3I(I + 1) + \frac{13}{8}\ ]/2(2I + 1).$$

$$F_b = \frac{4}{3} I(I + 1) + \frac{1}{2} (2I + 1) + \frac{1}{32} (2I + 1)^3. \qquad (2.57)$$

In case (c), the second moment of the central component is the same as Equation (2.55) given by Van Vleck for the unsplit line.

II. E. Homogeneous, Inhomogeneous, and Heterogeneous
       Interactions

As mentioned before, every single line is broadened or shifted by some mechanism. Three types of spectral line shapes, homogeneous, inhomogeneous and heterogeneous will result for a powder sample.

A homogeneous line is a sum of individual lines all

having the

and no shif

comes from

but are flu

with a spin

spin system

absorption

all the spi

with one a

interaction

"indistingu

flip-flop

also be tru

frequency

since energ

another.

If th

magnetic f

remarkably

those spi

condition.

in this s

interactio

have to be

different

overall re

of the ind

having the same line width (i.e. the same broadening $1/T_2^*$)
and no shift with respect to each other. If the line width
comes from some mechanism which are external to the system
but are fluctuating rapidly compared with the time associated
with a spin transition, then the thermal equilibrium of the
spin system will be maintained at all times. Therefore, the
absorption or emission of the energy will be distributed to
all the spins. In a liquid where all the spins are coupled
with one another or in a solid, where the dipole-dipole
interaction among the like spins makes the spins
"indistinguishable" in the frequency domain and where spin
flip-flop processes relax all the spins equally, this will
also be true. Therefore selective irradiation at a particular
frequency of the line causes saturation of the whole line
since energy will be quickly transferred from one spin to
another.

If the line width arises from variations in the local
magnetic fields, the physical response of the system is
remarkably different. Energy will be transferred only to
those spins whose local fields satisfy the resonance
condition. Further, the processes for spin-spin interactions
in this system will be slow as compared to the direct
interaction of the spins with the lattice because energy will
have to be transferred to the lattice in order for spins in
different local fields to come to equilibrium. Then the
overall response of the spin system will be a superposition
of the individual responses of the spin packets. Therefore an

inhomogeneo

lines will

by a distri

individual

packet, no

irradiation

pattern) ca

since coupl

sources of

(e.g. quad

anisotropie

inhomogenei

A het

packets, wh

to each oth

in NMR is

case dilute

"sea" of I

to the pa

interactior

other S sp

interactior

different

processes

spinning,

line of t

other hand

inhomogeneous line which is a superposition of individual lines will be observed and the lineshape will be determined by a distribution of the shifts. Although there may be some individual lifetime broadening connected with each spectral packet, no coupling between the packets exists. Selective irradiation at a particular frequency of the line (powder pattern) causes a saturation of only that part of the line since coupling to other spectral elements is excluded. Some sources of inhomogeneous broadening are anisotropy broadening (e.g. quadrupolar interactions, chemical shift and g anisotropies), dipolar interactions between unlike spins, and inhomogeneities in the applied magnetic fields.

A heterogeneous line is made up of individual spectral packets, which are distributed in frequency and are coupled to each other. The typical case where this behavior is found in NMR is in the case of heteronuclear spin coupling. In this case dilute S spins are coupled to a more or less isotropic "sea" of I spins via a few I spins which are strongly coupled to the part of the abundant I spins via dipole-dipole interaction. Some of the other I spins are in turn coupled to other S spins. The flip-flop processes of this dipole-dipole interaction among the I spins cause exchange between the different spectral parts of the S spins. If the flip-flop processes are quenched, which may be achieved by magic angle spinning, decoupling, or multiple pulse experiments, the NMR line of the S spin system become inhomogeneous. If on the other hand the flip-flop rate can be enhanced a homogeneous

line will r

line will result.

The fa

from the sp

of electron

dynamic pro

while magne

properties.

There

magnetic pr

and ferroma

the simple

metals, ex

paramagneti

when heated

that   para

connected.

important

these mate

CHAPTER III

MAGNETIC SUSCEPTIBILITY

The fascinating magnetic properties of materials arise from the spin of electrons or nuclei and the orbital motion of electrons. Magnetic resonance spectroscopy deals with the dynamic properties of the spins in a static magnetic field, while magnetic susceptibility is the study of static magnetic properties.

There are three main classes of solids as far as static magnetic properties are concerned: diamagnetic; paramagnetic; and ferromagnetic substances. Most insulators and about half the simple metals are diamagnetic. Some other insulators and metals, except for a few ferromagnetic substances, are paramagnetic. The ferromagnetic materials become paramagnetic when heated to sufficiently high temperatures, a fact showing that paramagnetism and ferromagnetism are intimately connected. The magnetic properties of electrides are very important to study the electron-electron interactions in these materials.

III. A. Defi

The res

characterize

$$\chi = \frac{M}{B}$$

where M is

per unit vo

symbol χ_v

parallel an

tensor. It

on a gram

gram suscep

susceptibil

$$\chi = \frac{\chi}{\text{density}}$$

In the cgs

ionic) sus

expressed

$$\chi_A = \chi \times a$$

$$\chi_M = \chi \times m$$

III. A. Definitions of Terms and Units

The response of materials in a static magnetic field is characterized by the susceptibility $\varkappa$, through the relation

$$\varkappa = \frac{M}{B} \tag{3.1}$$

where M is the magnetization, defined as the magnetic moment per unit volume, and B is the applied field. Quite often the symbol χ_v is used for $\varkappa$. In isotropic media B and M are parallel and $\varkappa$ is a scalar; for anisotropic materials, $\varkappa$ is a tensor. It is more convenient to express the susceptibility on a gram (χ) rather than on a unit volume ($\varkappa$) basis. The gram susceptibility is also called the mass or the specific susceptibility. It is related to the volume susceptibility by

$$\chi = \frac{\varkappa}{\text{density}} \tag{3.2}$$

In the cgs system the unit for χ is $cm^3 g^{-1}$. The atomic (or ionic) susceptibility (χ_A) and the molar susceptibility (χ_M) expressed in cgs units of $cm^3 mole^{-1}$ are given by

$$\chi_A = \chi \times \text{atomic weight} \tag{3.3}$$

$$\chi_M = \chi \times \text{molecular weight} \tag{3.4}$$

The ap

motion   of

magnetizati

Lenz's law.

temperature

diamagnetic

be attribu

structure o

gram-atom (

distributio

present on

susceptibil

$$\chi_A = - \frac{Ne^2}{6mc^2}$$

where N is

around the

electron r

the perman

of electr

susceptibi

susceptibi

III. B. Diamagnetism

The application of an external field to the orbital motion of an electron around a nucleus induces a magnetization in the opposite direction, in accordance with Lenz's law. Diamagnetic susceptibility is independent of both temperature and the applied field. Any significant changes in diamagnetic susceptibility with temperature in most cases may be attributed to a change in the physical or chemical structure of the material. The diamagnetic susceptibility per gram-atom (χ_A) depends primarily on the average radial charge distribution $\langle r^2 \rangle$, taken perpendicular to the field and is present only when an external field is present. The atomic susceptibility χ_A is given by the Langevin equation:

$$\chi_A = - \frac{Ne^2}{6mc^2} \sum_{i=1}^{z} \langle r_i^2 \rangle \qquad (3.5)$$

where N is Avogadro's number, z is the number of electrons around the nucleus, e and m are the charge and mass of the electron respectively, and c is the speed of light. However, the permanent magnetic moment arising from the unpaired spins of electrons which gives rise to a high paramagnetic susceptibility masks the very small diamagnetic susceptibility.

C. Parama

When a

the respons

Classically

with the f

produced by

which in th

than the

magnetic po

which each

field   in

randomizat

susceptibi

the Curie

$$\chi_{M} = \frac{C}{T}$$

where C is

When

permit th

align the

of known

"molecula

is the s

molecular

simplest

C.   Paramagnetism, Ferromagnetism and Antiferromagnetism

When a magnetic field is applied to noninteracting spins the response of the spin system is remarkably different. Classically, the tendency of the magnetic dipoles to orient with the field is counteracted by the randomizing effects produced by thermal energy kT (k is the Boltzmann constant), which in the room temperature region is several times greater than the magnetic energy of the dipoles. Hence very weak magnetic polarizations are observed in many paramagnetics, in which each dipole is able to orient itself parallel to the field independently of others. Experimentally the randomization effect is reflected in a decrease in susceptibility with increasing temperature. This is known as the Curie law:

$$\chi_M = \frac{C}{T} \qquad\qquad (3.6)$$

where C is the Curie constant.

When the distance between the spins is short enough to permit them to interact, the internal interaction tends to align the spins. First Weiss proposed that all interactions of known or unknown origins could be replaced by a single "molecular field" B_m, such that the total force on each spin is the sum of an externally applied field B and of the molecular field B_m. In the mean field approximation the simplest assumption for a molecular field is that B_m is

proportiona

$$B_m = \lambda M$$

From   the

calculated

$$\chi = \frac{C}{T - \theta};$$

The suscep

temperatur

magnetizat

Curie-Weis

susceptibi

Curie poin

$$\chi \propto \frac{}{(\ T -}$$

at tempera

    Heis

may be gi

of quant

magnetiza

momenta,

magnetic

subjected

proportional to the magnetization M:

$$B_m = \lambda M \qquad (3.7)$$

From the molecular field the susceptibility can be calculated:

$$\chi = \frac{C}{T - \theta}; \quad \theta = C\lambda. \qquad (3.8)$$

The susceptibility has a singularity at $T = \theta$. At this temperature and below there exists a spontaneous magnetization. This expression, which is called the Curie-Weiss law, describes fairly well the observed susceptibility variation in the paramagnetic region above the Curie point. Detailed calculations [39] predict

$$\chi \propto \frac{1}{(T - T_c)^{1.33}} \qquad (3.9)$$

at temperatures close to T_c.

Heisenberg [40] first showed that the Weiss local field may be given a direct and simple explanation in the language of quantum theory. His model suggests that spontaneous magnetization arises from a coupling of the spin angular momenta, S, rather than the total angular momenta. The magnetic atoms are assumed to interact in pairs and to be subjected to an applied field. This interaction is not solely

the magneti

magnetic fi

another spin

general too

interaction

which is

mechanical

Hamiltonian

$$\mathcal{H} = \mathcal{H}_H + \mathcal{H}_Z$$

$$= -2 \sum_{i<j} J_i$$

where J_{ij}

electrons

electrons

$$f_M(E) = \frac{1}{(2}$$

where $\bar{E}_M$ i

$n(M)$ is th

the z comp

square de

magnetic e

obtained:

the magnetic dipole-dipole interaction, which is due to the magnetic field produced by one spin at the position of another spin, because the magnetic dipolar interaction is in general too small to produce ferromagnetism. The predominent interaction is usually the so-called "exchange" interaction which is electrostatic in origin. This is a quantum mechanical consequence of the Pauli exclusion principle. The Hamiltonian for the entire crystal can be written as

$$\mathcal{H} = \mathcal{H}_H + \mathcal{H}_Z$$

$$= -2 \sum_{i<j} J_{ij} \mathbf{S}_i \cdot \mathbf{S}_j - g\mu B \sum_i S_i^z \qquad (3.10)$$

where J_{ij} is the exchange interaction constant of two electrons in states i and j. The distribution of levels of electrons with a given M may be approximated by the function

$$f_M(E) = \frac{n(M)}{(2\pi)^{1/2} \Delta_M} \exp\left(- \frac{(E - \overline{E}_M)^2}{\Delta_M^2} \right) \qquad (3.11)$$

where $\overline{E}_M$ is the mean value of the energy levels of given M, n(M) is the number states associated with different values of the z component of total magnetic moment and Δ_M^2 is the mean square deviation from this mean. With this assumption magnetic equations nearly equivalent to Weiss's equations are obtained:

$$\frac{M}{M_\infty} = \tanh \eta$$

in which

$$\eta = \frac{\mu B}{kT} + \frac{1}{2}$$

where z i

difference

be dropped,

equation:

$$\theta = 2J/k(1$$

In 19

ferromagnet

magnets as

problem to

function o

quqntity S

functional

essential

quantizati

diagonal,

zero. In

mechanics

truncated

$$\frac{M}{M_\infty} = \tanh \eta \qquad\qquad (3.12)$$

in which

$$\eta = \frac{\mu B}{kT} + \frac{1}{2} \left(\gamma - \frac{\gamma^2}{2}\right) \frac{M}{M_\infty} + \frac{\gamma^2}{4z} \left(\frac{M}{M_\infty}\right)^3 \qquad \left(\gamma = \frac{zJ}{kT}\right)$$

where z is the number of nearest neighbors. The only difference lies in the η term containing $(M/M_\infty)^3$. If it can be dropped, the Curie temperature is given by the following equation:

$$\theta = 2J/k(1 - \sqrt{1 - 8/z}).$$

In 1925 E. Ising [41] proposed a new model to treat ferromagnetism. Given a law of interaction between the little magnets associated with the spins, one can solve the Ising problem to yield the net magnetization of the system as a function of T and B. To simplify the interaction problem the quqntity $S_i \cdot S_j$ in Equation (3.10) is replaced by the simpler functional form $S_{iz}S_{jz}$. Hence this approximation leaves the essential physical situation intact because, if the quantization is along the z direction, only this part is diagonal, and expectation values of the other operators are zero. In addition, the Ising problem needs no quantum mechanics for its discussion, because all variables of the truncated Hamiltonian commute. The quantum variable S_z thus

becomes a s

sees that t

number of

states. St

calculate

entropy o

stabilizati

the one di

the disorde

the system

results o

Magnetism"

    The ma

$$\chi \sim \frac{1}{T} \exp(2$$

and the ze

$$c(T) = k(\frac{k}{J}$$

are obtai

one-dimens

functions

theory. T

range orde

to the

temperatur

becomes a scalar which can be either +1 or -1. However one sees that there is a combinatorial problem in calculating the number of configurations associated with each set of spin states. Statistical mechanics provides the formalism to calculate the properties of a collection of spins. The entropy of disordering the spins competes with the stabilization of the spin system due to ordering. Except for the one dimensional case there should be a transition from the disordered to the ordered state when the temperature of the system is lowered below the critical temperature. The results of the Ising model, based on "The Theory of Magnetism" by D. C. Mattis [41], will be discussed here.

The magnetic susceptibility

$$\chi \sim \frac{1}{T} \exp(2J/kT) \tag{3.13}$$

and the zero-field specific heat

$$c(T) = k\left(\frac{kT}{J} \cosh\frac{J}{kT}\right)^{-2} \tag{3.14}$$

are obtained by solving the Ising Hamiltonian of a one-dimensional ferromagnet. These quantities are continuous functions of T and differ considerably from mean field theory. They are plotted in Figure 9. The absence of long range order in this one dimensional model is closely related to the absence of spontaneous magnetization at any temperature T > 0 and to the lack of a phase transition.
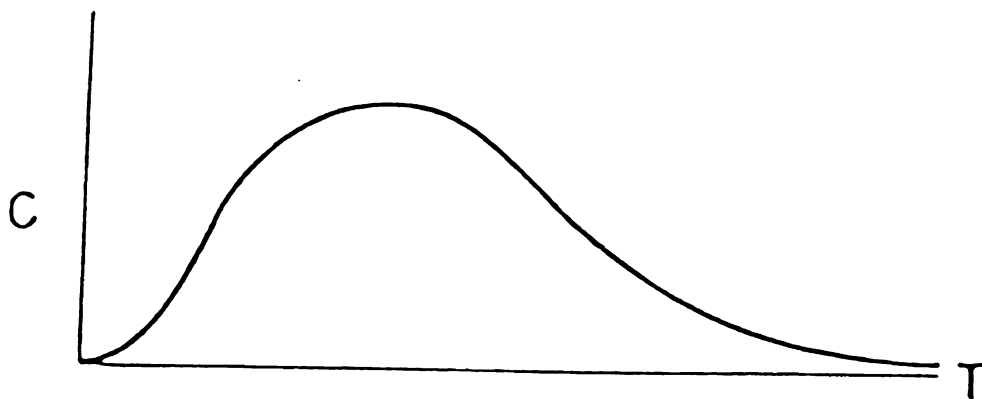
a)
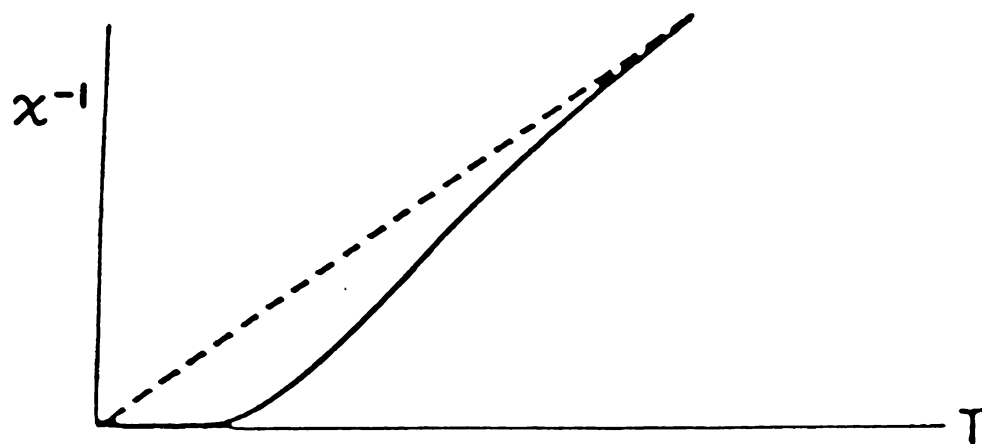
b)

Figure 9 Specific heat a) and Susceptibility b) of
one-dimensional Ising ferromagnet [42].

The t

antiferroma

is exactly

for the sp

net in the

L. Onsager

$M = (1 - x$

where J_1 a

particular

energy U(T

$U(T) = -Jc$

with $x =$

elliptic i

$$K(x) = \int_0^{\pi/}$$

When the

the speci

found as

expansion

for the m

The two-dimensional Ising model of ferromagnetism or antiferromagnetism is one of the rare many-body problems that is exactly soluble and shows a phase transition. The formula for the spontaneous magnetization of the rectangular Ising net in the absence of an external magnetic field was given by L. Onsager [42]:

$$M = (1 - x^{-2})^{1/8} \quad \text{with} \quad x = \sinh\frac{2J_1}{kT}\sinh\frac{2J_2}{kT} \tag{3.15}$$

where J_1 and J_2 are the two exchange interactions. For the particular case of the square net, $J_1 = J_2 = J$, the internal energy $U(T)$ is derived as

$$U(T) = -J\coth\frac{2J}{kT}\left(1 + \frac{2}{\pi}\left(2\tanh^2\frac{2J}{kT} - 1\right)K(x)\right) \tag{3.16}$$

with $x = 2\sinh(2J/kT)/\cosh^2(2J/kT)$ defined as the complete elliptic integral of the first kind,

$$K(x) = \int_0^{\pi/2}(1 - x^2\sin^2\phi)^{-1/2}d\phi.$$

When the internal energy is differentiated in turn to obtain the specific heat, a logarithmically singular behavior is found as shown in Figure 10. On the basis of exact series expansion methods, Fisher [44] has obtained the following law for the magnetic susceptibility:

Figure 10

Figure
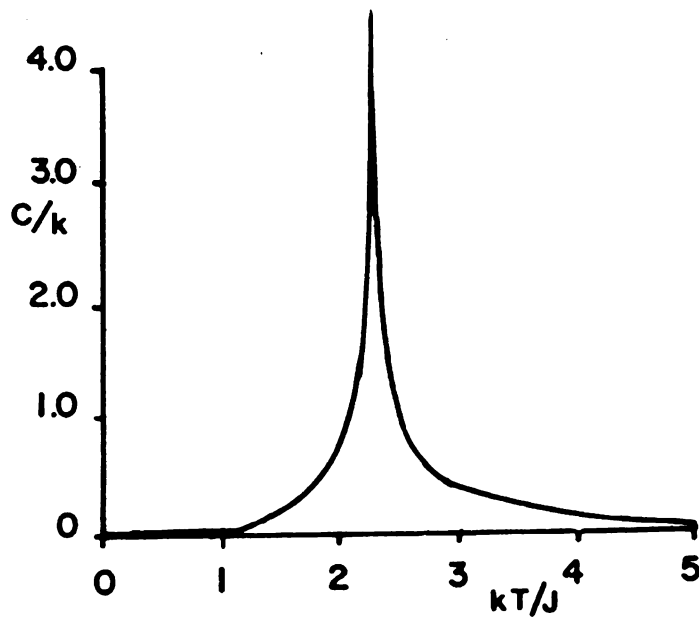
Figure 10 Exact specific heat C/k versus kT/J for isotropic
nearest-neighbor, square-lattice Ising model [45].
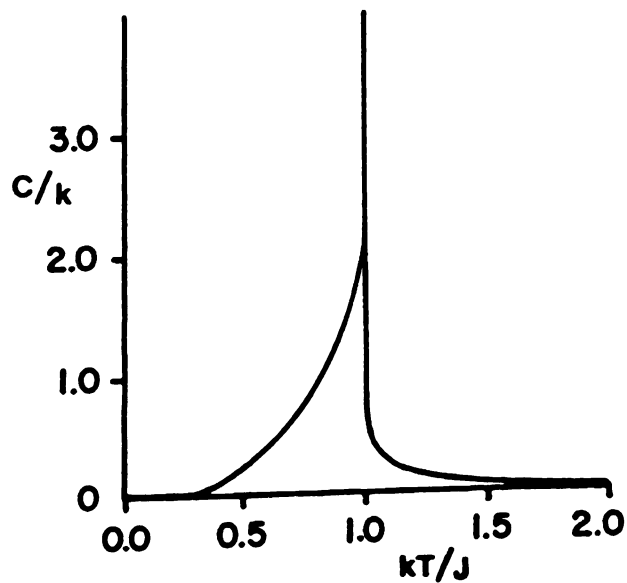
Figure 11 Specific heat C/k versus kT/J for isotropic,
nearest-neighbor, fcc Ising model. Results of
series methods exact everywhere except near Tc
[46].

$$\chi = \frac{Ng^2\mu^2}{kT_c} (1$$

In contrast

not valid w

Despit

physicists,

has not ye

expansions

indicated

two-dimensi

singularity

shown   in

three-dimer

$$\chi = \frac{Ng^2\mu^2}{kT_c} ($$

which is

the result

To ir

spin-wave

Slater [4

the probl

different

A   q

quantizat

The eleme

$$\chi = \frac{Ng^2\mu^2}{kT_c}(1 - \frac{T_c}{T})^{-1.75} \qquad T \gtrsim T_c \qquad\qquad (3.17)$$

In contrast to the Curie-Weiss law, Equation (3.17) is evidently not valid when $T \gg T_c$.

Despite intensive efforts by theoretical chemists, physicists, and mathematicians, the three-dimensional problem has not yet been solved. However, very highly accurate series expansions of the three-dimensional Ising model have indicated results similar to many features of the exact two-dimensional solution. For example, there is a logarithmic singularity in the specific heat. The specific heat curve is shown in Figure 11. Near the Curie temperature, the three-dimensional susceptibility obeys the law

$$\chi = \frac{Ng^2\mu^2}{kT_c}(1 - \frac{T_c}{T})^{-1.25} \qquad T \gtrsim T_c \qquad\qquad (3.18)$$

which is closer to the molecular field Curie-Weiss law than the result of the two-dimensional Ising model.

To improve Heisenberg's treatment of ferromagnetism the spin-wave theory was developed by Bloch [47] and extended by Slater [48]. Although this treatment casts a new light upon the problem of ferromagnetism, the results are not radically different from those of Heisenberg's theory.

A quantized spin wave is called a magnon. The quantization can be interpreted in terms of spin reversal. The elementary excitations of a spin system have a wavelike

form. Spi

orientatior

of magneti

Heisenberg'

which all e

atoms, each

the one-el

atomic fun

$E_0 = N(\varepsilon_0$

where ε_0

interactio

exchange :

atoms, an

ϕ_n are det

the spin

These N ft

of magnet

Bohr magn

$\phi_k = a_k \sum_n$

and have

$E_k = E_0 +$

form. Spin waves are oscillations in the relative orientations of spins on a lattice. Bloch constructed a set of magnetic wavefunctions that bear the same relation to Heisenberg's atomic wave functions and chose the state Ψ_0 in which all electron spins are parallel. Consider a system of N atoms, each of which has one valence electron and assume that the one-electron wave functions $\psi(r - r(n)) = \psi_n$ are like atomic functions. The energy of the state Ψ_0 is

$$E_0 = N(\varepsilon_0 + C - \frac{1}{2} Jz) \tag{3.19}$$

where ε_0 is the energy of a free atom, NC is the Coulomb interaction energy of the system, J is the Heisenberg exchange integral involving the ψ_n for pairs of neighboring atoms, and z is the number of nearest neighbors. The states ϕ_n are determinants of functions that differ from ϕ_0 in that the spin of an electron on the nth atom has been reversed. These N functions have the same energy and have a z component of magnetic moment equal to $(N - 2)\beta_e$, in which β_e is the Bohr magneton. The spin waves Φ_k are

$$\Phi_k = a_k \sum_n \exp(2\pi i k \cdot r(n)\phi_n) \tag{3.20}$$

and have the energy

$$E_k = E_0 + 2J \sum_\rho (1 - \exp(2\pi i k \cdot \rho)) \tag{3.21}$$

where ρ is

nearest ne:

small compe

in which t

is

$E(k_1, \cdots, k$

where

$\epsilon(k_\nu) = E_k$

The partit

by

$$f = \sum_{i=0}^{N/2} e$$

where $-\beta$

temperatu

may be re

$\epsilon(k) \simeq J$

Using th

M satisf

where ρ is summed over the vectors joining an atom with its nearest neighbors. As long as the number of spin waves is small compared with N, the energy of the crystal in a state in which there are i spin waves of wave number k_1, k_2, $\cdots$, k_i is

$$E(k_1, \cdots, k_i) = E_0 + \sum_{\nu=1}^{i} \epsilon(k_\nu) \qquad (3.22)$$

where

$$\epsilon(k_\nu) = E_k - E_0. \qquad (3.23)$$

The partition function f for the system of electrons is given by

$$f = \sum_{i=0}^{N/2} \exp\left(-\frac{E_0 - \beta_e B(N - 2i)}{kT}\right) \sum_{k_1, \cdots, k_i} \prod^{\nu=1, \cdots, i} \exp\left(-\frac{\epsilon(k_\nu)}{kT}\right) \qquad (3.24)$$

where $-\beta_e B(N - 2i)$ is the field interaction term. At low temperatures, when only the lowest levels are excited, $\epsilon(k)$ may be replaced by the value

$$\epsilon(k) \simeq J \sum (\rho \cdot k)^2. \qquad (3.25)$$

Using this approximation, Bloch found that the magnetization M satisfies the equation

$$\frac{M}{M_{\infty}} = 1 - \left(\frac{T}{\theta}\right)$$

where θ is

on the crys

Antif

constant J

them antip

on whether

state is

are paral

singlet.)

and spin

Heisenber

periodici

an arbit

obtain

propertie

more accu

There is

three di

simple

interact

theory c

down abo

exchange

so that

complet

$$\frac{M}{M_\infty} = 1 - (\frac{T}{\theta})^{3/2} \qquad\qquad (3.26)$$

where θ is the approximate Curie temperature, which depends on the crystal structure.

Antiferromagnetism arises when the exchange interaction constant J is negative between neighbors, tending to align them antiparallel. (Since J is positive or negative depending on whether the energy of the triplet state or of the singlet state is lower, this simply restates the fact that the spins are parallel in the triplet state and antiparallel in the singlet.) One can use Heisenberg's model, the Ising model, and spin wave theory to interpret antiferromagnetism. However Heisenberg's model has the following weaknesses. First the periodicity of the lattice is not taken into account. Second an arbitrary approximation (Equation (3.11)) is used to obtain the distribution of levels. Since the thermal properties are strongly dependent upon this distribution, a more accurate description is required for better calculation. There is at present no known simple derivation based on the three dimensional Ising model. Also real systems are not as simple as the Ising model since there are some other interactions besides the pairwise interactions. The spin wave theory can consider the periodicity of a crystal, but breaks down above T_c. The molecular field theory replaces all of the exchange interactions in the crystal by an effective field, so that certain properties of the $S_i \cdot S_j$ interaction are completely lost. If all of the exchange interactions are

considered

obvious co

crystal, t

exactly,

remainder

model [4

antiferrom

model modi

For a

given by

interactir

nonequival

i-spin.

neighbors

nearest n

Oguchi mo

the j spi

spin and

(with |J

Hamiltoni

$$\mathcal{H} = -g\mu B\cdot$$

where th

i-spin e

the i-sp

reduces

considered, the problem cannot be manageable. Therefore an obvious compromise is to consider some small section of the crystal, treat the exchange interactions within the section exactly, and assume the section to be coupled to the remainder of the crystal by an effective field. The Oguchi model [49] and the modified Oguchi model [50] of antiferromagnetism are based on this idea. Here the Oguchi model modified by Ohya-Nishiguchi will be described.

For a collection of spins, the Heisenberg Hamiltonian is given by Equation (3.10). Consider a pair of spins i and j interacting antiferromagnetically with each other and nonequivalently interacting with z nearest neighbors of the i-spin. The j-spin is excluded in counting the nearest neighbors. It is important to note that the number z of nearest neighbors in this model is equal to z - 1 in the Oguchi model where z is the coordination number, including the j spin. In addition to the interaction, J, between the i spin and the j spin, the inter-pair exchange interaction, J′ (with $|J'|\leq|J|$), is introduced in the system. Then the Hamiltonian can be written as

$$\mathcal{H} = -g\mu B \cdot (S_i + S_j) - 2JS_i \cdot S_j - 2J'(\sum_k S_k \cdot S_i + \sum_l S_l \cdot S_j) \qquad (3.27)$$

where the sums k and l go over the nearest neighbors of the i-spin except for the j-spin, and of the j-spin except for the i-spin, respectively. When J′ is equal to J, this model reduces to the Oguchi model. The terms S_k and S_l are replaced

by their t

the z axis

below the

field, the

and S_1 van

g is iso

reasonably

electrides

axis and

the Hamilt

$$\mathcal{H} = -2JS_i$$

where

$$a = -2xJ($$
$$b = -2xJ($$

The term

With the

and $(1/\sqrt{2}$

Equation

matrix T

$$E_1 = J(-$$
$$E_2 = J(1$$
$$E_3 = J(-$$

by their thermal mean expectation values, $\overline{S}$. If one chooses
the z axis (easy axis), along which the spins would line up
below the Néel temperature in the absence of an external
field, then the x and y components of the mean values of S_k
and S_l vanish. For the sake of simplicity, it is assumed that
g is isotropic and S is 1/2. This assumption may be
reasonably good for the trapped electrons in solids such as
electrides. By applying an external field B along the easy
axis and using two new parameters, $x = zJ'/J$ and $h = g\mu B/J$,
the Hamiltonian can be rewritten as

$$\mathcal{H} = -2J\mathbf{S}_i \cdot \mathbf{S}_j + aS_i^z + bS_j^z \tag{3.28}$$

where

$$a = -2xJ(-\overline{S} + \delta\overline{S}^z) - hJ$$
$$b = -2xJ(\overline{S} + \delta\overline{S}^z) - hJ$$

The term $\delta\overline{S}^z$ is the component added by the external field.
With the basis functions, $\alpha_i\alpha_j$, $(1/\sqrt{2})(\alpha_i\beta_j + \beta_i\alpha_j)$, $\beta_i\beta_j$,
and $(1/\sqrt{2})(\alpha_i\beta_j - \beta_i\alpha_j)$, the Hamiltonian matrix obtained from
Equation (3.28) can be diagonalized by a transformation
matrix T to yield the eigenvalues:

$$E_1 = J(-1 - 4x\delta\overline{S}^z - 2h)/2$$
$$E_2 = J(1 - 2R)/2$$
$$E_3 = J(-1 + 4x\delta\overline{S}^z + 2h)/2$$

$E_4 = J(1 +$

where

$R = (1 + 4$

The transf

$$T = \begin{pmatrix} 1 \\ 0 \\ 0 \\ 0 \end{pmatrix}$$

where sin

external

defined a

$\bar{S} + \delta\bar{S}^z =$

Since th

expand t

order te

$\bar{S} = \dfrac{}{R(\text{ex}}$

where j

is

$$E_4 = J(1 + 2R)/2 \tag{3.29}$$

where

$$R = (1 + 4x^2\overline{S}^2)^{1/2}$$

The transformation is

$$T = \begin{pmatrix} 1 & 0 & 0 & 0 \\ 0 & \cos\theta & 0 & -\sin\theta \\ 0 & 0 & 1 & 0 \\ 0 & \sin\theta & 0 & \cos\theta \end{pmatrix}. \tag{3.30}$$

where $\sin 2\theta = 2x\overline{S}/R$ and $\cos 2\theta = 1/R$. The magnetization in the external magnetic field along the z-axis is self-consistently defined as

$$\overline{S} + \delta\overline{S}^z = \mathrm{Tr}\{S^z \exp(-\beta\mathcal{H})\}/\mathrm{Tr}\{\exp(-\beta\mathcal{H})\}. \tag{3.31}$$

Since the terms containing h and $\delta\overline{S}^z$ are small, one can expand the right hand side of Equation (3.31). The zeroth order term which leads to the non-zero solution of $\overline{S}$ is

$$\overline{S} = \frac{-x\overline{S}\sinh(jR)}{R(\exp(j) + \cosh(jR))} \tag{3.32}$$

where $j = J/kT$. At the limit of $R = 1$, the Néel temperature is

$$j_{_N} = \frac{J}{kT}_{_N}$$

$$= \frac{1}{2} \ln\left(\begin{matrix} \\ \end{matrix}\right.$$

From the

susceptibi

$$\chi_{_{''}} = Ng\mu\left[\frac{\partial}{\partial}\right.$$

$$= \frac{1}{2} \frac{}{-j}$$

By a

perpendic

relation

$$2\delta\overline{S}^{x} = \text{Tr}$$

where the

$$\mathcal{H} = -2JS$$

$$= \mathcal{H}_{0} +$$

and

$$\mathcal{H}_{0} = -2$$

$$j_N = \frac{J}{kT_N}$$

$$= \frac{1}{2} \ln\left[\frac{x - 1}{x + 3}\right]. \tag{3.33}$$

From the first order term of Equation (3.31) the parallel susceptibility is obtained as

$$\chi_{\shortparallel} = Ng\mu\left(\frac{\partial \delta\bar{S}^z}{\partial B^z}\right)$$

$$= \frac{1}{2}\frac{Ng^2\mu^2\beta}{-jx + 1 + \exp(-j)\cosh(jR)} \tag{3.34}$$

By applying the external field along the x axis, the perpendicular susceptibility is obtained. The self-consistent relation becomes

$$2\delta\bar{S}^x = \mathrm{Tr}\{(S_i^x + S_j^x)\exp(-\beta\mathcal{H})\}/\mathrm{Tr}\{\exp(-\beta\mathcal{H})\} \tag{3.35}$$

where the Hamiltonian is

$$\mathcal{H} = -2JS_iS_j + 2Jx\bar{S}S_i^z - 2Jx\bar{S}S_j^x - (2Jx\delta\bar{S}^x + g\mu B^x)(S_i^x + S_j^x)$$

$$= \mathcal{H}_0 + \mathcal{H}_1 \tag{3.36}$$

and

$$\mathcal{H}_0 = -2JS_iS_j + 2Jx\bar{S}S_i^z - 2Jx\bar{S}S_j^x$$

$$\mathcal{H}_1 = - (2J\times$$

$$= \xi(S_i^x \ +$$

The eigenv

functions

(3.30):

$$E_{01} = -J/2$$
$$E_{02} = J(1$$
$$E_{03} = -J/2$$
$$E_{04} = J(1$$

According

component

$$\{T \exp[-\beta$$

$$+ \frac{\exp(}{}$$

where

$$T \mathcal{H}_1 T^{-1}$$

$$\mathcal{H}_1 = - (2J\varkappa\delta\bar{S}^x + g\mu B^x)(S_i^x + S_j^x)$$

$$= \xi(S_i^x + S_j^x)$$

The eigenvalues of $\mathcal{H}_0$ are obtained by using the same basis functions and the transformation matrix given by Equation (3.30):

$$E_{01} = -J/2$$

$$E_{02} = J(1 - 2R)/2$$

$$E_{03} = -J/2$$

$$E_{04} = J(1 + 2R)/2 \qquad (3.37)$$

According to Karplus and Schwinger's method [51], the component of the transformed matrix can be given by

$$\{T \exp[-\beta(\mathcal{H}_0 + \mathcal{H}_1)] T^{-1}\}_{ij} = \exp(-\beta E_{0i})\delta_{ij}$$

$$+ \frac{\exp(-\beta E_{0i}) - \exp(-\beta E_{0j})}{E_{0i} - E_{0j}} \{T \mathcal{H}_1 T\}_{ij}^{-1} \qquad (3.38)$$

where

$$T \mathcal{H}_1 T^{-1} = \frac{\xi}{\sqrt{2}} \begin{bmatrix} 0 & \cos\theta & 0 & \sin\theta \\ \cos\theta & 0 & \cos\theta & 0 \\ 0 & \cos\theta & 0 & \sin\theta \\ \sin\theta & 0 & \sin\theta & 0 \end{bmatrix}.$$

One can obt

Tr{exp(-β$\mathcal{H}$)

and the nu

Tr{(S$_i^x$ + S

From Equa

susceptib

$\chi_\perp$ = Ng$^2\mu$

where

ζ = (1 -

In the

coincide

(T$_N$ ≫ T)

One can obtain the denominator of Equation (3.35)

$$Tr\{\exp(-\beta\mathcal{H})\} = Tr\{\exp(-\beta\mathcal{H}_0)\}$$

$$= 2\exp(j/2)[1 + \exp(-j)\cosh(jR)] \qquad (3.39)$$

and the numerator of Equation (3.35)

$$Tr\{(S_i^x + S_j^x)\exp(-\beta\mathcal{H})\} = 2\xi(\frac{\exp(-\beta E_{01}) - \exp(-\beta E_{02})}{E_{01} - E_{02}} \cos^2\theta$$

$$+ \frac{\exp(-\beta E_{01}) - \exp(-\beta E_{04})}{E_{01} - E_{04}} \sin^2\theta).$$

$$(3.40)$$

From Equations (3.35), (3.39), and (3.40), the perpendicular susceptibility is derived as

$$\chi_\perp = Ng^2\mu^2\zeta/(-2Jx\zeta + 2JR(1 - R^2)[1 + \exp(-j)\cosh(jR)]) \quad (3.41)$$

where

$$\zeta = (1 - R^2)\exp(-j)\cosh(jR) + 2R - (1 + R^2)\exp[-j(1 - R)]$$

In the paramagnetic region ($\bar{S} = 0$), Equation (3.41) for $\chi_{\prime\prime}$ coincides with Equation (3.34) for $\chi_\perp$. At **high temperatures** ($T_N \gg T$), the susceptibilities take on a simple **form**:

$$\chi_{''} = \chi_{\perp} = \frac{N}{}$$

Then the We

$$\theta = J(\chi +$$

In the ant

with a d

constant

is given

$$\chi_{\perp 0} = - \frac{Ng}{}$$

The progr

thesis re

electrid

shown ir

critical

$\leq \chi < 1$,

there i

χ_{max},

temperat

the sus

and the

$$\chi_{/\!/} = \chi_{\perp} = \frac{Ng^2\mu^2}{4k} \cdot \frac{1}{T - J(x + 1)/2k}. \qquad (3.42)$$

Then the Weiss temperature θ becomes

$$\theta = J(x + 1)/2k. \qquad (3.43)$$

In the antiferromagnetic region $(R > 1)$, $\chi_{/\!/}$ decreases rapidly with a decrease in temperature, while $\chi_{\perp}$ gives a nearly constant value $\chi_{\perp 0}$ near absolute zero. The susceptibility $\chi_{\perp 0}$ is given by

$$\chi_{\perp 0} = -\frac{Ng^2\mu^2(x - 1)}{4Jx^2}. \qquad (3.44)$$

The program ANTIMAG (Appendix C) was written as part of this thesis research and was used to fit susceptibilities of some electrides. Some calculated magnetic susceptibilities are shown in Figure 12. At temperatures comparable to J/k, χ critically depends on the molecular field parameter, x. For $0 \leq x < 1$, the susceptibility curves show a broad maximum and there is no phase transition. The maximum susceptibility, χ_{max}, occurs at a temperature higher than the Néel temperature in the region where $1 \leq x < \sim2$. When x increases, the susceptibility at the Néel temperature approaches χ_{max} and the maximum on the susceptibility curve becomes sharp.
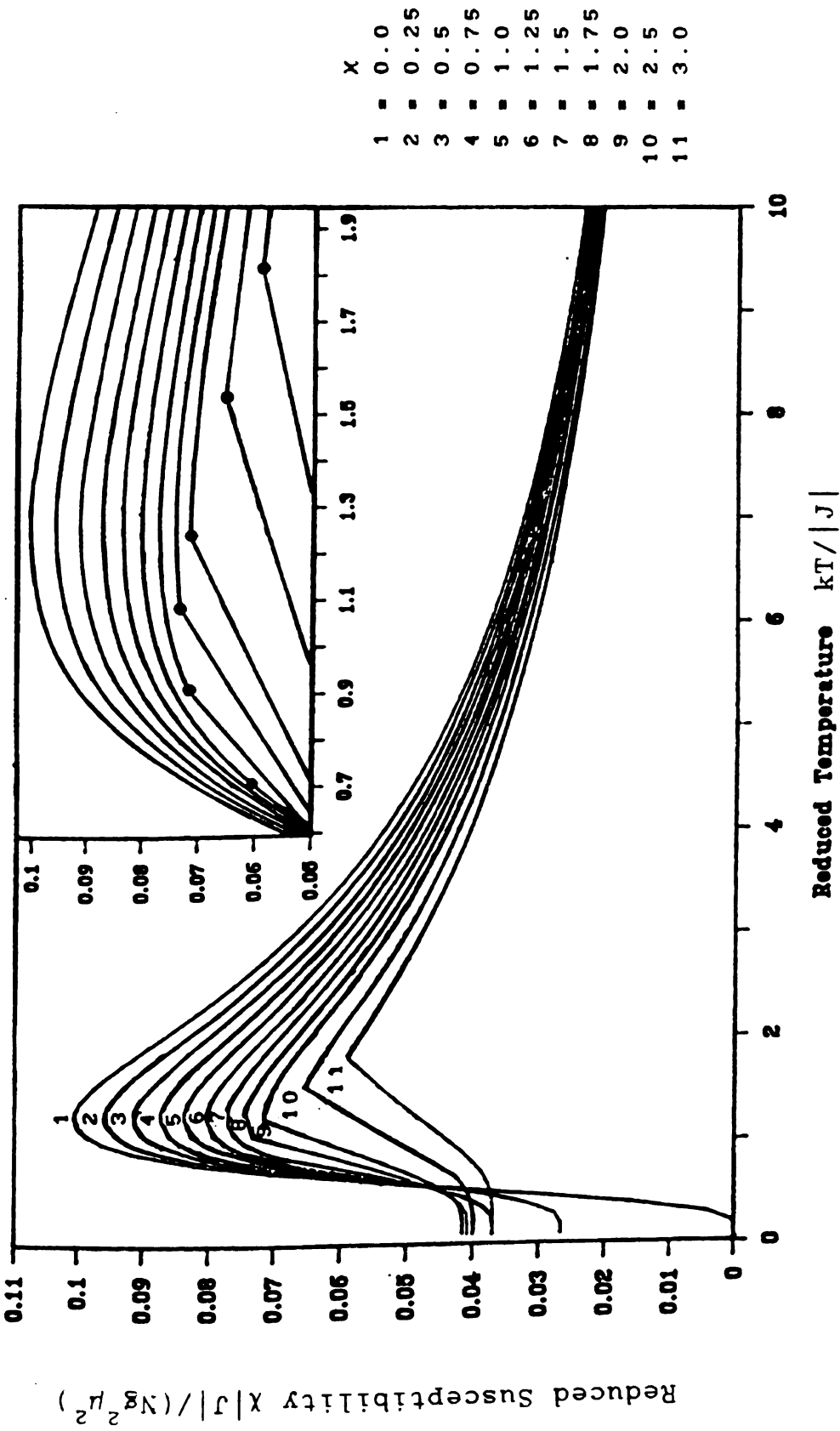
Figure 12 Calculated reduced magnetic susceptibility versus reduced temperature for x = 0.0 to 3.0. The Néel temperature are indicated on the curve in the inset.

IV. A. Sy

IV. A. 1.

Stoi

$X^- = Cl^-$

18C6, C22

salts) a

evaporat:

used fo

measurem

IV. A. 2

Abc

small be

added s

heated

the ref

had for

crystal

CHAPTER IV

EXPERIMENTAL METHODS

IV. A. Synthesis and Recrystallization of Model Salts

IV. A. 1. Method 1

Stoichiometric amounts of M^+X^- (M = Na^+, K^+, Rb^+, Cs^+; X^- = Cl^-, Br^-, I^-, SCN^-, $B(C_6H_5)_4^-$) and L (L = 12C4, 15C5, 18C6, C222) were dissolved in methanol (acetone for $B(C_6H_5)_4^-$ salts) at room temperature. Crystals formed upon very slow evaporation of the methanol. The crystals were collected and used for recrystallization and for solid state NMR measurements

IV. A. 2. Method 2

About 0.5 ml of saturated solution of M^+X^- was made in a small beaker at about $90°C$. A slight excess of complexant was added so that some crystals were formed. Then the beaker was heated to dissolve the crystals after which it was kept in the refrigerater to permit crystallization. After crystals had formed, the residual water was filtered off. Slightly wet crystals were obtained, squeezed between several dry filter

papers and

IV. A. 3.

Polyc

recrystal

ketone, o

was cover

the paraf

solvent.

listed i

prepare t

IV. B. Sy

E

IV. B. 1

The

and the

electrid

more co

electric

The syr

simpler

shown i

of a co

K-cell

papers and then dried in air.

IV. A. 3. Recrystallization

Polycrystalline samples were redissolved in a recrystallization solvent (mainly acetone, methyl ethyl ketone, or methanol) in a 50 ml Erlenmeyer flask. The flask was covered with a piece of parafilm and a small portion of the parafilm was lifted to allow very slow evaporation of the solvent. The model salts synthesized by these methods are listed in Table 7 together with the conditions used to prepare them.

IV. B. Synthesis and Recrystallization of Alkalides and
       Electrides

IV. B. 1. Synthesis

The purification procedure for solvents and metals [53] and the synthetic methods used to prepare alkalides and electrides [7] have been decribed in detail. However it was more complex and tedious to synthesize alkalides and electrides by using a synthesis apparatus called the "cow". The synthetic procedures have been improved by using a simpler apparatus called a K-cell (or Kim's cell). The K-cell shown in Figure 13 was designed by combining the advantages of a commercial H-cell [Kontes] and the cow. The evacuated K-cell and a metal ampoule [53] were taken into the

Table 7 Sy

Method 1

Method 2

Other
methods

Recrysta
llizatic

a Sample
  et al.
b Sample
  [18].

Table 7 Synthesis and recrystallization of model salts

	Solvent	Compound
Method 1	methanol	$Na^+15C5 \cdot SCN^-$, $Na^+18C6 \cdot Cl^-$, $Na^+18C6 \cdot Br^-$ $Na^+18C6 \cdot I^-$, $Na^+C222 \cdot Cl^-$, $Na^+C222 \cdot Br^-$ $Na^+C222 \cdot I^-$, $Cs^+(18C6)_2 \cdot I^-$, $Cs^+(15C5)_2 \cdot I^-$ $Cs^+18C6 \cdot SCN^-$, $Cs^+C222 \cdot SCN^-$, $Cs^+C222 \cdot I^-$ $Rb^+(15C5)_2 \cdot SCN^-$, $Rb^+C222 \cdot Br^-$, $K^+C222 \cdot SCN^-$ $K^+18C6 \cdot I^-$
	acetone	$Na^+18C6 \cdot SCN^-$, $Na^+C222 \cdot TPB^-$, $Cs^+18C6 \cdot TPB^-$ $Cs^+(18C6)_2 \cdot TPB^-$, $Cs^+(15C5)_2 \cdot TPB^-$, $Cs^+C222 \cdot TPB^-$,
	methanol toluene	$Cs^+18C6 \cdot I^- \cdot$Toluene
Method 2	water	$Na^+(12C4)_2 \cdot Cl^-$, $Na^+(12C4)_2 \cdot Br^-$ $Na^+(12C4)_2 \cdot I^-$, $Na^+(12C4)_2 \cdot SCN^-$ $Na^+15C5 \cdot Br^-$, $Na^+15C5 \cdot I^-$, $Na^+15C5 \cdot SCN^-$ $K^+(12C4)_2 \cdot I^-$, $K^+(12C4)_2 \cdot SCN$, $K^+(15C5)_2 \cdot I^-$ $K^+(15C5)_2 \cdot SCN^-$,
Other methods		Li^+TPB^{-a}
	THF/water	K^+TPB^{-a}, Rb^+TPB^{-a}, Cs^+TPB^{-a}
	1-propanol	$Cs^+(18C6)_2 \cdot SCN^{-b}$, $Cs^+18C6 \cdot I^{-b}$
Recrysta-llization	methanol	$Rb^+(15C5)_2 \cdot SCN^-$, $Cs^+18C6 \cdot SCN^-$,
	acetone	$Cs^+(15C5)_2 \cdot I^-$, $Na^+C222 \cdot Br^-$, $Na^+C222 \cdot TPB^-$ K^+TPB^-, Rb^+TPB^-, Cs^+TPB^-, $Cs^+C222 \cdot SCN^-$ $Cs^+18C6 \cdot TPB^-$, $Cs^+(18C6)_2 \cdot TPB^-$
	methyl ethyl ketone	$Cs^+(18C6)_2 \cdot I^-$

[a] Sample prepared according to the directions of Bhattacharyya et al. [52].
[b] Sample prepared according to the directions of Ellaboudy [18].

Sample
Fingers

Sample
Fingers

A

B
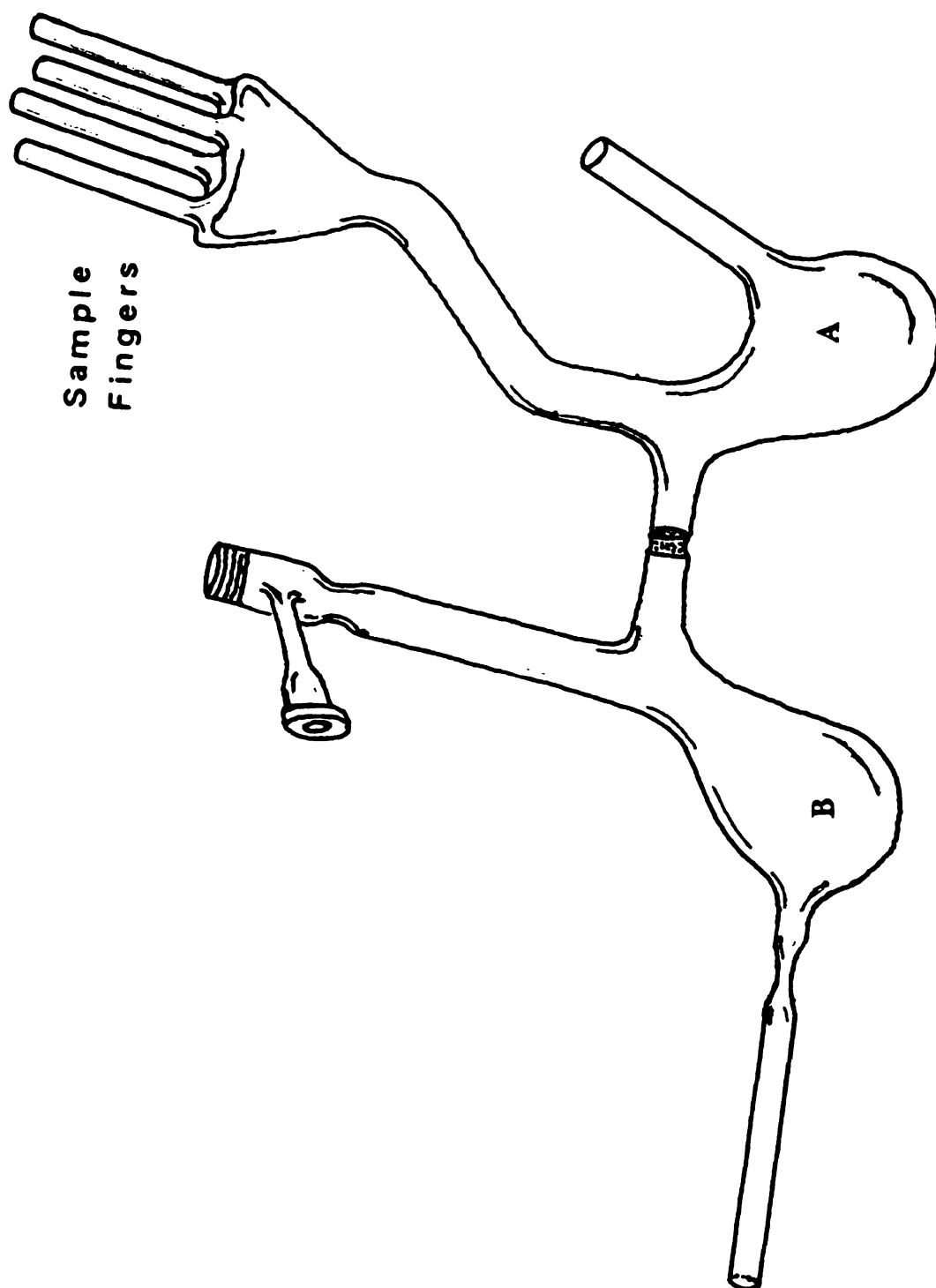
Figure 13 Apparatus for the synthesis of alkalides and electrides [K - cell].

helium-fi

through t

to which

sealed me

arm. The

unions (

removed

containi

small De

The Ultr

vacuum s

been mad

K-cell a

dimethyl

cooled

vacuum

and iso

solution

from ch

several

metal m

When t

poured

trimeth

crystal

keeping

Me_2O h

helium-filled box. The purified complexant [53] was loaded through the short side arm in the crystallization chamber A, to which the fingers for crystal harvest were attached. The sealed metal ampoule was broken and loaded in the long side arm. The side arms were sealed with two 3/8″ Ultra-torr unions (Cajon) and closed end glass caps. The K-cell was removed from the inert atmosphere box, the chamber A containing the complexant was cooled by liquid nitrogen in a small Dewar. The cell was then evacuated to 2×10^{-5} torr. The Ultra-torr unions and end caps were removed by making a vacuum seal-off of the side arms. After a metal mirror had been made by distillation, the side arm was removed and the K-cell allowed to thermally equilibrate. About 15 ml of dried dimethyl ether (Me_2O) was distilled onto the liquid nitrogen cooled complexant. The closed apparatus was removed from the vacuum line and placed in a cold bath that contained dry ice and isopropanol. When the complexant had been dissolved, the solution was poured onto the metal mirror. Me_2O was distilled from chamber B to chamber A and then poured back and forth several times to dissolve the complexant completely. The metal mirror was dissolved by gentle agitation of the K-cell. When the reaction was completed, the entire solution was poured into the crystallization chamber A. Diethyl ether, trimethylamine, or pentane was added as a co-solvent for crystallization. Me_2O was distilled into a waste bottle, while keeping a temperature gradient of about $10°C$. When most of Me_2O had been removed, the co-solvent was added one more

time. The

decanted

co-solven

the cryst

Finally t

bottle or

cell was

chamber

After di:

were imm

and stor

IV. B. 2

A s

mmole of

(either

in a co

NESLAB

was sca

At the

bath, f

distill

vacuum.

Na$^+$C222

refrige

time. The solution then became light blue and the solvent was decanted into chamber B. If washing was necessary, the co-solvent was redistilled onto the crystals. After washing the crystals, the co-solvent was again decanted to chamber B. Finally the solvent was distilled from chamber B to the waste bottle or to a liquid nitrogen trap under dynamic vacuum. The cell was removed from the vacuum line and the crystallization chamber side including "fingers" was cooled with dry ice. After distributing the crystals into the fingers, the fingers were immersed into liquid nitrogen in a Dewar, sealed off, and stored at $-80°C$ or at liquid nitrogen temperatures.

IV. B. 2. Recrystallization

A saturated methylamine solution containing about 1 or 2 mmole of $Na^+C222\cdot Na^-$ was prepared by addition of a co-solvent (either trimethylamine or diethyl ether) in a cell at $-20°$ C in a constant bath. The cell was placed in a programmable NESLAB LT-9 bath at $-20°$ C and then the crystal growing bath was scanned from $-20°$ C to $-70°$ C over a period of 48 hours. At the end of the scan the cell was placed in a $-70°$ C cold bath, followed by a decant. The decanted mother liquor was distilled off into a liquid nitrogen trap under dynamic vacuum. Some large single crystals and multiple crystals of $Na^+C222\cdot Na^-$ were harvested and stored in a vial in the refrigerator in the helium-filled dry box.

Samp

rotors wi

Co.. For

and end

tightened

coming a

Instrume

type of

rotor wa

rest to

centrifu

procedui

rates a

and el

atmosph

while i

probe.

or a h

with n

Cornin

After

Nicole

the or

T

NMR da

IV. C. NMR Experiments

Samples were loaded into cylindrical Delrin or Al_2O_3 rotors with Kel-F turbines and end caps from Doty Scientific Co.. For low temperature experiments special Kel-F turbines and end caps with center holes (Doty Scientific Co.) were tightened with Kel-F bolts and nuts to prevent them from coming apart. Also ZrO_2 rotors and Kel-F caps from Bruker Instruments, Inc. were used for the Bruker VAS probe. Each type of rotor was filled with fine powder and capped. The rotor was inserted into a stator and then brought slowly from rest to spinning at rates of 1 to 5 KHz. This allowed for centrifugal packing of the sample within the rotor. This procedure was repeated to achieve stable and high spinning rates and to enhance the signal to noise ratios. Alkalides and electrides were loaded under a cold dry nitrogen atmosphere. The samples were transferred to the spectrometer while in liquid nitrogen and inserted into the precooled NMR probe. Single crystals were mounted in a nitrogen glove bag or a helium-filled dry box onto Acrylic holders [Figure 14] with markers every 5°. Apiezon high vacuum grease or Dow Corning vacuum grease was employed for crystal mounting. After NMR experiments the crystal holder was mounted on a Nicolet P3F single crystal x-ray diffractometer to determine the orientation of the crystal with respect to the holder.

The program KINFIT [54] was used to fit single crystal NMR data. The program XTAL was also used to calculate (or to

Figure
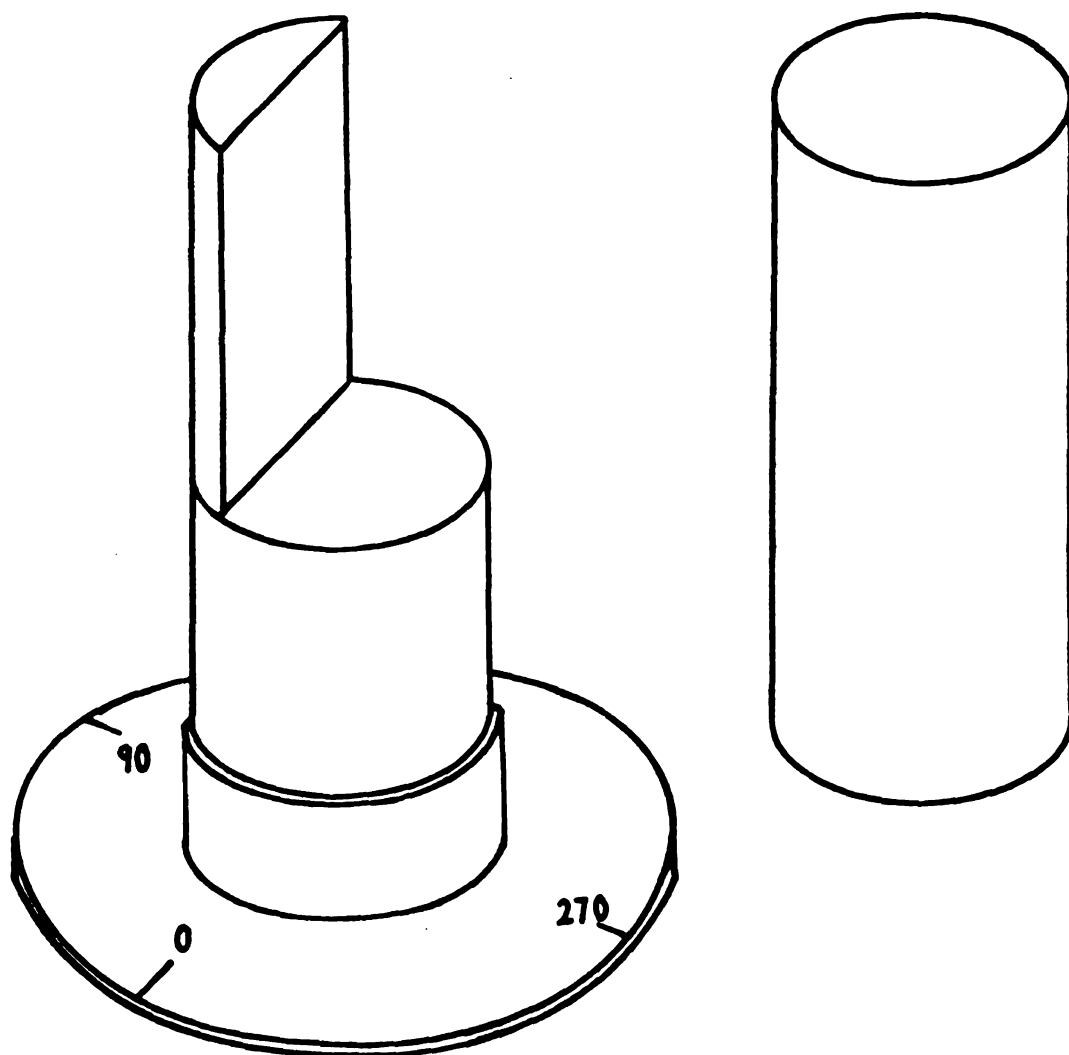
Figure 14 Single crystal holder and cap used in the single crystal NMR studies.

fit) reso

fitting w

with the

The

Bruker A}

or on a

1180 com}

mm o.d.

MHz and

capacito

to lower

23.61 MF

carried

home-bu:

obtaine

static

Univers

spectro

of Ill:

cold w

Extern;

determ

standa

for a:

Simple

during

fit) resonance frequencies in order to confirm that the fitting was correct. MAS and static spectra were simulated with the program VMASS (Appendix B).

The studies of Na^+ and Cs^+ salts were carried out on a Bruker AM 400 spectrometer equipped with a Bruker VAS probe or on a Bruker WH 180 spectrometer equipped with a Nicolet 1180 computer system and a Doty Scientific MAS probe using 7 mm o.d. rotors. This probe has a tunable range of 45 to 72 MHz and proton decoupling capabilities at 180 MHz. Additional capacitors were used with the tuning and matching capacitors to lower the probe tuning range for measurements of ^{133}Cs at 23.61 MHz and ^{39}K at 8.4 MHz. Single crystal NMR studies were carried out on the Bruker WH 180 spectrometer equipped with a home-built static probe. The ^{39}K and ^{87}Rb NMR spectra were obtained on a Bruker AM 400 spectrometer with a home-built static probe in the Department of Radiology at Michigan State University Clinical Center and an 11.7 Tesla home built spectrometer in the Department of Chemistry at the University of Illinois. A dewared NMR probe was used to keep the samples cold without cooling the electronic circuits or the magnet. External standards were used as secondary references to determine the chemical shifts; the chemical shifts of the standards were determined with respect to a value of 0.0 ppm for an infinitely dilute aqueous solution of the cation. Simple one pulse experiments with and without decoupling during acquisition were used for ^{23}Na and ^{133}Cs NMR studies.

In the case of ^{39}K and ^{87}Rb NMR, very weak free

induction

time, aft

the prob

with unw

distorti

eliminat

echo pul

destruct

construc

sequence

RD - P$_1$

where R

acquisi

θ_1 = x

θ_2 = x

θ_3 = $\bar{y}$

where

shifts

times

acquis

$\bar{x}$ $\bar{x}$ y

as fo

induction decay signals (FID) decayed within a very short time, after the strong observing pulse and before recovery of the probe circuits and receiver. Therefore the FID was mixed with unwanted extraneous signals, which produce a baseline distortion after Fourier transformation. In order to eliminate this probe ringdown, a 16 step phase cycling spin echo pulse sequence [55] was used. This phase cycling causes destructive interference of the noise signals and constructive interference of the echo signals. The pulse sequence is based on the Hahn spin echo which is given by:

$$RD - P_1(\theta_1) - D_1 - P_2(\theta_2) - D_2 - ACQ(\theta_3) \qquad (2.1)$$

where RD is a relaxation delay and ACQ is the time needed for acquisition. The phases of the pulses and the receiver were:

$$\theta_1 = x \ x \ x \ x \ y \ y \ y \ y \ \bar{x} \ \bar{x} \ \bar{x} \ \bar{x} \ \bar{y} \ \bar{y} \ \bar{y} \ \bar{y}$$

$$\theta_2 = x \ y \ \bar{x} \ \bar{y} \ x \ y \ \bar{x} \ \bar{y} \ x \ y \ \bar{x} \ \bar{y} \ x \ y \ \bar{x} \ \bar{y} \qquad (2.2)$$

$$\theta_3 = \bar{y} \ y \ \bar{y} \ y \ \bar{x} \ x \ \bar{x} \ x \ \bar{y} \ y \ \bar{y} \ y \ \bar{x} \ x \ \bar{x} \ x$$

where x, y, $\bar{x}$, $\bar{y}$ represent $0°$, $90°$, $180°$, and $270°$ phase shifts respectively. The intervals D_1 and D_2 are the delay times for echo formation between the two pulses and acquisition. Since the phases of the receiver were fixed (x x $\bar{x}$ $\bar{x}$ y y $\bar{y}$ $\bar{y}$), the phases of the two pulses have been modified as follows:

$\theta_1 = y\ y\ $

$\theta_2 = y\ \bar{y}\ $

The pulse

pulse fo

for soli

solution

sequence

quadrupo

[56], th

and this

Fortunat

used. Ir

circuits

pulse t

group,

enough.

echoes

elimina

procedu

lasts

differe

echo e

on the

a norr

buried

15 b)

$$\theta_1 = y \ y \ y \ y \ x \ x \ x \ x \ \bar{y} \ \bar{y} \ \bar{y} \ \bar{y} \ \bar{x} \ \bar{x} \ \bar{x} \ \bar{x} \tag{2.3}$$

$$\theta_2 = y \ \bar{y} \ x \ \bar{x} \ y \ \bar{y} \ x \ \bar{x} \ y \ \bar{y} \ x \ \bar{x} \ y \ \bar{y} \ x \ \bar{x}.$$

The pulse widths, P_1 and P_2 were used either a 45° or a 90° pulse for quadrupolar nuclei in solids. Usually a 90° pulse for solids was taken as half of a 90° pulse for aqueous solution. Spectra were obtained by using both a 45°-90° pulse sequence and a 90°-90° pulse sequence. Since the 90° pulse for quadrupolar nuclei depends on the QCC and nuclear spin I [56], the 90° pulse should be determined for every compound and this is impossible for compounds containing these nuclei. Fortunately, it was not important that accurate 90° pulses be used. Instead, a relatively good quality factor of the probe circuits was required. It seems that the shorter the 90° pulse the better. According to the experience of the Dye group, 90° pulses for liquid samples less than 14 µs are good enough. One desires the minimum delay time for formation of echoes that are free of ringing, since longer delays can eliminate the ringing but reduce signal intensity. The best procedure is to determine how long the probe ringdown signal lasts with an empty probe. Figure 15 illustrates the difference between a normal one pulse experiment and a spin echo experiment for [39]K NMR and the effect of the delay times on the spin echo spectra. Figure 15 a) shows a spectrum from a normal one pulse experiment, in which the KSCN peak is buried under the distorted base line. The spectrum in Figure 15 b) shows the partial removal of the baseline distortion
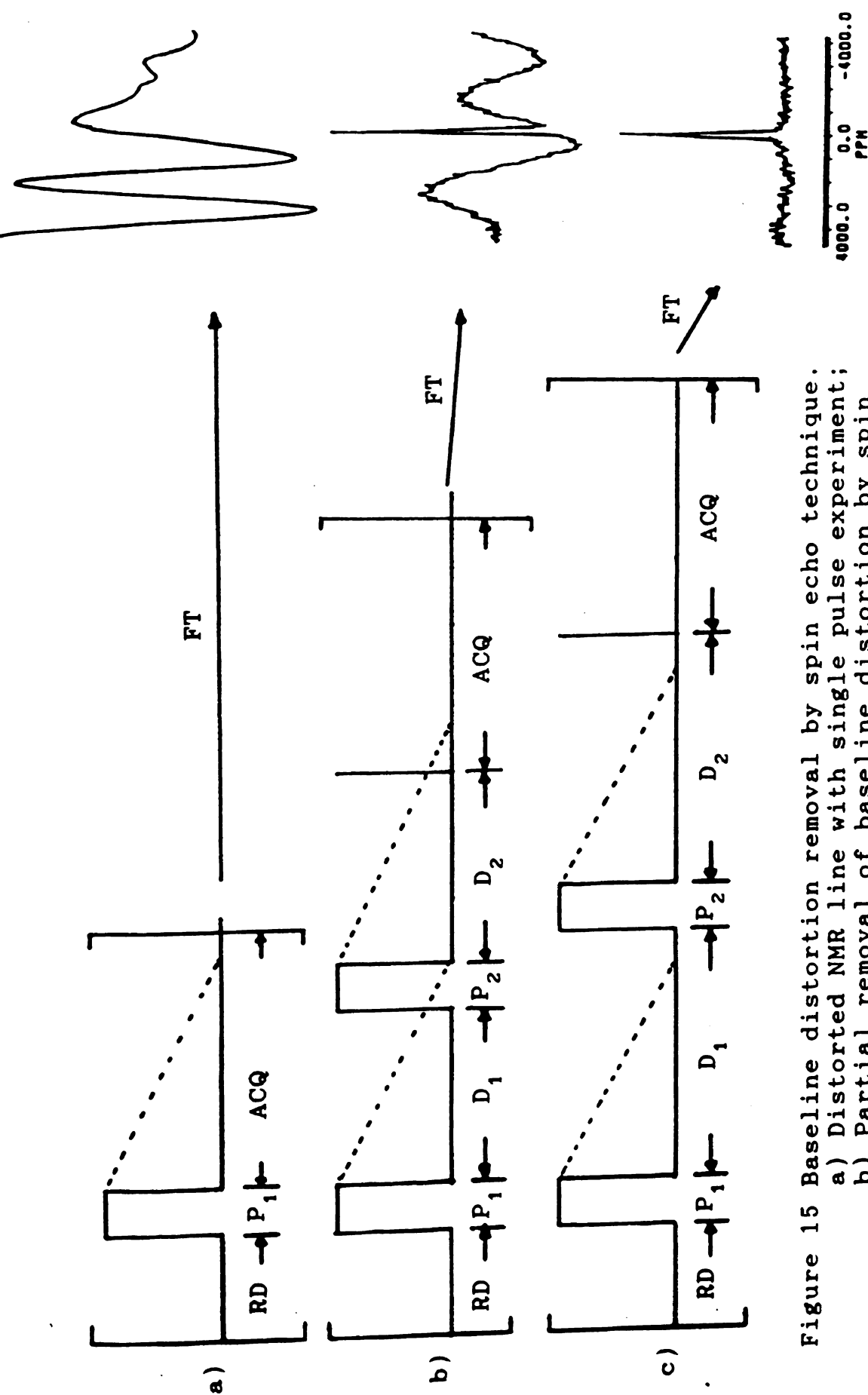
Figure 15 Baseline distortion removal by spin echo technique.
a) Distorted NMR line with single pulse experiment;
b) Partial removal of baseline distortion by spin
echo experiment with insufficient delays;
c) Distortion free NMR spectrum by spin echo
experiment with sufficient delays.

with two

spectrum

times wer

with two short delay times. However the most distortion free
spectrum shown in Figure 15 c) was obtained when long echo
times were used.

Thi

alkali r

model

studies

discuss

Chapter

V. A. A

V. A. 1

F:

crysta

Co. MA

result

spin 3

the pi

those

Hz.

signif

surrou

CHAPTER V

RESULTS AND DISCUSSIONS

This chapter is divided into two areas. The first is alkali metal NMR studies of alkalides, electrides and related model compounds. The second is magnetic susceptibility studies of electrides. The experimental data are analyzed and discussed based on the theories which were described in Chapters II and III and on the structures of the compounds.

V. A. Akali Metal NMR
V. A. 1. A Single Crystal NMR Study of $Na^+C222 \cdot Br^-$

Figure 16 shows the ^{23}Na NMR spectra of the single crystal $Na^+C222 \cdot Br^-$, obtained by using the Doty Scientific Co. MAS probe on a Bruker WH 180 spectrometer. The spectra result from three transitions of a quadrupolar nucleus with spin 3/2. The linewidth $\Delta\nu_{1/2}$ of the central transition of the proton coupled spectrum is about 2600 ± 200 Hz, while those of the proton decoupled spectra vary from 200 Hz to 500 Hz. This linewidth reduction suggests that there are significant interactions between the sodium nucleus and its surrounding protons. More discussions about dipolar

a)

b)

Figure
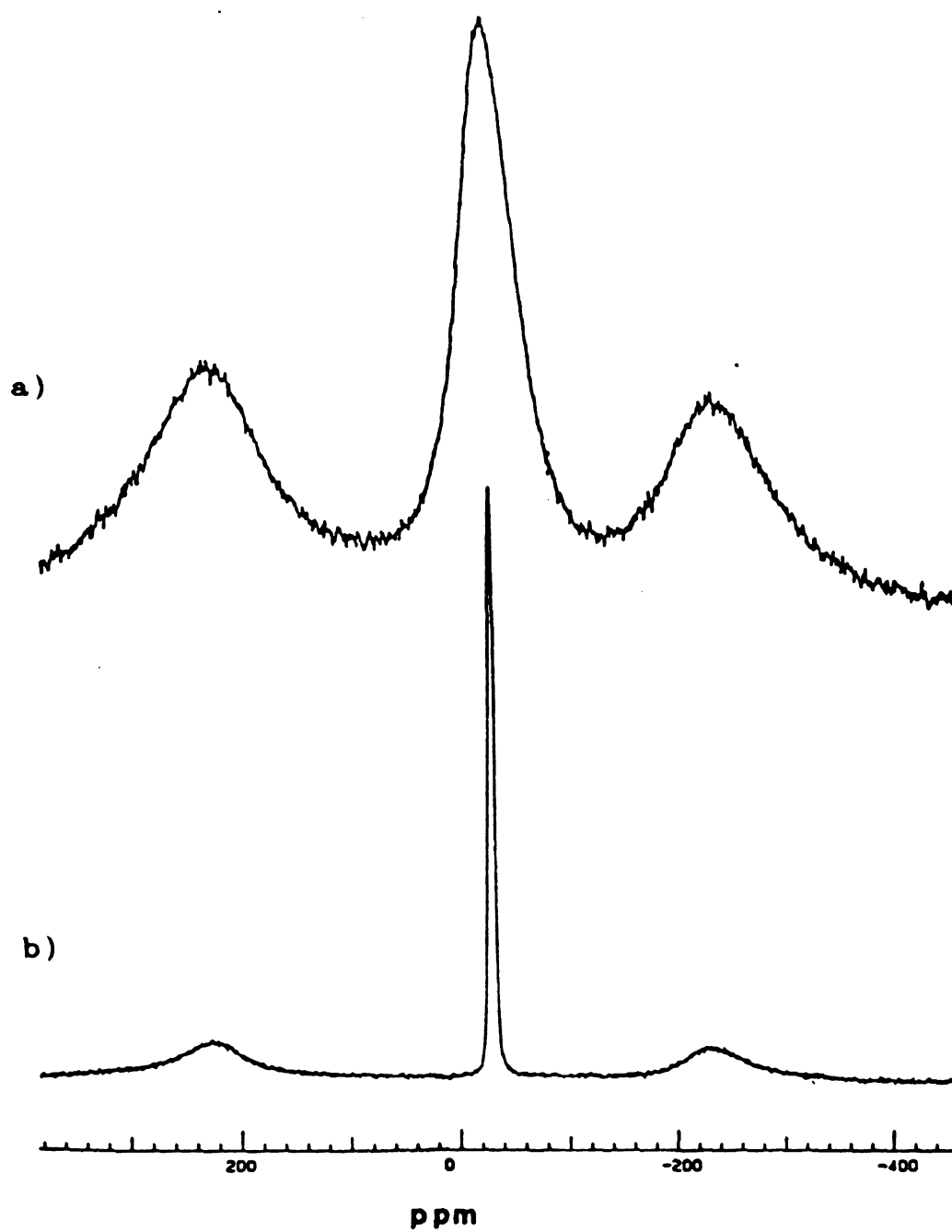
Figure 16 Single crystal ^{23}Na NMR spectra of Na$^+$C222·Br$^-$ at ν_L = 47.61 MHz.

a) Proton coupled; b) Proton decoupled.

interact

The

satellit

a distri

relaxati

orientat

magneti

orienta

satelli

Because

proport

central

is only

This i

relaxa

intera

on the

F

plot i

of t

envir

orien

syste

value

of th

by u

equat

interactions will be included in other sections.

The different linewidths of the central transition and satellites at various orientations indicate that there may be a distribution of quadrupolar coupling constants or that the relaxation time T_2^* of a single crystal varies with the orientation of the crystal with respect to the external magnetic field. However, it is very difficult to study this orientation dependent linewidth since only a few spectra show satellites within the sweep width of the spectrometer. Because the peak positions of the satellites are directly proportional to the QCC they are much broader than the central transition. The linewidth of the central transition is only slightly dependent on the orientation of the crystal. This implies that the effects of orientation dependent relaxation times, T_2 and T_1, orientation dependent dipolar interactions, or the distribution of electric field gradients on the linewidth of the central transition is small.

Figure 17 shows that the periodicity of the orientation plot is not π for a tilted goniometer. Although the structure of this compound is not known, an axially symmetric environment of Na^+ was assumed in order to fit the orientation plot. Without including CSA there is a slight systematic deviation between the experimental values and values calculated by using only the second order expression of the quadrupolar Hamiltonian. An excellent fit is obtained by using KINFIT [54] and XTAL (Appendix A), in which the equations include both first order CSA terms and second order
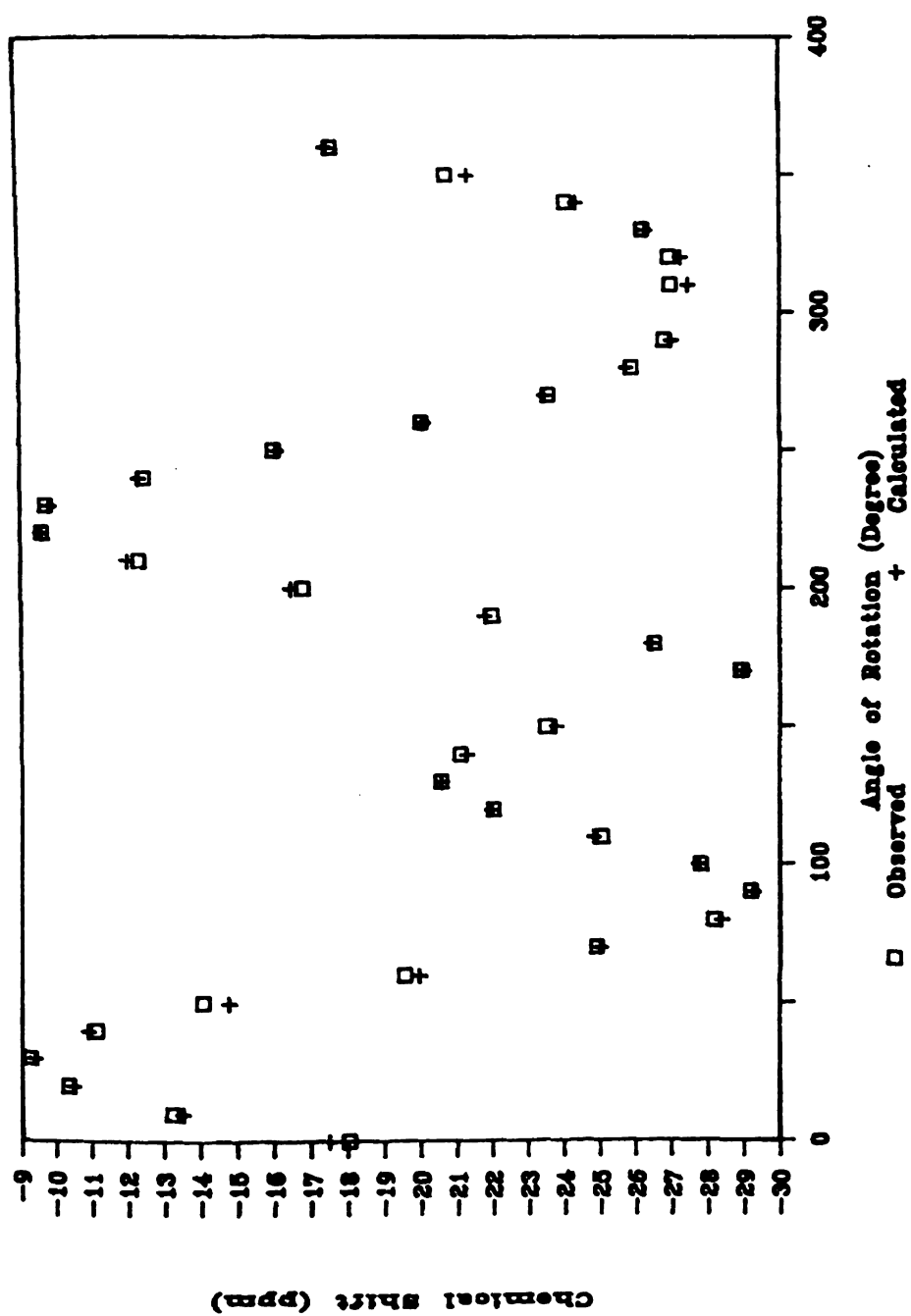
Figure 17 Angular dependence of the central transition of ^{23}Na in a single crystal $Na^+C222\cdot Br^-$.

quadrupo

determin

δ_{zz}= -14

0.605 MH

= 73.15

since t

symmetr

will be

salts

Because

of thi

correla

cannot

CSA ter

three-

A

χ, η^Q,

basis

obtain

powder

V. A.

alkal

was u

anion

quadrupolar terms. The chemical shift parameters thus determined are δ_{iso} = -16.25 ppm, δ_{XX} = δ_{YY} = -16.92 ppm, and δ_{ZZ} = -14.92 ppm. The quadrupolar coupling constant, χ, is 0.605 MHz , and the Eulerian angle angles are β = 48.31° and γ = 73.15°. The Eulerian angle α can be chosen arbitrarily since the resonance position of a nucleus with axially symmetric coupling tensors is independent of the angle α. As will be discussed later, the powder patterns of most Na^+C222 salts support an axially symmetric environment for Na^+. Because both the orientation of the crystal and the structure of this compound are unknown, information about the correlation between these tensors and the crystal structure cannot be obtained. Presumably, the principal Z axis of the CSA tensor and the quadrupolar coupling tensor lie along the three-fold axis.

A single crystal NMR study is the best way to determine χ, η^Q, and the chemical shift parameters, and provides a basis for understanding powder patterns. The parameters obtained will be used in order to calculate static and MAS powder patterns.

V. A. 2. A Single Crystal NMR Study of $Na^+C222 \cdot Na^-$

This is the first single crystal NMR study of an alkalide or electride. As mentioned in the Introduction, it was unknown whether the narrow single peaks of alkali metal anions are broadened by quadrupolar interactions. The single

crystal l

the peal

satellit

with I =

Fig

of the

respecti

frequenc

spectrun

decoupl

for a p

a singl

(2.55)

differe

and th

ration

arbitr

made.

intera

to us

chemi

cryst

tempe

centr

cryst

addi

crystal NMR spectrum shown in Figure 18 clearly proves that the peaks originate from a central transition and two satellite transitions of the half integer spin ^{23}Na nucleus with I = 3/2.

Figure 18 a and 18 b are the single crystal NMR spectra of the compound without and with proton decoupling, respectively, at an arbitrary orientation at the resonance frequency, 47.61 MHz. The linewidth of the proton coupled spectrum is about 2270 ± 100 Hz and that of the proton decoupled one is about 400 ± 50 Hz. A calculated linewidth for a powder sample of Na$^+$C222·Na$^-$ [17] is about 3670 Hz. For a single crystal, the term $\sum_{jk} (1 - 3\cos^2\theta_{jk})^2$ in Equation (2.55) cannot be replaced by its average value, 4/5. Thus a difference between the value observed for the single crystal and the value calculated for a powdered sample can be rationalized. The linewidth for a single crystal at an arbitrary orientation can be calculated but no attempt was made. The NMR line was broadened by strong dipolar interactions from many surrounding protons. It was necessary to use a proton decoupler in order to accurately measure chemical shifts and to improve the signal-to-noise ratio.

Figure 19 illustrates the spectra of the bronze single crystal of the compound at arbitrary orientations at a temperature of about -50 $^\circ$C. The chemical shifts of the central transitions for Na$^+$ vary with the orientation of the crystal due to the second order quadrupolar shift. In addition to the shift, the linewidth of Na$^+$ strongly depends
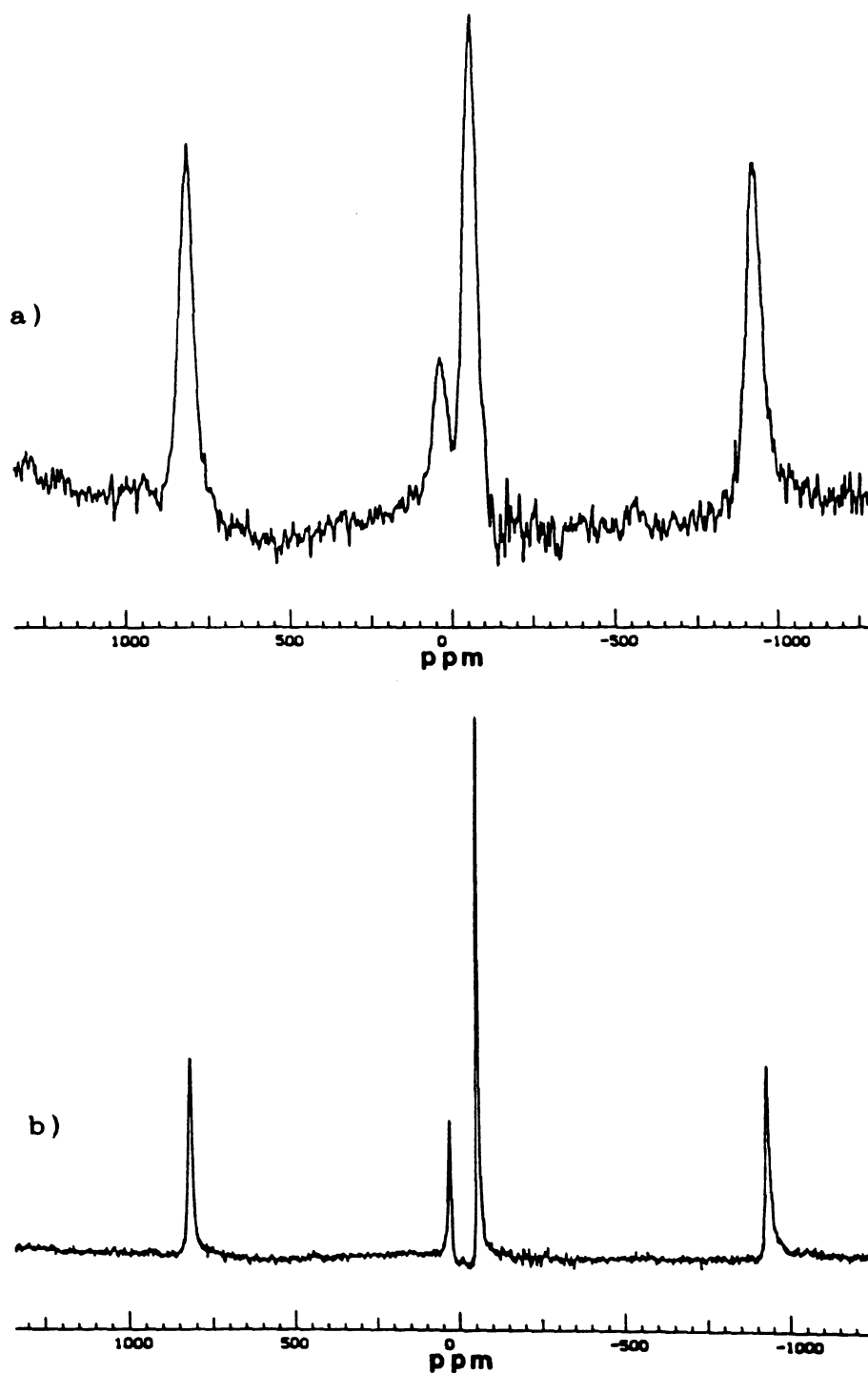
Figure 18 ^{23}Na NMR spectra of a single crystal Na^{+}C222·Na^{-} at ν_{L} = 47.61 MHz.

a) Proton coupled; b) Proton decoupled.
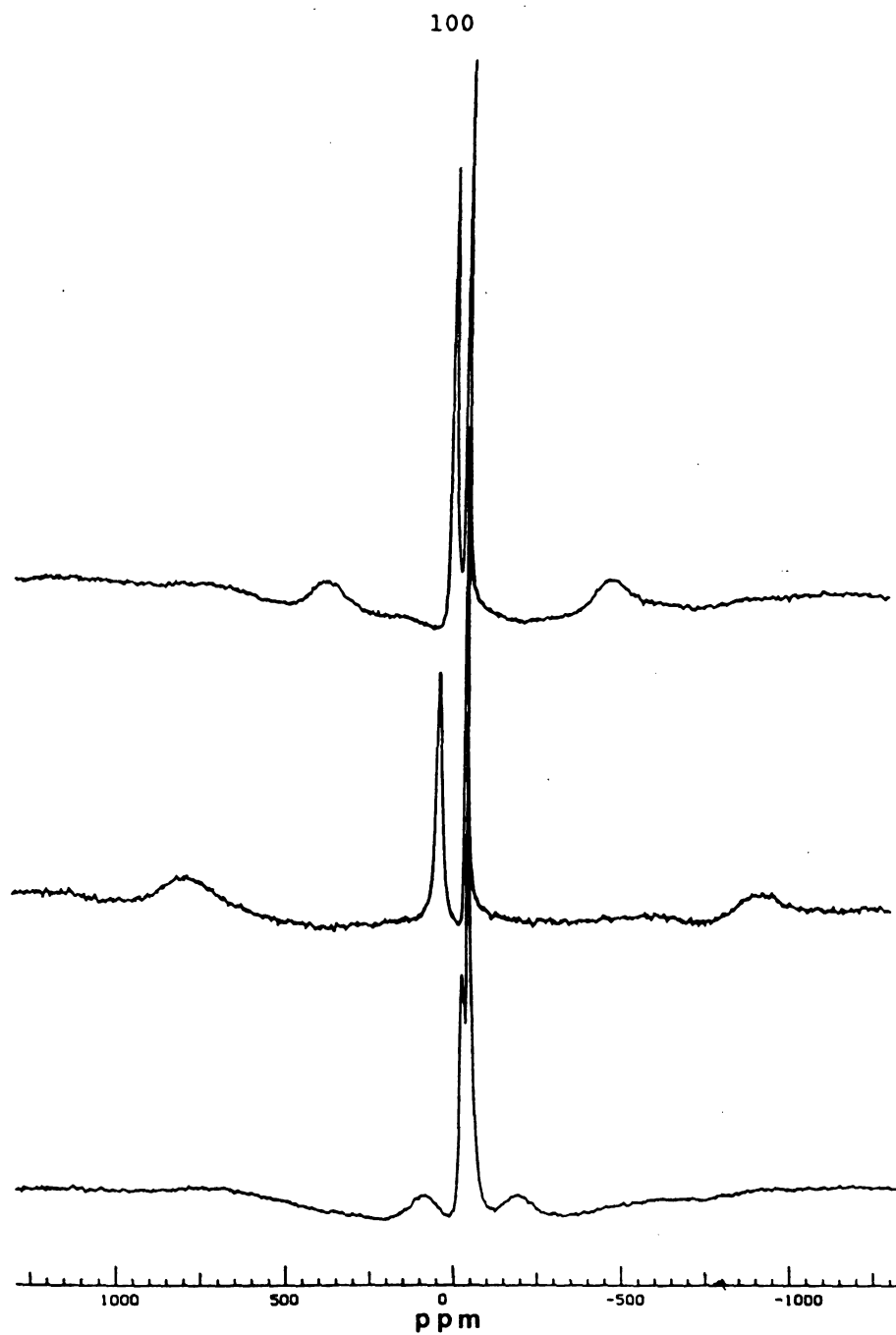
Figure 19 Single crystal ^{23}Na NMR spectra of Na$^+$C222·Na$^-$ at three different orientations, at ν_L = 47.61 MHz.

on the

external

relaxati

the full

effectiv

$\Delta\omega_{1/2}= 2$

with

$(T_2^*)^{-1}$

where t

second

linewi

β spi

fluctu

that

depend

impuri

and c

orien

shape

MAS s

patte

anisc

sodi

on the orientation of the crystal with respect to the external field because the encapsulated Na^+ has a different relaxation times T_2^* at different orientations. Frequently, the full width at half-height, $\Delta\omega_{1/2}$, is used to define an effective relaxation time, T_2^* by means of the relation

$$\Delta\omega_{1/2} = 2/T_2^* \qquad (5.1)$$

with

$$(T_2^*)^{-1} = T_2^{-1} + (2T_1)^{-1}$$

where the first term is the spin-spin relaxation rate and the second term is the field inhomogeneity contribution to the linewidth. The T_2 rate depends on the lifetimes of the α and β spin states, the T_1 rate is a contribution due to fluctuations in the energy difference between the two levels, that is, the z components of the local field. Orientation dependent relaxation times T_2 and T_1 due to paramagnetic impurities, dipolar interactions, quadrupolar interactions, and changes in these interactions due to defects can cause orientation dependent linewidths. Therefore the powder line shape of Na^+ of this compound might be distorted. However the MAS spectrum shown in Figure 20 is a good second order powder pattern due to the elimination of the orientation dependent anisotropy broadening by MAS. Satellite transitions of the sodium cation have not been seen in this experiment (a total
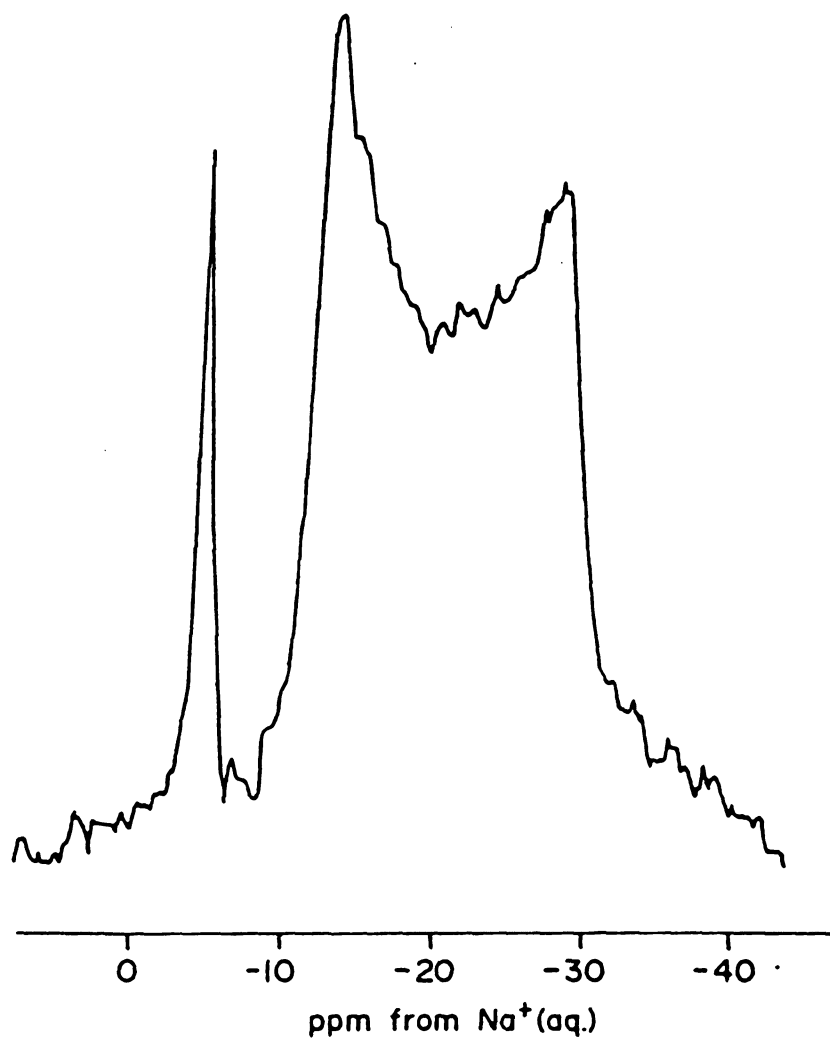
Figure 20 MAS ^{23}Na NMR spectrum of $Na^+C222 \cdot Na^-$ at ν_L = 52.94 MHz [17].

of 120

buried

sweepwid

Na⁻ is

the pos

orienta

interac

Th

black N

the res

freque

cation

crysta

room

partic

const

MHz.

chang

local

cause

stud:

prob:

thos

blac

diff

show

of 120 orientations). Presumably broad satellites must be buried under the baseline or are beyond the spectrometer sweepwidth. While the frequency of the central transition of Na^- is nearly independent of the orientation of the crystal, the positions of the satellite transitions vary with the orientation of the crystal due to the first order quadrupolar interactions.

The spectra shown in Figure 21 were obtained from a black $Na^+C222 \cdot Na^-$ crystal at room temperature. In contrast to the result with the bronze crystal at lower temperatures, the frequency of the central transition of the cryptated sodium cation is almost independent of the orientation of the crystal and the satellites of Na^+ in the black crystal at room temperature have occasionally been observed at particular orientations. Presumably, the quadrupolar coupling constant of Na^+ has been reduced to the range of 0.3 ~ 0.6 MHz. The reason for this change is not clear but a structural change with temperature (possibly a phase transition or a local structural change due to thermal motion of atoms) might cause the change. Both black and bronze crystals should be studied at different temperatures in order to solve this problem. However the peaks of Na^- are almost the same as those of the bronze crystal. This fact indicates that the black crystal still contained sodide ions.

The single crystal NMR spectra of two bronze crystals at different temperatures are shown in Figure 22. It clearly shows that the line is narrower at higher temperature,
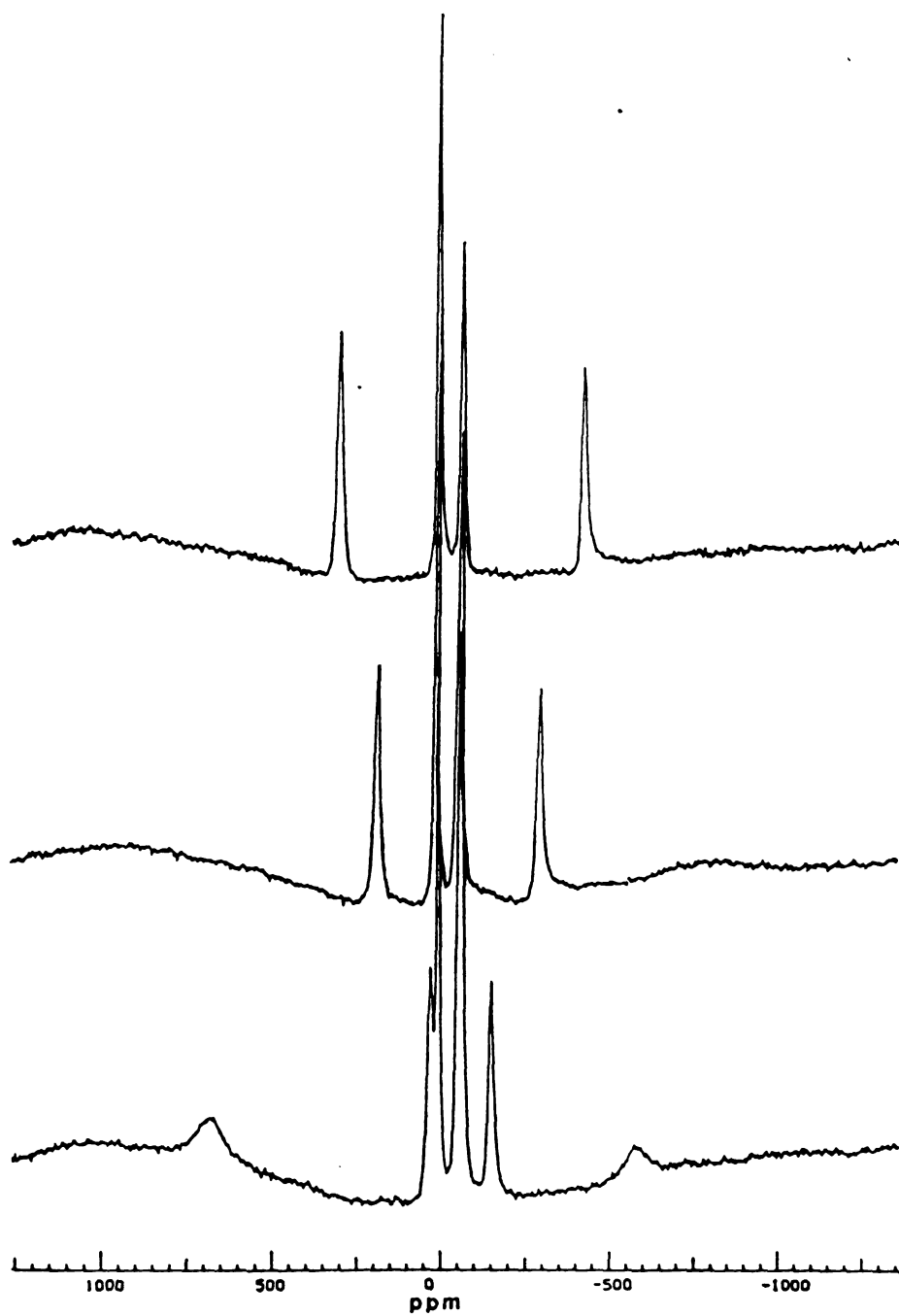
Figure 21 Three orientation dependent ^{23}Na NMR spectra at ν_L = 47.61 MHz for a black single crystal of Na$^+$C222·Na$^-$ at room temperature.
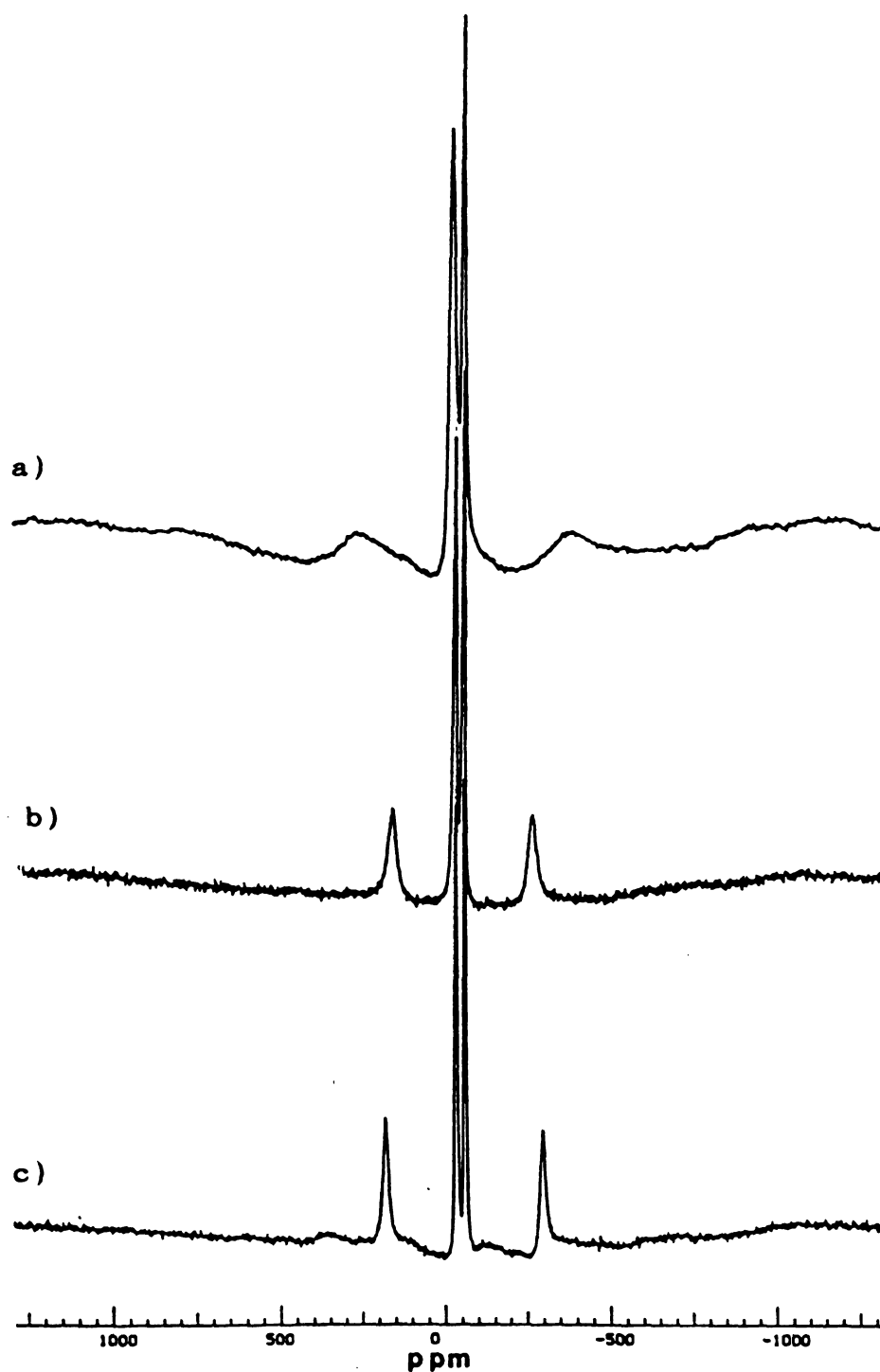
Figure 22 ^{23}Na NMR spectra of two single crystals of Na$^+$C222·Na$^-$ at different temperatures, at ν_L = 47.61MHz.
a) Crystal 1 at ~-50°C.;
b) Crystal 2 at ~-30°C.; c) Crystal 2 at ~-20°C.

probabl

cryptan

-4 °C

of 0.0

powder

F

single

around

edge

the c

orien

satell

to t

trans

chemi

a dev

i.e.

the

meth

usin

1.26

ppm

chem

are

iso

wer

val

probably due to line narrowing by the thermal motion of the cryptand. Later, an Na^- powder pattern of $Cs^+(18C6)2 \cdot Na^-$ at $-4\,^{\circ}C$ [57] was observed and a quadrupolar coupling constant of 0.090 MHz was obtained from the two singularities of the powder pattern of the satellites.

Figure 23 shows the orientation plots of one of the single crystals of $Na^+C222 \cdot Na^-$. The crystals were rotated around three orthogonal axes, one of which is parallel to an edge of the crystal. Figure 23a is the orientation plot of the central transitions for Na^+, while Figure 23b is the orientation plot of half of the distance between the two satellite transitions for Na^-. These transitions correspond to the first order quadrupolar shifts for either the transition (3/2,1/2) or the transition (-1/2,-3/2). The chemical shifts at 0° and 180° are slightly different due to a deviation of the principal axes from the goniometer axis, i.e. none of the principal axes are parallel to an edge of the single crystal. In this case, analysis by the Volkoff method [28] is very difficult. However KINFIT [54] analysis using XTAL (Appendix A) yielded a very accurate QCC, $\chi = 1.268 \pm .008$ MHz, isotropic chemical shift, $\delta_{iso} = -5.5 \pm 0.6$ ppm for Na^+ and QCC, $\chi = 0.1763 \pm 0.0003$ MHz, isotropic chemical shift, $\delta_{iso} = -61.8 \pm 0.9$ ppm for Na^-. The results are summarized in Table 8. A QCC, $\chi = 1.2 \pm 0.1$ MHz and an isotropic chemical shift, $\delta_{iso} = -6.5 \pm 0.5$ ppm for Na^+ [17] were obtained by simulation of the MAS spectrum and the values agreed well with the above results within experimental

a)

b)
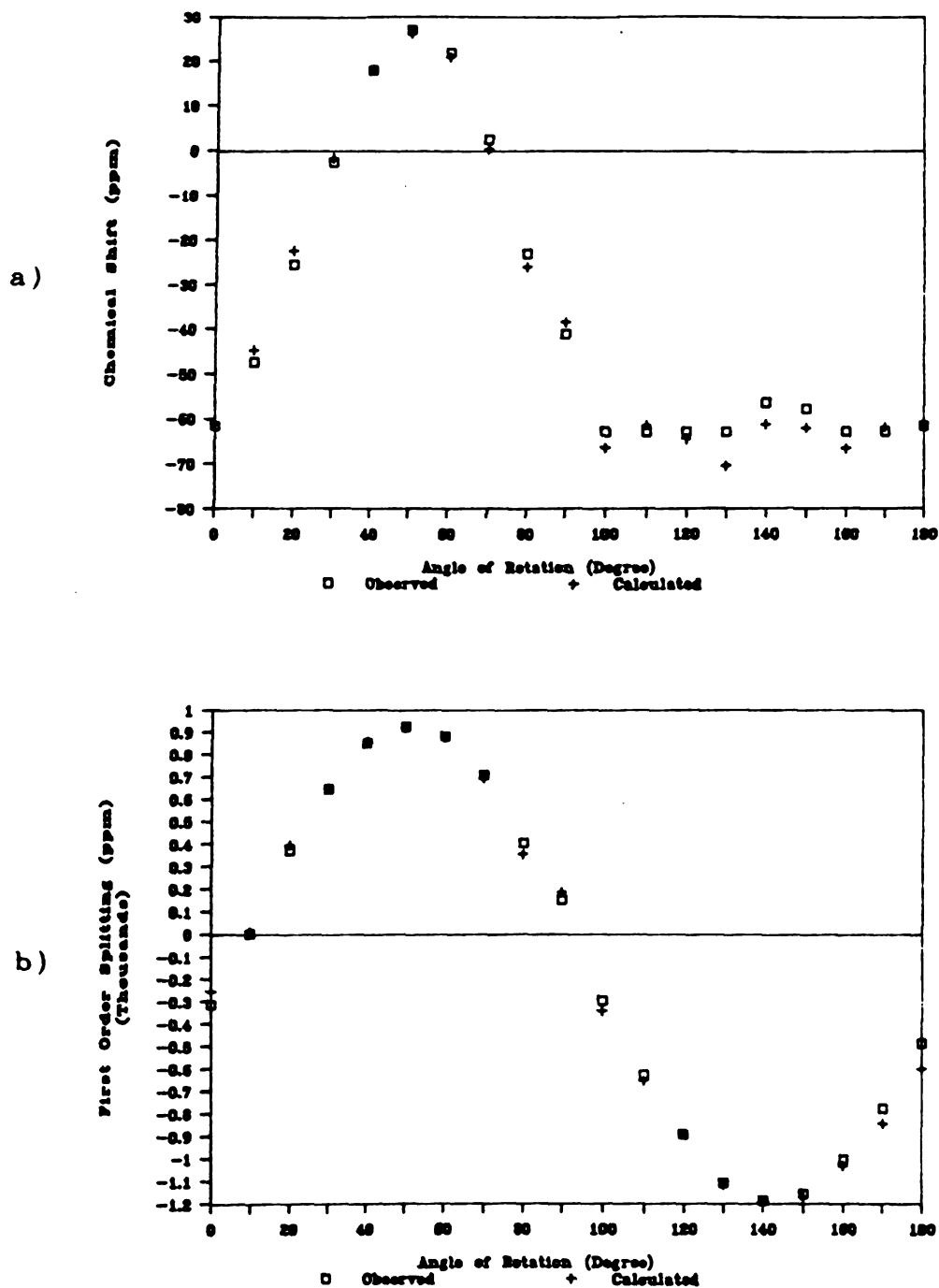
Figure 23 Angular dependence of the ^{23}Na NMR transitions in
a single crystal of Na$^+$C222·Na$^-$.
a) Chemical shift variation of the central
transition of Na$^+$;
b) Half the separation between the satellites of
Na$^-$.

Table 8

ax:
1

Na$^+$ 2

3

1,

1

Na$^-$ 2

1

*Resu

Table 8 The results obtained from a single crystal ^{23}Na NMR
study of Na$^+$C222·Na$^-$

	axis	χ, (MHz)	δ(ppm)	β(°)	γ(°)
Na$^+$	1	1.274±0.014	-6.2±0.98	60.83	38.27
	2	1.268±0.013	-5.1±0.92	56.39	148.87
	3	1.261±0.012	-5.3±0.81	48.38	42.62
	1,2,3	1.268±0.008[*]	-5.5±0.6[*]		
Na$^-$	1	0.1764±0.0004	-61.8±0.9	60.83	38.27
	2	0.1763±0.0005	-61.8±0.9	56.39	148.87
	3	0.1762±0.0009	-61.8±0.9	48.38	42.62
	1,2,3	0.1763±0.0003[*]			

[*]Results from multiple data set KINFIT analysis

error.

both

Presum

the sa

are d

chemic

tensor

experi

and

orien

sodiu

elect

This

unit

A. I

cati

pseu

plan

and

indi

requ

axi

pos

wit

tem

to

an

error. Principal axes and quadrupolar coupling tensors for both Na^+ and Na^- are parallel and axial respectively. Presumably the local symmetries for both Na^+ and Na^- are of the same type, even though the magnitudes of the interactions are different. There may be a small anisotropy of the chemical shift tensor associated with Na^+. However, the tensor was not extractable from data obtained in this experiment since the NMR peaks for both Na^+ and Na^- overlap and the NMR peaks for Na^+ are broadened at these orientations. The small quadrupolar coupling constant of the sodium anion implies that there is little perturbation of the electron cloud of Na^- from surrounding protons and charges. This compound is rhombohedral, with space group R32 [58]. The unit cell is hexagonal (Z = 3) with a = 8.83 Å and c = 29.96 Å. It can be described as closest-packed sodium cryptate cations with the sodium anions occupying the pseudo-octahedral holes. The sodium anions form parallel planes perpendicular to the three-fold axis. Also, both Na^+ and Na^- have a local three-fold symmetry axis, which indicates that they have axially symmetric tensors. This requires that one of the principal axes (the principal Z axis) is along the three fold axis. Unfortunately it was not possible to determine the absolute orientation of the crystal with respect to the goniometer since it is so air- and temperature-sensitive. In addition, the crystal was too large to handle conveniently in the X-ray diffractometer. There was an attempt to determine the absolute orientation of a crystal

before

crystal

gave di

Th

is one

study

has be

broade

satell

determ

Also

orient

coupl

V. A.

[8],

pres

insu

obta

unce

obs

pri

sin

dif

before measuring the single crystal NMR spectra, but the crystal turned black after the X-ray study, and as a result gave different spectra as mentioned previously.

This section shows that single crystal NMR spectroscopy is one of the most powerful techniques available for the study of alkali metals in alkalides and electrides. Also it has been shown that the NMR line of the sodide anion is broadened by quadrupolar interactions. The location of the satellites as a function of orientation provided an accurate determination of the quadrupolar coupling constant of Na^-. Also the variation of the frequency of the Na^+ signal with orientation yielded an accurate value of its quadrupolar coupling constant.

V. A. 3. A Single Crystal ^{133}Cs NMR Study and a Powder Lineshape of $Cs^+(15C5)_2 \cdot I^-$

The title compound was studied as a powder by our group [8], but the results differ from those obtained in the present study. The reasons for these differences are insufficient data collection, and the fact that information obtained from powder patterns contains relatively large uncertainties since the singularities of a powder pattern are obscured by line broadening. In order to obtain the six principal tensor values and the three Eulerian angles from a single crystal study, at least five to eight spectra at different orientations are required for an axially symmetric

or non-

the fac

paramet

shift

Q.C.C.

previo

62.0

and η^Q

Figure

proce

corre

trans

progr

obtai

dista

tens

Also

yiel

as t

Both

The

cou

$|V_{YY}$

tet

13.

fac

or non-axially symmetric case respectively. This is due to the fact that the line positions are functions of the unknown parameters, χ, η^Q, δ_{XX}, δ_{YY}, δ_{ZZ}, α, β, and γ. The chemical shift parameters δ_{iso} = 29 ppm, δ^{CSA} = 52 ppm, η^{CSA} = 0, and Q.C.C. χ = 0.427 MHz and η^Q = 0 were obtained from the previous study. In this study the tensor parameters δ_{XX} = 62.0 ppm, δ_{YY} = 46.1 ppm, δ_{ZZ} = -28.4 ppm, χ = 0.5810 MHz, and η^Q = 0.4755 were extracted by fitting the data shown in Figures 24 and 25 by Equation (2.18) with KINFIT [54]. This procedure is known as the Volkoff method [28]. In order to correct for the second order quadrupolar shift of the central transition (or the center of gravity of the satellites), the program XTAL (Appendix A) was used with the parameters obtained by fitting the pure quadrupolar splittings (the distances between transitions (3/2,1/2) and (-1/2,-3/2)). The tensors of ^{133}Cs and direction cosines are given in Table 9. Also, the least-squares fit of the data by Equation (2.35) yields three principal components of the CSA tensor as well as the quadrupolar coupling tensor and three Eulerian angles. Both methods gave the same results within experimental error. The principal axes of both the CSA and the quadrupolar coupling tensors are coincident; in addition $|V_{ZZ}| \geq |V_{XX}| \geq |V_{YY}|$ and $|\delta_{ZZ} - \delta_{iso}| \geq |\delta_{XX} - \delta_{iso}| \geq |\delta_{YY} - \delta_{iso}|$.

From the previously determined crystal structure [8] the tetragonal space group, I4, the unit cell dimensions, $a = b =$ 13.173 A, c = 16.645 A, and z = 4 were obtained with an R factor of 8.6 % and an R_w factor of 11.6 %. Because of the
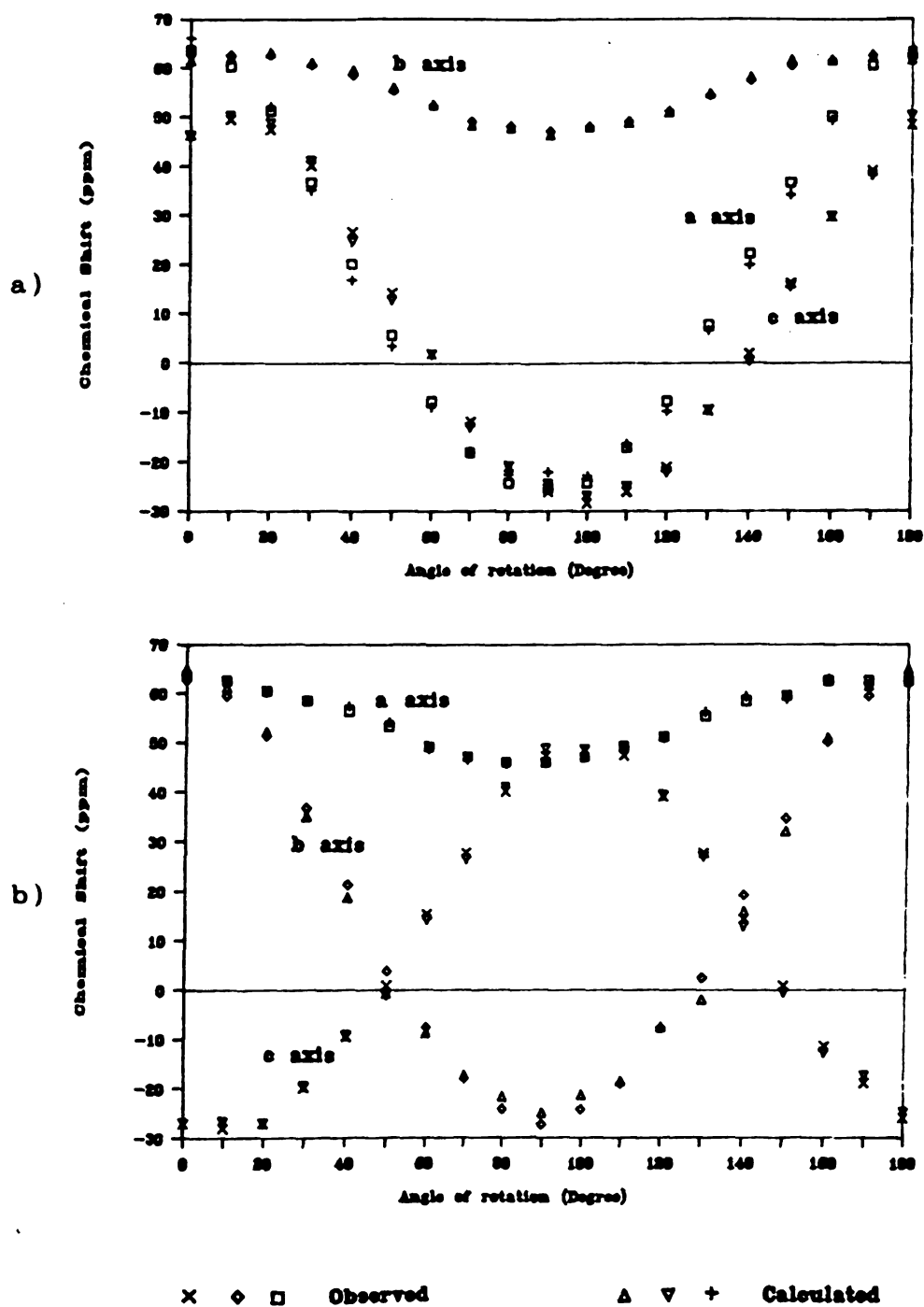
Figure 24 Angular dependence of the central transitions of Cs$^+$ in a single crystal Cs$^+$(15C5)$_2$·I$^-$.

a) Site A; b) site B.

lated

Table

A

CSA*—

B

A

QCC*-

I

CSA*

QCC*

χ**

*Re
**R
E.

Table 9 ^{133}Cs chemical shift, quadrupolar coupling tensors and direction cosines

		(ppm)	Eigen Vectors			E. Angles(°)	
CSA[*]	A δ_{XX}	62.0±0.7	0.0227	-0.0017	0.9997	α	1.3
	δ_{YY}	47.2±0.7	0.9860	0.1655	-0.0221	β	89.7
	δ_{ZZ}	-28.2±0.7	-0.1654	0.9862	0.0054	γ	80.5
	B δ_{XX}	61.6±0.7	0.0191	-0.0758	0.9969	α	4.5
	δ_{YY}	46.2±0.7	-0.1669	0.9829	0.0779	β	89.6
	δ_{ZZ}	-28.7±0.7	0.9858	0.1679	-0.0061	γ	170.3
QCC[*]	A A_{XX}	-1298.±2	0.0053	0.0041	1.0000	α	-0.4
	A_{YY}	-469.±10	0.9859	0.1674	-0.0059	β	90.2
	A_{ZZ}	1757.±5	-0.1674	0.9859	-0.0032	γ	80.4
	B A_{XX}	-1297.±2	0.0072	-0.0187	0.9998	α	1.1
	A_{YY}	-454.±10	-0.1779	0.9838	0.0196	β	90.2
	A_{ZZ}	1768.±10	0.9840	0.1780	-0.0038	γ	169.7

		(ppm)	Eulerian Angle (°) Site A	Site B
CSA[**]	δ_{XX}	62.0±0.7	α 0.	0.
	δ_{YY}	46.1±0.7	β 90.	90.
	δ_{ZZ}	-28.4±0.7	γ 80.	170.
QCC[**]	A_{XX}	-1297.±2	α 0.	0.
	A_{YY}	-461.±2	β 90.	90.
	A_{ZZ}	1758.±2	γ 80.	170.

χ^{**} = 0.5810 MHz η^{Q**} = 0.4755 A_{ZZ} = 3χ/[2I(2I - 1)]

[*]Results obtained by the Volkoff method
[**]Results from multiple data set KINFIT analysis with XTAL
E. Angles = Eulerian Angles

poor R

Nicole

solvi

symme

of th

infor

crown

succe

cryst

orier

envi

exac

sing

the

crys

show

from

ori

ext

(3/

gen

sit

sev

tr

wi

poor R factors, the diffraction data were redetermined with a Nicolet P3F diffractometer. So far, we have not succeeded in solving the structure of this compound due to the very high symmetry of the crystal. However, its space group must be one of the several space groups belonging to I4 or $I\bar{4}$. From this information, one can obtain some structural information. The crown ether sandwich unit lies on a screw axis which requires successive complexed cations along the c-direction in the crystal to be rotated by $90°$ about the c-axis. Thus, two orientations of the crown sandwich units exist. The environments of these different crown sandwich units are exactly the same chemically, but different magnetically.

Figures 26a and 26b show the ^{133}Cs NMR spectra of a single crystal of $Cs^+(15C5)_2 \cdot I^-$ with proton decoupling when the static magnetic field is directed along the crystallographic a and c axes, respectively. The central peak shown in Figure 26a is assigned to the (1/2,-1/2) transitions from the two magnetically different sites which at this orientation have the same environments with respect to the external magnetic field. The two peaks from the transition (3/2,1/2) of both sites also coalesce at this orientation. In general, however, two distinct sets of peaks from the two sites were observed as shown in Figures 26b and 26c. All seven transitions (2I = 7) from one site (A) and three transitions from the other (B) were detected within the sweep width of the spectrometer [Figures 26b and 26c].

The principal axes of both the CSA and the quadrupolar

Figure 26 ^{133}Cs NMR spectra of a single crystal
$Cs^+(15C5)_2 \cdot I^-$ at ν_L = 23.61 MHz.

a) B_0 is along the crystallographic a axis;

b) B_0 is along the crystallographic c axis;

c) At an arbitrary orientation.

tensors ar

plots in F

chemical s

the cryst

site A ar

and   the

respectiv

of $10°$ fr

related t

ions   ar

quadrupol

shift   ar

symmetric

tensors

and I^- i

interact

be very

an n-fo

which n

the carl

the loc

     Th

the   po

frequer

static

transit

patterr

tensors are coincident as can be noticed from the orientation plots in Figures 24 and 25. The X principal axes of both the chemical shift and the quadrupolar coupling tensor are along the crystallographic c-axis. The Y and Z principal axes at site A are about $10°$ away from the crystallographic a-axis and the b-axis in the counterclockwise direction, respectively. The Z principal axis at site B makes an angle of $10°$ from the b-axis towards the $-a$-axis, where site B is related to that at site A by the crystal symmetry. If the I^- ions are strongly related to the chemical shift and quadrupolar interactions, one might expect both the chemical shift and the quadrupolar coupling tensors to be axially symmetric since the structure is tetragonal. However, both tensors are nonaxially symmetric. If the distance between Cs^+ and I^- is large enough to diminish the effect of I^- on these interactions, the local environment of the complexed Cs^+ may be very important. It is probably impossible for Cs^+ to have an n-fold rotation or an n-fold rotation reflection axis for which n > 2. Even if there is a local symmetry axis, often the carbon atoms in the crown ethers are disordered [6]. Thus the local environment of Cs^+ may be highly asymmetric.

The spectra shown in Figure 27 are a MAS spectrum and the powder patterns of $Cs^+(15C5)_2 \cdot I^-$ at the resonance frequency, 52.482 MHz. Figure 27b shows an experimental static powder spectrum. The powder pattern of the central transition is very similar to an axially symmetric CSA powder pattern but it is nonaxially symmetric. Combination of the

a)

Figure 27 ^{133}Cs NMR spectra of a powdered sample of Cs$^+$(15C5)$_2 \cdot$I$^-$ at ν_L = 52.482 MHz.

    a) MAS spectrum with $\omega_r \approx$ 4 kHz;

    b) Observed static powder pattern;
    c) Computer simulated powder pattern.

b)

c

100(

a)

b)

800.0   500.0   200.0   0.0   -300.0   -600.0   -900.0
PPM

c)

1000   500   0   -500   -1000
ppm
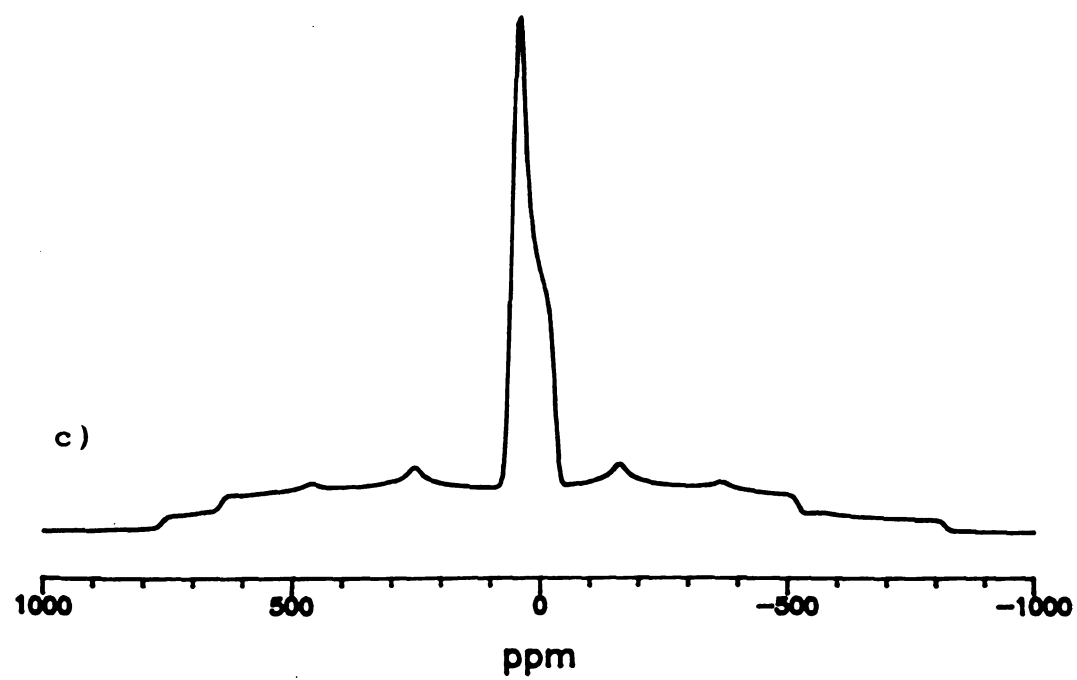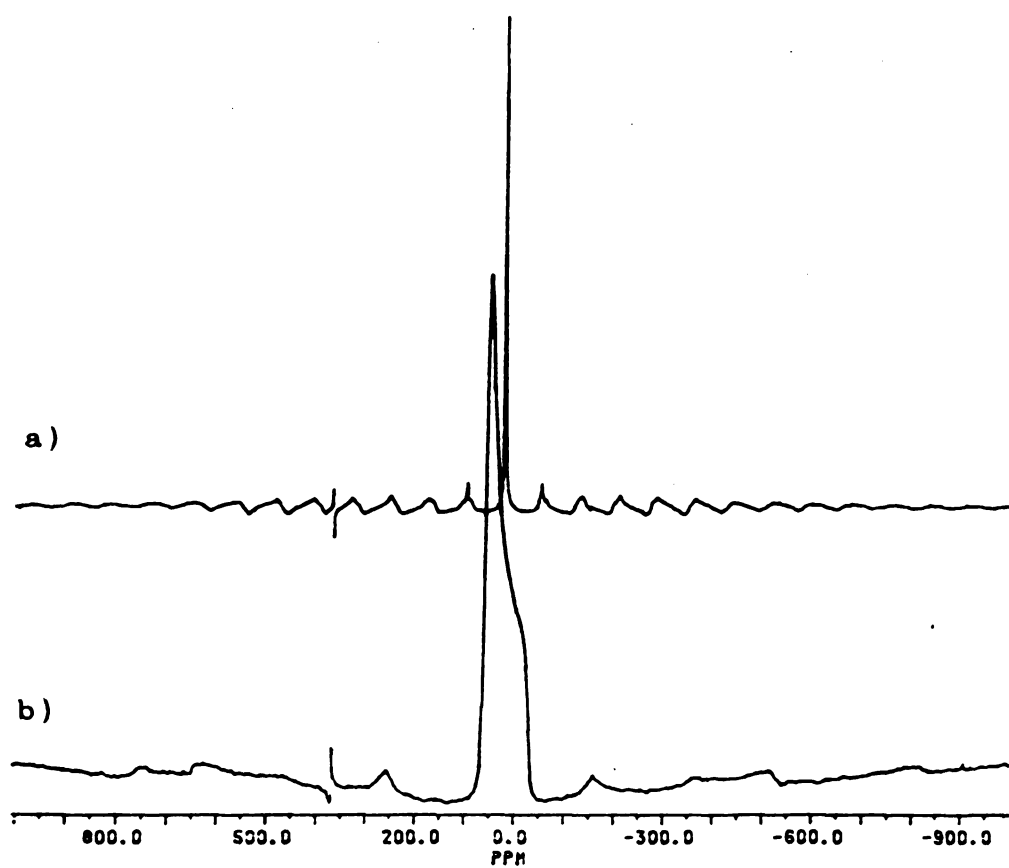
isotropic

and the

pattern

tensor s

extract

some oth

differen

simulate

crystal

fits ve

transiti

contribu

broadeni

satellit

transit

visible

order q

pattern

CSA wit

Fi

differe

MHz. Pr

interac

nuclei

than

intera

spectr

isotropic chemical shift from a MAS experiment (Figure 27a) and the chemical shifts at singularities of the powder pattern can provide evidence for a nonaxially symmetric tensor since $\delta_{iso} = 1/3 (\delta_{XX} + \delta_{YY} + \delta_{ZZ})$. It is dangerous to extract parameters from only a static powder pattern since some other experiments such as MAS and VAS can provide different information. The spectrum shown in Figure 27c is simulated by using the parameters obtained from the single crystal NMR study of $Cs^+(15C5)_2 \cdot I^-$. The simulated spectrum fits very well to the experimental one. The central transition is broadened mainly by CSA and a small contribution from dipolar interactions. Quadrupolar broadening is negligible for the central transition. The satellite transitions are very weak compared to the central transition. However, most of the singularities are clearly visible. The satellites are broadened primarily by first order quadrupolar interactions and the symmetry of the powder pattern of corresponding satellites is destroyed by mixing CSA with the quadrupolar contribution.

Figure 28 shows the ^{133}Cs MAS NMR spectra obtained with different spinning speeds at a resonance frequency of 23.61 MHz. Proton decoupling was used to minimize the Cs-H dipolar interactions. Because the dipolar interactions between cesium nuclei and protons are about 1 kHz, spinning speeds slower than 1 kHz cannot completely average out the dipolar interactions. Thus at low spinning speeds, broad bumpy spectra due to partial averaging of the dipolar interactions
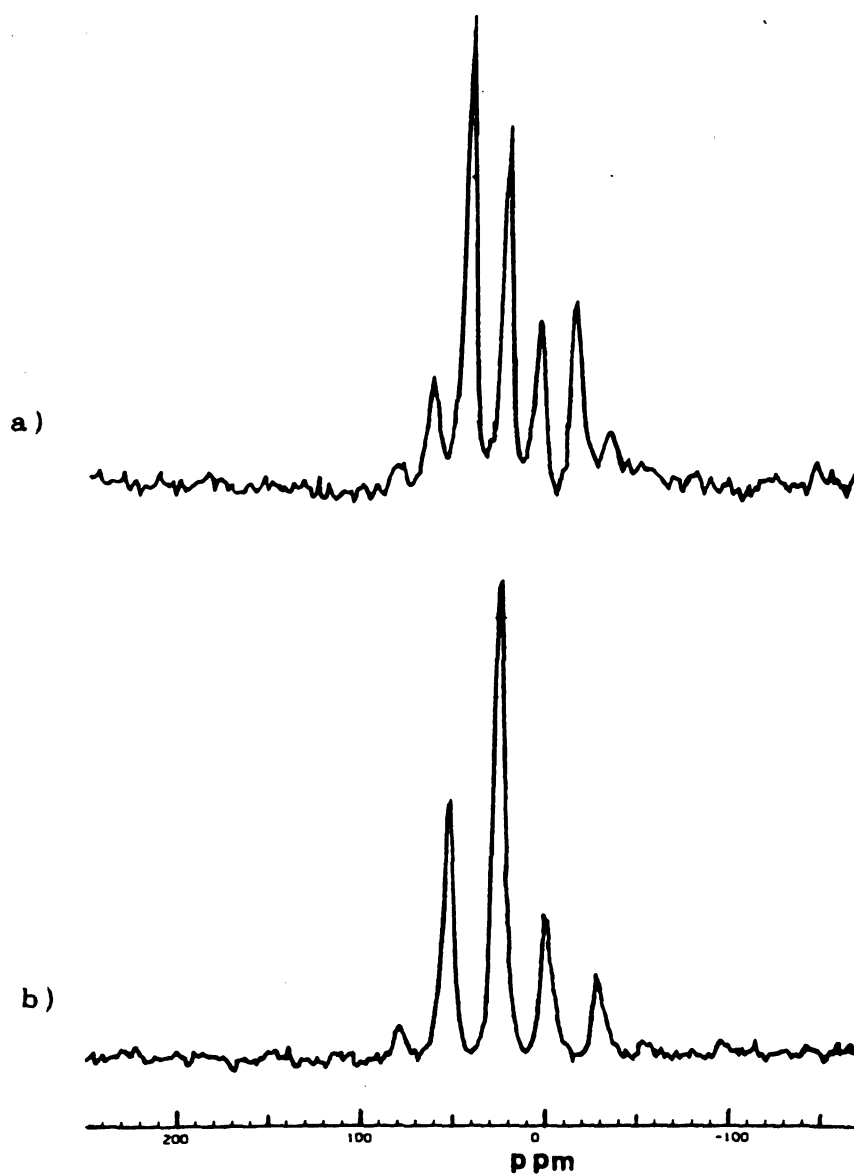
Figure 28 ^{133}Cs MAS NMR spectra of a powdered sample of $Cs^+(15C5)_2 \cdot I^-$ with decoupling at ν_L = 23.61 MHz. a) $\omega_r \approx$ 470 Hz; b) $\omega_r \approx$ 650 Hz.

were obse

proton d

under sl

inhomoger

spectra

Acc

interact

and dip

interact

spins (

studied

(i.e.,

being s

corresp

NMR lin

term ξ

spin i

propor

be obs

will b

strong

from

couple

wherea

system

ideas

aroun

were observed instead of narrow spinning sidebands without proton decoupling. The proton decoupled spectra obtained under slow spinning conditions are clearly broadened by inhomogeneous interactions. Also the proton coupled ^{133}Cs NMR spectra at slow spinning speed behave inhomogeneously.

According to Maricq, et al. [59], "when two or more interactions are present simultaneously (e.g., chemical shift and dipolar) the result is homogeneous if any of the interactions is homogeneous." In other words, if abundant spins (for example proton spins) around the nuclei to be studied (for example Cs) are strongly coupled to each other (i.e., homogeneous), then the NMR line of the spin system being studied (Cs) becomes homogeneous. This usage does not correspond exactly to that in the section II. E. since the NMR line of the spin system behaves inhomogeneously if the term $\xi^{(ij;D)}(t)$ (in equation 26 in reference [59]) for each spin in an array of spins with dipolar interactions is proportional to one another; However, "hole burning" cannot be observed in the resonance of such a system since energy will be quickly transferred from one spin to another due to strong dipolar interactions. In addition this is different from heterogeneous broadening. Only a few spin packets are coupled to each other in a heterogeneously broadened line, whereas all spin packets interact with each other in the spin system. Complexed cesium compounds are good models to test ideas about these interactions since the charge distribution around the cesium cation causes a relatively large chemical

anisotrop

If the ^{13}

origin, a

instead

broadened

obtained

shift par

pattern.

nearly t

for the

broadeni

4.7 kHz

Cs^+(15C5

may not

line of

will be

MAS exp

inhomog

is obse

when th

experim

given i

anisotropy and the organic complexant provides many protons. If the ^{133}Cs in $Cs^+(15C5)_2 \cdot I^-$ were completely homogeneous in origin, a single Lorentzian (or Gaussian) line would result instead of a normal powder pattern. However, a Gaussian broadened CSA powder pattern for the central transition was obtained for this compound and the simulation with chemical shift parameters yielded a matching static theoretical powder pattern. The lineshape of a proton decoupled spectrum is nearly the same as that of a proton coupled spectrum except for the extra broadening due to protons. The dipolar broadening is smaller than the width of CSA broadening (about 4.7 kHz at ν_L = 52.482 MHz). Therefore, the lineshape of $Cs^+(15C5)_2 \cdot I^-$ appears to involve inhomogeneous broadening and may not agree with the Maricq predictions. Whether the NMR line of the cesium compound follows the Maricq predictions will be clearly solved by a hole burning experiment or slow MAS experiments at higher field. If the line broadening is inhomogeneous, the FID with a train of rotational spin echos is observed (or spinning sidebands after Fourier transform) when the sample is slowly spun at the magic angle. More experimental evidence for inhomogeneous broadening will be given in Section V. A. 5.

V. A. 4.

S

In

yielded

It was

shifted

chemical

crystals

easily

quantita

pattern.

complexe

Qua

(for qu

(mainly

listed

static

Some re

30, 31

second

T

symmetr

Na^+C22

contai

symmet

betwee

V. A. 4. Lineshape Analysis of ^{23}Na NMR Spectra of Model
Salts that contain Na$^+$

In Section, V. A. 1., an NMR study of a single crystal yielded very accurate parameters associated with the nuclei. It was shown that the central transition of Na$^+$ is mainly shifted by second order quadrupolar interactions and that the chemical shift effect is negligible. However, good single crystals are not always available, while powdered samples are easily synthesized. Although the accuracy is limited, quantitative information can often be obtained from a powder pattern. In this section, ^{23}Na NMR spectra of various complexed sodium salts will be discussed.

Quadrupolar coupling constants, asymmetry parameters (for quadrupolar interactions) and chemical shift parameters (mainly isotropic chemical shifts) for Na$^+$ model salts are listed in Table 10. These values were obtained by simulating static and MAS spectra with or without proton decoupling. Some representative ^{23}Na NMR spectra are shown in Figures 29, 30, 31, and 32. These spectra have lineshapes typical of second order quadrupolar powder patterns.

The sodium NMR spectra of C222 compounds are axially symmetric except for Na$^+$C222·SCN$^-$. The structure of Na$^+$C222·I$^-$ [60] shows that the individual twin component contains two molecular species in a trigonal unit cell with symmetry P31c. Average distances between Na$^+$ and O and between Na$^+$ and N are 2.574 Å and 2.752 Å. Axially symmetric

Table 10

| ν_L | Co |
| MHz | |

Na
Na
Na
Na
Na

Na

Na

Na

47.61 | Na

Na
Na
Na

Na
Na
Na
N
N

N
105.84 | N
N

$^a\delta_{iso}$, χ

DN;Proto
DF;Proto

Table 10 NMR parameters obtained by simulations of the static and MAS ^{23}Na NMR spectra at two different fields

ν_L MHz	Compound	δ_{iso} ppm	QCC MHz	η^Q	Gaussian broadening, Hz Static DF	DN	Mass DN
	Na$^+$C222·Cl$^-$	-16	0.65	0	1200	150	55
	Na$^+$C222·Br$^-$ a	-16.2	0.605	0	1200	200	60
	Na$^+$C222·I$^-$	-9	1.05	0	1200	400	150
	Na$^+$C222·SCN$^-$	-10	1.0	0.5	1300	300	160
	Na$^+$C222·TPB$^-$	-8	0.5	0	1200	200	150
	Na$^+$(12C4)$_2$·Cl$^-$	-3	1.2	0	700	250	150
	Na$^+$(12C4)$_2$·Br$^-$	-3	1.2	0	800	350	150
	Na$^+$(12C4)$_2$·I$^-$	-3	1.0	0	650	200	120
47.61	Na$^+$(12C4)$_2$·SCN$^-$	0	1.2	0	1100	350	100
	Na$^+$15C5·Br$^-$	-5	1.1	0.4	500	250	60
	Na$^+$15C5·I$^-$	-5	0.81	0.4	750	170	90
	Na$^+$15C5·SCN$^-$	-1	0.8	1	900	500	300
	Na$^+$18C6·Cl$^-$	-10	2.2	0	800	350	---
	Na$^+$18C6·Br$^-$	-9	2.05	0	650	300	---
	Na$^+$18C6·I$^-$	-7	3.0	0.4	650	---	---
	Na$^+$18C6·SCN$^-$	-9	1.05	0.8	700	210	140
	Na$^+$18C6·TPB$^-$	-6	1.72	0.16	1000	600	250
	Na$^+$18C6·Cl$^-$	-10	2.2	0	800	---	200
105.84	Na$^+$18C6·Br$^-$	-9	2.1	0	650	---	200
	Na$^+$18C6·I$^-$	-7	3.0	0.4	1050	---	200

[a] δ_{iso}, χ, and η^Q obtained by a single NMR study

DN;Proton decoupled
DF;Proton coupled

Figure 29 ^{23}Na NMR spectra of Na$^+$C222·I$^-$ a), b), and c), and Na$^+$C222·SCN$^-$ d) at ν_L = 47.61 MHz.

a) Proton coupled static spectrum;
b) Proton decoupled static spectrum;
c) Proton decoupled MAS spectrum;
d) Proton decoupled static spectrum.
Observed (———)and simulated (···).

a)

b)

c)

400   300   200   100   0   -100   -200   -300   -40C
ppm

d)

80   60   40   20   0   -20   -40   -60   -80   -100
ppm
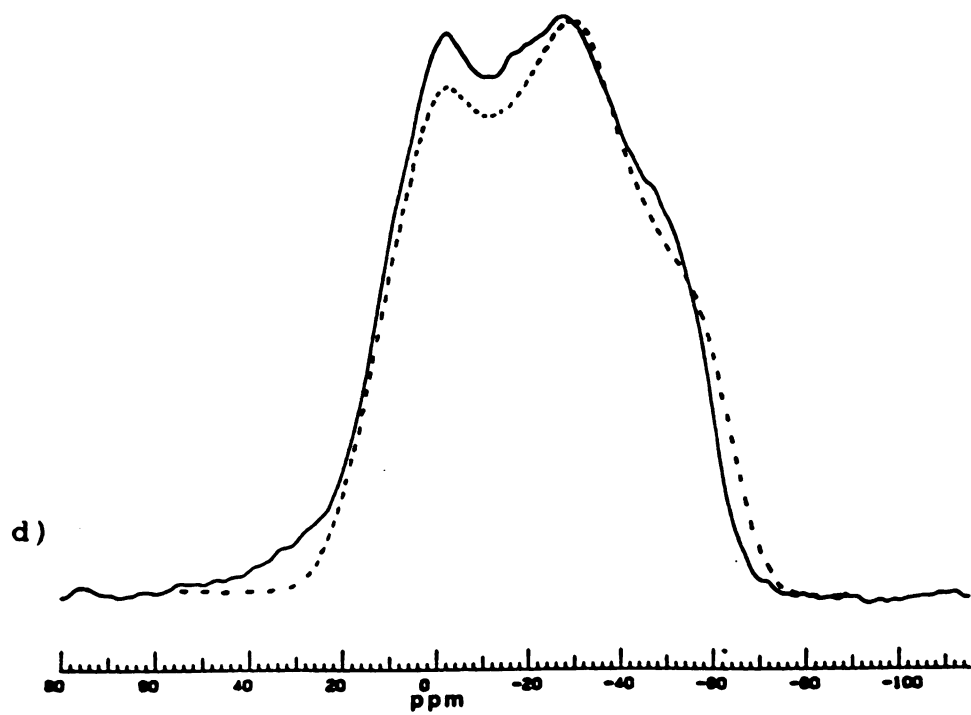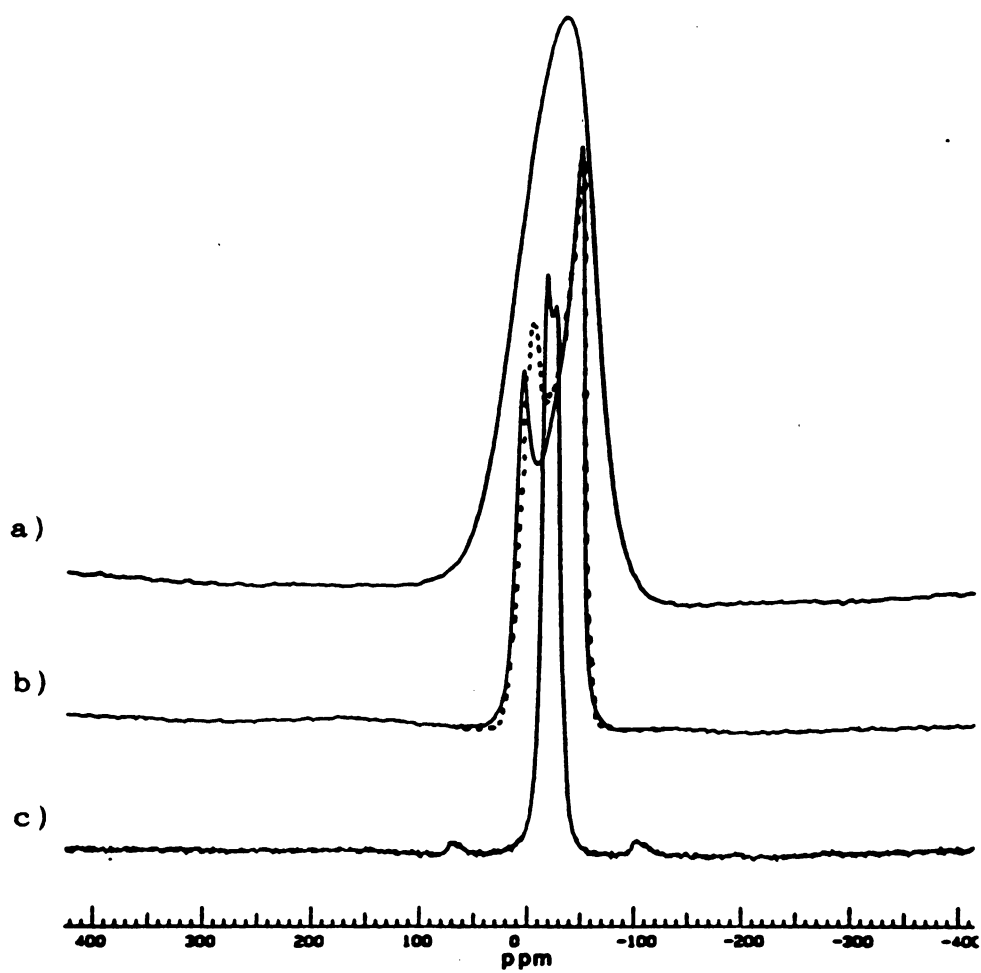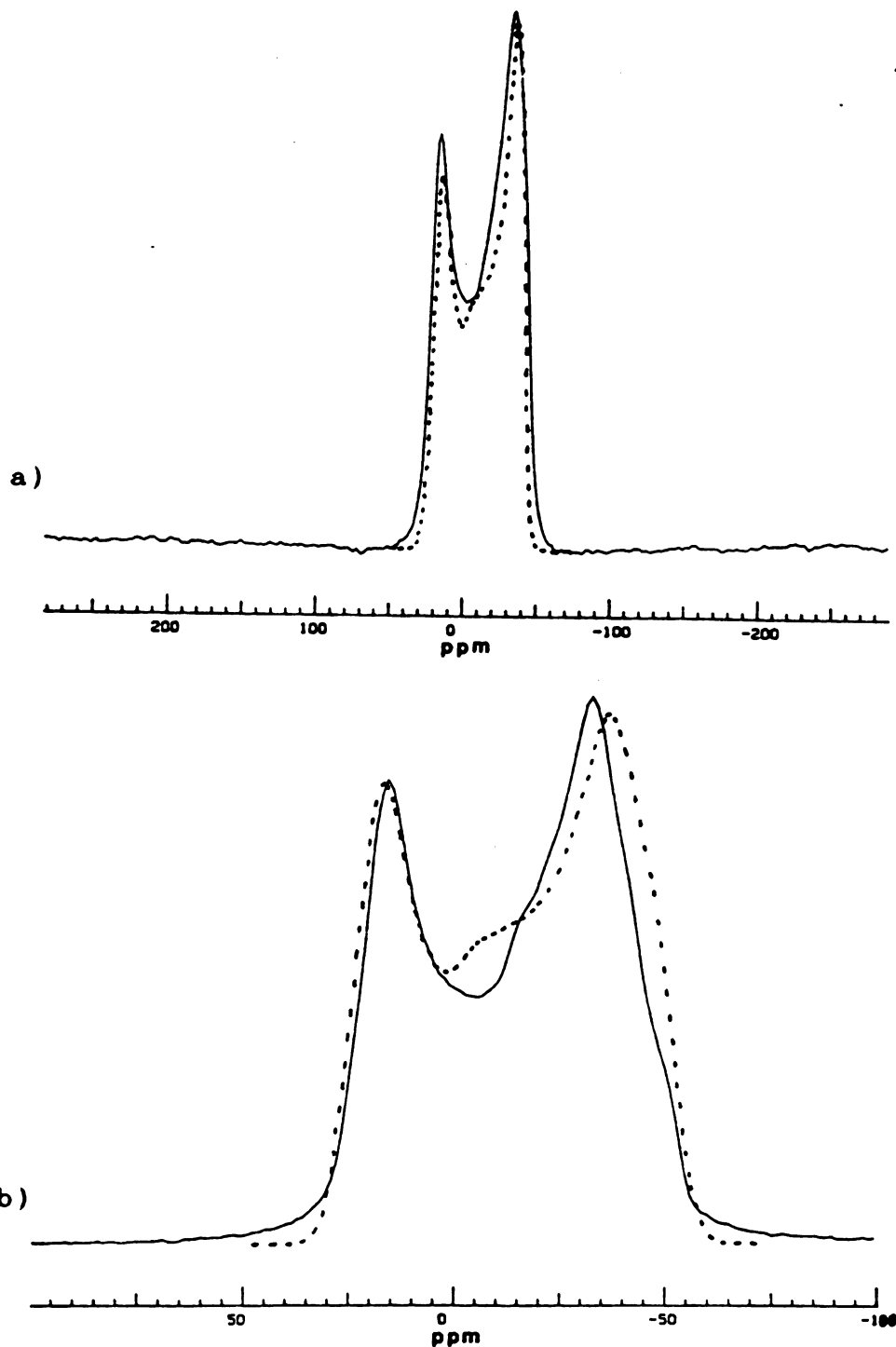
Figure 30 Proton decoupled static ^{23}Na NMR spectra of Na$^+$(12C4)$_2$·I$^-$ a) and Na$^+$(12C4)$_2$·TPB$^-$ b) at ν_L = 47.61 MHz. Observed (——) and simulated (···).
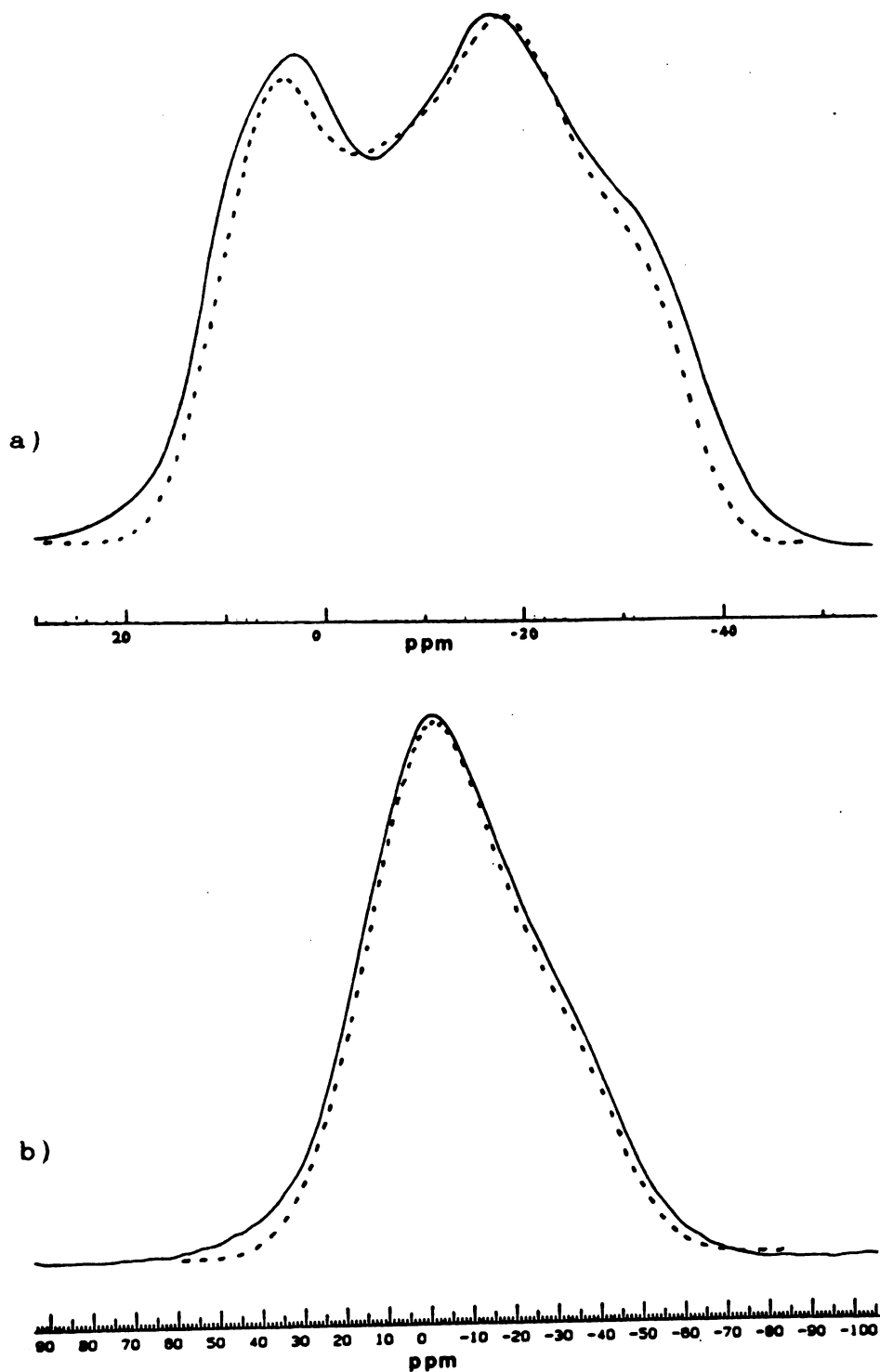
Figure 31 Proton decoupled static ^{23}Na NMR spectra of Na$^+$15C5·I$^-$ a) and Na$^+$15C5·SCN$^-$ b) at ν_L = 47.61 MHz. Observed (——) and simulated (···).

Figure 32 ^{23}Na NMR spectra of $Na^+18C6 \cdot Br^-$ a), $Na^+18C6 \cdot I^-$ b),
c), $Na^+18C6 \cdot SCN^-$ d) and e).

a) Proton decoupled static, $\nu_L = 47.61$ MHz;

b); d) Proton coupled static, $\nu_L = 105.482$ MHz;

c) Proton coupled MAS, $\nu_L = 105.482$ MHz;

e) Proton decoupled MAS, $\nu_L = 47.61$ MHz.

Observed (——), Simulated ($\cdots$).
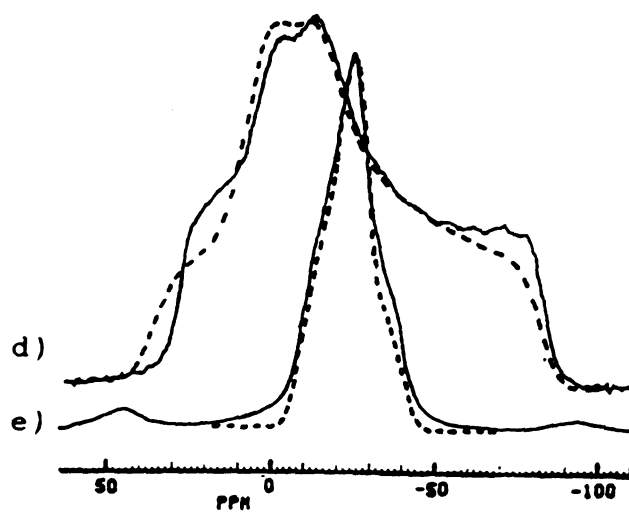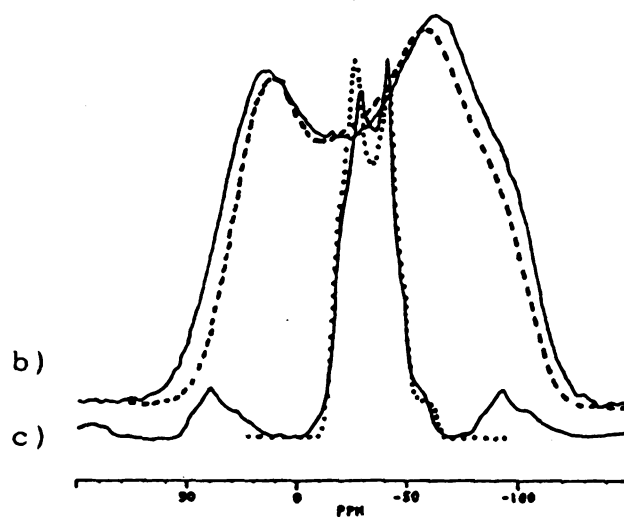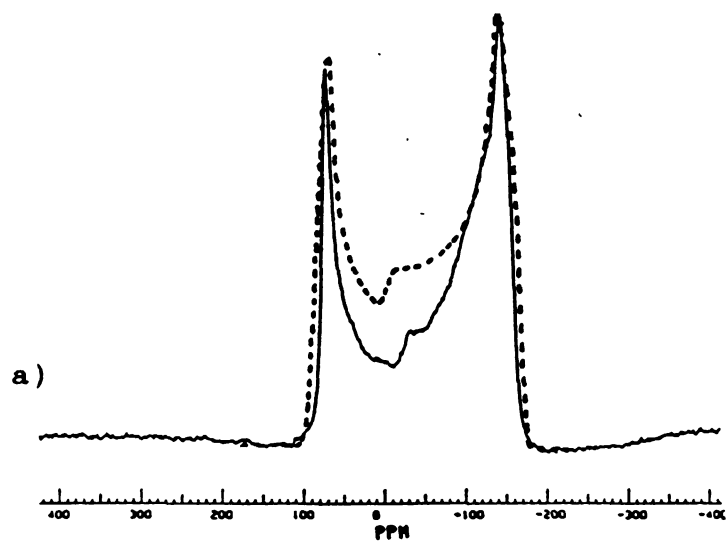
electric field gradient tensors were obtained from these compounds as expected from the local structure around Na^+. In general, any n-fold rotation or n-fold rotation reflection axis for which n > 2 requires $\eta = 0$ [61]. In $Na^+C222 \cdot SCN^-$ a stick-shaped SCN^- ion might cause deformation of a cryptand strand, which could cause a nonaxially symmetric electric field gradient. Presumably, changes in the structures due to different anions are responsible for the different QCC values observed.

Axially symmetric powder patterns of most $Na^+(12C4)_2$ ions with QCC of about 1.2 MHz imply that $Na^+(12C4)_2$ ions are in very similar environments in different salts. The lineshapes agree well with those expected from their structures. For example, $Na^+(12C4)_2$ has an approximate D_4 symmetry with two polyether rings, each of which obeys approximate C_4 symmetry [62]. Two crown ether rings form a square-antiprism arrangement [Figure 33]. The average distance between Na^+ and O is 2.497 Å. Sodium cations in $Na^+(12C4)_2$ are relatively well shielded from anions or intercrystalline water.

The distinctly nonzero asymmetry parameters of 15C5 compounds that contain Na^+ indicate asymmetric electronic environments around the sodium cations. The complexant 15C5 can form 1:1 compounds with sodium salts and thus cannot completely shield the Na^+ ion. Hence, anions or water molecules may interact with Na^+. In addition there may be no n-fold axis (n > 2) around Na^+ because of the asymmetry of
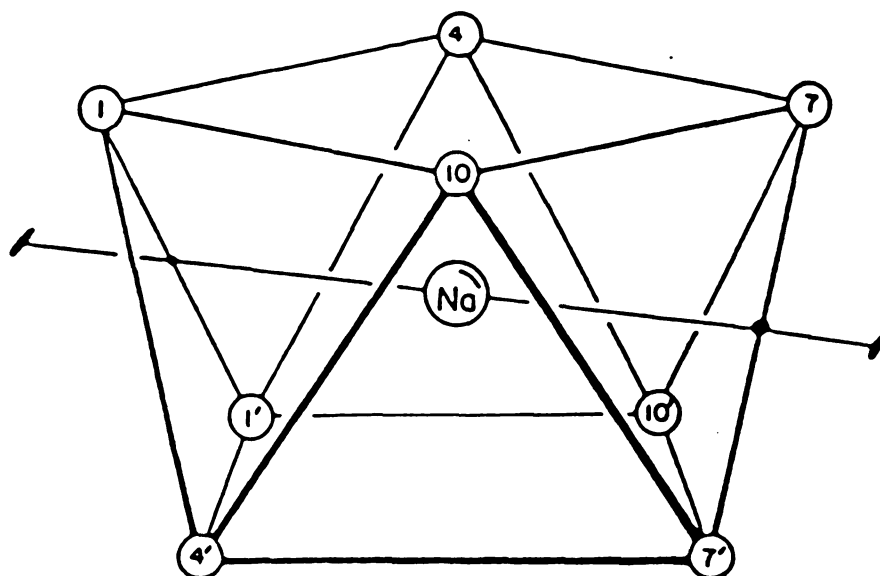
Figure 33 Square-antiprism arrangement of oxygen atoms in $Na^+(12C4)_2 \cdot Cl^- \cdot 5H_2O$. The inter-oxygen distances and the crystallographic two fold axis are shown.

15C5.

Na$^+$ ions in the cage of 18C6 have relatively large quadrupolar coupling constants except for Na$^+$18C6·SCN$^-$. The NMR spectra of Na$^+$18C6·Cl$^-$ and Na$^+$18C6·Br$^-$ are nearly axially symmetric while those of Na$^+$18C6·I$^-$, Na$^+$18C6·SCN$^-$, and Na$^+$18C6·TPB$^-$ are nonaxially symmetric. The structure of Na$^+$18C6·SCN$^-$ has been determined [62]. The six ether oxygens have a highly irregular conformation in which five approximately coplanar atoms surround Na$^+$. A water molecule and the remaining oxygen of the crown ether are bonded to form a distorted pentagonal bipyramidal coordination of the cation [Figure 34]. The distances between Na$^+$ and O range from 2.321 Å to 2.623 Å. The water oxygen is the shortest distance away from Na$^+$. The average distance between Na$^+$ and O is 2.516 Å. An asymmetry parameter of 0.8 for this compound is easily explained by the highly distorted coordination structure. Although Na$^+$ is present in a highly distorted crown ether molecule, it has a relatively small QCC. Structural asymmetry gives rise to big asymmetry parameters without having large QCC values. It seems that 18C6 is too large for Na$^+$ but that the flexibility of the crown ether molecule allows it to form different coordination structures.

The ^{23}Na NMR spectra of most compounds obtained at a Larmor frequency of 47.61 MHz show the second order quadrupolar powder pattern. It was not possible to obtain MAS powder patterns of some 18C6 compounds with about 4kHz spinning speed at the resonance frequency of 47.61 MHz due to
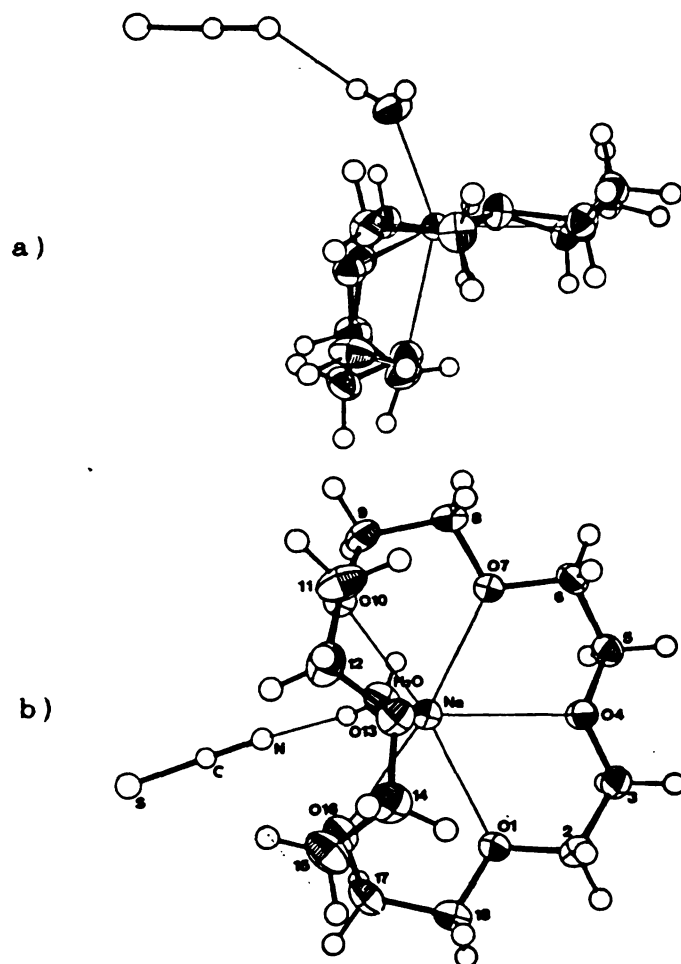
Figure 34 Local structure of Na$^+$18C6·SCN$^-$.
a) View along a direction in the mean plane;
b) View in a direction normal to the mean plane.

large quadrupolar interactions. Except for $Na^+18C6 \cdot Cl^-$, $Na^+18C6 \cdot Br^-$, $Na^+18C6 \cdot I^-$ and $Na^+18C6 \cdot TPB^-$, most compounds at a ^{23}Na Larmor frequency of 105.842 MHz gave broad structureless lineshapes due to small quadrupolar and large dipolar interactions. At this frequency, static and MAS powder patterns for sodium 18C6 halides and tetraphenylborate were obtained. These spectra are much narrower than the spectra obtained at a resonance frequency of 47.61 MHz. This demonstrates that the quadrupolar linewidth for a second order powder pattern are inversely proportional to the external field, and hence the resonance frequency.

Although there are many protons, inhomogeneously broadened quadrupolar ^{23}Na NMR lines were observed. The Gaussian broadening in Table 10 is almost half the full width at half height. Although the values of the Gaussian broadening contributions have relatively large errors, rough estimation about the extent of dipolar interactions can be obtained. In general, C222 compounds have the largest proton dipolar interactions since the linewidths are greatly reduced by proton decoupling. The structure of $Na^+C222 \cdot I^-$ is known but the coordinates for the protons are not available. However the calculated proton dipolar contribution to the static linewidth (full width at half height) of Na^+ in $Na^+C222 \cdot Na^-$ is 3340 Hz [17]. Excellent agreement between the observed width (3700 Hz below $-20^{\circ}C$) and the calculated value (3670 Hz) considering both dipolar and quadrupolar contributions was obtained. However, the static linewidth of
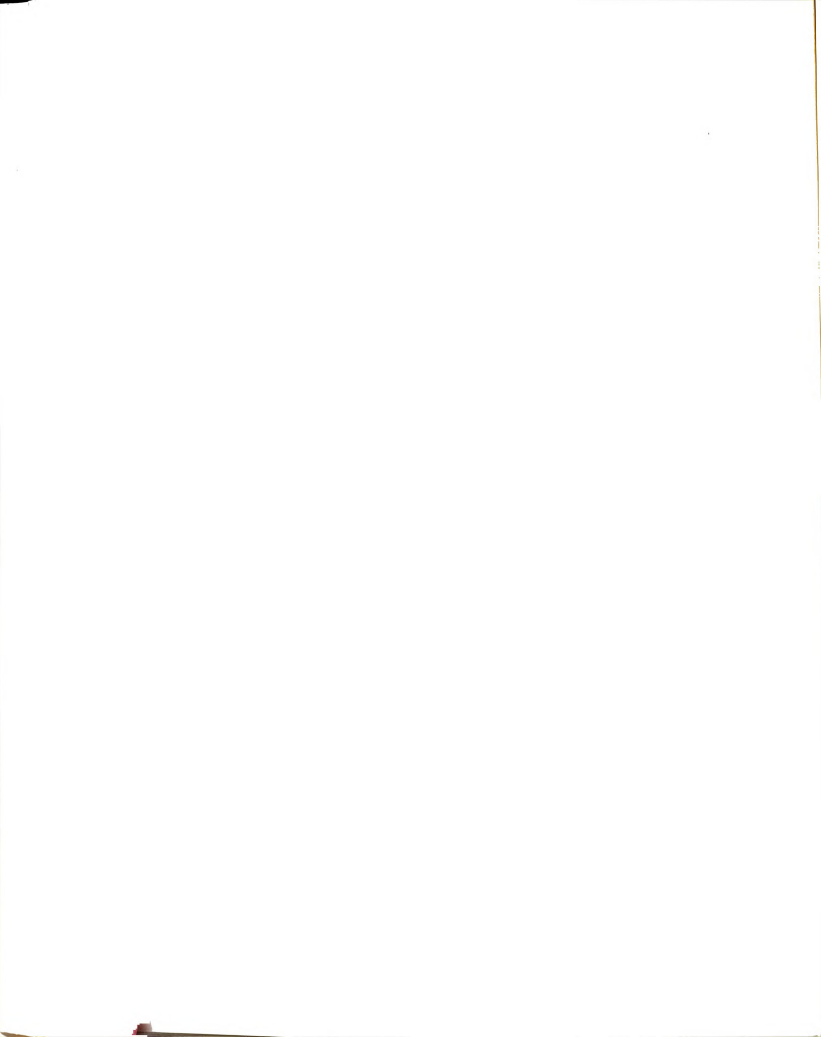
most C222 compounds is about 2400 Hz at room temperature. Significant motional narrowing at room temperature might cause the linewidth reduction. A recent study of the ^{23}Na relaxation time in $Cs^+(18C6)_2 \cdot Na^-$ showed that T_2^* increases with temperatures and changes dramatically above ~0 $^\circ$C [57]. The calculated dipolar contributions from protons within a 6 Å radius from Na^+ in $Na^+(12C4)_2 \cdot Cl^- \cdot 5H_2O$ and $Na^+18C6 \cdot SCN^- \cdot H_2O$ are 3800 Hz and 3950 Hz, respectively, using Van Vleck equations for a powder sample. Linewidths for 12C4 and 18C6 compounds vary from ~1000 Hz to 2000 Hz, depending on the compound. Linewidth reduction of these crown ether compounds by decoupling is much smaller than that of C222 compounds. The dipolar interactions in the crown compounds are weaker than those in the C222 salts as shown by data obtained from the static proton coupled spectra. This implies that motion of the crown ring is much easier than that of a cryptand. The crown ethers might have rotational motion about an axis normal to the ring plane as well as vibrational motion. Only limited vibrational motions are allowed for the cryptands since their ether chains are bonded to the two end nitrogens. With proton decoupling, the residual dipolar interactions vary from ~150 Hz to ~600 Hz in static experiments. MAS studies further reduce the linewidths to about 100 ~ 350 Hz. Without proton decoupling, the NMR lines were additionally broadened by proton dipolar interactions such that the singularities of the quadrupolar powder pattern were masked.

Second order quadrupolar powder patterns of complexed
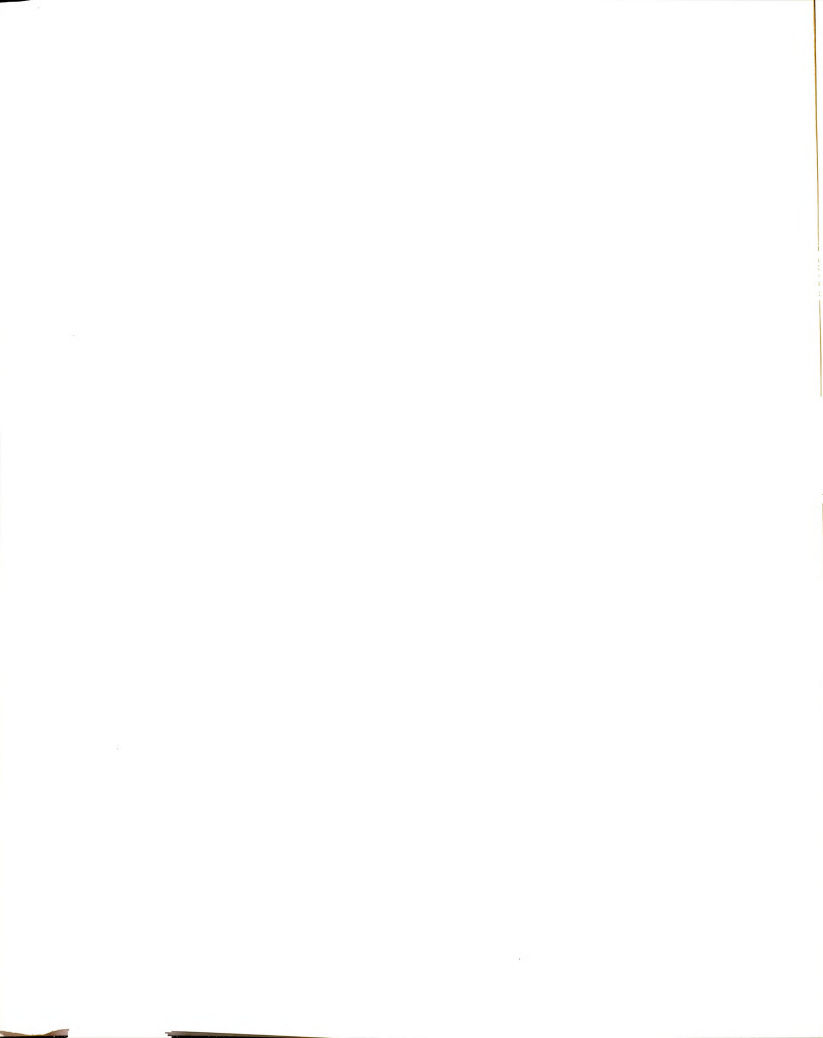
sodium salts were discussed in this section. It is very important to examine samples both with and without proton decoupling and with both static and with MAS techniques at different fields in order to extract useful NMR parameters.

V. A. 5. Lineshape Analysis of ^{133}Cs NMR Spectra of Cesium
        Model Salts

A variety of complexed cesium salts were very carefully reexamined in order to investigate the anisotropic interactions of Cs$^+$ with the surrounding environment. Complexed cesium cations provide very good examples of both chemical shift anisotropy and quadrupolar interactions in addition to dipolar effects. These interactions vary significantly with the coordination structures.

Figures 35, 36, and 37 show the ^{133}Cs NMR spectra of three cesium C222 salts. Cryptated cesium cations have suprisingly large quadrupolar coupling constants of about 1 MHz. No appreciable spinning sidebands in comparison with other Cs compounds and no powder patterns of satellites were observed from MAS and static experiments. Pure second order quadrupolar powder patterns were obtained from MAS experiments at a frequency of 23.61 MHz since MAS eliminated the CSA contribution, and different Cs$^+$C222 compounds showed different MAS powder patterns. With proton decoupling at the same field, unusual static powder patterns were obtained because of the combination of CSA and quadrupolar
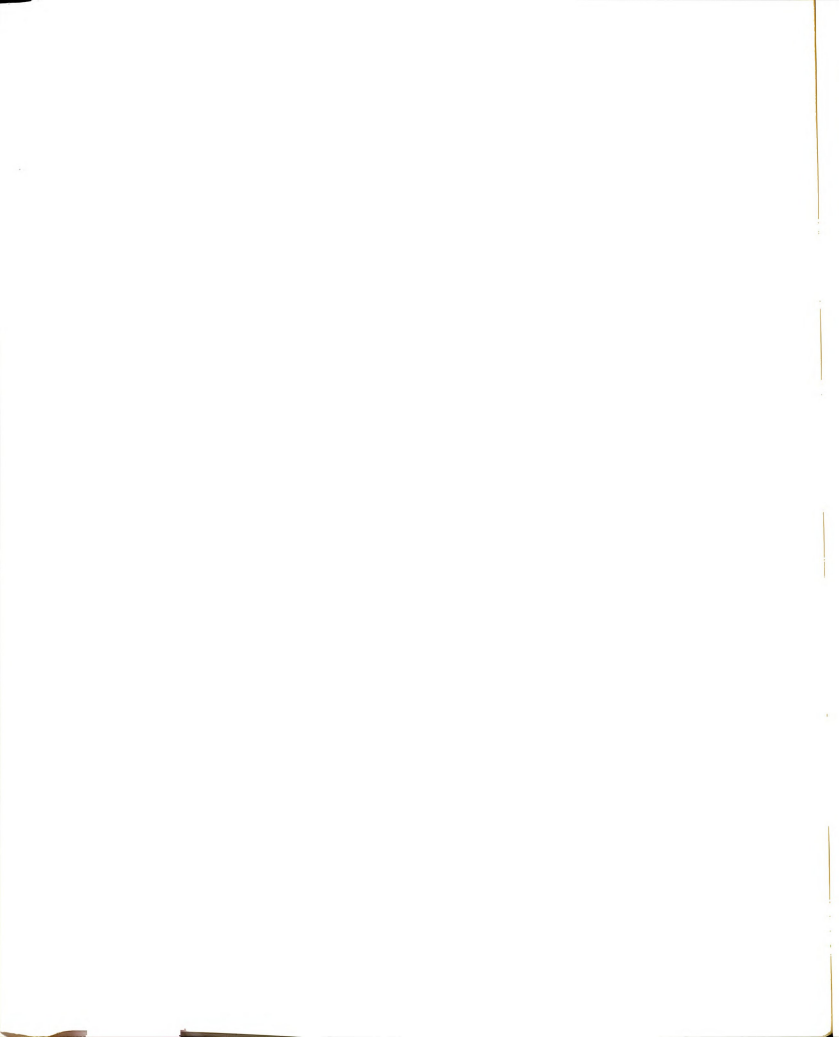
Figure 35 ^{133}Cs NMR spectra of $Cs^{+}C222 \cdot I^{-}$.
a) Proton coupled static, $\nu_{L} = 52.482$ MHz;
b) Proton decoupled static, $\nu_{L} = 23.61$ MHz;
c) Proton decoupled MAS, $\nu_{L} = 23.61$ MHz.
Observed (——), Simulated (·····).
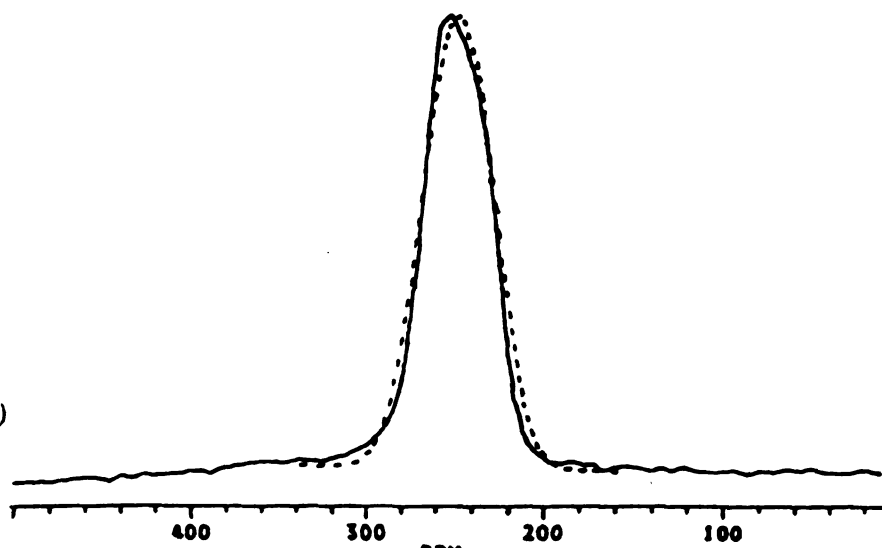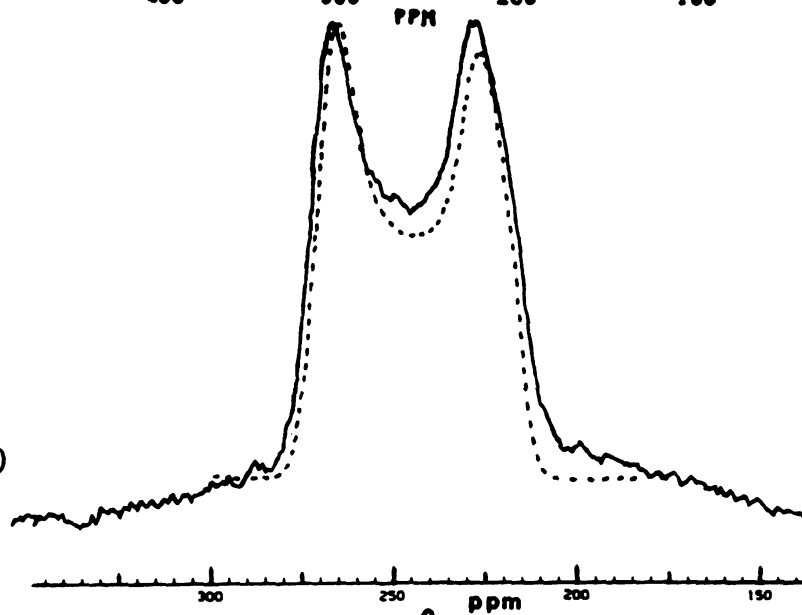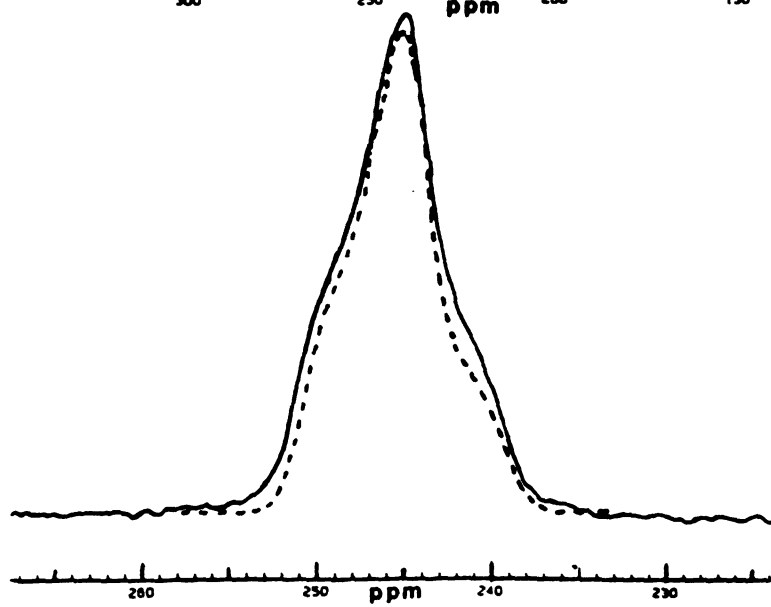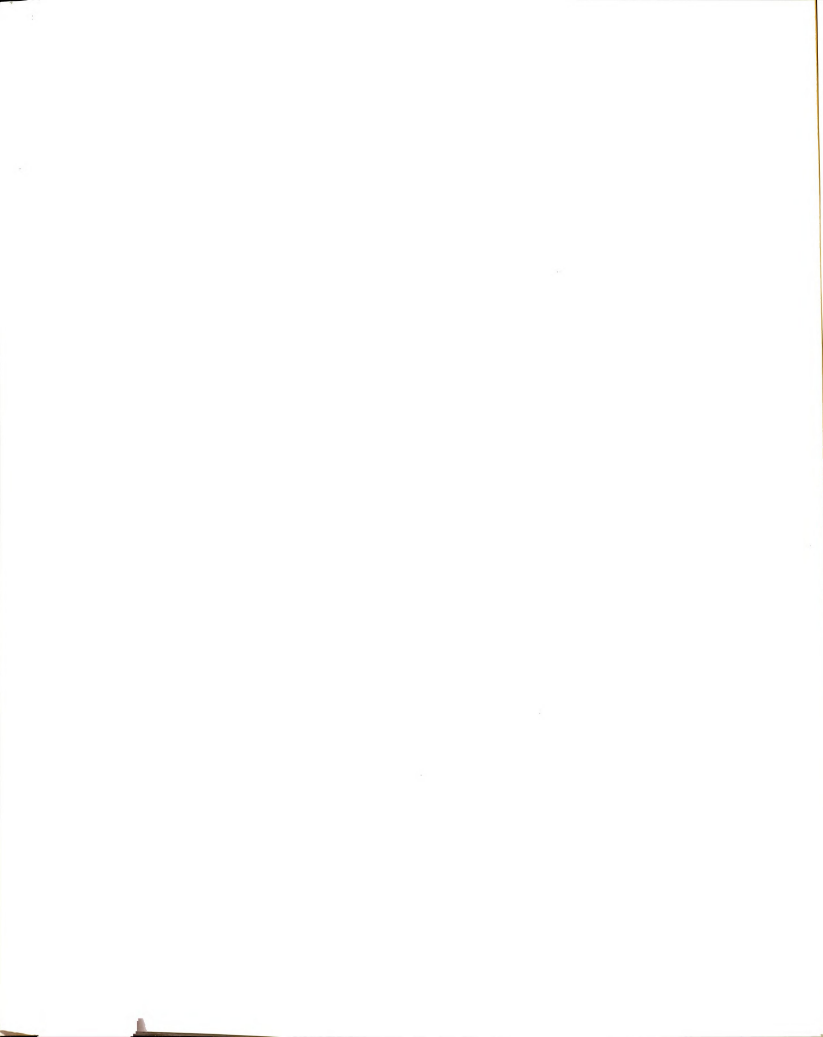
Figure 36 ^{133}Cs NMR spectra of Cs$^+$C222·SCN$^-$.
a) Proton coupled static, ν_L = 52.482 MHz;
b) Proton coupled MAS, ν_L = 52.482 MHz;
c) Proton decoupled static, ν_L = 23.61 MHz;
d) Proton decoupled MAS, ν_L = 23.61 MHz.
Observed (——),Simulated (····, -·-·-).

143

a)

b)

c)

d)
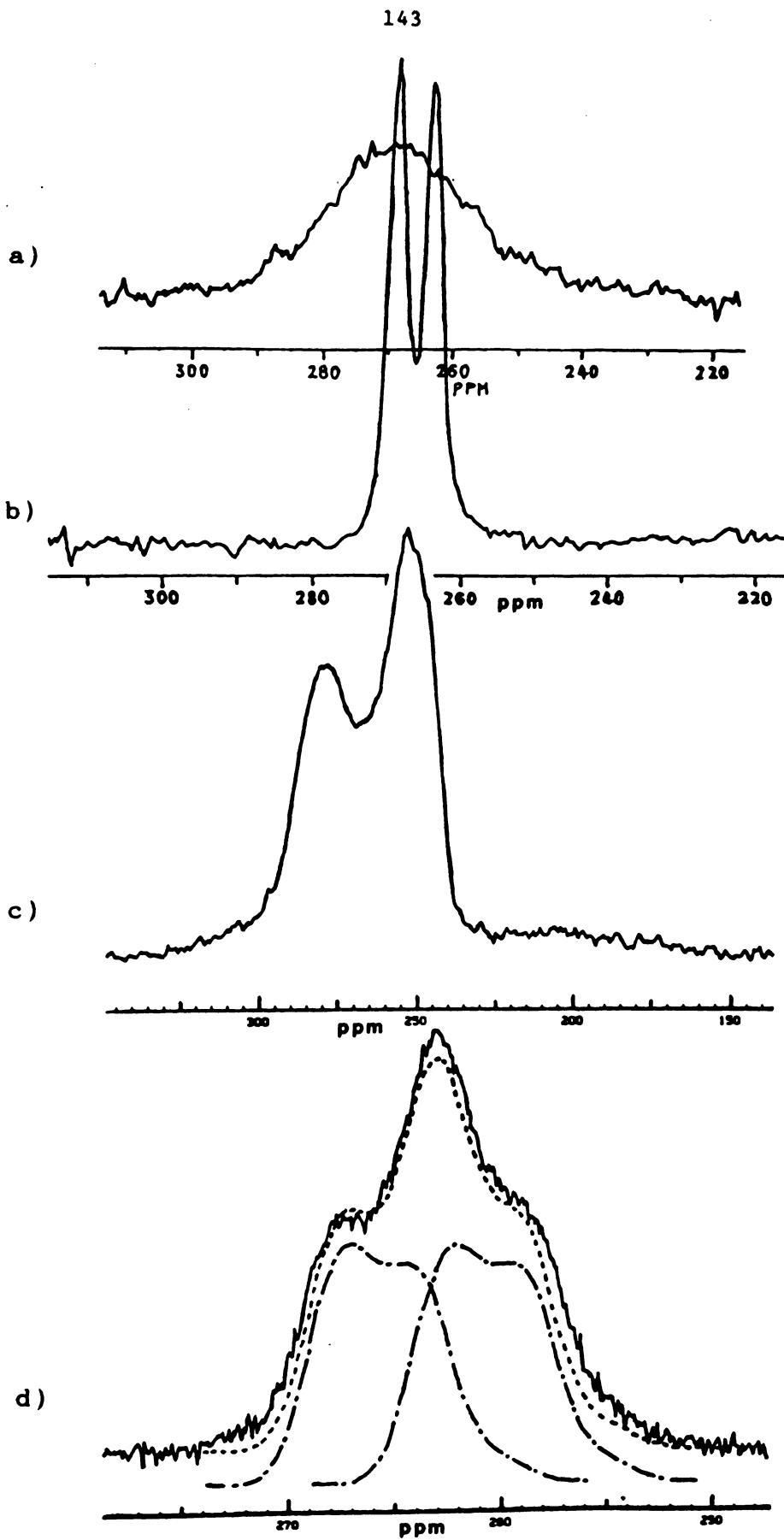
Figure 37 ^{133}Cs NMR spectra of $Cs^+C222 \cdot TPB^-$.

a) Proton coupled MAS, ν_L = 52.482 MHz;

b) Proton decoupled static, ν_L = 23.61 MHz;

c) Proton decoupled MAS, ν_L = 23.61 MHz.

Observed (——), Simulated ($\cdots$).
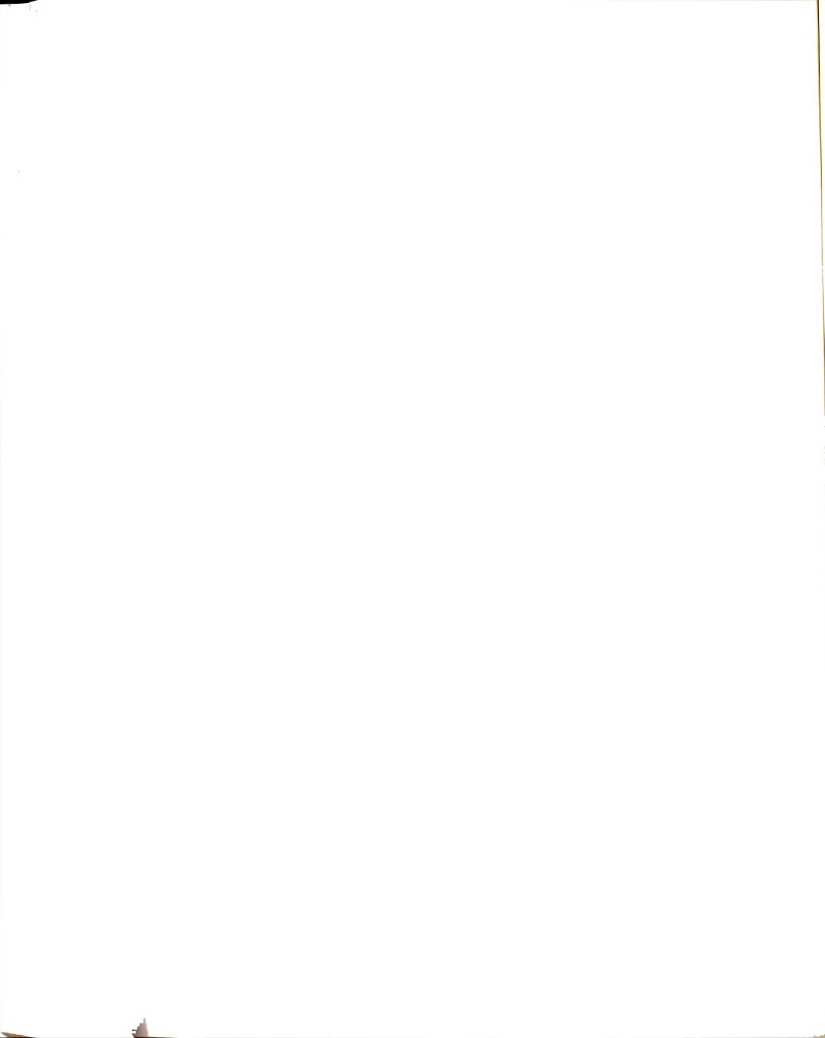
a)
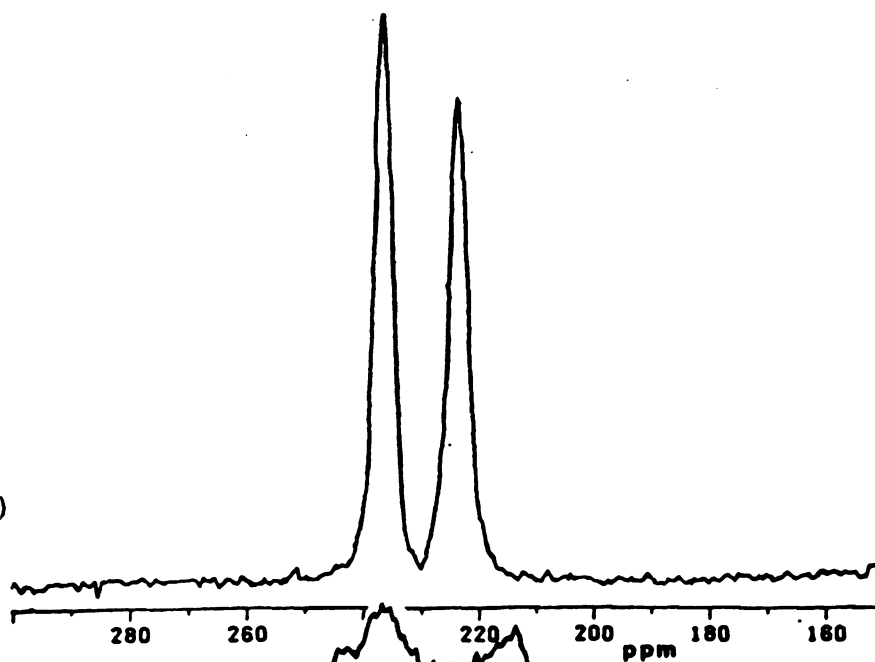
b)

c)
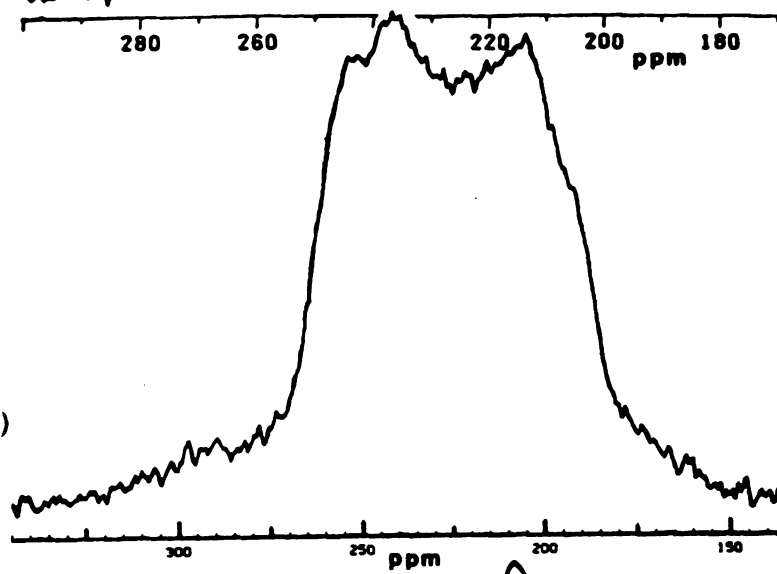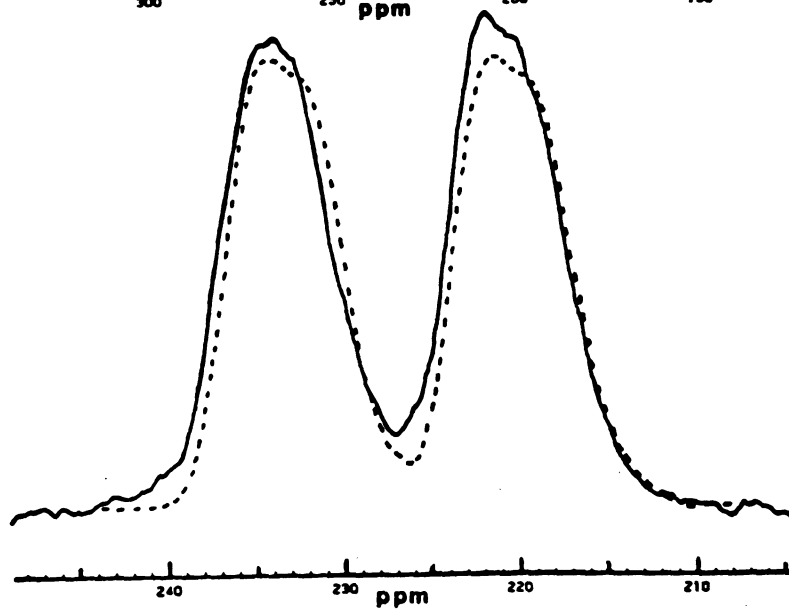
interactions. The structural changes due to different anions causes significant changes in lineshapes. At a frequency of 52.482 MHz, where quadrupolar broadening is smaller, the powder patterns primarily reflected CSA and proton dipolar coupling. A proton decoupler was not available at this frequency. Proton dipolar interactions broadened NMR lines and hindered this study. Fortunately, $Cs^+C222 \cdot I^-$ showed a single powder pattern corresponding to a single site in the structure. However two salts, $Cs^+C222 \cdot TPB^-$ and $Cs^+C222 \cdot SCN^-$ showed two powder patterns corresponding to two magnetically different sites. It was therefore extremely difficult to simulate static powder patterns from these samples since the two powder patterns, each broadened by CSA and quadrupolar interactions, overlap.

Figure 38 shows the ^{133}Cs NMR spectra of three sandwiched compounds, $Cs^+(18C6)_2 \cdot I^-$, $Cs^+(18C6)_2 \cdot TPB^-$, and $Cs^+(18C6)_2 \cdot SCN^-$. These yielded good powder patterns for all transitions, indicating small quadrupolar coupling constants. The NMR lineshape of $Cs^+(18C6)_2 \cdot I^-$ is nearly axially symmetric, while that of $Cs^+(18C6)_2 \cdot TPB^-$ is very asymmetric. Their local symmetries must be greatly different.

In contrast, the one-to-one complexes in $Cs^+18C6 \cdot I^-$, $Cs^+18C6 \cdot TPB^-$, $Cs^+18C6 \cdot SCN^-$, and $Cs^+18C6 \cdot I^- \cdot$toluene showed spectra [Figures 39 and 40], which consist of a large CSA broadened central transition and quadrupolar broadened satellites that also show CSA broadening. Highly asymmetric local structures of the Cs^+18C6 moiety are responsible for

Figure 38 Proton coupled static ^{133}Cs NMR spectra of $Cs^+(18C6)_2\cdot TPB^-$ a), $Cs^+(18C6)_2\cdot SCN^-$ b), and $Cs^+(18C6)_2\cdot I^-$ c) at $\nu_L = 52.482MHz$. Observed (——), Simulated (····).
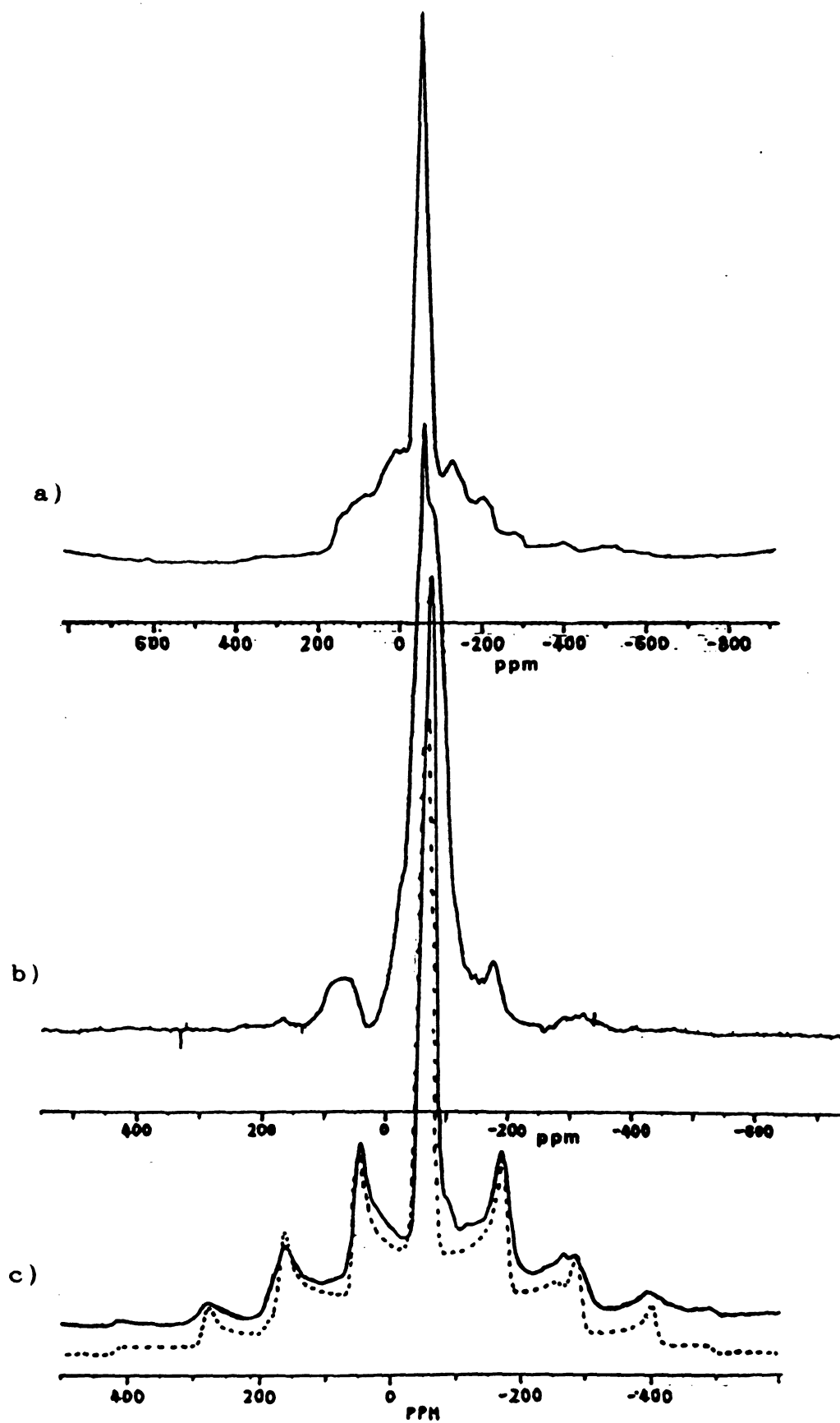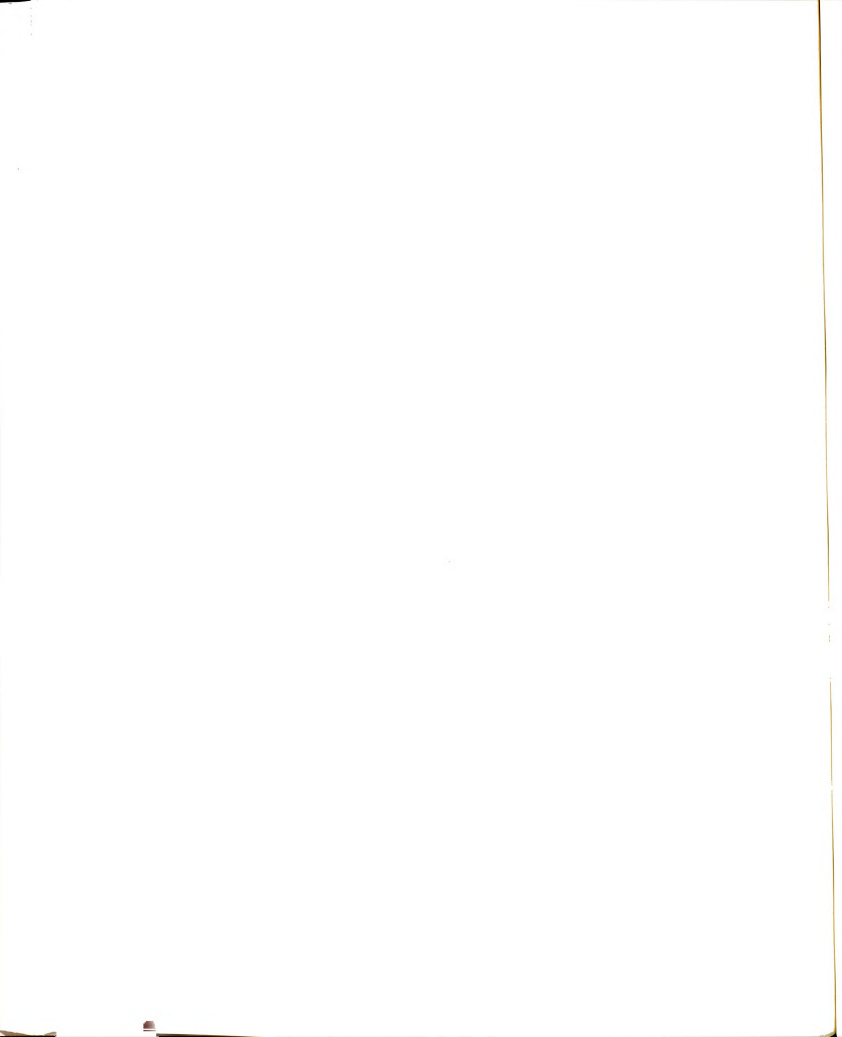
Figure 39 Proton coupled static ^{133}Cs NMR spectra of
Cs$^+$18C6·I$^-$ a), Cs$^+$18C6·TPB$^-$ b), and Cs$^+$18C6·SCN$^-$ c)
at ν_L = 52.482 MHz.
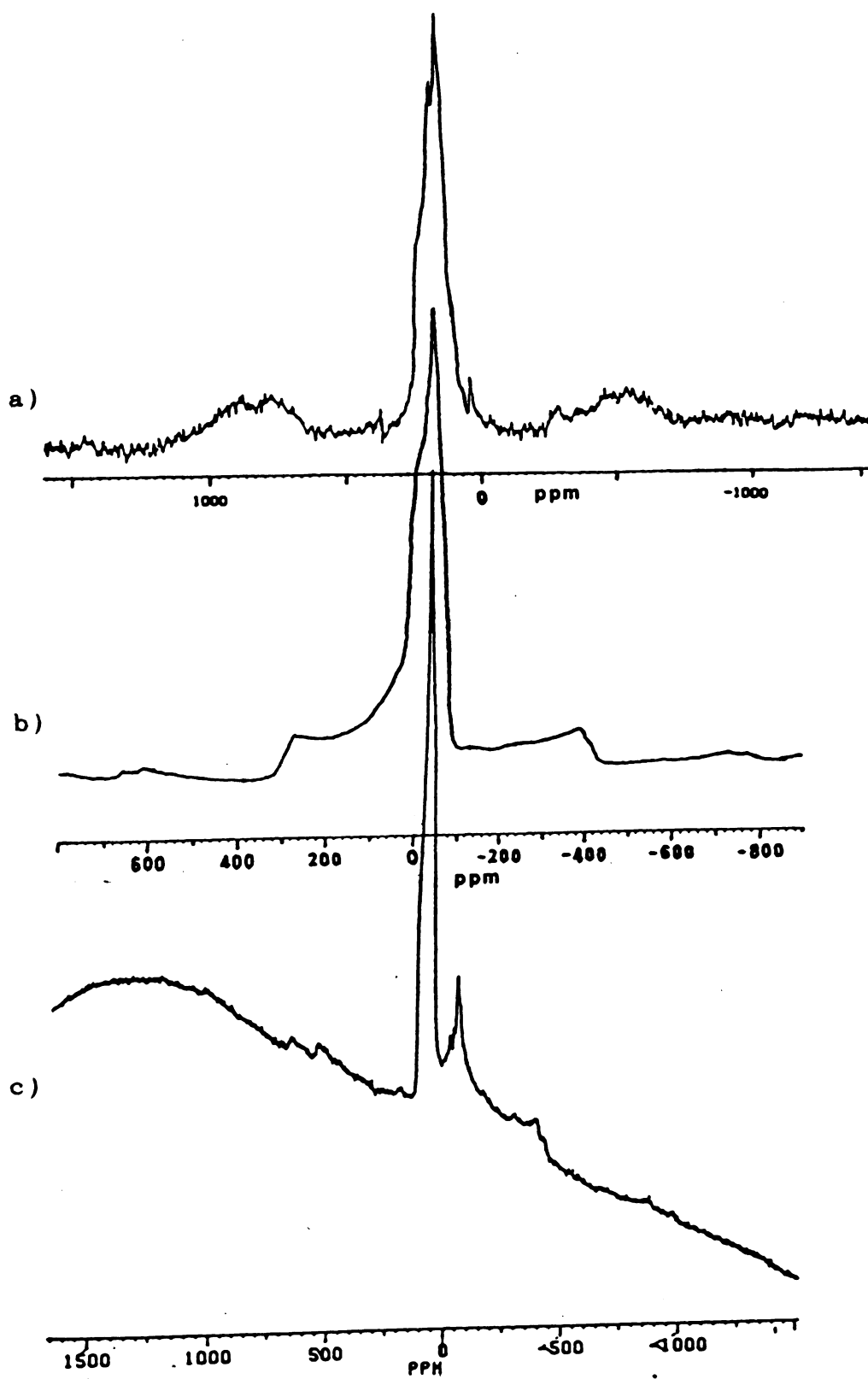
Figure 40 Proton coupled static ^{133}Cs NMR spectra of
Cs$^+$18C6·I$^-$·Toluene at ν_L = 52.482 MHz.

a) Observed;
b), c), d), e), f) and g) Simulated.

a)

χ = 0.33 MHz η = 0.14
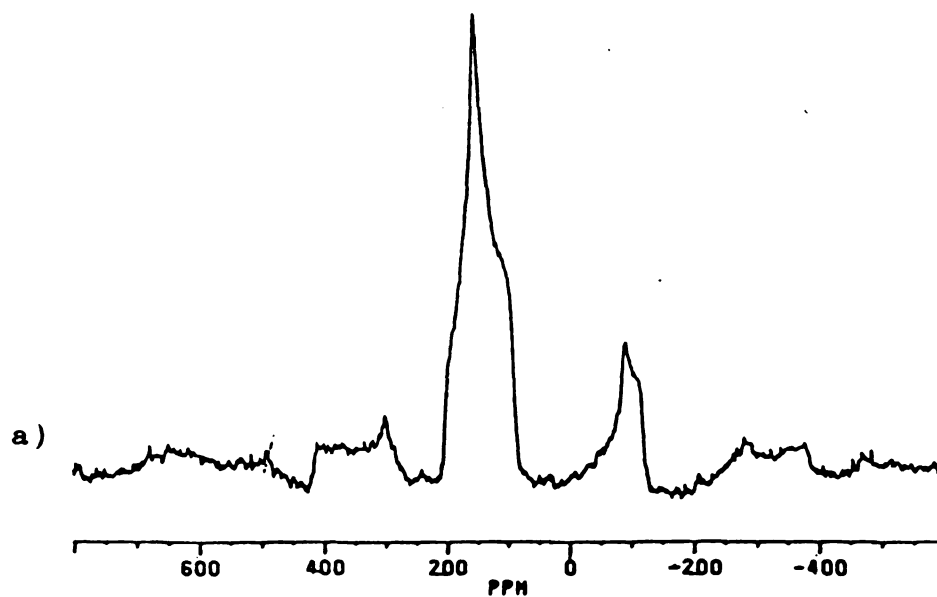
	δ_{XX}	δ_{YY}	δ_{ZZ} (ppm)
b)	145	100	200
c)	100	145	200
d)	100	200	145
e)	145	200	100
f)	200	145	100
g)	200	100	145
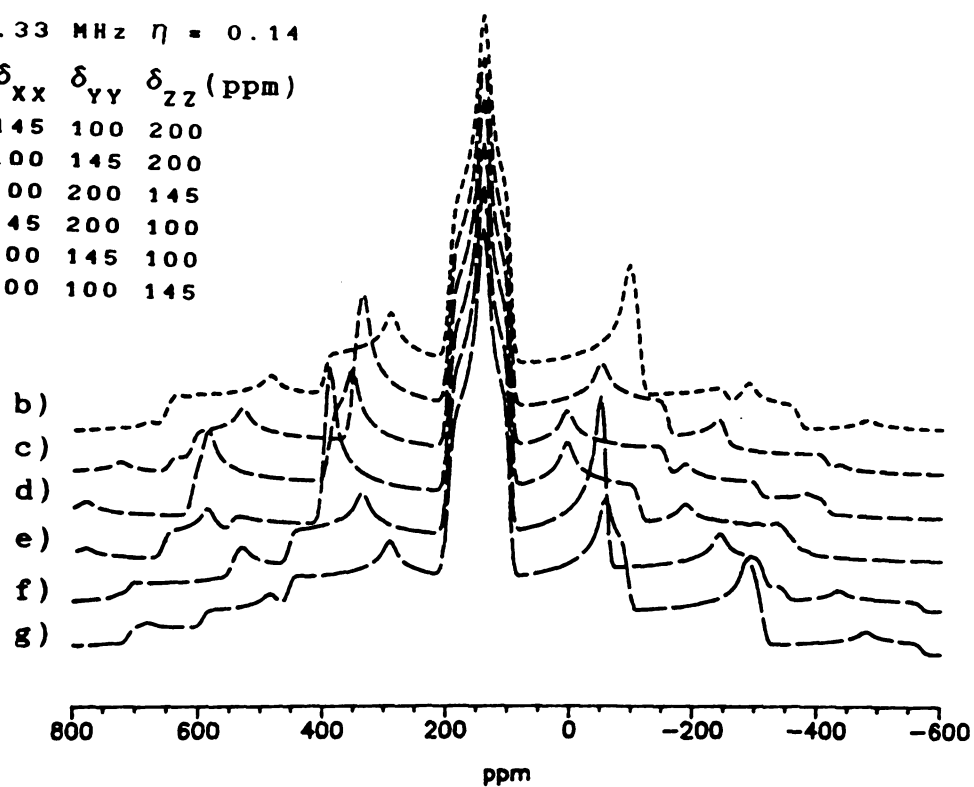
these large anisotropic broadenings. The structures of two salts, $Cs^+18C6 \cdot SCN^- \cdot H_2O$ [64] and $Cs^+18C6 \cdot I^- \cdot$ toluene [65] were determined and they show that the two highly asymmetric complexed cesium cations are bridged by either SCN^- or I^- in these compounds [Figure 41].

MAS and static spectra of $Cs^+(15C5)_2 \cdot TPB^-$ are shown in Figure 42. The lineshape of the central transition does not correspond to a nucleus in an axially symmetric environment like that of $Cs^+(15C5)_2 \cdot I^-$. The isotropic chemical shift is 39.9 ppm from a MAS experiment and two principal CSA tensor elements, ~-10 ppm and ~90 ppm can be obtained from two singularities of the static powder pattern. From this information the hidden chemical shift tensor element can be calculated as ~40 ppm by using $\delta_{iso} = 1/3 \ (\delta_{XX} + \delta_{YY} + \delta_{ZZ})$.

Some ^{133}Cs MAS NMR spectra at slow spinning speed are shown in Figure 43. Spinning sidebands cover the spectral range of the static powder patterns. This clearly indicates that all ^{133}Cs NMR spectra are inhomogeneously broadened, even in the presence of strong proton-proton interactions.

The results from simulations or estimations are listed in Table 11.

The range of the isotropic chemical shifts of Cs^+C222 is from ~226 ppm to ~270 ppm with an average value of about 250 ppm. The chemical shifts of inclusive complexes of Cs^+ with C222 in various solutions occur at ~240 ppm. Thus the chemical shifts of C222 model salts are quite sensitive to the minor changes in local structures of Cs^+. The large
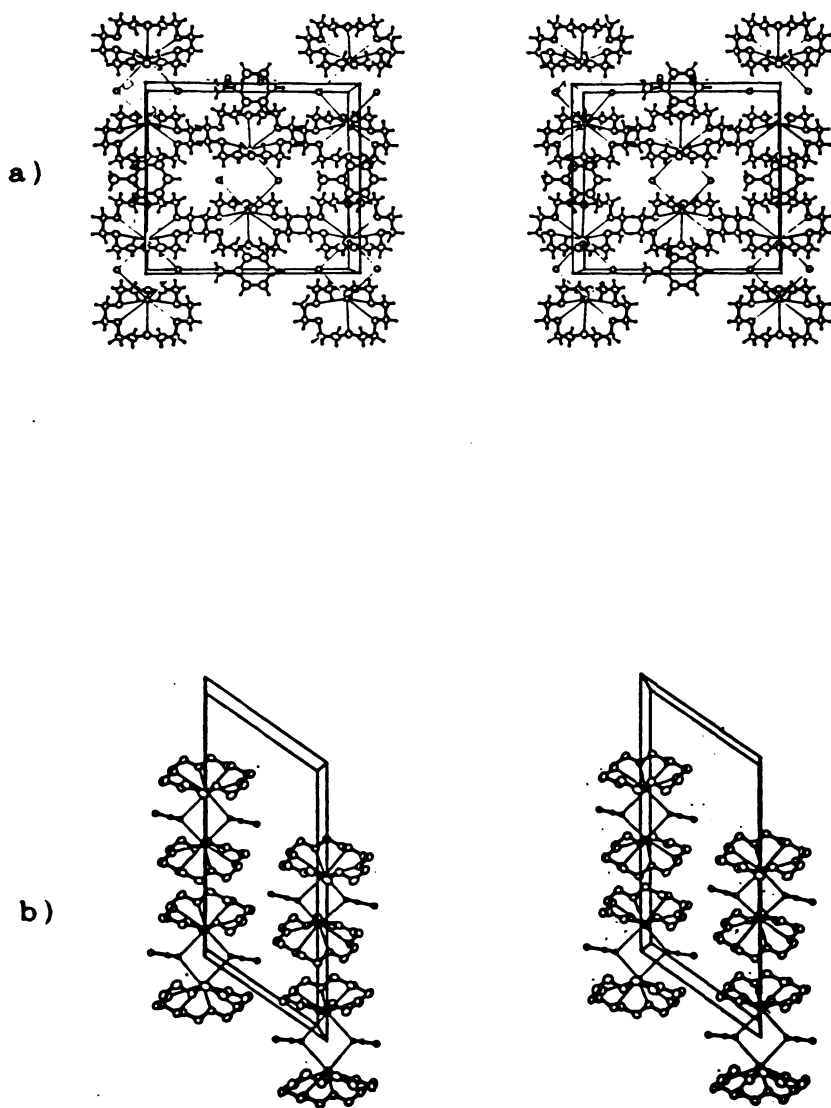
Figure 41 Stereoscopic view of the crystal structures of
Cs⁺18C6·I⁻·Toluene a) and Cs⁺18C6·SCN⁻ b) [64].
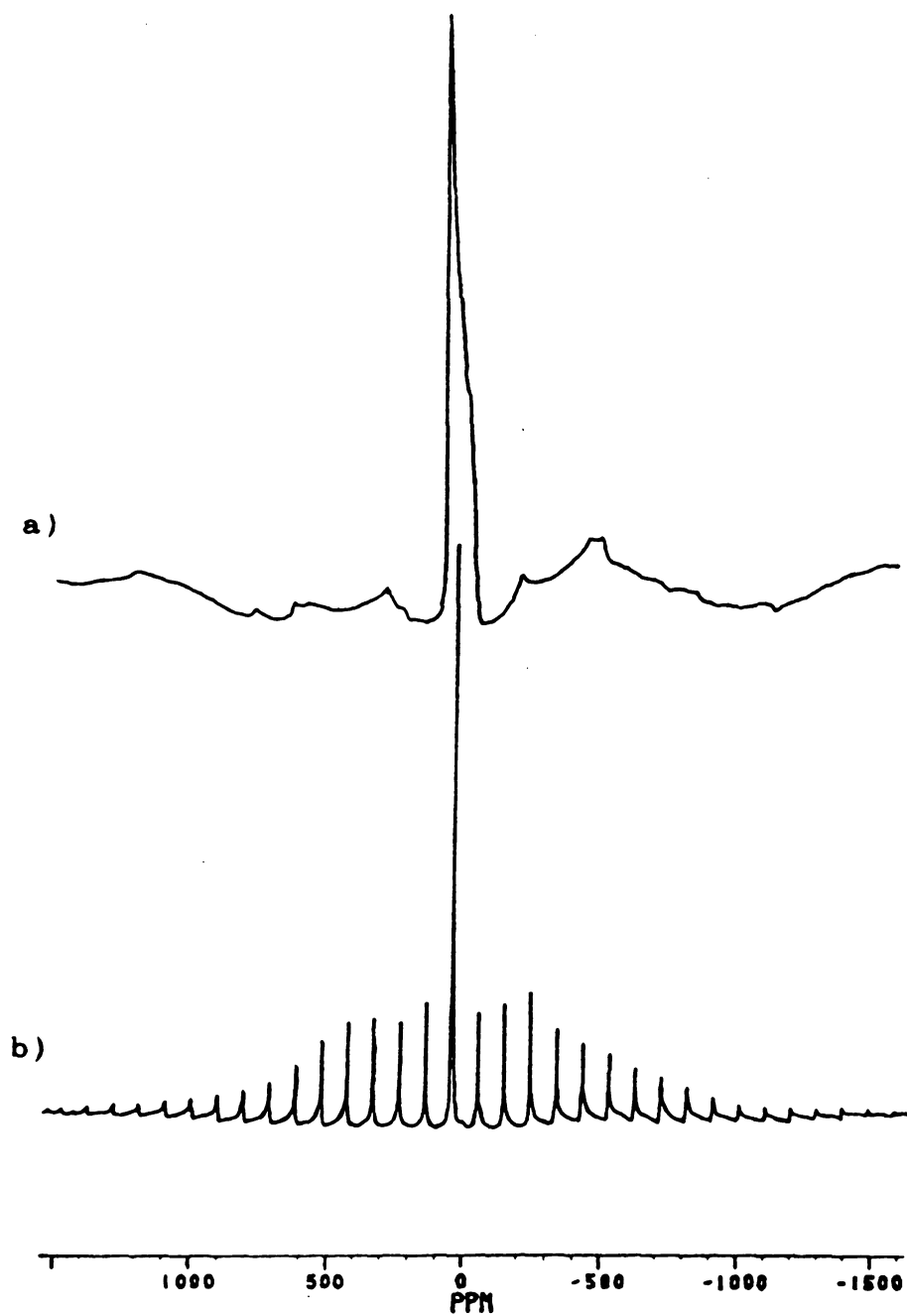
Figure 42 Proton coupled ^{133}Cs NMR spectra of
Cs$^+$(15C5)$_2$·TPB$^-$ at ν_L = 52.482 MHz.
a) Static; b) MAS.

Figure 43 ^{133}Cs MAS NMR spectra at ν_L = 52.482 MHz under slow spinning conditions.

b) $Cs^+C222 \cdot TPB^-$, $\omega_r \approx 1$ kHz;

c) $Cs^+C222 \cdot TPB^-$, $\omega_r \approx 2$ kHz;

a) $Cs^+18C6 \cdot TPB^-$, $\omega_r \approx 1$ kHz.
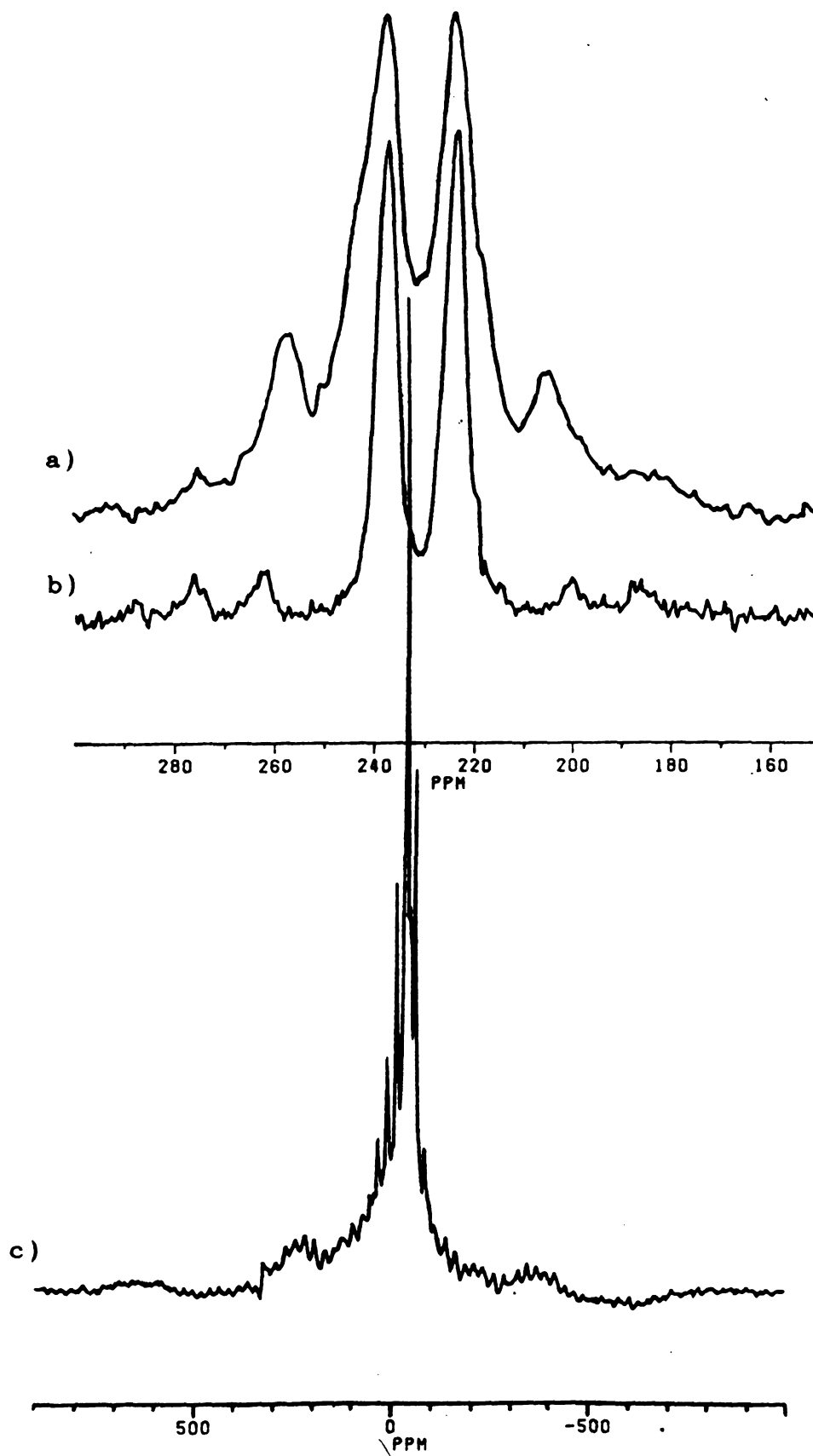
Table 11 A summary of the ^{133}Cs NMR results

Compound	δ_{XX}	δ_{YY} (ppm)	δ_{ZZ}	δ_{MAS}^{***}	QCC (MHz)	η^Q
Cs$^+$(15C5)$_2$·TPB^{-**}	-10	40	90	39.9	0.625	0.4
Cs$^+$18C6·I^{-**}	130	150	240	158.4	---	---
Cs$^+$18C6·I$^-$·ϕCH$_3^*$	145	100	200	144.1	0.33	0.14
Cs$^+$18C6·SCN^{-**}	35	68	110	69	---	---
Cs$^+$18C6·TPB^{-**}	-85	-51	7	-41	0.5	0
Cs$^+$(18C6)$_2$·I^{-*}	-65	-65	-40	-52.5	0.17	0
Cs$^+$(18C6)$_2$·SCN^{-**}	---	---	---	-61	---	---
Cs$^+$(18C6)$_2$·TPB^{-**}	-75	-45	-30	-51.1	---	---
Cs$^+$C222·I^{-*}	270	258	227	245.8	1.	0.8
Cs$^+$C222·SCN^{-*}	265	265	265	265.2	1.	0.3
	270	270	270	270.3	1.	0.3
Cs$^+$C222·TPB^{-*}	225	225	225	223.3	1.	0.4
	238	238	238	236.8	1.	0.4

[*] Parameters obtained by simulations.
[**] Estimated parameters.
[***] Chemical shift at maximum height, ν_L = 52.482 MHz.
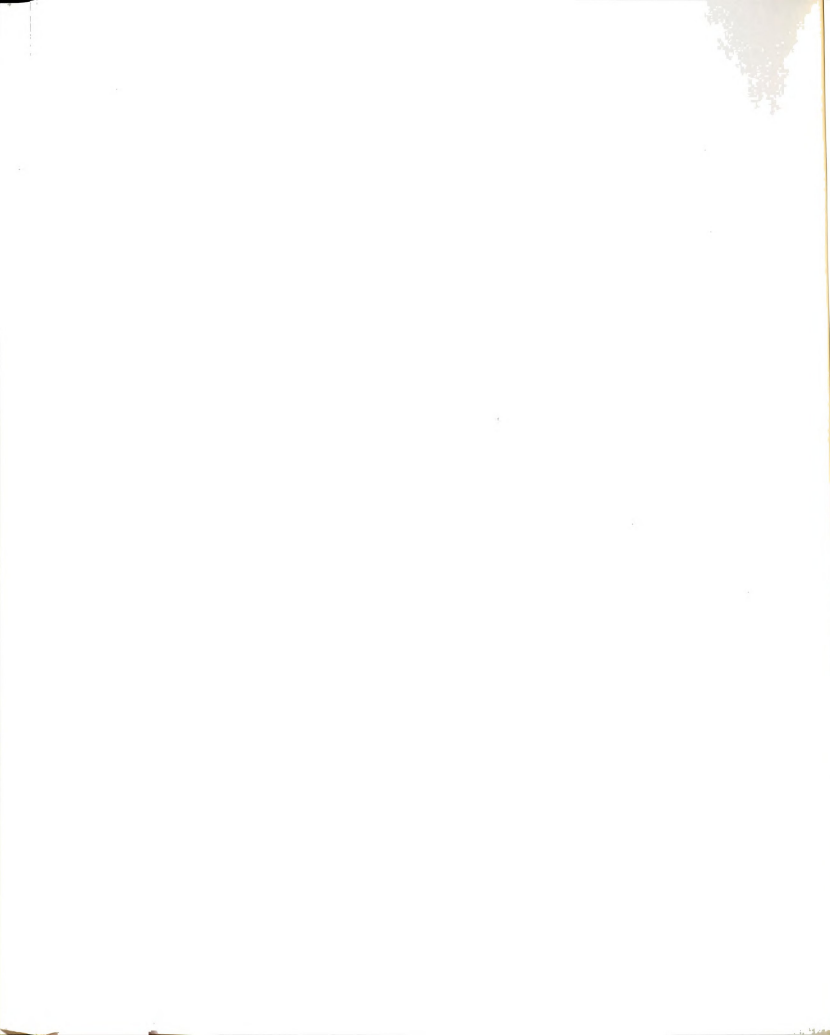
paramagnetic shifts for Cs^+C222 compounds are considered to result from electron donation from ether oxygens to Cs^+ due to overlap of the electron wavefunctions of the cesium with nonbonding p orbital of the oxygen and nitrogen atoms of C222. Encapsulation of Cs^+ in a cage that is "too small" enhances the effect.

The 18C6 sandwich compounds show fairly constant isotropic chemical shifts of -52.5 ppm, -51.1 ppm, and -61 ppm for I^-, tetraphenylborate, and SCN^- respectively. These chemical shifts are fairly close to the chemical shifts observed for Cs^+ at high 18C6 concentrations in various solvents. This invariance to the anionic environment and solvent implies that Cs^+ is well screened by the crown ethers from interactions with the anion or solvent.

The one-to-one salts, $Cs^+18C6 \cdot I^-$ and $Cs^+18C6 \cdot I^- \cdot$toluene have isotropic chemical shifts of about 158.4 ppm and 144.1 ppm. The isotropic chemical shifts of $Cs^+18C6 \cdot SCN^-$ and $Cs^+18C6 \cdot TPB^-$ are 69 ppm and -41 ppm. The structure of the $Cs^+18C6 \cdot I^- \cdot$toluene compound shows that the toluene molecules are trapped in a cage of the protons of the crown ethers and that two Cs^+ ions and two I^- ions form an ion contact square which is screened by two crowns from the toluene molecules [Figure 41]. Thus, nearly the same isotropic chemical shifts can be expected for the two iodide salts. Although the structure of $Cs^+18C6 \cdot SCN^- \cdot H2O$ is similar to that of $Cs^+18C6 \cdot I^- \cdot$toluene, the isotropic chemical shift of the SCN^- salt is very much different from that of the I^- salt. The

smaller paramagnetic shift of the SCN^- salt can be attributed to lower electron donicity of a SCN^- group. The most diamagnetically shifted Cs^+ of $Cs^+18C6 \cdot TPB^-$ among one-to-one compounds may result from a diamagnetic shielding ring current effect of the phenyl groups. This ring current effect is supported by the structure of the compound [65].

The NMR study of $Cs^+(15C5)_2 \cdot I^-$ has been described in an earlier section. Its isotropic chemical shift of 23 ppm is very close to those of $Cs^+(15C5)_2 \cdot Na^-$, $Cs^+(15C5)_2 \cdot K^-$ and $Cs^+(15C5)_2 \cdot Rb^-$ [8]. However, the isotropic chemical shift, δ_{iso} = 40.0 ppm, of $Cs^+(15C5)_2 \cdot TPB^-$ differs by 17 ppm from that of the iodide salt. It is difficult to discuss the reason for this behavior without crystal structures. In general, the isotropic chemical shifts of the 15C5 compounds are more paramagnetically shifted than those of the 18C6 sandwich compounds. This could result from shorter mean interatomic distances. Table 12 lists mean interatomic distances between Cs^+ and O.

As listed in Table 11, the C222 salts show different asymmetry parameters for different compounds which are very sensitive to the local structures of these compounds. Even if two sites in the crystal are chemically equivalent, they are magnetically nonequivalent in some compounds and have different chemical shifts. This indicates that NMR can probe very small changes in the local structure.

The principal axes for only the quadrupolar coupling tensor are labeled according to Equation (2.31) and the

Table 12 Mean interatomic distances between Cs^+ and O

Compound	Distance (Å)	Reference
$Cs^+(15C5)_2 \cdot e^-$	3.154 ± 0.09	80
$Cs^+(15C5)_2 \cdot K^-$	3.102 ± 0.07	6
$Cs^+(15C5)_2 \cdot I^-$	3.108 ± 0.148	8
$Cs(18C6)_2 \cdot e^-$	3.352 ± 0.105	8
$Cs(18C6)_2 \cdot Na^-$	3.357 ± 0.111	8
$Cs(18C6)_2 \cdot Cs^-$	3.314 ± 0.202	6
$CsC222 \cdot Cs^-$	2.958 ± 0.07	6
$CsC222 \cdot Cs^{-*}$	2.986 ± 0.098	6
$CsC222 \cdot SCN^-$	2.966 ± 0.007	20
$CsC222 \cdot SCN^{-*}$	2.983 ± 0.065	20

*Cs-N interatomic distances included.

coincidence of both CSA and quadrupolar principal axes was assumed in order to simulate powder patterns. Even with this simplification there are six combinations between the elements of the two tensors and there is no preferential order to use for the elements of CSA tensor once the quadrupolar coupling tensor has been defined. Thus, η^Q varies from zero to one but η^{CSA} can be zero, negative or positive if $\eta^{CSA} = (\delta_{YY} - \delta_{XX})/(\delta_{ZZ} - \delta_{iso})$. In a real spin system the chemical shift tensor is fixed relative to the quadrupolar coupling tensor. In fact it is very difficult to assign tensor elements without a single crystal NMR study or simulations for the six possible cases. Six simulated spectra and a spectrum of $Cs^+18C6 \cdot I^- \cdot$ toluene are shown in Figure 40. They show exactly the same CSA powder pattern for the central transition but different powder patterns for the satellites. Only one of them (Figure 40b) is very similar to the real spectrum. The two tensors are

$$\begin{bmatrix} -0.188 & 0 & 0 \\ 0 & -0.142 & 0 \\ 0 & 0 & 0.33 \end{bmatrix}$$

for a quadrupolar coupling tensor in MHz and

$$\begin{bmatrix} 145 & 0 & 0 \\ 0 & 100 & 0 \\ 0 & 0 & 200 \end{bmatrix}$$

for a chemical shift tensor in ppm. If one chooses the following convention for both tensors:

$$|R_{33} - R_{iso}| \geq |R_{11} - R_{iso}| \geq |R_{22} - R_{iso}|,$$

the quadrupolar coupling tensor is the same as with the other convention but the chemical shift tensor becomes

$$\begin{bmatrix} 100 & 0 & 0 \\ 0 & 145 & 0 \\ 0 & 0 & 200 \end{bmatrix}$$

and appropriate Eulerian angles between the two axis systems would be required to calculate the powder pattern. In this way both η^Q and η^{CSA} can be in the range between 0 and 1 since $\eta = (R_{22} - R_{11})/(R_{33} - R_{iso})$. However this makes it very complicated to calculate the powder pattern. In contrast either convention yielded the same tensors for $Cs^+(15C5)_2 \cdot I^-$ (section V. A. 3.).

This section has shown powder patterns due to CSA, first order and second order quadrupolar effects, and a mixture of both. Isotropic chemical shifts and anisotropies were discussed with their structures. In addition the importance of the convention for choosing principal axes was described. All of the ^{133}Cs NMR spectra observed here are inhomogeneously broadened.

V. A. 6. A study of ^{39}K and ^{87}Rb NMR spectra by the spin echo method.

The spectrum of KSCN shown in Figure 44 was obtained by using the phase cycled spin echo pulse train described in the previous chapter. It has been expanded to demonstrate the second order static powder pattern. Simulation of this spectrum yielded a QCC, χ = 0.65 MHz and an asymmetry parameter, η = 0.8.

Figures 45 and 46 show the observed ^{39}K NMR spectra of the iodide and thiocyanate salts of $K^+(12C4)_2$, $K^+(15C5)_2$, K^+18C6, and K^+C222 respectively. The sharp NMR line of $K^+(12C4)_2 \cdot I^-$ implies that the coordination structure of the complexed cation may be very similar to a cubic structure which has a QCC, $\chi \approx 0$ MHz. The NMR lines of the 15C5 salts are broader than those of the 12C4 salts but don't show any satellite powder pattern. The range of the estimated QCC is probably from 0.3 to 0.6 MHz. Although the two 15C5 molecules may form a quite symmetrical coordination environment around K^+, it may not be as symmetrical as that of the 12C4 salt. The nonaxially symmetric environment of the corresponding Cs^+ salt has been discussed in the previous section. However the SCN^- salt of 12C4 showed only a very broad line at a resonance frequency of 23.32 MHz and was not detectable at a resonance frequency of 18.673 MHz. $K^+(15C5)_2 \cdot SCN^-$ had an axially symmetric second order powder pattern with QCC, χ = 1.75 MHz. Unlike $K^+(12C4)_2 \cdot I^-$, the electronic environment of
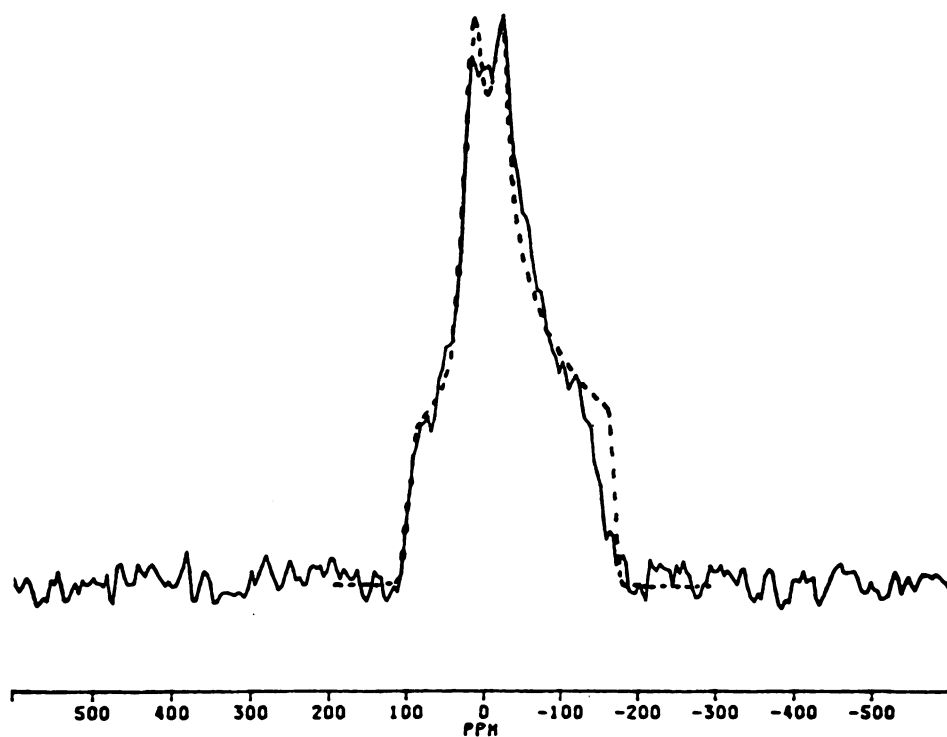
Figure 44 ^{39}K spin echo NMR spectra of K^+SCN^- at ν_L = 18.67 MHz. Observed (——), Simulated (····).
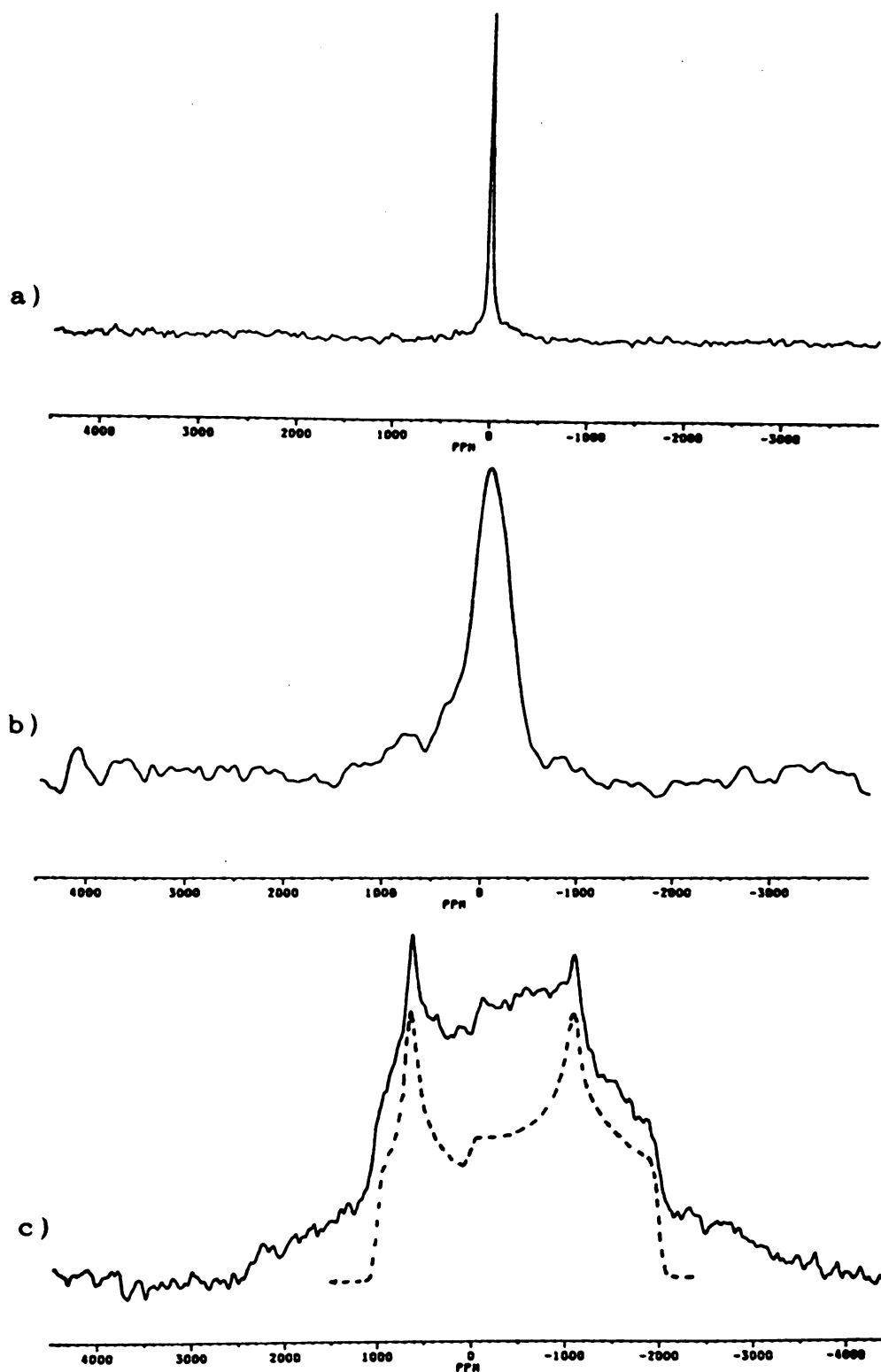
Figure 45 ^{39}K spin echo NMR spectra of $K^+(12C4)_2 \cdot I^-$ a),
$K^+(15C5)_2 \cdot I^-$ b), and $K^+ 18C6 \cdot I^-$ c) at ν_L = 18.67
MHz. Observed (——), Simulated ($\cdots$).

Figure 46 ^{39}K spin echo NMR spectra of $K^+(12C4)_2 \cdot SCN^-$ a), $K^+(15C5)_2 \cdot SCN^-$ b), $K^+18C6 \cdot SCN^-$ c), at $\nu_L = 23.32$ MHz and $K^+C222 \cdot SCN^-$ d) at $\nu_L = 18.67$ MHz. Observed (——), Simulated (····).

a)

b)

c)

d)
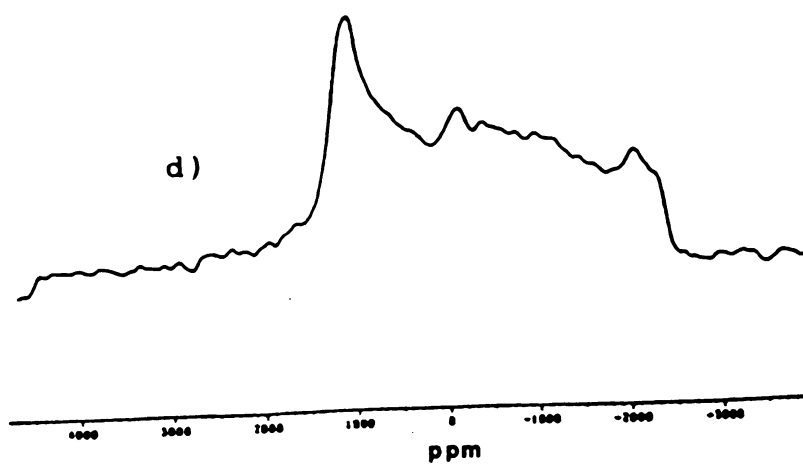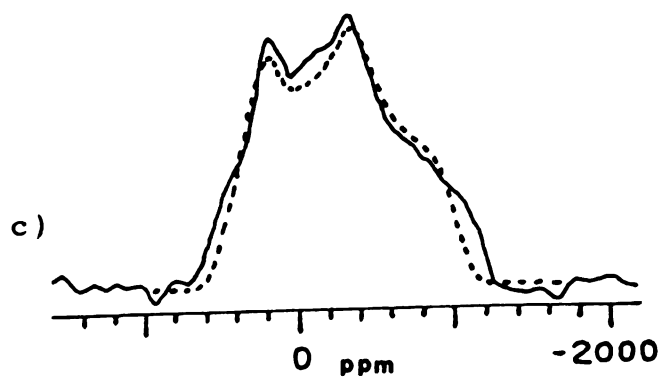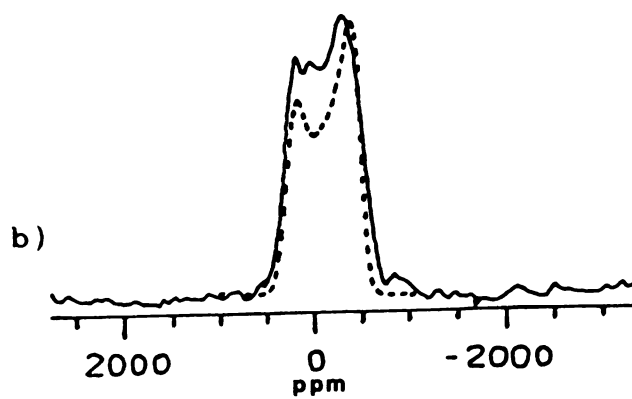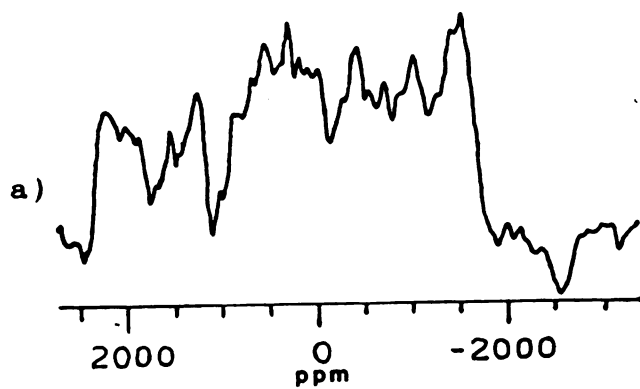
$K^+(12C4)_2 \cdot SCN^-$ might be distorted by forming a staggered sandwich compound or by the intrusion of the SCN^- or water of crystallization into or between the crown rings. Surprisingly the electronic environment of $K^+(15C5)_2 \cdot SCN^-$ is not distorted as much as that of $K^+(12C4)_2 \cdot SCN^-$. In contrast to the two classes of sandwich compounds, the complexed K^+ has only a single crown ether ring and thus cannot be shielded by the 18-crown-6 molecule. This allows the potassium cation to interact with I^-, SCN^- or protons [66]. Hence, a quite asymmetric environment can be expected. Simulation of the spectrum of $K^+18C6 \cdot I^-$ yields a QCC, χ = 2.5 MHz, and an asymmetry parameter, η = 0.3. Surprisingly, very strong quadrupolar interactions have been observed with all C222 salts. The several spectra of the C222 salts are doubtful because of the distorted lineshapes or bad signal to noise ratio.

In general the results with ^{87}Rb NMR measurements are less successful than those with ^{39}K NMR measurements. This can be explained by the large quadrupole moment and Sternheimer antishielding factor of ^{87}Rb [67].

Figure 47 shows the spectra of $Rb^+18C6 \cdot Cl^-$ and $Rb^+18C6 \cdot SCN^-$. It seems that the lineshapes are mainly quadrupolar mixed with some CSA. The estimated QCC and the asymmetry parameter of these compounds are; $\chi \approx 6$ MHz, $\eta^Q \approx 0.75$, $\chi \approx 4.5$ MHz, and $\eta^Q \approx 1$, respectively.

Recently, the ^{87}Rb spectrum of $Rb^+C222 \cdot Br^-$ [68] was observed with a VXR-300 NMR spectrometer with 2 MHz

a)

b)
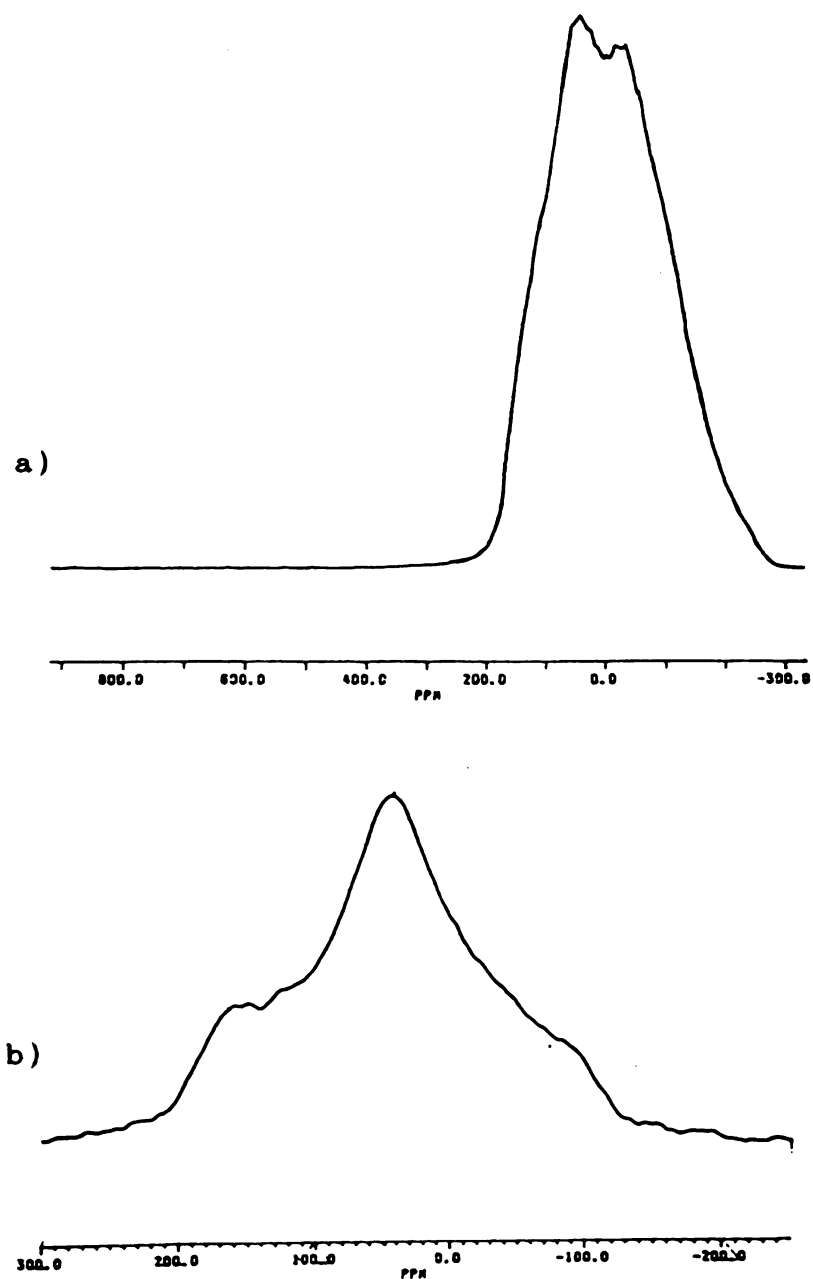
Figure 47 ^{87}Rb spin echo NMR spectra of Rb$^+$18C6·Cl$^-$ a) and Rb$^+$18C6·SCN$^-$ b) at ν_L = 130.93 MHz.

sweepwidth capability. It is shown in Figure 48, and has a linewidth of about 520 kHz. In this case the strength of the quadrupolar interaction is comparable to that of the Zeeman interaction. This explains why the ^{87}Rb and ^{39}K NMR signals of some Rb$^+$ and K$^+$ salts could not be detected by using a spectrometer with ~150 kHz sweepwidth capability.

Fortunately the ^{39}K and ^{87}Rb spin echo NMR spectra of alkalides and electrides are much better than those of the model salts. Figure 49 shows the ^{39}K NMR spectra for K$^+$(15C5)$_2$·e$^-$, K$^+$(15C5)$_2$·K$^-$, K$^+$(15C5)$_2$·Na$^-$, and K$^+$18C6·K$^-$. The peak of K$^+$(15C5)$_2$·e$^-$ at 47 ppm clearly indicates that it is for K$^+$ and this compound is a genuine electride, while K$^+$(15C5)$_2$·K$^-$ shows only a single sharp peak at -101 ppm, which is a proof of K$^-$. The potassium cation in K$^+$(15C5)$_2$·K$^-$ may be in a very unsymmetrical environment unlike that of the corresponding electride. However, K$^+$(15C5)$_2$·Na$^-$ has a peak at -89 ppm. This could be either K$^-$ or K$^+$, but this peak was assigned for the latter since ^{23}Na NMR showed clearly an Na$^-$ NMR peak [19]. However, the possibility of a mixture of the sodide and the potasside cannot be excluded. The total linewidth of the NMR spectrum of K$^+$18C6·K$^-$ is almost the same as that of K$^+$18C6·SCN$^-$, indicating that it may be a K$^+$ NMR spectrum with a QCC of ~1.7 MHz and an asymmetry parameter of 1. The formation of dimers or chains such as in the compounds, K$^+$C222·K$^-$ [69], Rb$^+$C222·Rb$^-$ [69], and Rb$^+$18C6·Rb$^-$ [69] might distort the NMR lineshape; however, the triangular shaped peak of K$^+$18C6·K$^-$ could result from either K$^+$ or K$^-$;
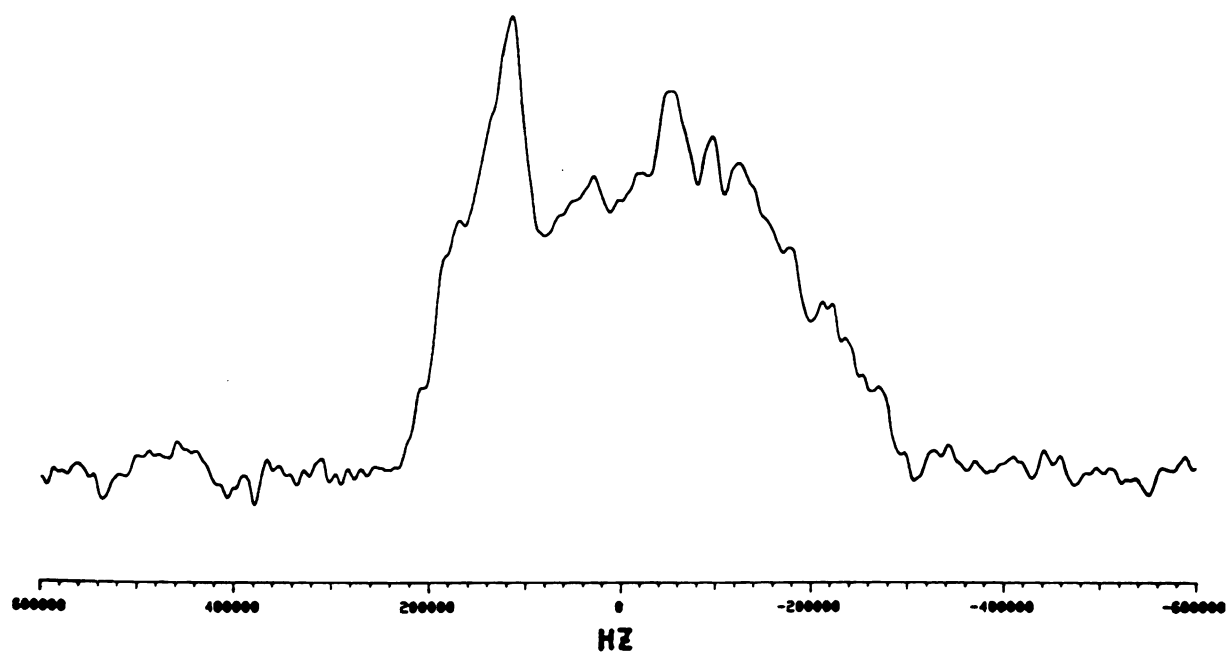
Figure 48 ^{87}Rb spin echo NMR spectra of $Rb^{+}C222 \cdot Br^{-}$ at ν_{L} = 98.16 MHz.

Figure 49 ^{39}K spin echo NMR spectra of alkalides and
electrides containing crown ethers.
a) $K^+(15C5)_2 \cdot e^-$, ν_L = 23.32 MHz;
b) $K^+(15C5)_2 \cdot K^-$, ν_L = 18.67 MHz;
c) $K^+(15C5)_2 \cdot Na^-$, ν_L = 18.67 MHz;
d) $K^+18C6 \cdot K^-$, ν_L = 23.32 MHz.
Observed (——), Simulated (····).
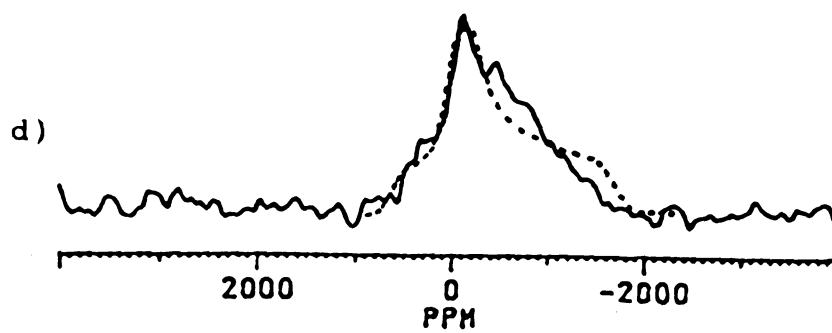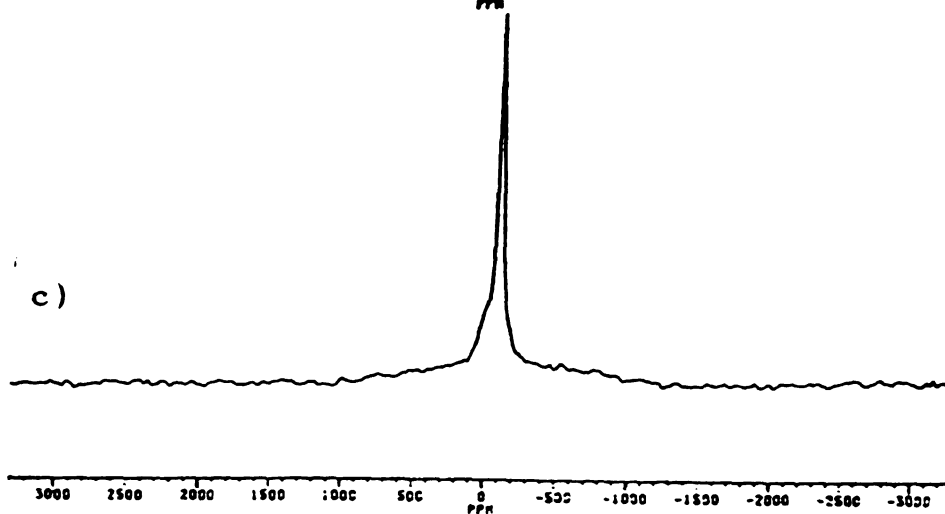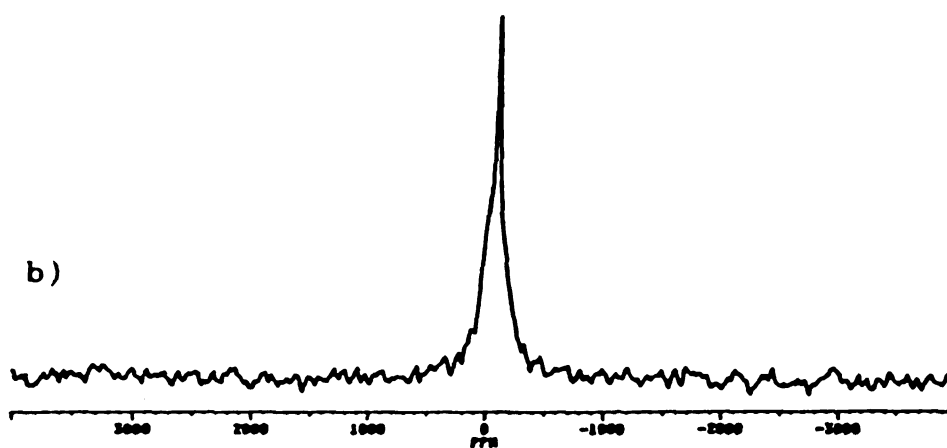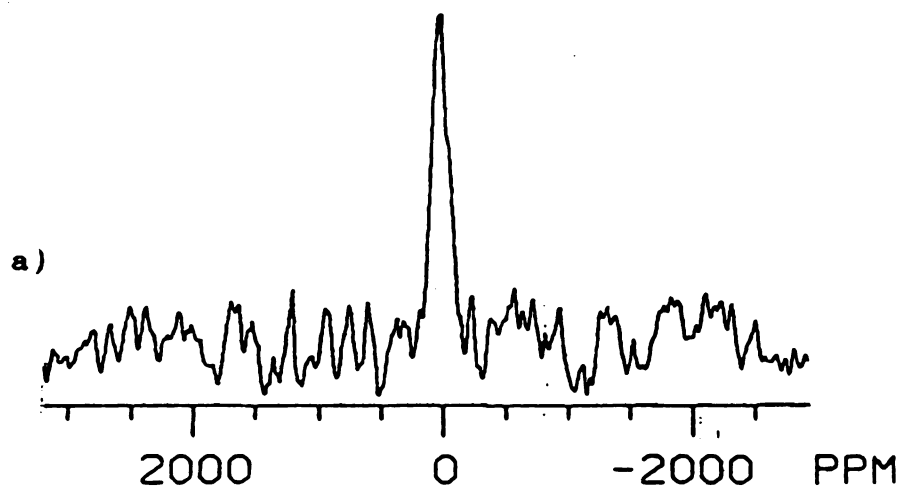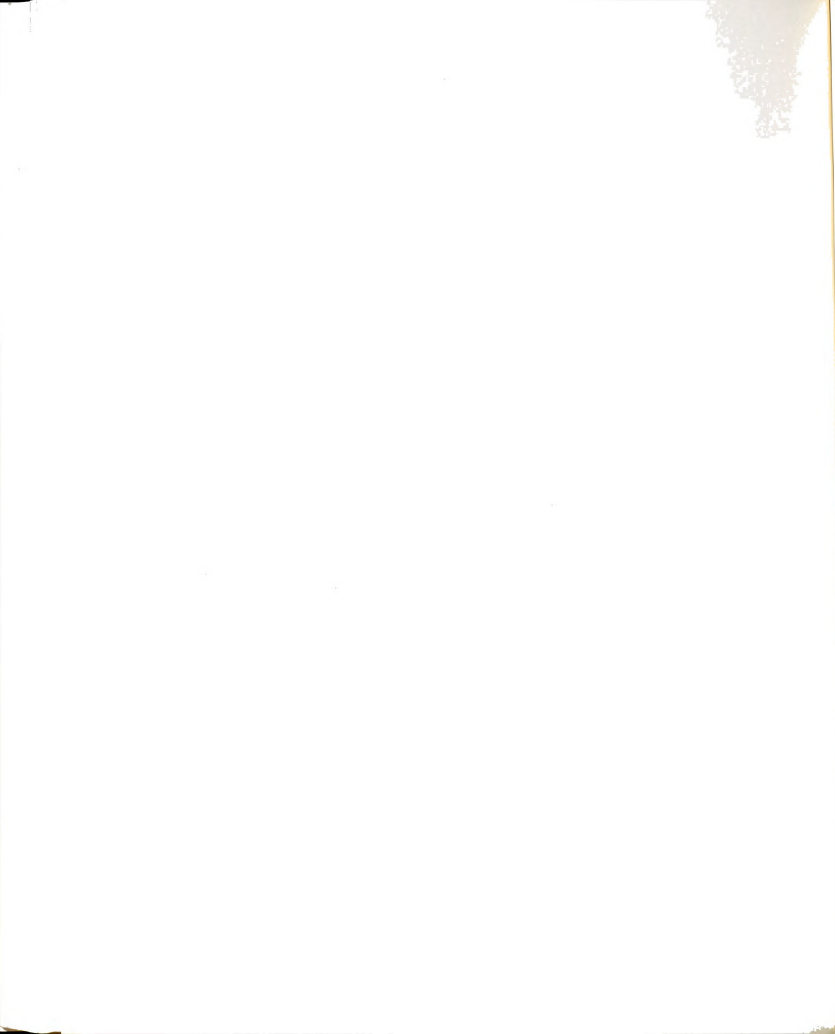
more likely K^+.

The spectra shown in Figure 50 are obtained from $K^+C222 \cdot e^-$, $K^+C222 \cdot K^-$, and $K^+C222 \cdot Na^-$, respectively. The NMR line of $K^+C222 \cdot Na^-$ is an almost typical quadrupolar powder pattern with a QCC, $\chi = 2.65$ MHz and an asymmetry parameter, $\eta = 0.25$. However, the distorted lineshapes of K^+ for the corresponding electride and potasside have been observed. The field dependence of these spectra showed that they are mainly broadened by the second order quadrupolar interaction. The reason for the lineshape distortion is unclear. The K^+ spectra for both $K^+C222 \cdot e^-$ and $K^+C222 \cdot K^-$ show almost the same linewidth and lineshape as expected from their similar packing structure [6]. Even though their detailed structures are different, the packing of the cations and the anions (or anionic sites) are very similar in these compounds. The estimated QCC for K^+ in both cases is ~2.7 MHz. In contrast the structure of $K^+C222 \cdot Na^-$ [6] is completely different from those of the potasside and electride. In the sodide, $K^+C222 \cdot Na^-$, the anions are isolated in the structure, whereas pairs of K^- and e^- are very close to one another in $K^+C222 \cdot K^-$ and $K^+C222 \cdot e^-$ respectively. The cationic NMR spectra indicate that the nature of the counteranion (K^- or e^-) is less important than the nature of the packing and that K^+ in the potasside is very similar to that in the electride. The quadrupolar lineshape for K^- in $K^+C222 \cdot K^-$ is consistent with the dimer structure of K^- and indicates a substantial perturbation from spherical symmetry. This is the first
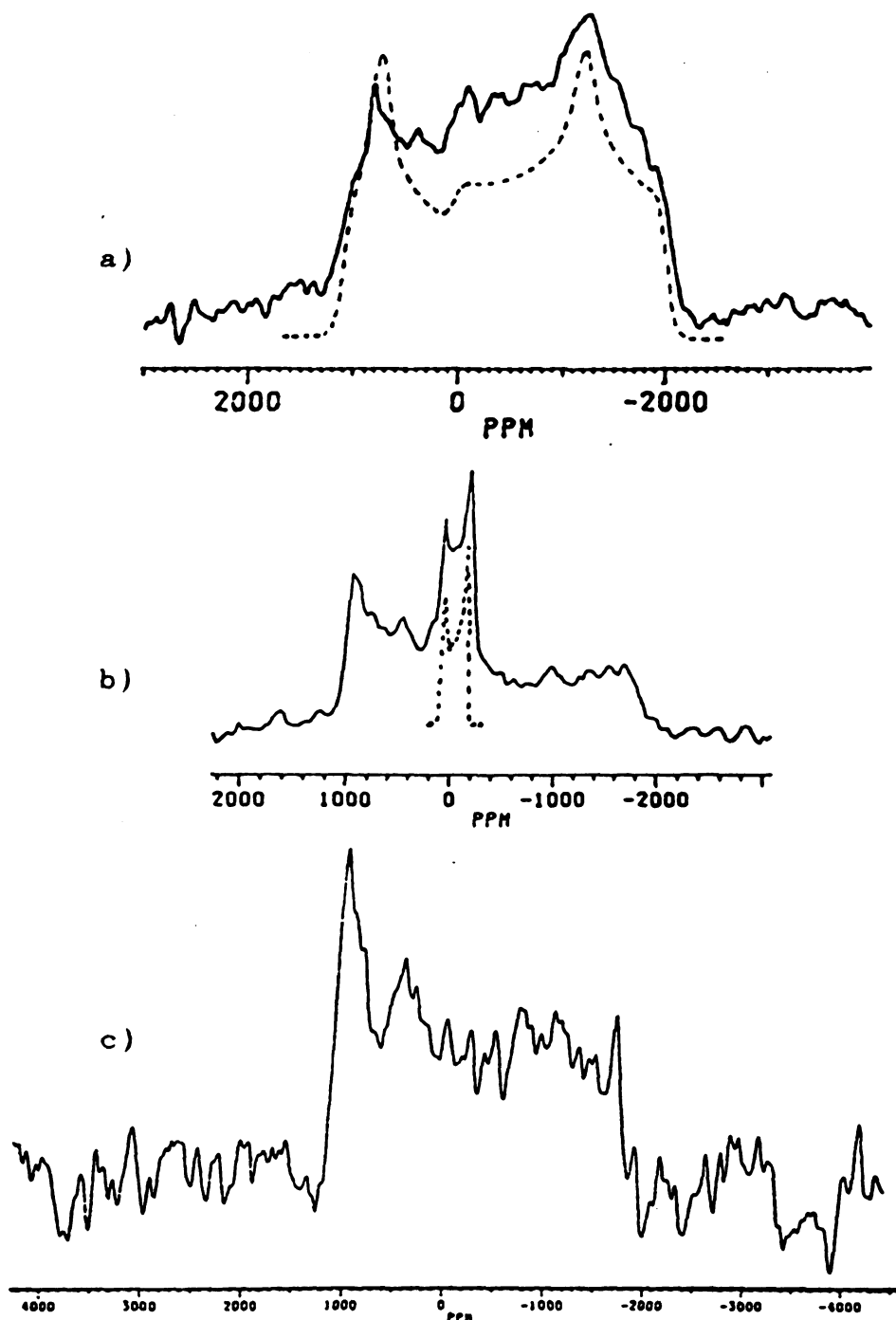
Figure 50 ^{39}K spin echo NMR spectra of alkalides and
electrides containing C222 at ν_L = 18.67 MHz.
a) $K^+C222\cdot Na^-$; b) $K^+C222\cdot K^-$; c) $K^+C222\cdot e^-$.
Observed (——), Simulated ($\cdots$).

second order quadrupolar powder pattern (QCC = 0.8 MHz and η = 0) obtained for an alkali metal anion. When the electron density distribution is distorted from spherical shape, the higher energy state can be mixed into the lower states according to the calculation of Sternheimer [70]. A "bond" between two akali metal anions may be formed by mixing the ns orbitals with low lying excited states such as (n - 1)d orbitals.

Figure 51 shows the ^{87}Rb NMR spectra of $Rb^+(15C5)_2 \cdot Rb^-$ and $Rb^+(15C5)_2 \cdot e^-$. It is difficult to extract information from the broad, noisy spectrum of $Rb^+(15C5)_2 \cdot e^-$, but an approximate QCC, $\chi \approx 6$ MHz is estimated. Only the Rb^- peak has been observed from $Rb^+(15C5)_2 \cdot Rb^-$. This is similar to the result obtained from the ^{39}K NMR spectrum of $K^+(15C5)_2 \cdot K^-$ and indicates that the complexed cations of both the rubidide and the potasside may have very similar environments.

The ^{87}Rb NMR spectra of two rubidium 18C6 alkalides are shown in Figure 52. The lineshape of $Rb^+18C6 \cdot Na^-$ is not characteristic of the second order quadrupolar pattern, but yields an approximate QCC, $\chi \approx 6.5$ MHz. The spectrum of $Rb^+18C6 \cdot Rb^-$ at the resonance frequency of 163.6 MHz shows both Rb^+ and Rb^- peaks on a distorted baseline. Unfortunately, the experiment could not be repeated. Another synthesis of this compound did not yield good spectra at the resonance frequency of 130.9 MHz, even though many attempts were made. The fact that the Rb^+ spectra for both $Rb^+18C6 \cdot Na^-$ and $Rb^+18C6 \cdot Rb^-$ show similar powder patterns may indicate
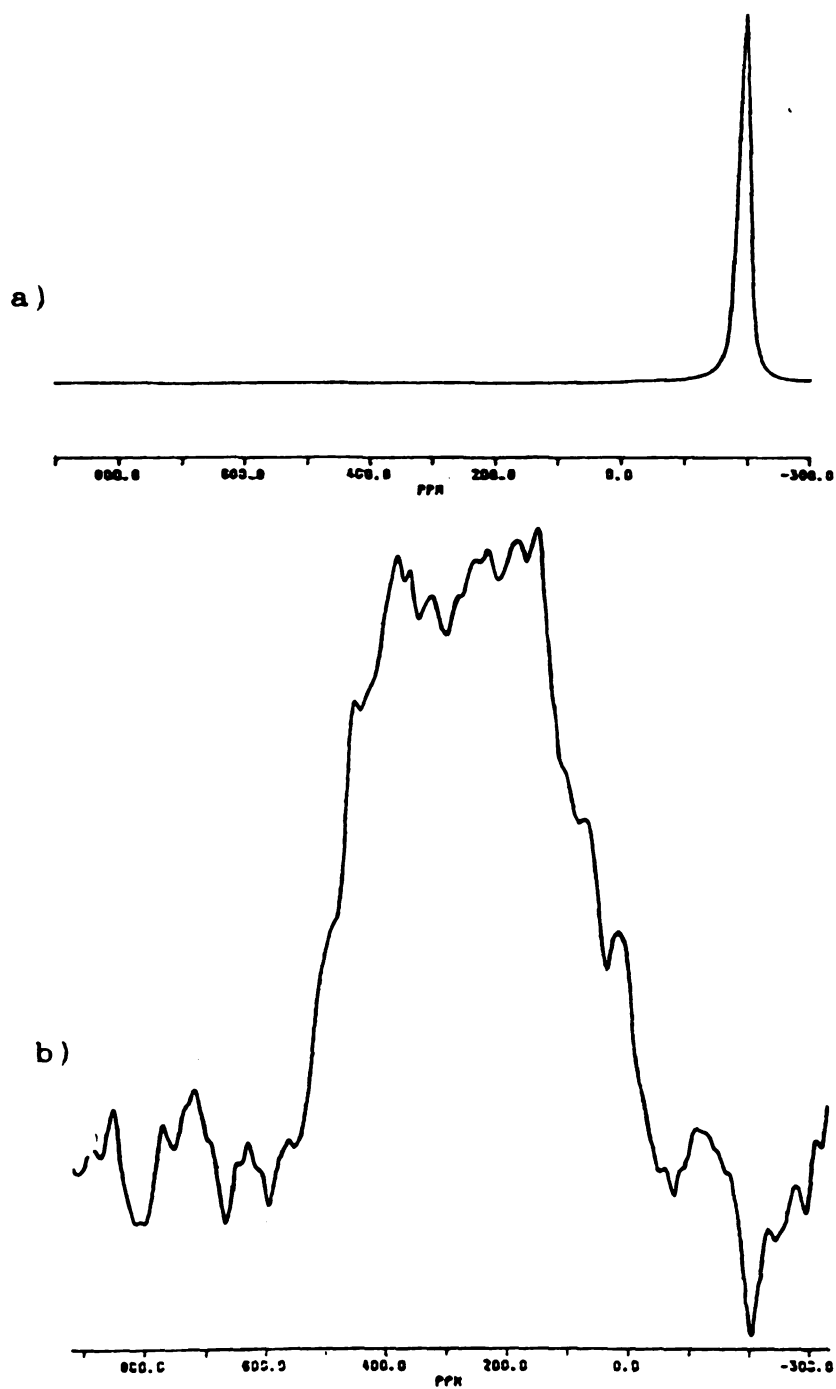
Figure 51 ^{87}Rb spin echo spectra of $Rb^{+}(15C5)_{2} \cdot Rb^{-}$ a) and $Rb^{+}(15C5)_{2} \cdot e^{-}$ b) at ν_{L} = 130.93 MHz.
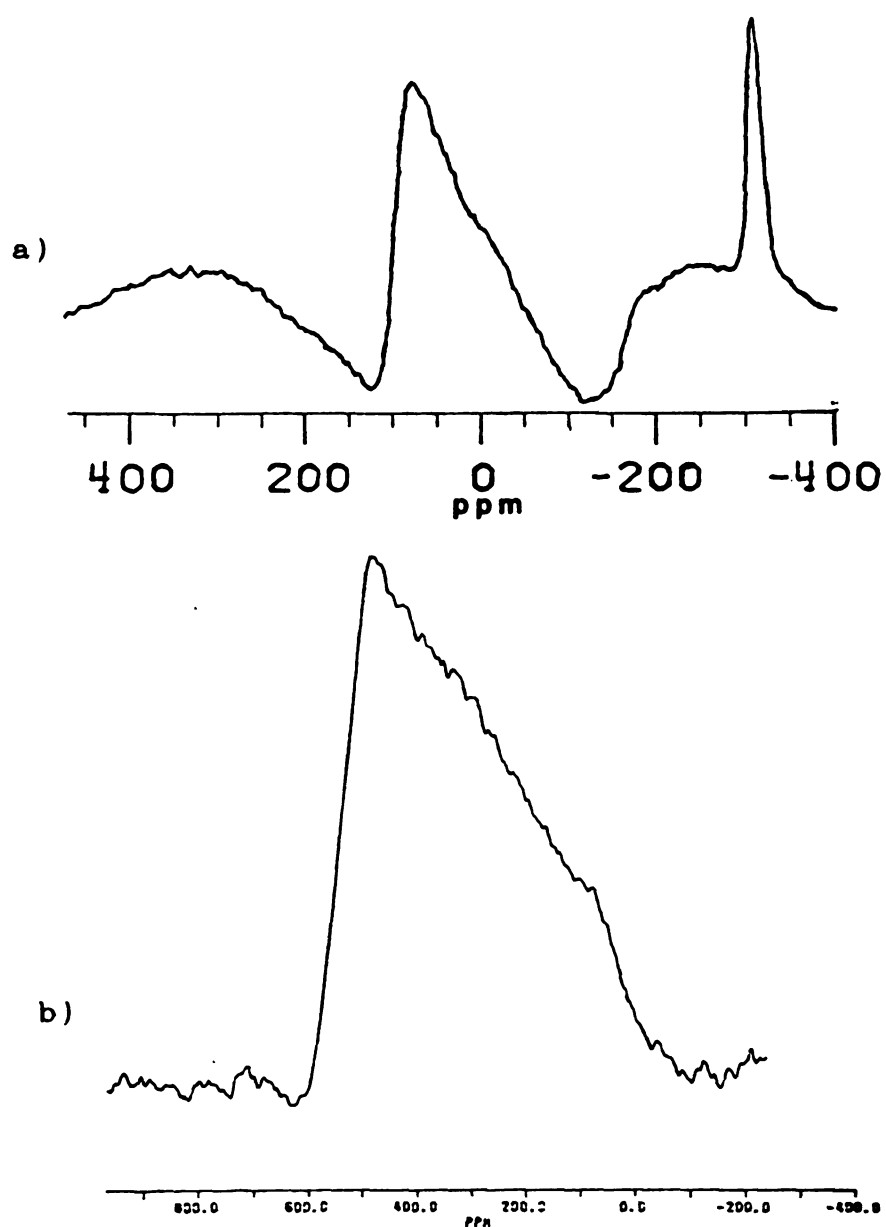
Figure 52 ^{87}Rb spin echo spectra of Rb$^+$18C6·Rb$^-$ a) at ν_L = 163.7 MHz and Rb$^+$18C6·Na$^-$ b) at ν_L = 130.93 MHz.

that their structures are very similar.

An extremely broad NMR spectrum of $Rb^+C222 \cdot Rb^-$ is shown in Figure 53. The structure of this compound is known and it is isostructural with the corresponding potassium potasside, $K^+C222 \cdot K^-$. The calculated QCC's are about 18.6 MHz and 3.7 MHz for Rb^+ and Rb^- in $Rb^+C222 \cdot Rb^-$ respectively.

$$\chi_{Rb} = \chi_K \cdot \left[\frac{(1 + \gamma_{Rb})Q_{Rb}}{(1 + \gamma_K)Q_K} \right] \tag{5.2}$$

It was assumed that the electric field gradients for both Rb^+ and Rb^- in $Rb^+C222 \cdot Rb^-$ are the same as those for the corresponding potassium ions in $K^+C222 \cdot K^-$ and Sternheimer antishielding factors were taken into account. Table 13 is a list of the values for quadrupole moments [71] and Sternheimer antishielding factors [72] used for calculation. The observed spectrum is probably that of Rb^- since the peak of Rb^+ in this compound may be extremely broadened by strong quadrupolar interactions as indicated by calculated results. A Ramsey's paramagnetic term might shift δ_{iso} for the homonuclear rubidide as a result of the formation of a dimer. In contrast, the isotropic chemical shift (which could not be determined accurately) is quite far from the sharp Rb^- peak expected at ~ -195 ppm and a spectrum for Rb^- could be broadened unexpectedly. Thus it could be assigned to the spectra for Rb^+. However it is not possible to assign the spectrum of either Rb^+ or Rb^- with certainty because of the
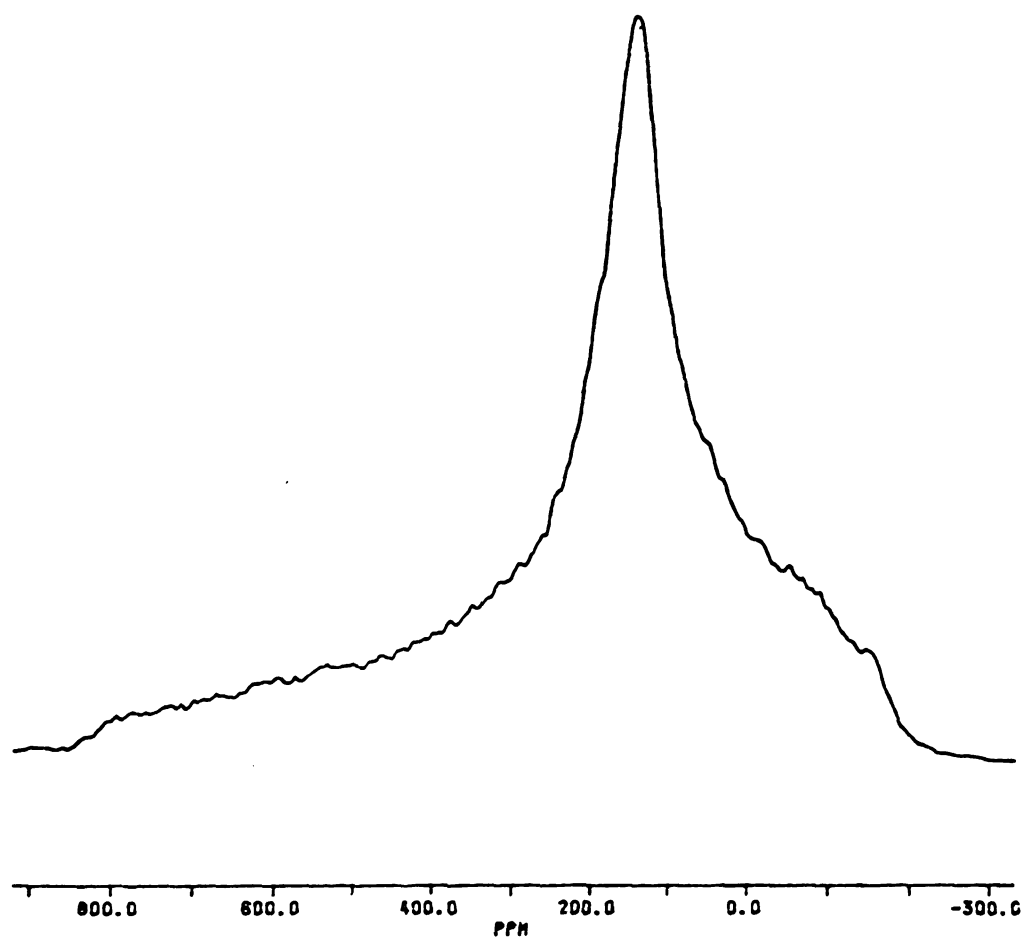
Figure 53 ^{87}Rb spin echo spectrum of Rb$^+$C222·Rb$^-$ at ν_{L} = 130.93 MHz.

Table 13 Nuclear quadrupole moments and Sternheimer antishielding factors for K and Rb

	$Q(\times 10^{-28} m^2)$[a]	Antishielding factor[b]
$^{39}K^+$	0.049	-18.82
$^{39}K^-$	0.049	-46.35
$^{87}Rb^+$	0.13	-47.2
$^{87}Rb^-$	0.13	-79.05

[a] See Reference 71.
[b] See Reference 72.

Table 14 ^{39}K and ^{87}Rb NMR parameters

Compound	QCC(MHz)	η^Q	δ (ppm)
KSCN*	0.65	0.8	10
K$^+$(12C4)$_2$·I^{-}**	~0		
K$^+$(15C5)$_2$·I^{-}**	0.3~0.6		
K$^+$(15C5)$_2$·SCN^{-}*	1.75	0	0
K$^+$18C6·I^{-}*	2.5	0.3	
K$^+$18C6·SCN^{-}*	2.1	0.5	0
Rb$^+$18C6·Cl^{-}*	6.	0.75	17
Rb$^+$18C6·SCN^{-}**	4.5	1.	40
K$^+$(15C5)$_2$·e^{-}**	0.3~0.6		
K$^+$(15C5)$_2$·Na^{-}**	0~0.6		
K$^+$(15C5)$_2$·K^{-}**	~0		
K$^+$18C6·K^{-}*	1.8	1.	-100
K$^+$C222·Na^{-}*	2.65	0.25	0
K$^+$C222·$\underline{K}^{-}$*	0.8	0.	0
$\underline{K}^+$C222·K^{-}**	2.7	?	
K$^+$C222·e^{-}**	2.7	?	
Rb$^+$(15C5)$_2$·e^{-}**	6	?	
Rb$^+$18C6·Na^{-}**	6.5		

*Parameters obtained by simulations.
**Estimated parameters.

large linewidth and distorted lineshape. The results with ^{39}K

and ^{87}Rb model salts are summarized in Table 14.

There are some plausible guesses for the causes of the lineshape distortion: (1) quadrupolar interaction with large CSA; (2) quality of the instrument such as the quality of an excitation pulse B_1; (3) the orientation dependent relaxation time T_2^*; and (4) validity of the second order perturbation theory when applied to strong quadrupolar interactions. The first may be ruled out for ^{39}K NMR because the effects are mainly quadrupolar as discussed above, but it seems that the Rb^+ NMR spectra are broadened by both quadrupolar and chemical shift interactions. The second may also be eliminated since the lineshapes of other salts such as $K^+18C6 \cdot I^-$ and $K^+C222 \cdot Na^-$ obtained under the same experimental condition are correct. The orientation dependent relaxation times (T_2 and T_1), orientation dependent dipolar interactions, or distribution of orientation dependent quadrupolar coupling constants due to crystal defects could be responsible for this distortion . Large CSA effects might be a good factor for the distortion of rubidium signals. Another factor is that the second order perturbation calculation might be invalid because the magnitude of the quadrupolar interaction is so large.

This section has shown that the spin echo technique is a very useful tool for the study of the local environments of the ^{39}K and ^{87}Rb nuclei. However, an NMR spectrometer with a 2 MHz sweepwidth capability would be required for some

compounds. Also, pure nuclear quadrupole resonance studies of these compounds might yield more information.

V. A. 7. Chemical Shifts of Alkali Metal Tetraphenylborates

Unusual chemical shifts of alkali metal tetraphenylborates (M^+TPB^-, M = Li, Na, K, Rb, Cs) which have large anions were observed when their NMR spectra were measured as model compounds for the NMR study of alkalides and electrides. Alkali metal borohydrides were also measured in order to demonstrate that these unusual chemical shifts of tetraphenylborate salts are related to the ring current of the phenyl groups.

The origin of the chemical shift is the induced magnetic moment of electrons due to the orbital motions of the electrons. It is well known that the ring current of organic aromatic compounds [73] shield or deshield protons around aromatic rings depending on the locations of the protons. Recently, the proton NMR results and structures of 2,8,17-Trithia[$4^{5,12}$][9]metacyclophane [74], its trisulfone and [$3^{4,10}$][7]Metacyclophane [75] showed the effect of aromatic ring current on the chemical shifts of their methine protons, -1.68 ppm, -2.79 ppm (2.16~2.21 Å from the ring) and -4.03 ppm (1.78 Å from the ring) respectively.

Not many studies of the effect of ring currents have been made for nuclei other than protons. Table 15 shows the chemical shifts of simple alkali metal halides, alkali metal

Table 15 MAS NMR chemical shifts of alkali metal nuclei in some alkali metal salts

Anion	Li^+	Na^+	K^+ (ppm)	Rb^+	Cs^+
Cl^-	-2.8	7.7	46.7	125	228
Br^-	----	5.6	54.5	179	260
I^-	----	-2.9	----	----	284
TPB^-	-7.3	-45[*]	-92[**]	-175[**]	-261.4
BH_4^-	-0.4	-7.1	24.5	91.5	205.8
TPB^{-a}	-26.	-26.7	-25.7	-25.5	-25.2
BH_4^{-a}	-60.1	-61.7	-57.4	-54.3	-47.6

[a] ^{11}B NMR chemical shifts, The chemical shifts are referenced to saturated boric acid solution.
[*] The chemical shift obtained by simulations of the static and MAS spectra.
[**] The chemical shifts obtained by simulations of the static spectra.

anions, alkali metal borohydrides, and alkali metal tetraphenylborates. The M^+ chemical shifts of the halides and the borohydrides from those in their gaseous state increase with atomic number and this can be explained by Ramsey's "paramagnetic" terms [76]. The "paramagnetic" contribution depends on the energy of appropriate excited states and the degree of overlap with neighboring atoms or ions. It vanishes for electrons in s orbitals which have zero angular momentum. The calculated or observed chemical shifts of M^+_{gas}, M_{gas}, and M^-_{gas} are very close together (within a few ppm) and have no "paramagnetic" shift [77]. However, in condensed phases there may be considerable contribution to a shift if low-lying excited states are available. For the same metal, the heavier salt has the more "paramagnetic" shift for M^+ in M^+X^- (X = Cl, Br, I, etc., and M = K, Rb, Cs). This can be explained by the electron donicity of the halides to the empty orbitals of the cations. This is not the case for Na^+X^-; the paramagnetic contribution to the chemical shift of Na^+ may be small, so that the effect of the small diamagnetic contribution from the halide ions can be seen. According to the chemical shift change of the alkali metal borohydrides, there must be a "paramagnetic" contributions due to the electron donation by BH_4^-, which may not therefore be considered as a hard sphere anion. The ^{11}B chemical shifts of BH_4^- in these salts support the existence of electron donation; boron nuclei are deshielded in going from the lithium salt to the cesium salt. This is very surprising

because there are no nonbonding electrons in BH_4^-. It seems that the electron donicity of BH_4^- is smaller than that of Cl^- according to their chemical shifts and probably depends on the gap between the ground state and the excited states of the cation. If there is bonding character between M^+ and phenyl rings, it will cause a paramagnetic shift rather than a diamagnetic shift. Therefore the large diamagnetic shifts observed in the alkali metal NMR of M^+TPB^- in comparison with alkali metal halides and borohydrides must to be interpreted as the result of the ring current. This conclusion is strongly supported by the structure of these salts. They are very similar in structure and belong to a tetragonal space group [78,79]. For example, K^+ is sitting on the four phenyl rings of the two nearest tetraphenylboron anions [Figure 54a], which form a trigonal pyramid around the K^+ ion. Figure 54b shows that K^+ is almost touching the π electron cloud of the phenyl rings. Presumably, the effect of the ring current can be divided into two parts, i.e. direct and indirect. The direct effect in ppm might have to be constant for each nucleus if their structures are exactly the same, although in practice they would be different slightly. On the other hand, the indirect effect should be proportional to the number of the electrons around the nucleus; if the nuclei feel local fields from phenyl rings due to the ring current, then the electrons must also feel the local fields. Hence this secondary effect might perturb the chemical shifts of alkali metal tetraphenylborates in the observed way. However, it is

a)

b)
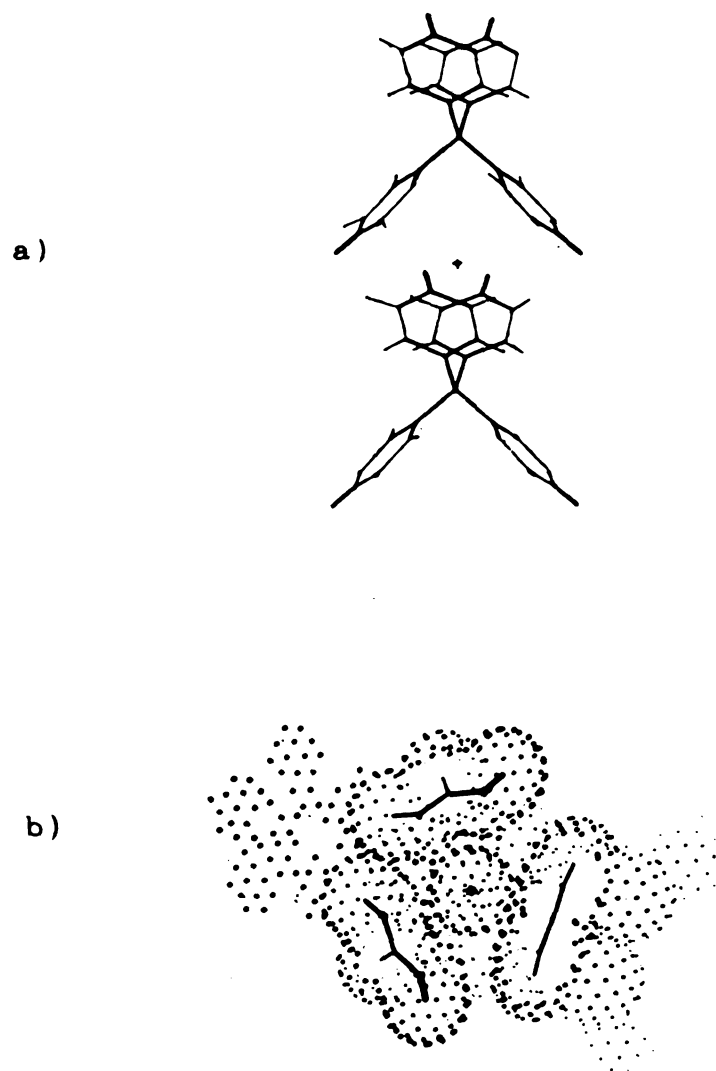
Figure 54 Computer generated structure of K^+TPB^-
a) Tetrahedral arrangement of the four phenyl rings;
b) Cross-section showing K^+ on the phenyl rings.

difficult to theoretically interpret these unusal chemical shifts and the proposed explanation is only qualitative.

A single sharp NMR peak was obtained from MAS experiments with $M^+BH_4^-$ due to its cubic structure [80]. Figure 55 shows the ^7Li NMR spectra of Li^+TPB^-. The static spectrum is broadended by a large dipolar interaction with protons. The proton decoupled spectrum may be broadened by residual dipolar interactions or unresolved quadrupolar interactions. A MAS experiment with proton decoupling averages out most of the residual broadening, yielding a single narrow peak at -7.3 ppm. The small quadrupole moment and Sternheimer antishielding factor of ^7Li make identification of Li^+ easy but Li^+ NMR spectra provide no further information because there are no appreciable anisotropic interactions. Figures 56, 57, and 58 show ^{23}Na, ^{39}K, ^{87}Rb, and ^{133}Cs NMR spectra of M^+TPB^-. Simulation of these spectra yielded QCC and chemical shift parameters shown in Table 16. Cs and Rb have relatively large chemical shift anisotropies, while Na has only a small chemical shift anisotropy. From the ^{39}K NMR spectrum it was impossible to obtain information about CSA due to the noisy spectrum. It was very difficult to observe ^{133}Cs NMR from Cs^+TPB^- and ^{39}K NMR from K^+TPB^- because of an extremely long spin lattice relaxation time and very low sensitivity, respectively. In this study, the relaxation delays for Cs^+ were 10 to 20 seconds. The results from the ^{39}K spin echo NMR spectrum were confirmed by two different chemical shifts for a single
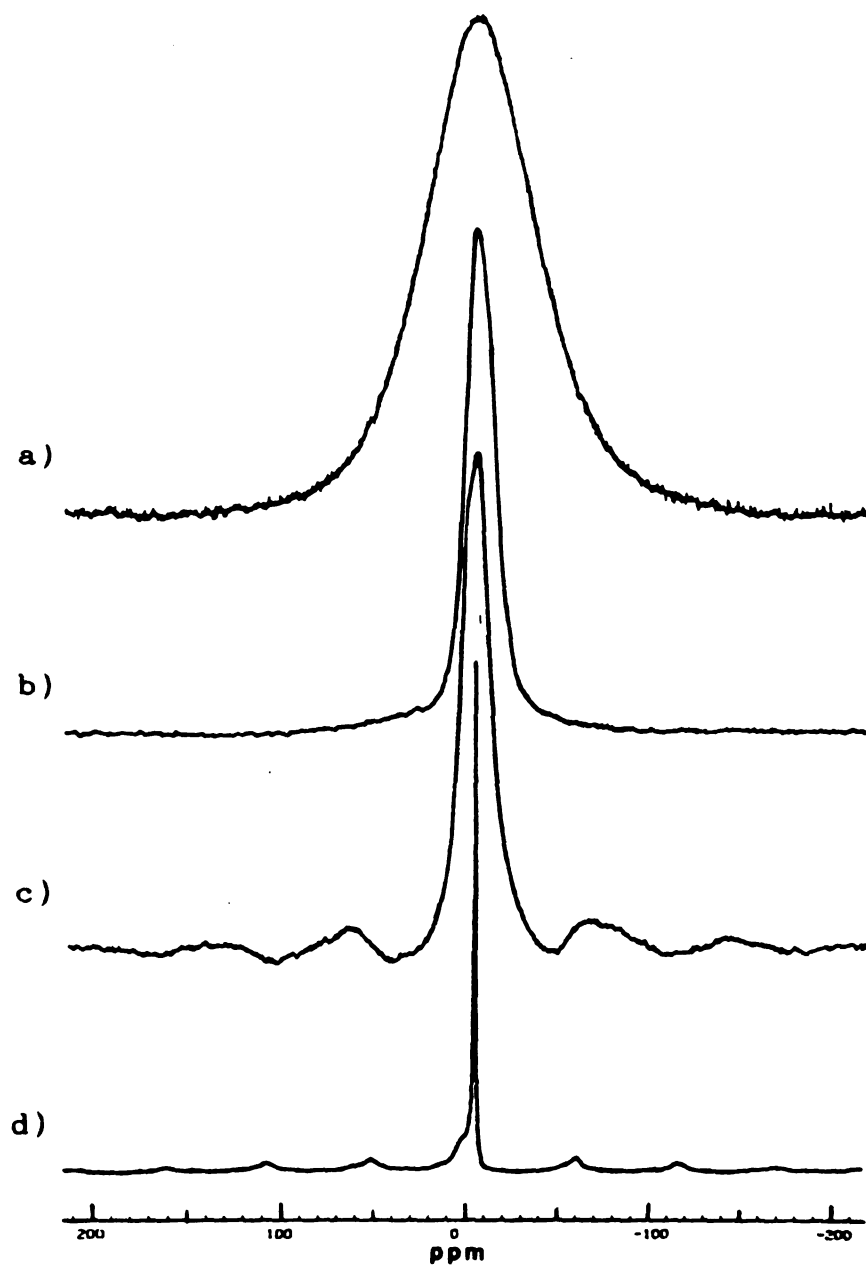
Figure 55 ^{7}Li NMR spectra of Li$^+$TPB$^-$ at ν_L = 69.95 MHz.

   a) Proton coupled static;
   b) Proton decoupled static;
   c) Proton coupled MAS; d) Proton decoupled MAS.
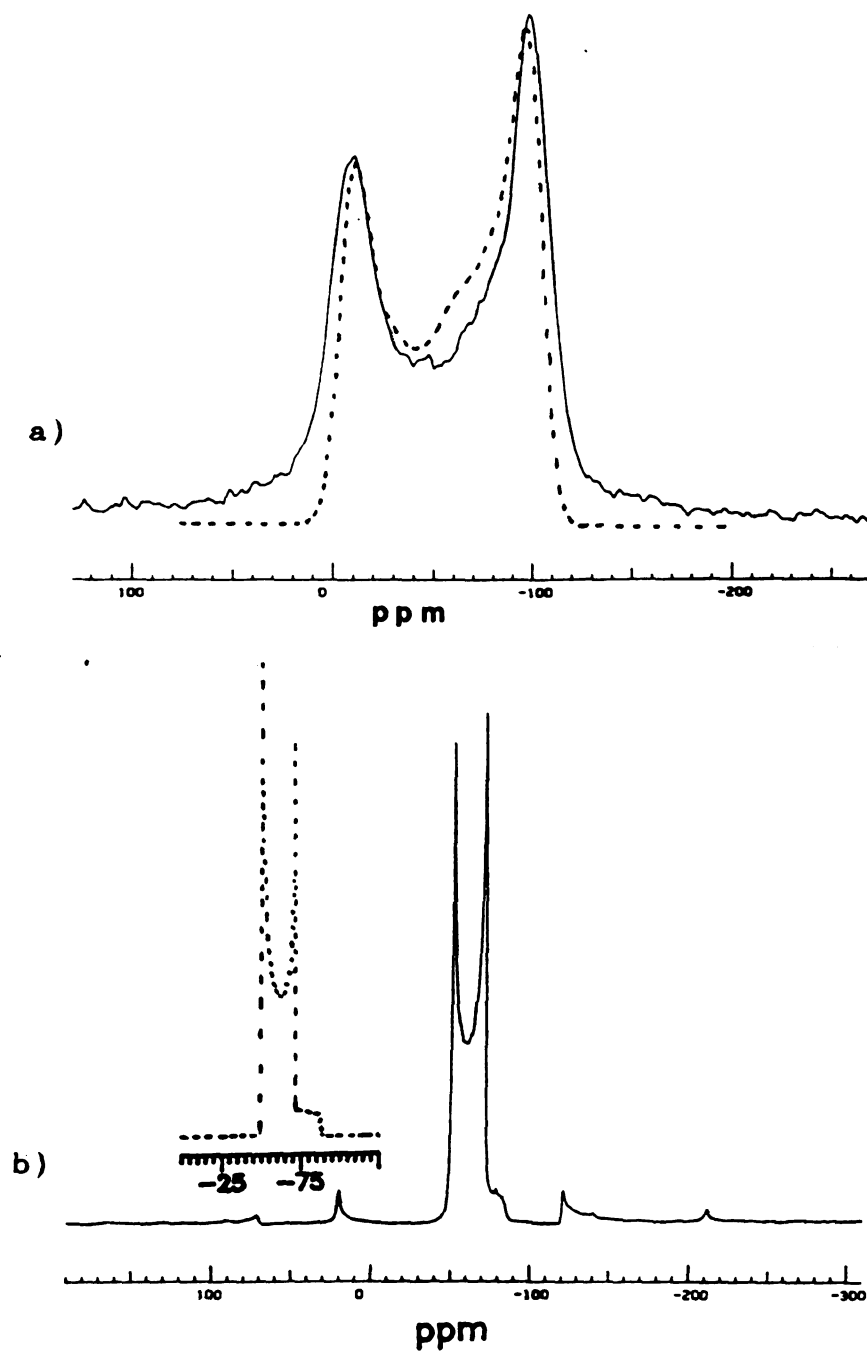
Figure 56 ^{23}Na NMR spectra of Na$^+$TPB$^-$ at ν_L = 47.61 MHz.

a) Proton decoupled static;
b) Proton decoupled MAS.
Observed (——), Simulated (·····).
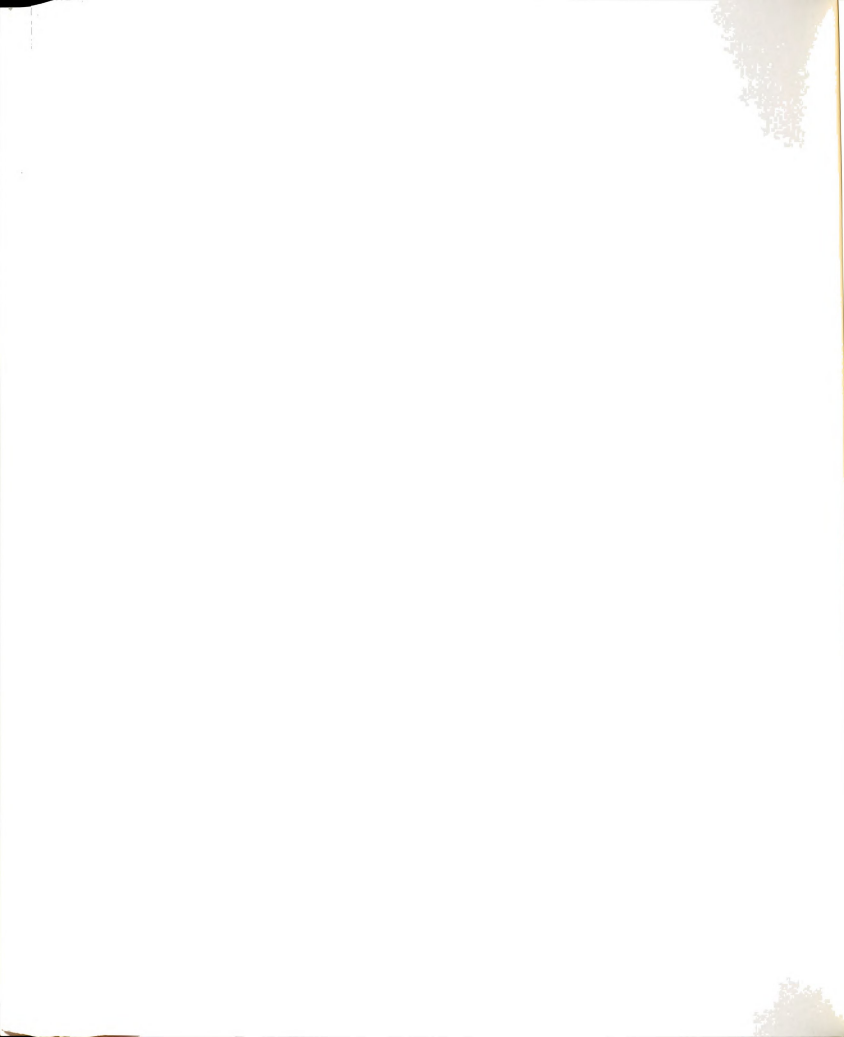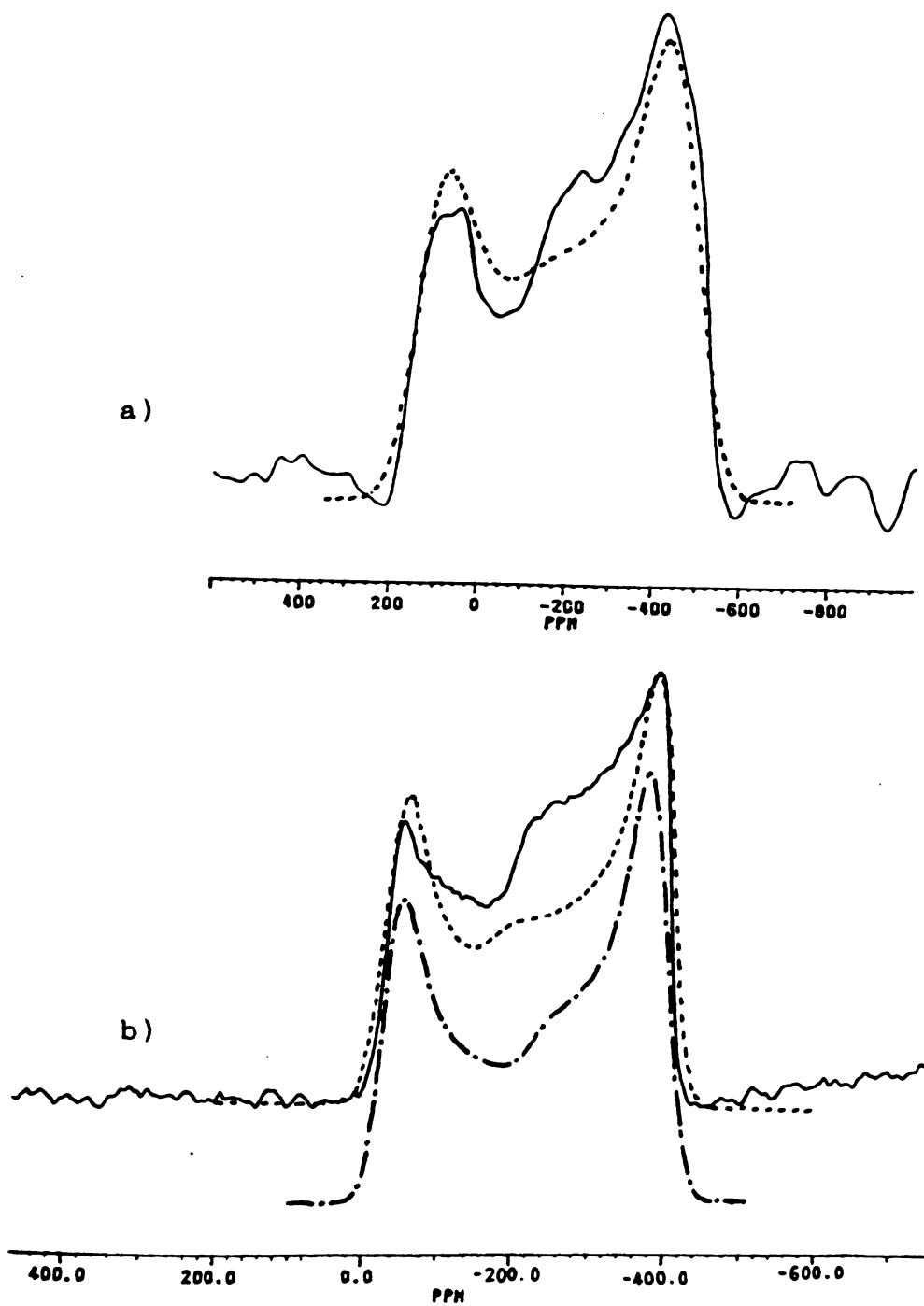
Figure 57 ^{39}K spin echo NMR spectrum of K^{+}TPB^{-} a) at ν_L = 18.67 MHz and ^{87}Rb spin echo NMR spectrum of Rb^{+}TPB^{-} b) at ν_L = 130.93 MHz.

Observed (——), Simulated (····, ─·─··─).
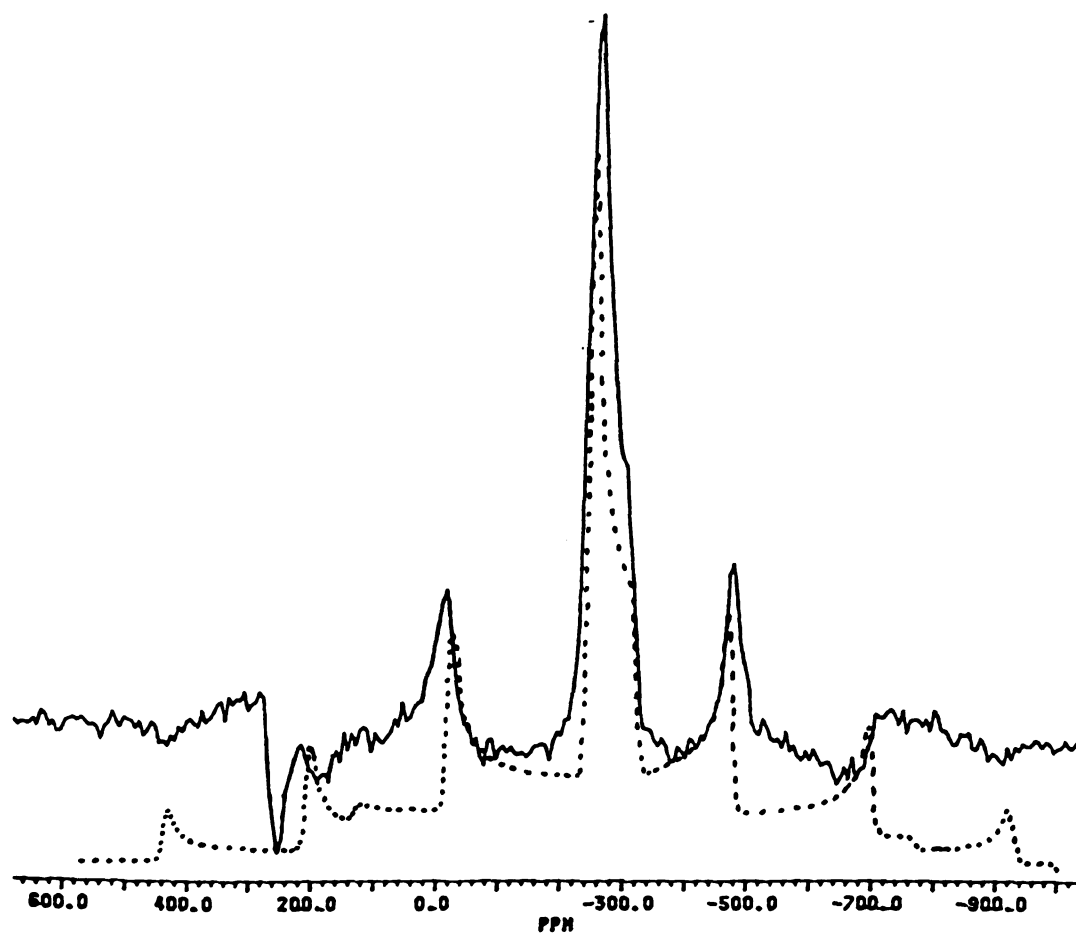
Figure 58 Proton coupled static ^{133}Cs NMR spectrum of
Cs$^+$TPB$^-$ at ν_L = 52.482 MHz.

Observed (——), Simulated (·····).

Table 16 Alkali metal NMR parameters for M^+TPB^- obtained by simulations

	$\delta_{XX} = \delta_{YY}$ (ppm)	δ_{ZZ} (ppm)	QCC (MHz)
NaTPB	-40	-55	1.23
KTPB	-92	-92	1.26
RbTPB[*]	-150	-225	6.5
RbTPB[**]	-160	-160	7.0
CsTPB	-235	-310	0.34

[*] See Figure 57b (-·-·-).
[**] See Figure 57b (·····).

crystal of K^+TPB^- at two different orientations within the chemical shift range of the powder pattern.

In this section, the chemical shifts of simple alkali metal salts and alkali metal tetraphenylborate salts were qualitatively described. Theoretical questions about highly shielded alkali metal cations remain unresolved.

V. B. Magnetic Properties of Some Electrides
V. B. 1. Magnetic Properties and Structures

In the previous chapter the exchange interactions were shown to be very important in describing the magnetic behavior of antiferromagnetic or ferromagnetic samples. The behavior depends on the overlap of the wavefunctions of the electrons and decreases rapidly with the distance between electrons. Since it arises from quantum mechanical exchange of the electrons it is known as the direct exchange. It is possible that the magnetic ions (electrons in electrides) have their magnetic interaction mediated by the electrons in their common nonmagnetic neighbors. This type of magnetic interaction is called superexchange. In this case the charges of the magnetic ions do not overlap directly, but they have overlap with the same non-magnetic ion. This is known as indirect exchange, in which a magnetic interaction is mediated by interactions with the intervening electrons. Often, conduction electrons are involved. Perhaps direct and indirect exchanges are important in electrides. Therefore,

the environments of the trapped electrons in the electride salts are of crucial importance in determining the interactions between the electrons.

The structures of three electrides, $Cs^+(18C6)_2 \cdot e^-$, $Cs^+(15C5)_2 \cdot e^-$, and $K^+C222 \cdot e^-$ have been recently solved. First, the localized electride, $Cs^+(18C6)_2 \cdot e^-$ behaves as a Curie-Weiss paramagnet [22]. It is monoclinic with Z = 4 and the cell parameters are: a = 13.075 Å, b = 15.840 Å, c = 17.359 Å, β = 92.30°, and V = 3592.3 Å^3 [81]. Second, $Cs^+(15C5)_2 \cdot e^-$ is triclinic with one molecule per unit cell [82]. The distances between the nearest neighbor electrons are the same as the cell parameters: a = 8.60 Å, b = 8.89 Å, c = 9.94 Å, α = 102.91°, β = 90.06°, γ = 97.74°, and V = 733.1 Å^3. It behaves as a classical antiferromagnet [8]. Finally, the structure of $K^+C222 \cdot e^-$ is monoclinic C2/c with a = 12.129 Å, b = 20.692 Å, c = 21.519 Å, V = 5378 Å^3, and Z = 8 [25]. The susceptibilities and the structure of this compound indicate that there is a strong coupling between pairs of electrons with weak interactions from neighbor pairs [25]. The distance between electrons, the channels in the structures, or formation of magnetic superlattice might cause different magnetic behavior of the electrides, but the reason for the susceptibility behavior is unclear. From the macroscopic point of view, trapped electron density through the material might be related. The electron densities are 1.113×10^{-3} Å^{-3}, 1.364×10^{-3} Å^{-3}, 1.488×10^{-3} Å^{-3} for $Cs^+(18C6)_2 \cdot e^-$, $Cs^+(15C5)_2 \cdot e^-$, $K^+C222 \cdot e^-$ respectively. This

reflects the strength of magnetic interactions in these material. More structures of electrides such as $K^+(15C5)_2 \cdot e^-$, $Rb^+(15C5)_2 \cdot e^-$, and $Li^+PMPCY \cdot e^-$, etc. may provide information in understanding magnetic behavior of electrides microscopically.

V. B. 2. Application of the Modified Oguchi Theory of Magnetism

Although there were several attempts [83] to fit the experimental magnetic susceptibility results of $Li^+C211 \cdot e^-$ over a wide range of temperatures using a Curie-Weiss equation or Wojciechowski's equation [84], these expression did not fit the experimental susceptibility data. Figure 59 shows the magnetic susceptibility data for $Li^+C211 \cdot e^-$. The experimental values shown in Figure 59 were provided by J. Skowyra and measured on an S.H.E. variable temperature susceptometer with a Superconducting Quantum Interference Device (SQUID). Calculated values were obtained by using KINFIT [54] and ANTIMAG (Appendix C). The magnetic susceptibility of a powdered sample can be written as:

$$\chi_{av} = 1/3 \ (\chi_\perp + \chi_{\prime\prime}) \tag{5.3}$$

where $\chi_{\prime\prime}$ and $\chi_\perp$ are given by Equations (3.34) and (3.41) respectively. Practically, the susceptibility data were fit to the following equation:
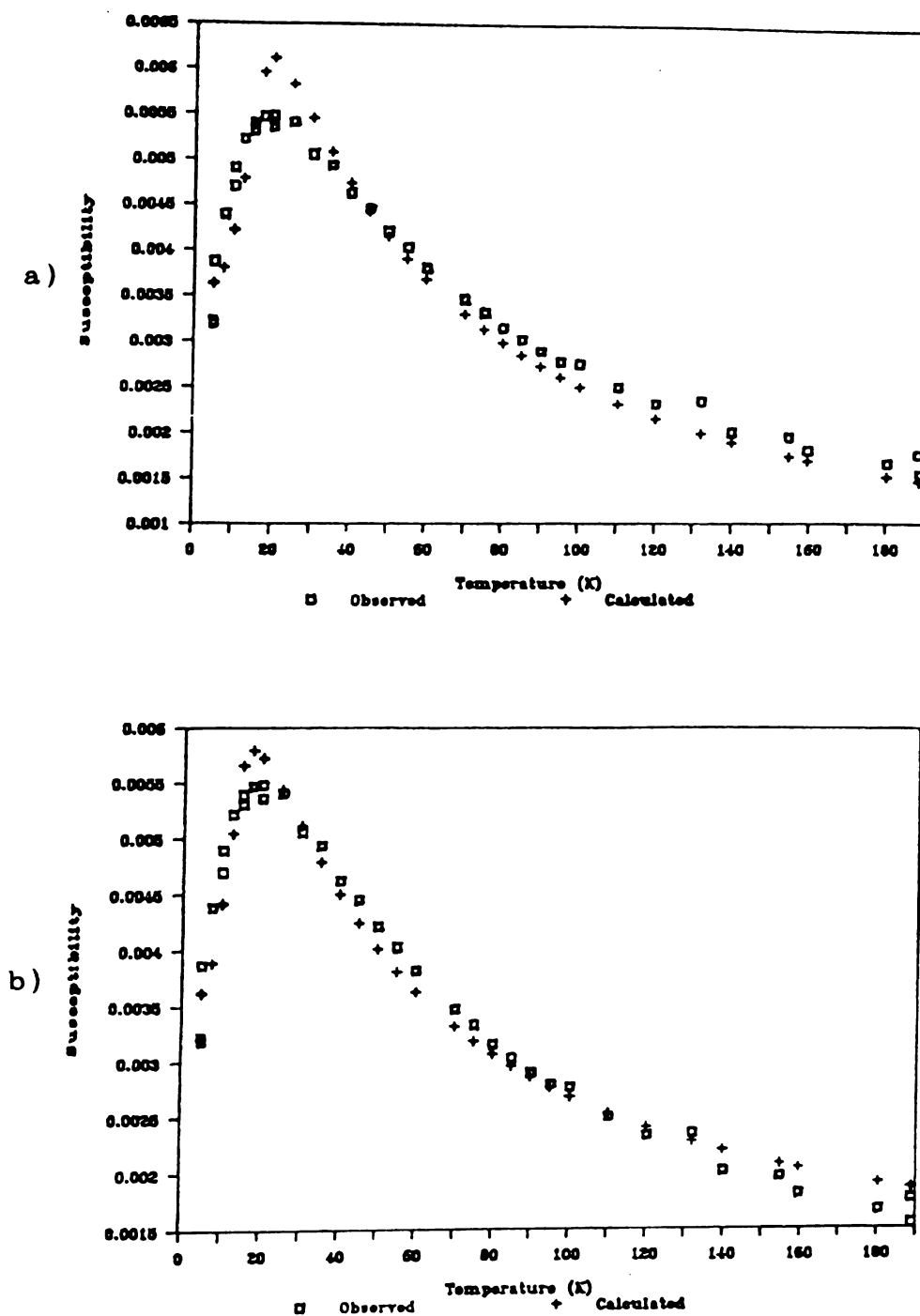
Figure 59 Magnetic susceptibility of $Li_4^+C211 \cdot e^-$.
a) $C = 0.0$; b) $C = 7.43 \times 10^{-4}$.

$$\chi_{calc} = F\chi_{av} + C \tag{5.4}$$

where F and C are correction factors. The term F can account for loss of magnetization due to impurities such as $M^+C \cdot M^-$ or decomposition products. Diamagnetic impurities and the uncompensated background can be accounted for in the C term. The parameters from the KINFIT analysis [54] are listed in Table 17. Regardless of the correction factor F, average values of J/k, the Weiss temperature and a molecular field parameter are about -13.9 ± 1.3 K, -20.6 ± 1.5 K and 1.96 ± 1.3, respectively. The parameter J'/k can be calculated as -13.6 K, -9.1 K, -6.8 K, -5.5 K, and -4.5 K for $z = 2$, 3, 4, 5, and 6, respectively, since the structure of this compound is not known. If the number of the nearest neighbors is 3, the strength of the interaction between pairs is appreciable compared with that of the interaction between an i-j pair. Even if $z = 6$, it is 1/3 of J. Therefore the molecular field is quite strong as the temperature at the maximum susceptibility indicates. A Néel temperature of 17.0 K was obtained from these fittings.

The magnetic susceptibility of $Li^+C211 \cdot e^-$ was explained by the theory of magnetism by Ohya-Nishiguchi [49]. It is a promising theory to interpret the magnetic behavior of some other electrides.

Table 17 Parameters obtained by KINFIT analysis of
Li$^+$C211·e$^-$ magnetic susceptibility data

J/k (K)	θ (K)	T_N (K)	x	F (%)	C
-13.6±0.5	-19.3±0.7	15.5	1.96	62.3±3.3	7.43 × 10^{-4}
-14.2±0.8	-22.0±0.8	18.5	2.09	82.4±2.4	0.

CHAPTER VI

CONCLUSIONS AND SUGGESTIONS FOR FUTURE WORK

VI. A. Conclusions

Three salts, $Na^+C222 \cdot Br^-$, $Na^+C222 \cdot Na^-$, and $Cs^+(15C5)_2 \cdot I^-$ were studied by a single crystal NMR method. Single crystal NMR studies yielded accurate values of the parameters associated with nuclear spin interactions. From ^{23}Na and ^{39}K NMR studies of alkalides, it was found that the NMR spectra of two alkali metal anions, Na^- and K^- are broadened by quadrupolar interactions. Numerous complexed alkali metal salts were investigated by static and MAS experiments with or without proton decoupling at different fields. A phase cycled spin echo technique was used to study complexed alkali metal salts that contained K and Rb. Distorted powder patterns from some K and Rb salts were obtained and further investigation is needed for these compounds. Sodium-23 NMR spectra of complexed salts showed that their powder patterns are mainly quadrupolar in origin. Also, single crystal ^{23}Na NMR studies of $Na^+C222 \cdot Br^-$ and $Na^+C222 \cdot Na^-$ proved that the central transition of Na^+ is shifted by second order quadrupolar interactions and that CSA is almost negligible. For the

heavier nuclei, more CSA was observed. Strong quadrupolar interactions for [133]Cs in cesium C222 salts were observed and second order quadrupolar powder patterns were observed by MAS at a Larmor frequency of 23.61 MHz. Unusal static powder patterns result from the simultaneous presence of chemical shift and quadrupolar interactions. Static CSA powder patterns were obtained from most complexed cesium salts at higher field (ν_L = 52.482 MHz). Most dipolar and chemical shift interactions were averaged by spinning samples at an angle of 54.74°, leaving a single sharp peak at the isotropic chemical shift or a second order quadrupolar powder pattern. First order quadrupolar interactions are theoretically averaged to zero; however, numerous spinning sidebands resulted, since the spinning speed is slow compared to the magnitude of the first order quadrupolar interactions. An NMR study of alkali metal tetraphenylborates showed that they are the most diamagnetically shielded alkali metal cations known to date. Inhomogeneously broadened NMR lines were observed from complexed alkali metal salts in spite of strong proton-proton interactions. In summary, the external magnetic field dependence of some interactions on NMR lines is described in Table 18.

This study has proven that solid state NMR spectroscopy is a very powerful technique for the identification of species in solids and for the study of anisotropic interactions between a nucleus and its surrounding environment. Single crystal NMR is the best way

Table 18 External magnetic field effect on NMR lineshapes

Interaction	ppm	Hz
Dipolar	$\propto 1/B_0$	independent
CSA	independent	$\propto B_0$
First order quadrupolar	$\propto 1/B_0$	independent
Second order quadrupolar	$\propto 1/B_0^2$	$\propto 1/B_0$

to obtain the elements of anisotropic coupling tensors. Information from a static powder pattern is not enough to obtain parameters associated with anisotropic interactions. Therefore, both static and MAS (or VAS) experiments with or without proton decoupling at different fields are strongly recommended.

A study of the magnetic susceptibility of $Li^+C211 \cdot e^-$ demonstrated that Oguchi's theory of magnetism as modified by Ohya-Nishiguchi is a very promising way to investigate the magnetic susceptibilities of electrides.

VI. B. Suggestions for Future Work

(1) Since quadrupolar broadened NMR spectra for alkali metal anions have been observed for three alkalides but not much besides MAS-NMR studies of other compounds have been attempted, the NMR behavior of various alkalides and electrides should be reexamined in detail.

(2) More single crystal NMR studies can be done with a good single crystal NMR probe with proton decoupling and low temperature capabilities. One of the best single crystal NMR (or EPR) candidates is $K^+C222 \cdot Na^-$ because of its orthorhombic structure and stability at room temperature.

(3) ^{13}C and proton NMR studies of alkalides and electrides by cross-polarization, multipulse, two dimensional NMR, etc. may provide new information.

(4) Interactions other than quadrupolar interactions

may be separated by two dimensional NMR studies of alkali metal nuclei.

(5) Theoretical studies of unusal lineshapes of some alkalides and electrides such as $K^+C222 \cdot K^-$ and $K^+C222 \cdot e^-$ are challenging.

(6) Single crystal magnetic susceptibility studies of electrides, $K^+C222 \cdot e^-$, $Cs^+(15C5)_2 \cdot e^-$, and $Li^+PMPCY \cdot e^-$, etc. will provide more information about electron-electron interactions.

APPENDICES

APPENDICES

APPENDIX A

          PROGRAM XTAL
C
C   AUTHOR
C   JINEUN KIM
C   JAMES L. DYE*
C   *DEPARTMENT OF CHEMISTRY
C   MICHIGAN STATE UNIVERSITY
C   EAST LANSING, MI 48824 U.S.A.
C
C   THE PROGRAM "XTAL.FOR" COMPUTES CHEMICAL SHIFTS
C   CORRESPONDING TO NUCLEAR MAGNETIC RESONANCE TRANSITIONS
C   WHICH RESULT FROM THE SPIN HAMILTONIAN WITH NUCLEAR
C   ZEEMAN, QUADRUPOLE AND CHEMICAL SHIFT TERMS. THE
C   QUADRUPOLE AND CHEMICAL SHIFT TERMS ARE TREATED AS
C   PERTURBATIONS ON THE ZEEMAN TERM, AND ARE CORRECT
C   THROUGH SECOND ORDER AND FIRST ORDER RESPECTIVELY. THE
C   SINGLE CRYSTAL NMR PEAK POSITIONS ARE CALCULATED BY
C   SETTING THE EULERIAN ANGLES, ALPHA, BETA, AND GAMMA,
C   WHICH ARE DEFINED WITH RESPECT TO THE GONIOMETER AXIS
C   SYSTEM. (A.R. Edmonds, Angular Momentum in Quantum
C   Mechanics, Princeton University Press) IF BOTH TENSORS
C   ARE AXIALLY SYMMETRIC, THE EULERIAN ANGLE ALPHA IS
C   MEANINGLESS. IT CAN BE AN ARBITRARY NUMBER. THE ANGLE
C   VAN IS DEFINED AS AN ANGLE BETWEEN MAGNETIC FIELD
C   DIRECTION AND THE ROTATION AXIS. EACH TRANSITION
C   INTENSITY IS PROPORTIONAL TO I(I+1)-M(M-1). TOTAL
C   TRANSITIONS TO BE CALCULATED ARE 2I*TOTAL ANGLE OF
C   ROTATION(ANG)/ANGLE OF ROTATION(XI).
C   THE PRINCIPAL AXIS SYSTEM OF THE QUADRUPOLAR COUPLING
C   TENSOR (Xq,Yq,Zq) IS DEFINED SO THAT THE ABSOLUTE
C   MAGNITUDE OF Vzz AND Vyy CAN BE THE LARGEST AND THE
C   SMALLEST RESPECTIVELY. ETA IS DEFINED AS: ETA = (Vyy -
C   Vxx)/Vzz. THE ELEMENTS (SSX,SSY,SSZ) OF THE CHEMICAL
C   SHIFT TENSOR ARE CHOSEN IN THE SAME PRINCIPAL AXIS
C   SYSTEM AS THE QUADRUPOLAR COUPLING TENSOR, SPECIFICALLY,
C
C   **
C   *   Xq // Xcs, Yq // Ycs, AND Zq // Zcs.   *
C   **
C   SSX, SSY, AND SSZ ARE IN PPM SCALE. THERE IS NO
C   PREFERENTIAL ORDER OF THE CSA TENSOR ELEMENTS. THERE ARE

```
C      6 COMBINATIONS WITH THE QUADRUPOLAR COUPLING TENSOR.
C      THIS PROGRAM CANNOT CALCULATE NMR TRANSITION FREQUENCIES
C      OF THE NUCLEUS, WHICH HAS NONCOINCIDENT PRINCIPAL AXIS
C      SYSTEMS.
C   INPUT
C      TITLE OF RUN                                          18A4
C      SPIN,VL,VAN,TRAN                          FREE FORMAT
C      SPIN           NUCLEAR SPIN
C      VL             LARMOR FREQUENCY IN MHZ
C      VAN            VARIABLE ANGLE IN DEGREE
C      TRAN           SELECTS TRANSITIONS TO BE CALCULATED
C EQQ,ETA,SSX,SSY,SSZ                            FREE FORMAT
C      EQQ            QUADRUPOLAR COUPLING CONSTANT IN MHZ
C      ETA            ASYMMETRIC PARAMETER OF ELECTRIC FIELD
C                     GRADIENT AT  NUCLEAR SITE
C      SSX,SSY,SSZ  CHEMICAL SHIFT PARAMETERS IN PPM
C ALPA,BETA,GAMA,XI,ANG                          FREE FORMAT
C      ALPA,BETA,GAMA: EULERIAN ANGLES IN DEGREE
C      XI: ANGLE INCREMENT OF EACH ROTATION IN DEGREE(CONSTANT)
C      ANG: MAXIMUM(TOTAL) ANGLE OF ROTATION
C
C   OUTPUT
C      XL,CHEM,DMAG,FIRS,MULTI,SECO,FNN
C         XL         XL*XI = SUM OF THE ANGLE ROTATED
C         CHEM       CHEMICAL SHIFT ANISOTROPY(PPM)
C         DMAG       M
C         FIRS       FIRST ORDER SATELLITE TRANSITION(PPM)
C         MULTI      I(I+1)-M(M-1)
C         SECO       SECOND ORDER SHIFT FOR EACH TRANSITION(PPM)
C         FNN        SUM OF CSA, FIRST ORDER, AND SECOND ORDER
C                    SHIFT(PPM)
C**************************************************************
C
C    XTAL.DAT (AN EXAMPLE OF DATA FILE)
C
C      TEST  CS(15C5)2+
C      3.5,23.61,90,3.5
C      .15,.5,60,40,-30
C      0,90,170,10,180
C**************************************************************
C
       IMPLICIT REAL*8 (A-H,O-Z)
       CHARACTER*20 F20,F21
       DIMENSION TITLE(18),S(10)
       DIMENSION SGM(100),CGM(100),S2G(100),C2G(100)
       DIMENSION A(10),B(10),C(10),INT(10),D(10)
C
C***************** OPEN FILES ***********************
C
7      WRITE(*,20)
       READ(*,40,ERR=7) F20
       OPEN(UNIT=1,FILE=F20,STATUS='OLD')
8      WRITE(*,30)
       READ(*,40,ERR=8) F21
```

```
        OPEN(UNIT=2,FILE=F21,STATUS='NEW')
C
C********************* FORMAT *************************
C
10      FORMAT(/)
20      FORMAT(' ENTER INPUT FILE NAME')
30      FORMAT(' ENTER OUTPUT FILE NAME')
40      FORMAT(A)
50      FORMAT(9H   ALPHA =,F7.3,1X,8H   BETA =,F7.3,1X,9H   GAMMA
=,F7.3,
     *1X,17H VARIABLE ANGLE =,F7.3)
60      FORMAT(9H    SPIN =,F4.1,5X,14HLAMROR FREQ. =,F7.3,
     *5X,21HQUAD. COUPL. CONST. =,F7.3,5X,13HASYMM. PAR.
=,F7.4)
70      FORMAT(29H   CHEM. SHIFT PARAMETERS;SSX=,F9.3,1X,4HSSY=,
F9.3,1X,
     *4HSSZ=,F9.3)
80      FORMAT(19H  ISO. CHEM. SHIFT=,F9.3,1X,18HCHEM. SHIFT
DELTA=,F9.3,
     *1X,16HCHEM. SHIFT ETA=,F5.3)
90      FORMAT(1X,31HDELTA M = 1 TRANSITIONS BETWEEN,F5.1,4H
AND,F5.1,
     *5H ONLY)
100     FORMAT(3X,'NO',5X,'CSA',6X,'M',2X,'SATELLITE',2X,
'MULTI',
     *2X,'SECOND',2X,'PEAK PPM')
110     FORMAT(1X,F5.1,1X,F9.3,1X,F4.1,1X,F9.3,1X,I4,1X,F9.3,
1X,F9.3)
120     FORMAT(1H1)
130     FORMAT(18A4)
140     FORMAT(2X,18A4)
150     FORMAT(' ENTER TITLE')
160     FORMAT(' ENTER SPIN (3/2 = 1.5)')
170     FORMAT('        LARMOR FREQUENCY IN MHZ')
180     FORMAT('        VARIABLE ANGLE VAN')
190     FORMAT('        TRANSITIONS TO BE CALCULATED')
200     FORMAT(' SPIN,VL,VAN,TRAN')
210     FORMAT(' ENTER QUADRUPOLE COUPLING CONSTANT')
220     FORMAT('        ASYMMETRY PARAMETER FOR QUADRUPOLE
TERMS')
230     FORMAT('        3 CSA TENSOR PRINCIPAL VALUES IN PPM')
240     FORMAT(' EQQ,ETA,SSX,SSY,SSZ')
250     FORMAT(' ENTER 3 EULERIAN ANGLES;ALPHA,BETA,GAMMA')
260     FORMAT('        ANGLE INCREMENT OF EACH ROTATION;XI')
270     FORMAT('        TOTAL ANGLE OF ROTATION;ANG')
280     FORMAT(' ALPA,BETA,GAMA,XI,ANG')
C*****************************************************
IO=2
C
C******************* INPUT DATA ********************
C
C       WRITE(*,150)
C       WRITE(*,160)
C       WRITE(*,170)
```

```
C       WRITE(*,180)
C       WRITE(*,190)
C       WRITE(*,200)
C       READ(*,*)SPIN,VL,VAN,TRAN
C       WRITE(*,210)
C       WRITE(*,220)
C       WRITE(*,230)
C       WRITE(*,240)
C       READ(*,*)EQQ,ETA,SSX,SSY,SSZ
C       WRITE(*,250)
C       WRITE(*,260)
C       WRITE(*,270)
C       WRITE(*,280)
C       READ(*,*)ALPA,BETA,GAMA,XI,ANG
        READ(1,130)TITLE
        READ(1,*)SPIN,VL,VAN,TRAN
        READ(1,*)EQQ,ETA,SSX,SSY,SSZ
        READ(1,*)ALPA,BETA,GAMA,XI,ANG
C****************************************************************
C
C       VARIABLE ANGLE
C
        THE=3.141593*VAN/180.
        SAL=SIN(THE)
        CAL=COS(THE)
        SCA=SAL*CAL
        SSA=SAL*SAL
        SSB=2.*SSA-1.
        CCA=(1.+CAL*CAL)/2.
        DCB=-SSB
        TCT=(3.*CAL*CAL-1.)/2.
C       EULERIAN ANGLE ALPHA
        ALP=3.141593*ALPA/90.
        STP=SIN(ALP)
        CTP=COS(ALP)
C       EULERIAN ANGLE BETA
        BTA=3.141593*BETA/180.
        SBT=SIN(BTA)
        CBT=COS(BTA)
        CSB=CBT*SBT
        CCB=CBT*CBT
C       EULERIAN ANGLE GAMMA
        J=ANG/XI+1
        DO 300 I=1,J
        YI=I-1.
        ROT=3.141593*(GAMA+YI*XI)/180.
        SG=SIN(ROT)
        CG=COS(ROT)
        CSG=2.*SG*CG
        CCG=2.*CG*CG-1.
        SGM(I)=SG
        CGM(I)=CG
        S2G(I)=CSG
        C2G(I)=CCG
```

```
300     CONTINUE
        CSIGMA=(SSX+SSY+SSZ)/3.
        CDEL=SSZ-CSIGMA
        IF (CDEL.EQ.0.) GO TO 350
        CETA=(SSY-SSX)/CDEL
        GO TO 400
350     CETA=0.
400     CSISO=CSIGMA/1.E6
        CSDEL=CDEL/1.E6
        S(1)=SSX
        S(2)=SSY
        S(3)=SSZ
405     CONTINUE
        DO 420 K=1,2
        LA=K+1
        DO 410 L=LA,3
        IF(S(K).LE.S(L)) GO TO 420
        SK=S(K)
        S(K)=S(L)
        S(L)=SK
410     CONTINUE
420     CONTINUE
        IF(S(2).LT.S(1)) GO TO 405
        IF(ABS(S(1)-CSIGMA).LE.ABS(S(3)-CSIGMA)) GO TO 430
        IF(ABS(S(1)-CSIGMA).GT.ABS(S(3)-CSIGMA)) S1=S(1)
        S(1)=S(3)
        S(3)=S1
430     CSDELTA=S(3)-CSIGMA
        IF(CSDELTA.EQ.0) GO TO 440
        CSETA=(S(2)-S(1))/CSDELTA
        GO TO 445
440     CSETA=0
445     VQ=EQQ
        TRAX=-TRAN
        SIX=SQRT(6.)
C
C***************** OUTPUT FOR PARAMETERS ******************
C
        WRITE(IO,120)
        WRITE(IO,140) TITLE
        WRITE(IO,10)
        WRITE(IO,60) SPIN,VL,VQ,ETA
        WRITE(IO,10)
        WRITE(IO,70) SSX,SSY,SSZ
        WRITE(IO,10)
        WRITE(IO,80) CSIGMA,CSDELTA,CSETA
        WRITE(IO,10)
        WRITE(IO,50) ALPA,BETA,GAMA,VAN
        WRITE(IO,10)
        WRITE(IO,90) TRAN,TRAX
        WRITE(IO,10)
        WRITE(IO,100)
C*************************************************************
        ETA=-ETA
```

```
        CSETA=-CETA
        SS1=SPIN*(SPIN+1.)
        IF(SPIN - 0.5) 450,450,500
450     VQQ = 0.0
        GO TO 550
500     VQQ=3.*VQ/(2.*SPIN*(2.*SPIN-1.))/VL
550     FACT=VQQ*VQQ/12.
        XMAG=-TRAN+1.
        MAG=1
600     CONTINUE
        XX1=XMAG*(XMAG-1.)
        A(MAG)=24.*XX1-4.*SS1+9.
        B(MAG)=6.*XX1-2.*SS1+3.
        C(MAG)=-VQQ*(XMAG-.5)
        D(MAG)=XMAG
        INT(MAG)=SS1-XX1
        IF(XMAG.GE.TRAN) GO TO 650
        XMAG=XMAG+1.
        MAG=MAG+1
        GO TO 600
650     CONTINUE
        MGMX=MAG
        ECP=ETA*CTP
        CON=(3.-ECP)*CSB/SIX
        SON=ETA*STP*SBT/SIX
        CTW=((3.+ECP)+(-3.+ECP)*CCB)*.5/SIX
        STW=ETA*STP*CBT/SIX
        FR=.5*(-1.+ECP+(3.-ECP)*CCB)
        ANI=.5*(-1.+CSETA*CTP+(3.-CSETA*CTP)*CCB)
        CCO=(3.-CSETA*CTP)*CSB/SIX
        CSO=CSETA*STP*SBT/SIX
        CCT=(3.+CSETA*CTP+(-3.+CSETA*CTP)*CCB)*.5/SIX
        CST=CSETA*STP*CBT/SIX
        DO 700 L=1,J
        DO 700 M=1,MGMX
        XL=L-1.
        CS1L=CON*CGM(L)-SON*SGM(L)
        CS2L=CON*SGM(L)-SON*CGM(L)
        CS3L=CTW*C2G(L)-STW*S2G(L)
        CS4L=CON*CGM(L)+SON*SGM(L)
        CS5L=CTW*C2G(L)+STW*S2G(L)
        CS6L=CTW*S2G(L)+STW*C2G(L)
        SAT=TCT*FR+.5*SIX*SSA*CS5L-SIX*SCA*CS4L
        F1R=-SCA*CS3L+DCB*CS4L+.5*SIX*SCA*FR
        F1I=SAL*CS6L-CAL*CS2L
        F2R=CCA*CS3L+SCA*CS4L+.25*SIX*SSA*FR
        F2I=CAL*CS6L+SAL*CS2L
        CAN=CSDEL*(TCT*ANI+.5*SIX*SSA*(CCT*C2G(L)+CST*S2G(L))
       *-SIX*SCA*(CCO*CGM(L)+CSO*SGM(L)))
        DMAG=D(M)
        MULTI=INT(M)
        VLCC=CSISO+CAN
        FST=C(M)*SAT
        SND=FACT*((F1R*F1R+F1I*F1I)*A(M)-(F2R*F2R+F2I*F2I)*
```

```
B(M))
      CHEM=VLCC*1.E6
      FIRS=FST*1.E6
      SECO=SND*1.E6
      FNN=(VLCC+FST+SND)*1.E6
      WRITE(IO,110) XL,CHEM,DMAG,FIRS,MULTI,SECO,FNN
700   CONTINUE
      STOP
      END
```

APPENDIX B

```
        PROGRAM VMASS
C
C       JINEUN KIM
C       J. L. DYE*
C       *DEPARTMENT OF CHEMISTRY
C        MICHIGAN STATE UNIVERSITY
C        EAST LANSING MI 48824 U. S. A.
C         PROGRAM POWPAT
C         QCPE PROGRAM 154
C         POWDER PATTERNS AND SPECTRA CORRESPONDING TO NMR
C         TRANSITIONS
C                   ***POWPAT PROGRAM***
C       H.S. STORY AND D. KLINE   DEPARTMENT OF PHYSICS
C             STATE UNIVERSITY OF NEW YORK AT ALBANY
C POWPAT PROGRAM COMPUTES AND PLOTS POWDER PATTERNS AND
C SPECTRA CORRESPONDING TO NUCLEAR MAGNETIC RESONANCE
C TRANSITIONS WHICH RESULT FROM THE SPIN HAMILTONIAN WITH
C NUCLEAR ZEEMAN, QUADRUPOLE AND CHEMICAL SHIFT TERMS, SEE,
C FOR EXAMPLE, NARITA, UMEDA AND KUSUMOTO, J. CHEM.
C PHYS.44,2719 (1966). OR BAUGHER, TAYLOR, OJA AND BRAY
C UNPUBLISHED BROWN UNIVERSITY REPORT.
C THE QUADRUPOLAR AND CHEMICAL SHIFT TERMS ARE TREATED AS
C PERTURBATIONS ON THE ZEEMAN TERM, AND ARE CORRECT
C THROUGH SECOND ORDER AND FIRST ORDER RESPECTIVELY. THE
C POWDER PATTERN IS SIMULATED BY SETTING THE CRYSTAL AT A
C LARGE NUMBER OF ANGLES, THETA AND PHI ON A REGULAR GRID
C IN COSINE THETA SPACE. THE FREQUENCIES ARE THEN COMPUTED
C AND A DENSITY FUNCTION OR POWDER PATTERN CONSTRUCTED. THE
C POWDER PATTERN IS THEN CONVOLUTED WITH A GAUSSIAN (OR
C GAUSSIAN DERIVATIVE TO PRODUCE A SPECTRUM SIMULATING THAT
C OBTAINED FROM A WIDE-LINED SPECTROMETER (DERIVATIVE
C MODE)). THIS PROGRAM ASSUMES THAT ALL TRANSITIONS HAVE
C THE SAME LINEWIDTH.
C  NOTE--- IF THE POWDER PATTERN EXTENDS BEYOND THE RANGE
C OF PPMIN OR PPMAX, THE RESULTING STEP WILL PRODUCE A
C RESPONSE IN THE CONVOLUTED SPECTRUM. THUS PEAKS AT THE
C ENDS OF THE SPECTRA ARE TO BE DISREGARDED.
C
C *** DATA ENTRY                                 FORMAT ***
C
C  TITLE OF RUN                                     18A4
C  SPIN,XM,PS,VL,PPMIN,PPMAX,ALP,DUMMY,NORM         FREE
C  EQQ,ETA,SSX,SSY,SSZ,SIGHZ,WEIGHT,TRAN            FREE
C
C     DATA LIST
C  SPIN            NUCLEAR SPIN
C  XM              NUMBER OF POINTS OF SPHERE DIVISION
C  PS              NUMBER OF FREQUENCIES AT WHICH POWDER
C                  PATTERN AND SPECTRUM WILL BE COMPUTED.
C  VL              LARMOR FREQUENCY
C  PPMIN,PPMAX     MINIMUM AND MAXIMUM CHEM. SHIFTS IN
```

```
C                          POWDER PATTERN AND SPECTRUM.
C       ALP                VARIABLE ANGLE
C       DUMMY              NUMBER TO ADD A BACKGROUND SPECTRUM
C       NORM               NORMALIZE INTENSITY, IF NORM = 1
C       EQQ                NUCLEAR QUADRUPOLE COUPLING CONSTANT
C       ETA                ASYMMETRY PARAMETER OF ELECTRIC FIELD
C                          GRADIENT AT NUCLEAR SITE
C
C       SSX,SSY,SSZ        CHEMICAL SHIFT PARAMETERS(NOT SHELDING)
C
C       SIGHZ              GAUSSIAN BROADENING IN HZ
C       WEIGHT             RELATIVE WEIGHT TO BE ASSIGNED TO SITE
C       TRAN               SELECTS TRANSITIONS TO BE INCLUDED
C       A GRID IS ESTABLISHED IN COSINE THETA, PHI SPACE WITH
C       EACH COORDINATE HAVING XM INCREMENTS, SO THAT THE GRID
C       IS XM*XM, IF THE QUADRUPOLAR COUPLING AND CHEMICAL SHIFT
C       TENSORS ARE GENERAL. IF BOTH ARE AXIAL, THE PHI ROTATION
C       IS NOT DONE. VL,PMIN, PMAX, AND EQQ ARE IN MEGAHERTZ. ETA
C       AND WEIGHT ARE DIMENSIONLESS. THE PRINCIPAL AXIS SYSTEM
C       OF THE QUADRUPOLAR COUPLING TENSOR (Xq, Yq, Zq) IS
C       DEFINED SO THAT THE ABSOLUTE MAGNITUDE OF Vzz AND Vyy CAN
C       BE THE LARGEST AND THE SMALLEST RESPECTIVELY. ETA IS
C       DEFINED AS: ETA = (Vyy - Vxx)/Vzz. THE ELEMENTS (SSX,
C       SSY, SSZ) OF THE CHEMICAL SHIFT TENSOR ARE CHOSEN IN THE
C       SAME PRINCIPAL AXIS SYSTEM AS QUADRUPOLAR COUPLING
C       TENSOR, SPECIFICALLY,
C             ***********************************************
C             **   Xq // Xcs, Yq // Ycs, AND Zq // Zcs.  **
C             ***********************************************
C       SSX, SSY, AND SSZ ARE IN PPM SCALE. THERE IS NO
C       PREFERENTIAL ORDER OF THE CSA TENSOR ELEMENTS. IN
C       GENERAL, THERE ARE 6 COMBINATIONS WITH THE QUADRUPOLAR
C       COUPLING TENSOR. IF THE PRINCIPAL AXES OF THE QUADRUPOLAR
C       COUPLING TENSOR AND THE CSA TENSOR ARE NONCOINCIDENT,
C       THIS PROGRAM HAS TO BE MODIFIED IN ORDER TO SET EULERIAN
C       ANGLES BETWEEN TWO PRINCIPAL AXIS SYSTEMS.
C
C       SIG IS THE GAUSSIAN HALFWIDTH EXPRESSED AS A FRACTION OF
C       THE TOTAL RANGE PMAX-PMIN. THE PATTERNS WILL INCLUDE THE
C       INTENSITY FROM ALL ADJACENT LEVEL TRANSITIONS BETWEEN THE
C       TRAN AND -TRAN. FOR EXAMPLE, IF TRAN IS SET EQUAL TO .5
C       FOR HALF ODD-INTEGRAL SPIN, THEN ONLY THE CENTRAL
C       TRANSITION WILL BE DONE. IF TRAN IS SET TO 1.5 THEN THE
C       CENTRAL TRANSITION PLUS TWO ADJACENT SATELLITES WILL BE
C       INCLUDED. THE WEIGHTING FACTOR I(I+1)-M(M-1) FOR THE
C       SATELLITE INTENSITIES IS INCLUDED. I IS THE SPIN AND M IS
C       THE MAGNETIC QUANTUM NUMBER.
C       THIS PROGRAM SIMULATES VARIABLE ANGLE SAMPLE SPINNING NMR
C       SPECTRA (NOT SPINNING SIDEBANDS).IF FAST SPINNING CAN
C       AVERAGE FIRST ORDER SATELLITES TO ZERO, THE SIMULATION
C       PROGRAM WHICH USES AVERAGE HAMILTONIAN THEORY WILL BE
C       APPROPRIATE (M. M. MARICQ AND J. S. WAUGH,
C       J. CHEM. PHYS. 70, 3300(1977).
C       STATIC  SPECTRA CAN BE SIMULATED BY SETTING THE VARIABLE
```

```
C     ANGLE ALP = 0.
C     * DUMMY = FACTOR TO DETERMINE IF SIMULATION IS TO BE
C     NORMAL(ANY NUMBER WHICH IS NOT EQUAL TO 2) OR IF
C     SIMULATION IS TO ADD IN A BACKGROUND SPECTRUM FROM A
C     FILE(SPECTRUM.DAT). THE VL,PPMIN,PPMAX, AND PS MUST BE
C     THE SAME TO ADD. THE RELATIVE RATIOS BETWEEN THE SITES
C     SHOULD BE USED. NORM SHOULD BE 0. AN ARRAY P(K) STORES
C     FREQUENCIES.
C     THE UNIT 2 OUTPUT FILE ' F21    ' KEEPS PARAMETERS.
C     THE UNIT 1 OUTPUT FILE ' F22    ' HAS CHEMICAL SHIFTS
C     AND CORRESPONDING FREQUENCIES.
C     THE UNIT 4 FILE IS A DATA FILE TO EXECUTE THIS PROGRAM.
C
C     VMASS1.DAT
C     *TEST1
C     *3.5,23.61,1000,1000,-1000,1000,0,0,0
C     *0.1,0.1,-12,-12,24,100,1,3.5
C
C     VMASS2.DAT
C     *TEST2
C     *1.5,47.61,360,100,-100,100,0,0,0
C     *1,0,0,0,0,200,1,.5
C
C     VMASS3.DAT
C     *TEST3
C     *1.5,47.61,360,100,-100,100,54.7356,0,0
C     *1.3,0,10,10,10,100,1,.5
C
C     VMASS4.DAT
C     *TEST4
C     *3.5,23.61,360,100,-50,50,0,0,0
C     *0,0,35,15,-30,50,1,.5
C
C     VMASS5.DAT
C     *TEST5
C     *1.5,47.61,360,100,-100,100,0,0,0
C     *1.3,0,10,10,10,150,1,.5
C
C     VMASS6.DAT
C     *TEST6
C     *1.5,47.61,360,100,-100,100,0,2,0
C     *1.3,0,10,10,10,150,25,.5
C
C     1.THE RESULT OF TEST1 IS A Cs SPECTRUM AT 180 MHz WHICH
C       SHOWS 7 TRANSITIONS AND CHEMICAL SHIFT ANISOTROPY(1 hr.
C       at IBM PC XT WITH MATH. COPROCESSOR).
C     2.THE TEST2 YIELDS CENTRAL TRANSITION OF Na AT 180 MHz
C       WHICH IS PURE QUADRUPOLAR SECOND ORDER PATTERN (WITHIN
C       1 min. at IBM PC XT WITH MATH. COPROCESSOR).
C     3.THE TEST3 DEMONSTRATES A MAS SPECTRUM OF TEST5 WITH
C       ISOTROPIC CHEMICAL SHIFT 10 PPM.
C     4.THE TEST4 SIMULATES PURE CHEMICAL SHIFT ANISOTROPY
C       POWDER PATTERN.
C     5.THE TEST5 YIELDS SECOND ORDER QUADRUPOLE POWDER
```

```
C           PATTERN WITH ISOTROPIC CHEMICAL SHIFT 10PPM.
C     6.IF THIS COMPOUND HAS 80% TEST2 SITES AND 20% TEST5
C        SITES THE SUM OF THE SPECTRA CAN BE GENERATED BY USING
C        VMASS6.DAT AND SPECTRUM.DAT WHICH IS RENAMED
C        FROM THE OUTPUT OF VMASS2.DAT.
C
C     DIMENSIONS OF PARAMETERS WHICH AGREE WITH EACH OTHER ARE
C     COUPLED AND SHOULD BE RESET ACCORDINGLY, IF MODIFICATION
C     IS NECESSARY.
C     IMPLICIT REAL*8 (A-H,O-Z)
      CHARACTER*20 F20,F21,F22
      DIMENSION TITLE(18),G(1000),GT(1000),KG(1000),ST(1000)
      DIMENSION COD(1000),CXD(1000),COSTP(1000)
      DIMENSION HT(1000),P(1000),PPM(1000),INT(10)
      DIMENSION BO1(10),BO2(10),BO3(10),BO4(10)
      DIMENSION BO5(10),BO6(10),BO7(10),S(10)
C
C     OPEN FILES
C
7     WRITE(*,76)
      READ(*,78,ERR=7) F20
      OPEN(UNIT=4,FILE=F20,STATUS='OLD')
8     WRITE(*,72)
      READ(*,78,ERR=8) F21
      OPEN(UNIT=1,FILE=F21,STATUS='NEW')
9     WRITE(*,74)
      READ(*,78,ERR=9) F22
      OPEN(UNIT=2,FILE=F22,STATUS='NEW')
C
C*********************** FORMAT ***********************
C
12    FORMAT(/)
14    FORMAT(9H    SPIN =,F4.1,5X,21HQUAD. COUPL. CONST. =,
     F7.3
     *,5X,13HLARMOR FRQ. =,F7.3,5X,13HASYMM. PAR. =,F7.4)
16    FORMAT(16H    SPHERE DIV. =,F5.0,1X,26HNO. POINTS TO BE
     PLOTTED =,
     *F5.0,1X,16HMIN CHEM SHIFT =,F8.2,1X,16HMAX CHEM SHIFT
     =,F8.2)
18    FORMAT(28H CHEM. SHIFT
     PARAMETERS;SSX=,F7.2,1X,4HSSY=,F7.2,1X,
     *4HSSZ=,F7.2)
20FORMAT(' ISO CHEM SHIFT=',F7.2,1X,'CHEM SHIFT
     DELTA=',F8.3,1X,
     *'CHEM SHIFT ETA=',F7.2)
22    FORMAT(22HGAUSSIAN BROADENNING =,F7.5,1X,20HGAUSSIAN
     LINEWIDTH =,
     *F10.5,4H KHZ)
24FORMAT(1X,31HDELTA M = 1 TRANSITIONS BETWEEN,F5.1,4H
     AND,F5.1,
     *5H ONLY)
26     FORMAT(1H1)
28     FORMAT(18A4)
30     FORMAT(2X,18A4)
```

```
32      FORMAT(2X,17H VARIABLE ANGLE =,F10.7)
34      FORMAT(2X,'ENTER TITLE')
36      FORMAT(2X,'ENTER SPIN (FOR EXAMPLE I=7/2--->3.5)')
38      FORMAT(8X,'LARMOR FREQUENCY IN MHZ')
40      FORMAT(8X,'NUMBER OF POINTS FOR ANGLES (<1001)')
42      FORMAT(8X,'NUMBER OF POINTS FOR PLOT  (<1001)')
44      FORMAT(8X,'PLOT MINIMUM IN PPM (FOR EXAMPLE -100)')
46      FORMAT(8X,'PLOT MAXIMUM IN PPM (FOR EXAMPLE 100)')
48      FORMAT(8X,'VARIABLE ANGLE (54.7356 FOR MASS, 0 FOR
STATIC)')
50      FORMAT(8X,'DUMMY (0 FOR NORM. SIM., 2 TO ADD A
SPECTRUM)')
52      FORMAT(36H SPIN,VL,XM,PS,PPMIN,PPMAX,ALP,DUMMY)
54      FORMAT(2X,'ENTER QUADRUPOLE COUPLING CONSTANT IN MHZ')
56      FORMAT(8X,'ASYMMETRY PARAMETER OF EFG')
58      FORMAT(8X,'3 CSA TENSOR PRINCIPAL COMPONENTS IN PPM')
60      FORMAT(8X,'GAUSSIAN BROADENING IN HZ')
62      FORMAT(8X,'RELATIVE INTENSITY')
64      FORMAT(8X,'TRANSITIONS TO BE CALCULATED(.5 FOR CENTRAL
     *TRANSITION)')
66      FORMAT(38H EQQ,ETA,SSX,SSY,SSZ,SIGHZ,WEIGHT,TRAN)
68      FORMAT(2E12.4)
70      FORMAT('*** THE SPECTRUM.DAT FILE HAS BEEN ADDED.
     *  ADD THE PARAMETER FILE ***')
72      FORMAT(' ENTER OUTPUT FILE NAME')
74      FORMAT(' ENTER OUTPUT PARAMETER FILE NAME')
76      FORMAT(' ENTER INPUT PARAMETER FILE NAME')
78      FORMAT(A)
80      FORMAT(' WEIGHT = ',1F10.6)
82      FORMAT(8X,'1 FOR NORMALIZATION')
        IO=2
C
C       *************** INPUT PARAMETER  *****************
C
C       WRITE(*,34)
C       READ(*,28)TITLE
C       WRITE(*,36)
C       WRITE(*,38)
C       WRITE(*,40)
C       WRITE(*,42)
C       WRITE(*,44)
C       WRITE(*,46)
C       WRITE(*,48)
C       WRITE(*,50)
C       WRITE(*,52)
C       WRITE(*,82)
C       READ(*,*)SPIN,VL,XM,PS,PPMIN,PPMAX,ALP,DUMMY,NORM
C       WRITE(*,54)
C       WRITE(*,56)
C       WRITE(*,58)
C       WRITE(*,60)
C       WRITE(*,62)
C       WRITE(*,64)
C       WRITE(*,66)
```

```
C       READ(*,*)EQQ,ETA,SSX,SSY,SSZ,SIGHZ,WEIGHT,TRAN
        READ(4,28)TITLE
        READ(4,*)SPIN,VL,XM,PS,PPMIN,PPMAX,ALP,DUMMY,NORM
        READ(4,*)EQQ,ETA,SSX,SSY,SSZ,SIGHZ,WEIGHT,TRAN
C******************************************************************
        IF(XM.GT.1000.) XM=1000.
        IF(PS.GT.1000.) PS=1000.
        IF(XM.LT.1.) XM=360.
        IF(PS.LT.1.) PS=100.
        M=XM
        NS=PS
        PMIN=VL+(PPMIN*VL/1.0E6)
        PMAX=VL+(PPMAX*VL/1.0E6)
        PR=PMAX-PMIN
        GIP=(PS-1.)/PR
        ANG=3.141593*ALP/180.
        CAL=COS(ANG)
        CXC=CAL*CAL
        CTC=CXC*CXC
        THC=3.*CXC-1.
        TTC=.25*THC
        DO 100 I=1,M
        XI=I
        U=(XI-.5)/XM
        UXU=U*U
        COD(I)=UXU
        CXD(I)=UXU*UXU
        TPHI=3.141593*(XI-.5)/XM
        COSTP(I)=COS(TPHI)
100     CONTINUE
        DO 110 K=1,NS
        G(K)=0.
        GT(K)=0.
        KG(K)=0.
        ST(K)=0.
        XK=K
        P(K)=PMIN+(XK-1.)*PR/(PS-1.)
        PPM(K)=(P(K)-VL)*1.0E6/VL
110     CONTINUE
        SIGKC=SIGHZ/1000.
        SIG=SIGHZ/PR*1.E-6
        CSIGMA=(SSX+SSY+SSZ)/3.
        CSDEL=SSZ-CSIGMA
        IF(CSDEL.EQ.0.) GO TO 120
        CETA=(SSY-SSX)/CSDEL
        GO TO 130
120     CETA=0.
130     CISO=CSIGMA/1.E6
        CDEL=CSDEL/1.E6
        S(1)=SSX
        S(2)=SSY
        S(3)=SSZ
131     CONTINUE
        DO 134 K=1,2
```
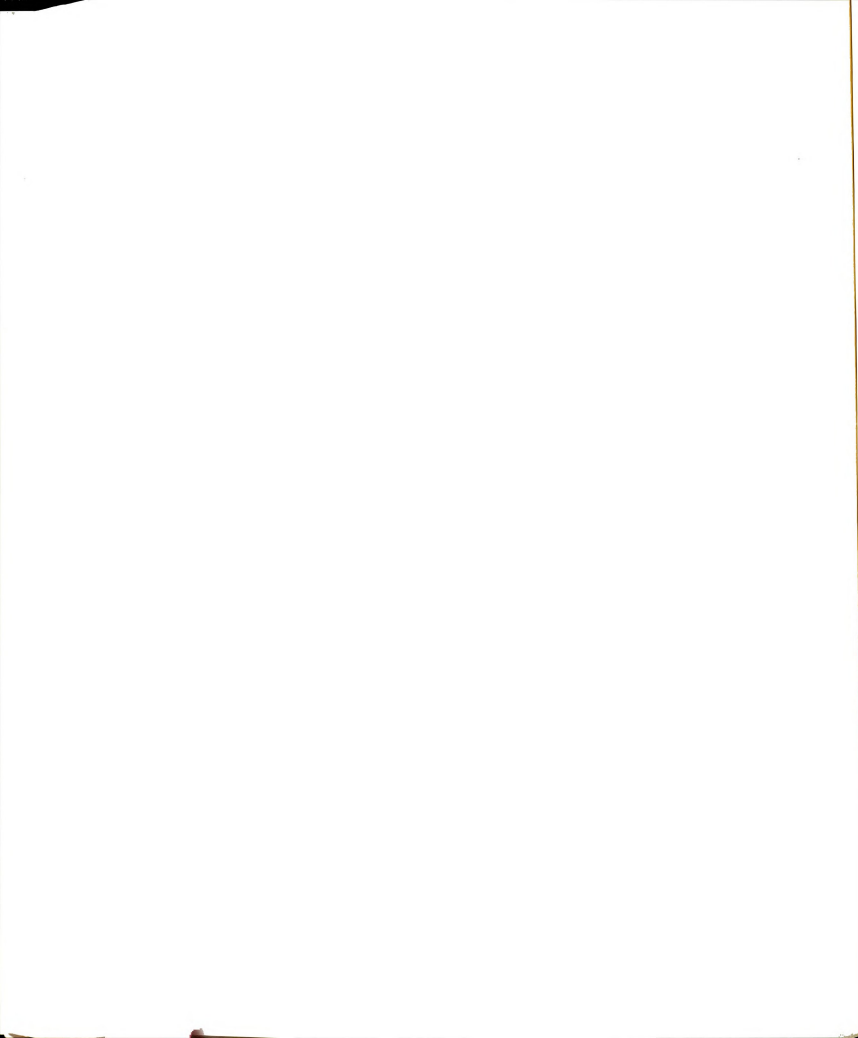
```
          LA=K+1
          DO 132 L=LA,3
          IF(S(K).LE.S(L)) GO TO 132
          SK=S(K)
          S(K)=S(L)
          S(L)=SK
132       CONTINUE
134       CONTINUE
          IF(S(2).LT.S(1)) GO TO 131
          IF(ABS(S(1)-CSIGMA).LE.ABS(S(3)-CSIGMA)) GO TO 136
          IF(ABS(S(1)-CSIGMA).GT.ABS(S(3)-CSIGMA)) S1=S(1)
          S(1)=S(3)
          S(3)=S1
136       CSDELTA=S(3)-CSIGMA
          IF(CSDELTA.EQ.0) GO TO 138
          CSETA=(S(2)-S(1))/CSDELTA
          GO TO 139
138       CSETA=0
139       VQ=EQQ
          TRAX=-TRAN
C
C************* OUTPUT FOR INPUT PARAMETER *****************
C
          WRITE(IO,26)
          WRITE(IO,30)TITLE
          WRITE(IO,12)
          WRITE(IO,16)XM,PS,PPMIN,PPMAX
          WRITE(IO,12)
          WRITE(IO,14)SPIN,VQ,VL,ETA
          WRITE(IO,12)
          WRITE(IO,18)SSX,SSY,SSZ
          WRITE(IO,20)CSIGMA,CSDELTA,CSETA
          WRITE(IO,12)
          WRITE(IO,24)TRAN,TRAX
          WRITE(IO,12)
          WRITE(IO,32)ALP
          WRITE(IO,12)
          WRITE(IO,22)SIG,SIGKC
          WRITE(IO,12)
          WRITE(IO,80)WEIGHT
C*********************************************************************
          CSETA=-CETA
          ETA=-ETA
          EE=ETA*ETA
          EE6=EE/6.
          SS1=SPIN*(SPIN+1.)
          IF(SPIN-0.5) 140,140,150
140       VQQ=0.0
          GO TO 160
150       VQQ=3.*VQ/(2.*SPIN*(2.*SPIN-1.))
160       FACT=VQQ*VQQ/(12.*VL)
          VLC=VL*CDEL
          VCC=VLC*CSETA
          VIS=VL*(1.+CISO-.25*THC*CDEL)
```

```
        FATA=FACT*ETA
        XMAG=-TRAN+1.
        MAG=1
170     CONTINUE
        XX1=XMAG*(XMAG-1.)
        A=24.*XX1-4.*SS1+9.
        B=6.*XX1-2.*SS1+3.
        C=-VQQ*(XMAG-.5)
        VMA=.5*A*(1.-CTC)-.125*B*(1.+6.*CXC+CTC)
        VMB=.5*A*(1.-3.*CXC+4.*CTC)-.5*B*(1.-CTC)
        VMC=1.5*A*(CXC-CTC)-.375*B*(1.-2.*CXC+CTC)
        VCEC=VCC+ETA*C
        VLCC=VLC+C
        BO1(MAG)=-TTC*C+FACT*(.375*VMA+EE6*VMB+.25*VMC)
        BO2(MAG)=TTC*VCEC+FATA*(.25*VMA-.5*VMC)
        BO3(MAG)=FACT*EE*(VMA/24.-VMB/6.+.25*VMC)
        BO4(MAG)=3.*TTC*VLCC+FACT*((EE6-.75)*VMA+(1.5-EE6)*VMB-
1.5*VMC)
        BO5(MAG)=-TTC*VCEC+FATA*(-VMB+2.*VMC)
        BO6(MAG)=FACT*(.375*VMA-1.5*VMB+2.25*VMC)
        BO7(MAG)=FATA*(-.25*VMA+VMB-1.5*VMC)
        INT(MAG)=SS1-XX1
        IF(XMAG.GE.TRAN) GO TO 190
180     XMAG=XMAG+1
        MAG=MAG+1
        GO TO 170
190     CONTINUE
        MGMX=MAG
        MM=M
        IF(SSX.EQ.SSY.AND.ETA.EQ.0.) MM=1
        AMP=WEIGHT/MM
        DO 200 J=1,MM
        CTP=COSTP(J)
        CXP=CTP*CTP
        DO 200 MAG=1,MGMX
        BOC=BO3(MAG)*CXP
        EUN1=VIS+BO1(MAG)+BO2(MAG)*CTP+BOC
        EUN2=BO4(MAG)+BO5(MAG)*CTP-2.*BOC
        EUN3=BO6(MAG)+BO7(MAG)*CTP+BOC
        MULTI=INT(MAG)
        DO 200 I=1,M
        FNN=EUN1+EUN2*COD(I)+EUN3*CXD(I)-PMIN
        NN=FNN*GIP+1.5
        IF(NN.LT.2.OR.NN.GT.NS) GO TO 200
        KG(NN)=KG(NN)+MULTI
200     CONTINUE
        DO 210 LL=1,NS
        GTLL=KG(LL)*AMP
        GT(LL)=GTLL
210     CONTINUE
        CALL SHIFT(NS,GT)
        CALL CONVOL(NS,SIG,GT,0,ST)
        IF(DUMMY.NE.2) GO TO 230
        OPEN(UNIT=3,FILE='SPECTRUM.DAT',STATUS='OLD')
```
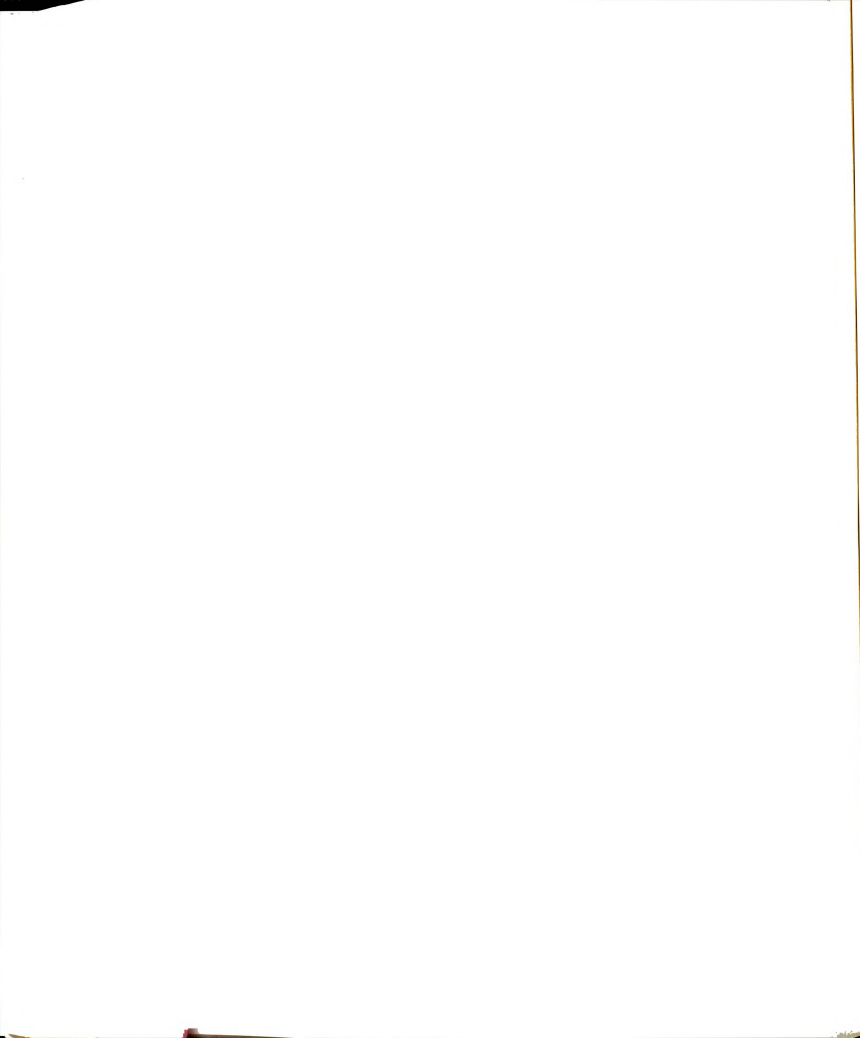
```
      READ(3,68)(PPM(K),HT(K),K=1,PS)
      WRITE(*,70)
      DO 220 N=1,PS
      ST(N)=ST(N)+HT(N)
220   CONTINUE
230   CONTINUE
      IF(NORM.NE.1) GO TO 240
      CALL UNITY(NS,ST)
C******************** OUTPUT *************************
240   WRITE(1,68)(PPM(K),ST(K),K=1,PS)
      STOP
      END
C
C
      SUBROUTINE CONVOL(NS,SIGMA,G,NDERIV,SA)
C     CONVOL DOES A CONVOLUTION OF THE NTH GAUSSIAN DERIVATIVE
C     WITH AN ARBITRARY FUNCTION. N IS 0,1,2, OR 3. ENTRY IS NS
C     POINTS, SIGMA THE GAUSSIAN HALF-WIDTH, G CONTAINING THE
C     FUNCTION TO BE CONVOLUTED AND NDERIV THE VALUE OF N. THE
C     OUTPUT IS IN SA.
C
C     IMPLICIT REAL*8 (A-H,O-Z)
      DIMENSION G(1000),SA(1000),XSTORE(1000)
      IF(SIGMA.LE.0.) RETURN
      RX=1./(2.*(SIGMA*NS)**2)
      SQRX=RX**.5
      DO 28 L=1,NS
      SA(L)=0.
      XL=L-1
      POW=XL*XL*RX
      IF(POW-30.) 26,27,27
26    XSTORE(L)=EXP(-POW)
29    GO TO 28
27    XSTORE(L)=0.
28    CONTINUE
      IF(NDERIV.LT.0.OR.NDERIV.GT.3) NDERIV=1
      MOVE=NDERIV+1
      GO TO (20,30,40,50) MOVE
20    CONTINUE
      DO 22 I=1,NS
      DO 22 J=1,NS
      XXX=I-J
      IF(XXX) 23,24,24
23    L=J-I+1
      GO TO 22
24    L=I-J+1
22    SA(J)=SA(J)+G(I)*XSTORE(L)
      RETURN
30    CONTINUE
      DO 32 I=1,NS
      DO 32 J=1,NS
      XXX=I-J
      IF(XXX) 33,34,34
33    L=J-I+1
```

```
          GO TO 32
34        L=I-J+1
32        SA(J)=SA(J)+G(I)*XSTORE(L)*XXX*SQRX
          RETURN
40        CONTINUE
          DO 42 I=1,NS
          DO 42 J=1,NS
          XXX=I-J
          IF(XXX) 43,44,44
43        L=J-I+1
          GO TO 42
44        L=I-J+1
42        SA(J)=SA(J)+G(I)*XSTORE(L)*(1.-2.*XXX*XXX*RX)
          RETURN
50        CONTINUE
          DO 52 I=1,NS
          DO 52 J=1,NS
          XXX=I-J
          IF(XXX) 53,54,54
53        L=J-I+1
          GO TO 52
54        L=I-J+1
52        SA(J)=SA(J)-G(I)*XSTORE(L)*(-6.*XXX*SQRX
         *+4.*XXX*XXX*XXX*RX*SQRX)
          RETURN
          END
C
C
          SUBROUTINE SHIFT(N,G)
C    SHIFT SUBTRACTS A FIXED AMOUNT FROM THE POWDER PATTERN TO
C    MINIMIZE THE EFFECTS OF THE CONVOLUTION AT THE ENDS OF
C    THE SIMULATED SPECTRUM.
C
C    IMPLICIT REAL*8 (A-H,O-Z)
          DIMENSION G(1000)
          GMIN=G(1)
          DO 1 I=2,N
          IF(GMIN.LE.G(I)) GO TO 1
          GMIN=G(I)
1         CONTINUE
          DO 2 I=1,N
          G(I)=G(I)-GMIN
2         CONTINUE
          RETURN
          END
C
          SUBROUTINE UNITY(N,ST)
C    UNITY NORMALIZES INTENSITY AFTER CONVOLUTION (MAXIMUM
C    PEAK HEIGHT = 1.).
C    IMPLICIT REAL*8 (A-H,O-Z)
          DIMENSION ST(1000)
          STMAX=ST(1)
          DO 1 I=1,N
          IF(STMAX.GE.ST(I)) GO TO 1
```

```
        STMAX=ST(I)
1       CONTINUE
        DO 2 I=1,N
        ST(I)=ST(I)/STMAX
2       CONTINUE
        RETURN
        END
```

APENDIX C

```
      PROGRAM ANTIMAG
C
C     JINEUN KIM
C     JAMES L. DYE*
C          *DEPARTMENT OF CHEMISTRY
C           MICHIGAN STATE UNIVERSITY
C           EAST LANSING MI 48824 U.S.A.
C
C     THIS IS THE PROGRAM TO FIND THE ROOTS OF THE ZEROTH
C     ORDER SUSCEPTIBILITIES AND CALCULATE THE MAGNETIC
C     SUSCEPTIBILITIES. REF;BULL.CHEM.SOC.JPN. V52 P3480 1979,
C     PROG.THEOR.PHYS. V13 P148 1955
C     NUMERICAL RECIPES;THE ART OF SCIENTIFIC COMPUTING,
C     WILLIAM PRESS ET.AL. CAMBRIDGE UNIV. PRESS, CHAPTER 9.
C     CALC=THEORETICAL SUSCEPTIBILITY
C     SUS,SLJ,SRJ;;SUSCEPTIBILITIES
C     SRED,SRLJ,SRRJ:: REDUCED SUSCEPTIBILITIES.
C     TR=REDUCED TEMPERATURE
C     MOLECULAR FIELD PARAMETER AK=(Z-1)*J'/J
C
C     INPUT
C     ENTER 444. IN THE ANTIMAG.TEM;FOR THE NEEL TEMPERATURE
C     ENTER 999. IN THE ANTIMAG.TEM;FOR PROGRAM STOP
C
C     ANTIMAG.TEM (AN EXAMPLE INPUT FILE)
C     2
C     4
C     6
C     8
C     10
C     13
C     16
C     20
C     25
C     30
C     35
C     40
C     45
C     50
C     60
C     70
C     80
C     90
C     100
C     120
C     140
C     160
C     180
C     200
C     250
C     300
```

```
C       444
C       999
C
C       THE INTERACTIVE INPUTS ARE AJ,WT,EFF. (AN EXAMPLE)
C       COUPLING CONSTANT           AJ=-J/k   (14.2)    FREE  FORMAT
C       WEISS TEMPERATURE           WT        (-22 )    FREE  FORMAT
C       EFFECTIVE SPIN NUMBER(%) EFF          (82.5)    FREE  FORMAT
C
C
        IMPLICIT REAL*8 (A-H,O-Z)
        CHARACTER*20 F20,F21
7       WRITE(*,10)
        READ(*,30,ERR=7) F20
        OPEN (UNIT=1,FILE=F20,STATUS='OLD')
8       WRITE(*,20)
        READ(*,30,ERR=8) F21
        OPEN (UNIT=2,FILE=F21,STATUS='NEW')
C******************** FORMAT *************************
10      FORMAT(' ENTER INPUT FILE NAME : TEMPERATURE')
20      FORMAT(' ENTER OUTPUT FILE NAME')
30      FORMAT(A)
40      FORMAT(29H COUPLING CONSTANT -J/k = AJ=)
50      FORMAT(19H WEISS TEMPERATURE=)
60      FORMAT(20H  WEISS TEMPERATURE=,F10.5,2H K)
70      FORMAT(25H EFFECTIVE SPIN #(%) EFF=)
80      FORMAT(27H  COUPLING CONSTANT AJ=-J/k,F10.5,2H K)
90      FORMAT(31H  MOLECULAR FIELD PARAMETER AK=,F10.5)
100     FORMAT(23H  EFFECTIVE SPIN # EFF=,F10.5,2H %)
110     FORMAT(5X,3H TR,6X,5H SRED,8X,5H SRLJ,6X,5H SRRJ,6X,4H
TEM,
       *4X,5H CALC,5X,4H SLJ,4X,4H SRJ,8X,2H R,6X,4H SUS)
120     FORMAT(1X,F9.3,1X,E10.4,1X,E10.4,1X,E10.4,1X,F10.4,
       *1X,F8.6,1X,F8.6,1X,F8.6,1X,F10.5,1X,E10.4)
130     FORMAT(45X,7H T NEEL)
C********************************************************************
        NN=100
        WRITE(*,40)
        READ(*,*)AJ
        WRITE(*,50)
        READ(*,*)WT
        WRITE(2,60) WT
        WRITE(*,70)
        READ(*,*)EFF
        WRITE (2,80) AJ
        AK=-2.*WT/AJ-1.
        WRITE (2,90) AK
        WRITE (2,100) EFF
        WRITE (2,110)
200     READ (1,*) TEM
        IF ((TEM.EQ.444.).AND.(AK.GT.1.)) GO TO 444
        IF (TEM.GE.999.) GO TO 999
        AKB=1.38054E-23
        AJJ=AJ*AKB
        BJ=-AJ/TEM
```

```fortran
      TR=-1./BJ
      IF (AK.LE.1.) GO TO 400
      BN=LOG((AK-1.)/(AK+3.))/2
      IF (BJ.GE.BN) GO TO 400
      ABA=ABS(BJ*AK)
      IF (LOG(ABA)+ABA.GT.85.) GO TO 300
      X1=1.
      X2=AK+1.E-6
      CALL ZBRAK(FM,BJ,AK,X1,X2,NN,XB1,XB2)
      XACC=1.E-10*(XB1+XB2)/2
      ROOT=RTSAFE(BJ,AK,XB1,XB2,XACC)
      RJ=ROOT
      IF (ABS(BJ*(1.+RJ)).GT.85.) GO TO 300
      EBJ=EXP(-BJ)
      CBR=COSH(BJ*RJ)
      CHA=1.+EBJ*CBR
      CHB=(1.-RJ)**2*EBJ*CBR+2*RJ-(RJ**2+1.)*EBJ*EXP(BJ*RJ)
      CAB=-AK*CHB+RJ*(1.-RJ**2)*CHA
      SRLJ=AJ/2./TEM/(CHA-AK*BJ)
      SRRJ=-CHB/2./CAB
      GO TO 350
300   SRLJ=0.
      SRRJ=.25*(AK-1.)/AK**2
350   SRED=(SRLJ+2.*SRRJ)/3.
      CALC=2.07616E-23/AJJ*SRED
      SLJ=2.07616E-23/AJJ*SRLJ
      SRJ=2.07616E-23/AJJ*SRRJ
      SUS=CALC*EFF/100.
      GO TO 550
444   BJ=BN
      TR=-1./BJ
      TEM=-AJ/BJ
      WRITE (2,130)
      GO TO 400
400   RJ=1
      IF (ABS(2.*BJ).GT.87.) GO TO 450
      CHC=1.-BJ*AK+EXP(-BJ)*COSH(BJ)
      SRED=AJ/2./TEM/CHC
      GO TO 500
450   SRED=0.
500   SRLJ=SRED
      SRRJ=SRED
      CALC=2.07616E-23/AJJ*SRED
      SLJ=CALC
      SRJ=CALC
      SUS=CALC*EFF/100.
      GO TO 550
550   WRITE (2,120)TR,SRED,SRLJ,SRRJ,TEM,CALC,SLJ,SRJ,RJ,SUS
      GO TO 200
999   STOP
      END
C
C
      FUNCTION ZESUS(BJ,AK,X)
```

```fortran
      IMPLICIT REAL*8 (A-H,O-Z)
      ZESUS=X*EXP(BJ)+X*COSH(BJ*X)+AK*SINH(BJ*X)
      RETURN
      END
C
C
      SUBROUTINE DFUNC(BJ,AK,X,FM,DF)
      IMPLICIT REAL*8 (A-H,o-Z)
      FM=ZESUS(BJ,AK,X)
      DZESUS=EXP(BJ)+(1.+BJ*AK)*COSH(BJ*X)+BJ*X*SINH(BJ*X)
      DF=DZESUS
      RETURN
      END
C
C
      SUBROUTINE ZBRAK(FX,BJ,AK,X1,X2,NN,XB1,XB2)
      IMPLICIT REAL*8 (A-H,O-Z)
      X=X1
      DX=(X2-X1)/NN
      FP=ZESUS(BJ,AK,X)
      DO 10 I=1,100
      X=X+DX
      FX=ZESUS(BJ,AK,X)
      IF (FX/ABS(FX)*FP/ABS(FP).GT.0.) GO TO 7
      XB1=X-DX
      XB2=X
      RETURN
7     FP=FX
10    CONTINUE
      RETURN
      END
C
C
      FUNCTION RTSAFE(BJ,AK,X1,X2,XACC)
      IMPLICIT REAL*8 (A-H,O-Z)
      MAXIT=100
      CALL DFUNC(BJ,AK,X1,FL,DF)
      CALL DFUNC(BJ,AK,X2,FH,DF)
      IF (FL.GE.0.) GO TO 10
      XL=X1
      XH=X2
      GO TO 20
10    XH=X1
      XL=X2
      SWAP=FL
      FL=FH
      FH=SWAP
20    DO 60 J=1,MAXIT
      RTSAFE=0.5*(XL+XH)
      DXOLD=ABS(XH-XL)
      DX=DXOLD
      CALL DFUNC(BJ,AK,RTSAFE,F,DF)
      DFF=(DF-F)/ABS(DF-F)
      IF (((RTSAFE-XH)*DFF)*((RTSAFE-XL)*DFF).LT.0.
```
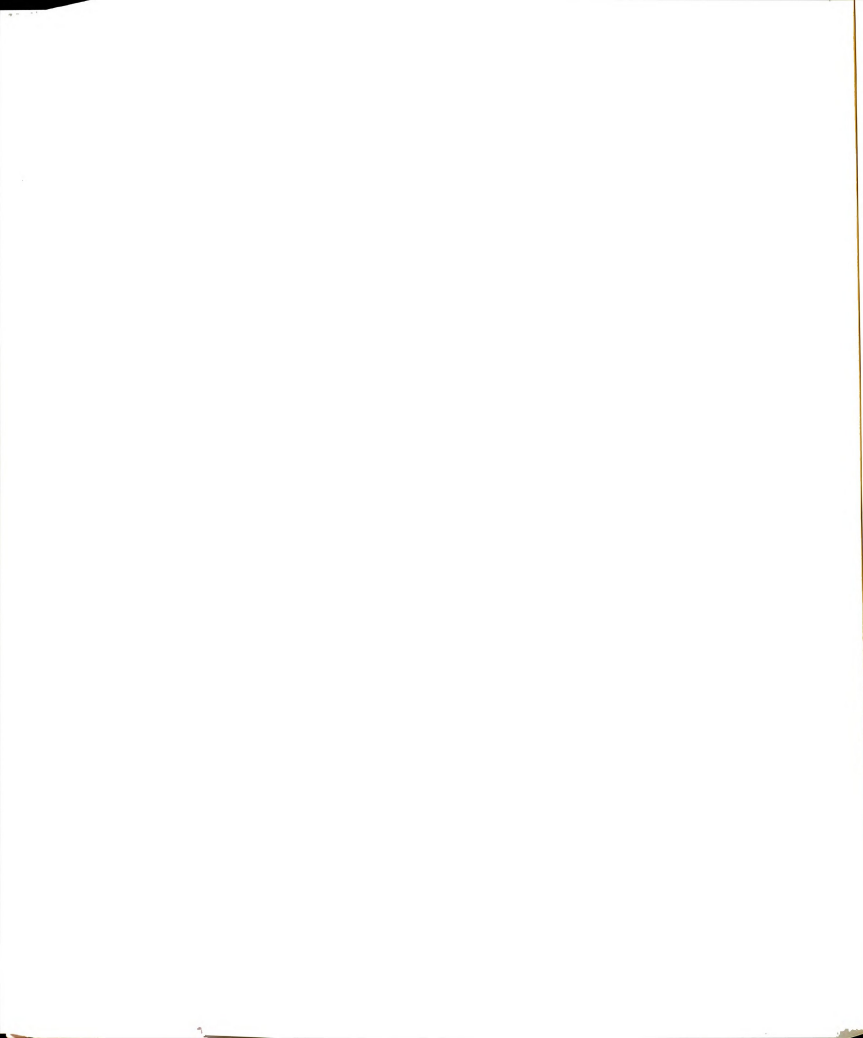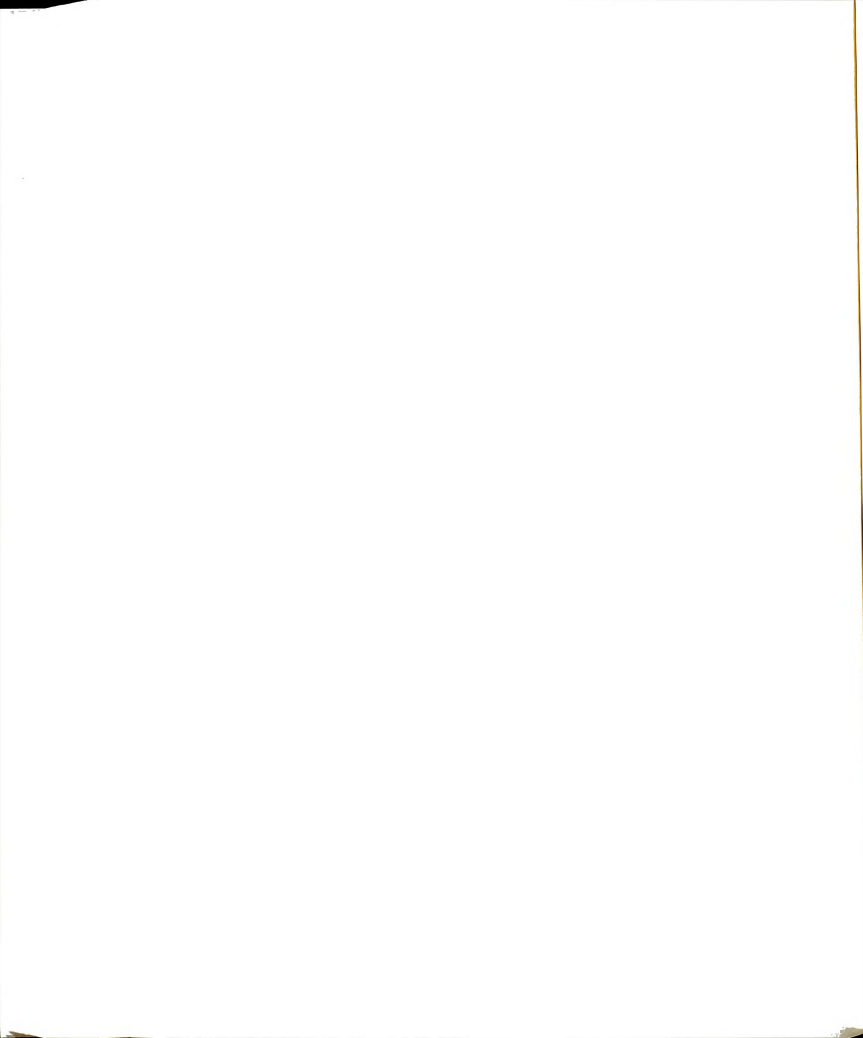
```
     *.AND.ABS(2.*F).LE.ABS(DXOLD*DF)) GO TO 30
      DXOLD=DX
      DX=(XH-XL)/2.
      IF (XL.EQ.RTSAFE) RETURN
      XACC=(1.E-10)*(XH+XL)/2.
      GO TO 40
30    DXOLD=DX
      DX=F/DF
      TEMP=RTSAFE
      RTSAFE=RTSAFE-DX
      IF (TEMP.EQ.RTSAFE) RETURN
40    IF (ABS(DX).LT.XACC) RETURN
      CALL DFUNC(BJ,AK,RTSAFE,F,DF)
      IF (F.GT.0.) GO TO 50
      XL=RTSAFE
      FL=F
      GO TO 60
50    XH=RTSAFE
      FH=F
60    CONTINUE
      RETURN
      END
```

LIST OF REFERENCES

1. J. L. Dye, *Prog. Inorg. Chem.*, 32, 327 (1984).

2. J. L. Dye and M. G. DeBacker, *Ann. Rev. Phys. Chem.*, 38, 271 (1987).

3. J. L. Dye, J. M. Ceraso, M. T. Lok, B. L. Barnett and F. J. Tehan, *J. Am. Chem. Soc.*, 96, 608 (1974).

4. A. Ellaboudy and J. L. Dye, *J. Am. Chem. Soc.*, 105, 6490 (1983).

5. M. G. DeBacker, J. L. Dye, R. S. Bannwart and S. A. Solin, *J. Am. Chem. Soc.*, in press.

6. R. H. Huang, Ph. D. Dissertation, Michigan State University (1987).

7. J. L. Dye, *J. Phys. Chem.*, 88, 3842 (1984).

8. S. B. Dawes, Ph. D. Dissertation, Michigan State University (1986).

9. O. Fussa, Ph. D. Dissertation, Michigan State University (1986).

10. M. E. Kuchenmeister and J. L. Dye, *J. Am. Chem. Soc.*, 111, 935 (1989).

11. J. M. Ceraso and J. L. Dye, *J. Chem. Phys.*, 61, 1585 (1974).

12. R. Concepcion and J. L. Dye, *J. Am. Chem. Soc.*, 109, 7203 (1987).

13. A. Ellaboudy, M. L. Tinkham, B. VanEck, J. L. Dye and P. B. Smith, *J. Phys. Chem.*, 88, 3852 (1984).

14. S. B. Dawes, A. S. Ellaboudy, and J. L. Dye, *J. Am. Chem. Soc.*, 109, 3508 (1987).

15. M. L. Tinkham and J. L. Dye, *J. Am. Chem. Soc.*, 107, 6129 (1985).

16. M. L. Tinkham, A. Ellaboudy, J. L. Dye, and P. B. Smith, *J. Phys. Chem.*, 90, 14 (1986).

17. A. Ellaboudy and J. L. Dye, *J. Magn. Reson.*, 66, 491 (1986).

18. A. S. Ellaboudy, Ph. D. Dissertation, Michigan State University (1984).

19. M. L. Tinkham, Ph. D. Dissertation, Michigan State University (1985).

20. P. D. Moras, B. Metz, and R. Weiss, *Acta. Cryst.*, B29, 388 (1973).

21. M. L. Tinkham, M. S. Thesis, Michigan State University (1982).

22. D. Issa, A. Ellaboudy, R. Janakiraman, and J. L. Dye, *J. Phys. Chem.*, 88, 3847 (1984).

23. M. E. Kuchenmeister, Ph. D. Dissertation, Michigan State University (1989).

24. J. S. Landers, J. L. Dye, A. Stacy, and M. J. Sienko, *J. Phys. Chem.*, 85, 1096 (1981).

25. R. H. Huang, M. K. Faber, K. J. Moeggenborg, D. L. Ward, and J. L. Dye, *Nature*, 331, 599 (1988).

26. M. E. Rose, "Elementary Theory of Angular Momentum", John Wiley, New York (1957).

27. M. Mehring, "Principles of High Resolution NMR in Solids", Springer-Verlag Berlin Heidelberg New York (1983).

28. G. M. Volkoff, *Can. J. Phys.*, 31, 820 (1953).

29. R. L. Cook and F. C. De Lucia, *Am. J. Phys*, 30, 1433 (1971).
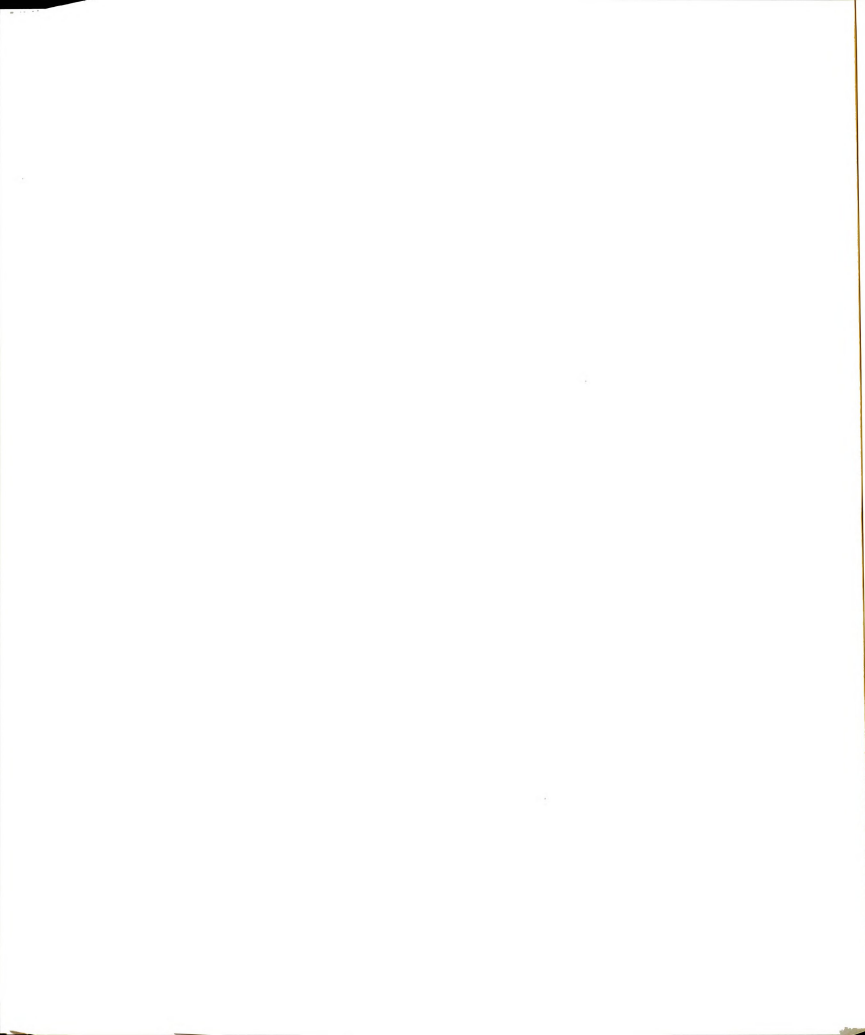
30. K. Narita, J. Umeda, and H. Kusumoto, *J. Chem. Phys*, <u>44</u>, 2719 (1966).

31. J. F. Baugher, P. C. Taylor, T. Oja, and P. J. Bray, *J. Chem. Phys.*, <u>50</u>, 4914 (1969).

32. A. Naito, S. Ganapathy, and C. A. McDowell, *J. Magn. Reson.*, <u>48</u>, 367 (1982).

33. S. Ganapathy, S. Schramm, and E. Oldfield, *J. Chem. Phys.*, <u>77</u>, 4360 (1982).

34. J. Herzfeld and A. E. Berger, *J. Chem. Phys.*, <u>73</u>, 6021 (1980).

35. C. Ye, B. Sun, and G. E. Maciel, *J. Magn. Reson.*, <u>70</u>, 241 (1986).

36. A. Abragam, "The Principles of Nuclear Magnetism", Clarendon Press, Oxford (1961).

37. J. H. Van Vleck, *Phys. Rev.*, <u>74</u>, 1168 (1948).

38. K. Kambe and J. K. Ollom, *J. Phys. Soc. Japan*, <u>11</u>, 50 (1956).

39. C. Domb in "Magnetism, Vol. II A", ed. G. T. Rado and H. Suhl, Academic Press (1965).

40. W. Heisenberg, *Z. Physik*, <u>49</u>, 619 (1928).

41. E. Ising, *Z. Physik*, <u>31</u>, 253 (1925).

42. D. C. Mattis, "The Theory of Magnetism; An Introduction to the Study of Cooperative phenomena", Harper and Row, New York (1965).

43. L. Onsager, *Phys. Rev.*, <u>65</u>, 117 (1944).

44. M. E. Fisher, *J. Math. Phys.*, <u>4</u>, 278 (1963).

45. G. H. Wannier, *Rev. Mod. Phys.*, <u>17</u>, 50 (1945).

46. C. Domb, *Phyl. Mag. Suppl*, <u>9</u>, 245 (1960).

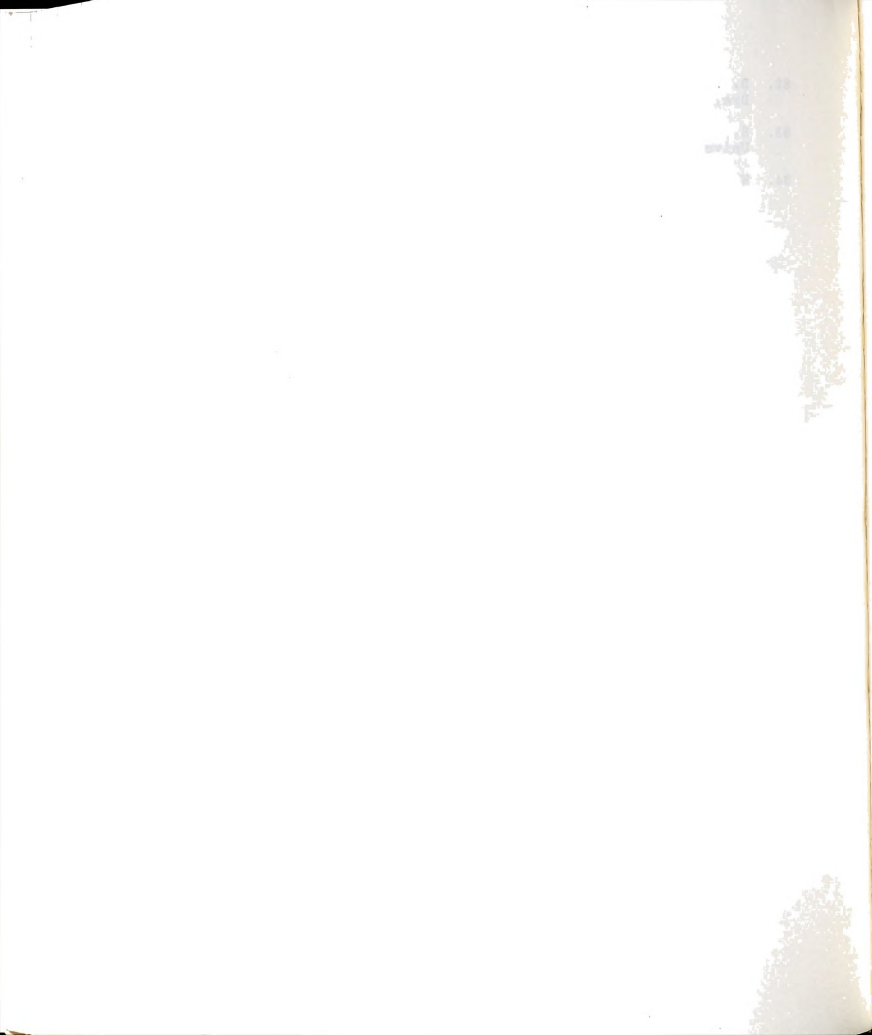47. F. Bloch, *Z. Physik*, <u>61</u>, 206 (1931).

48. J. C. Slater, *Phys. Rev.*, 52, 198 (1937).

49. T. Oguchi, *Prog. Theo. Phys.*, 13, 148 (1955).

50. H. Ohya-Nishiguchi, *Bull. Chem. Soc. Japan*, 52, 3480 (1979).

51. R. Karplus and J Schwinger, *Phys. Rev.*, 73, 1020 (1948).

52. D. N. Bhattacharyya, C. L. Lee, J. Smid, and M. Szware, *J. Phys. Chem.*, 69, 608 (1965).

53. J. L. Dye, *J. Phys. Chem.*, 84, 1084 (1980).

54. J. L. Dye and V. A. Nicely, *J. Chem. Educ.*, 48, 443 (1971).

55. A. C. Kunwar, G. L. Turner, and E. Oldfield, *J. Magn. Reson.*, 69, 124 (1986).

56. D. Fenzke, D. Freude, T. Fröhlich, and J. Hasse, *Chem. Phys. Lett.*, 111, 171 (1984).

57. L. E. H. McMills, Ph. D. Dissertation, Michigan State University (1989).

58. F. J. Tehan, B. L. Barnett, and J. L. Dye, *J. Am. Chem. Soc.*, 96, 7203 (1974).

59. M. M. Maricq and J. S. Waugh, *J. Chem. Phys.*, 70, 3300 (1979).

60. P. D. Moras and R. Weiss, *Acta. Cryst.*, B29, 396 (1973).

61. M. H. Cohen and F. Reif in "Solid State Phys, Vol. 5", ed. F. Seitz and D. Turnbull, Academic Press, New york (1957).

62. F. P. Van Remoortere and F. P. Boer, *Inorg. Chem.*, 13, 2071 (1974).

63. M. Dobler, J. D. Dunitz, and P. Seiler, *Acta. Cryst.*, B30, 2741 (1974).

64. M. Dobler and R. P. Phizackerley, *Acta. Cryst.*, B30, 2748 (1974).
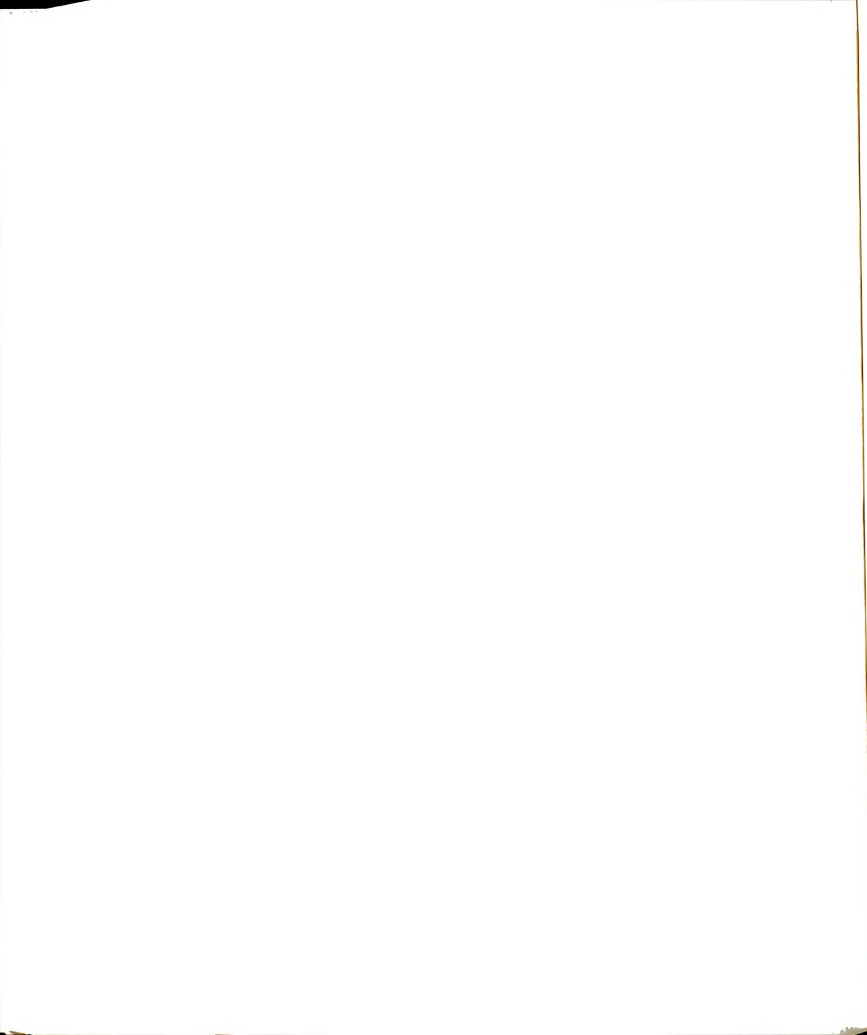
65. D. L. Ward, A. Ellaboudy, J. Kim, and J. L. Dye, unpublished results.

66 P. Seiler, M. Dobler, and J. D. Dunitz, *Acta. Cryst.*, B30, 2744 (1974).

67. E. A. Lucken, "Nuclear Quadrupole Coupling Constants", Academic Press, New York (1969).

68. J. Kermit, A. Ellaboudy, J. Kim, L. E. H. McMills, J. L. Eglin, and J. L. Dye, unpublished results.

69. R. H. Huang, D. L. Ward, and J. L. Dye, *J. Am. Chem. Soc.*, in press.

70. R. Sternheimer, *Phys. Rev.*, 84, 244 (1951).

71. R. K. Harris, "Nuclear Magnetic Resonance Spectroscopy", Pitman London (1983).

72. A. Ellaboudy, N. C. Pyper, and P. P. Edwards, to be published.

73. C. W. Haigh and R. B. Mallion, *Prog. NMR Spec.*, 13, 303 (1980).

74. R. A. Pascal, Jr. and R. B. Grossman, *J. Org. Chem.*, 52, 4616 (1987).

75. R. A. Pascal, Jr., R. B. Grossman, and D. Van Engen, *J. Am. Chem. Soc.*, 109, 6878 (1987).

76. N. F. Ramsey, *Phys. Rev.*, 77, 567 (1950).

77. N. C. Pyper and P. P. Edwards, *J. Am. Chem. Soc.*, 108, 78 (1986).

78. S. Arnott and S. C. Abrahams, *Acta. Cryst.*, 11, 449 (1958).

79. K. Hoffmann and E. Weiss, *J. Organometal. Chem.*, 67, 221 (1974).

80. S. C. Abrahams and J. Kalnajs, *J. Chem. Phys.*, 22, 434 (1954).

81. S. B. Dawes, D. L. Ward, R. H. Huang, and J. L. Dye, *J. Am. Chem. Soc.*, 108, 3534 (1986).
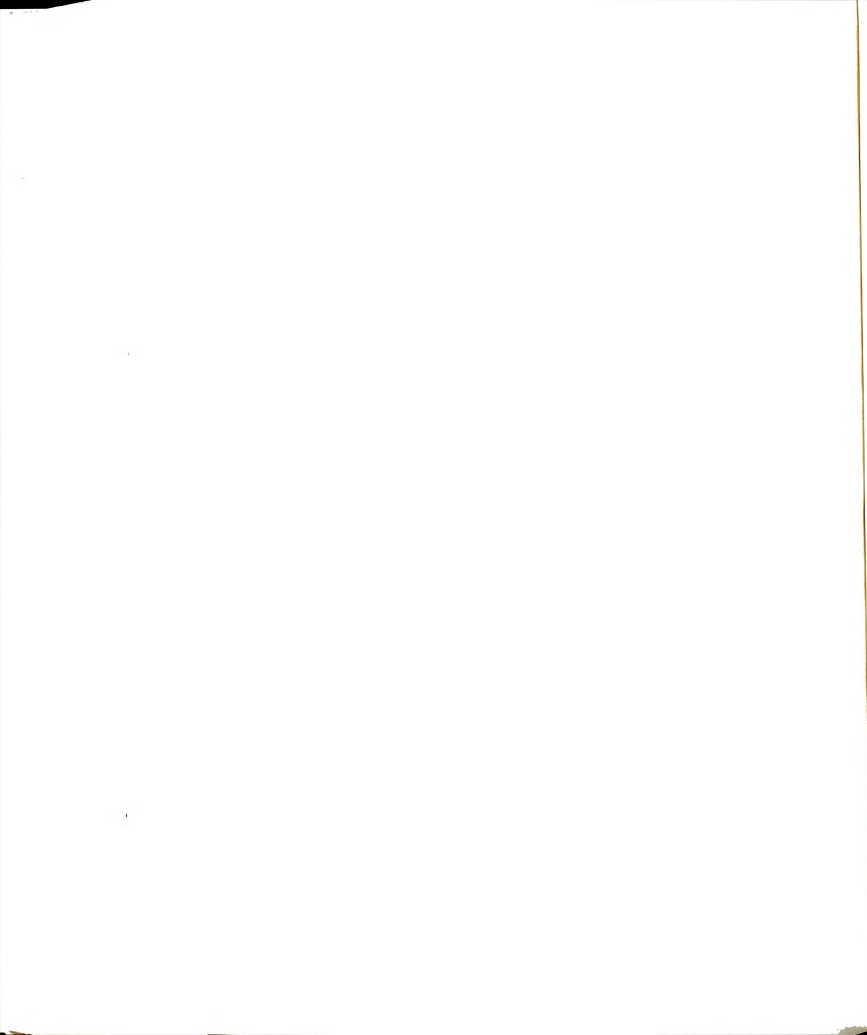
82. D. L. Ward, R. H. Huang, M. E. Kuchenmeister, and J. L. Dye, to be published.

83. S. Landers, Ph. D. Dissertation, Michigan State University (1981).

84. W. Wojciechowski, *Inorg. Chim. Acta.*, 319 (1967).